

UNIVERSITY OF READING



A General synthesis of π -Conjugated Materials

Thesis presented for the degree of Doctor of Philosophy

Long Chen

Seen and Approved for Submission by

Professor H.M. Colquhoun and Dr. B.W. Greenland

November 2016

Abstract

The work presented in this thesis explores the potential of using the Zincke salts of viologen derivatives to produce n-type (electron accepting) conjugated oligomers, polymers and macrocycles.

The cyclocondensation reaction between rigid, electron-rich aromatic diamines and di-Zincke salts has been harnessed to produce a series of conjugated oligomers containing up to twelve aromatic/heterocyclic residues. These oligomers exhibit discrete, multiple redox processes accompanied by dramatic changes in electronic absorption spectra. Comparison of the CVs of all of the unimers and dimers shows a strong correlation between the half wave potentials ($E_{1/2}$) and the pK_b values of the amine residues of the endgroups: higher pK_b values for the endgroups increase the energy required to reduce the viologen species. The measured conductivities of selected unimers, dimers and trimers showed that as either the length or area of conjugation increases, the thin film conductivity tends to increase. In addition, some of the oligomeric species showed interesting photocurrent characteristics under irradiation at visible wavelengths.

Lastly, a novel fully π -conjugated macrocycle which contained two 4,4'-bipyridinium residues was synthesised by cycloaddition of a di-Zincke salt with *m*-terphenyl diamine. It was found to be suitable to bind electron rich aromatic derivatives. Two [2] pseudo-rotaxanes incorporating this novel cyclophane were studied. The results clearly demonstrated that binding occurred by inclusion of the guest into the cavity of the macrocycle. The binding constant of the complexes was found to be correlated to the number of face-to-face π -stacking interactions within the supramolecular structure.

The results of this work will contribute towards a greater understanding of the electronic properties of viologen based materials. In particular, the identification of the correlation between the pK_b values of a broad range of aromatic end groups and the $E_{1/2}$ value of the viologens could have great value for designing a broad range of systems including nano-machines, electrochromic displays and novel catalysts.

Declaration

I confirm that this is my own work and the use of results and material from other sources has been properly and fully acknowledged.

Acknowledgements

I would like to thank my both my supervisors. Firstly, Prof Howard Colquhoun for his kind help and continued support during my PhD. Many thanks must also go to Dr Barny Greenland for patience and help throughout all 4 years, especially proof reading the final thesis.

I would like to thank Prof. František Hartl for his patient help in electrochemistry.

I would like to express my many thanks to Dr. Helen Wilcock (Loughborough) and Dr. Chris Wedge (Warwick) for their help with EPR spectra measurements.

I am also grateful to Drs. Olga Efremova, Jean-Sebastien Bouillard and Ali Adawi at University of Hull for use of equipment and training in thin film casting and electronic conductivity studies. In addition, I would like to thank Elodie Vivier for measuring some solid-state thin film conductivities after I returned to Reading.

A big thanks to the technical support provided by the Chemistry Department, including NMR, mass spectrometry and X-ray. I thank all of them for their daily help.

Finally, I would like to thank my parents for their love and support.

List of Abbreviations

Å	ångström
BBB	polybenzimidazobenzophenthroline
BBL	polybenzimidazobenzophenthroline
CB	conduction band
CBPQT ⁴⁺	cyclobis(paraquat- <i>p</i> -phenylene)
CPQ	1,1'-bis(<i>p</i> -cyanophenyl)-4,4'-bipyridilium
CV	cyclic voltammetry
DCMT	dicyanomethylene-terthiophene
DMF	N,N-dimethylformamide
DMP	9,10-dimethylphenazine
DSC	differential scanning calorimetry
ϵ	molar extinction coefficient
$E_{1/2}$	half wave potential
ECDs	electrochromic devices
Eq	equivalents
eV	electron volt
FETs	field effect transistors
g	gram
HOMO	highest occupied molecular orbital
HOSO	highest occupied spin orbital
Hz	hertz
I	current
IR-SEC	infra-red spectroelectrochemistry
ITO	indium tin oxide
LEDs	light-emitting diodes
LUMO	lowest unoccupied molecular orbital
m.p.	melting point

mmol	millimole
MS	mass spectrometry
MSTJ	two-terminal molecular switch tunnel junction
NP	naphthalene
NTCDA	1,4,5,8-naphthalenetetracarboxylic dianhydride
NTCDI	naphthalenetetracarboxylic diimide
ppm	parts per million
PPV	poly(p-phenylene-vinylene)
PVDs	photovoltaic devices
S	siemens
SWV	squarewave voltammetry
TBAPF ₆	tetrabutylammonium hexafluorophosphate
TCNQ	7,7,8,8-tetracyanoquinodimethanide
TEA	triethylamine
TFA	trifluoroacetic acid
THF	tetrahydrofuran
UPy	2-ureido-4[1h]-pyrimidinone
UV-vis	ultraviolet–visible spectroscopy
UV-vis SEC	ultraviolet-visible spectroelectrochemical
V	voltage
VB	valence band
δ	chemical shift (in ppm) downfield from tms
σ	conductivity
ν	frequency
Ω	ohm

Contents

Abstract	i
Declaration	ii
Acknowledgements	iii
List of Abbreviations	iv
List of Figures	5
Chapter 1 Introduction	1
1.1. Introduction and aims of the thesis	2
1.2. The electronic structure of organic semiconductors	3
1.3. Electronic structures of p-type and n-type semiconductors	6
1.4. Applications of conjugated semiconductors	8
1.4.1. Polymers for light-emitting diodes	8
1.4.2. Polymers for photovoltaic cells (PV).....	10
1.4.3. Organic Thin-Film Transistors (TFT).....	14
1.4.4. Summary of organic semiconductor development	17
1.5. Structure and properties of viologens	17
1.5.1. Viologens in electrochromic devices	18
1.5.2. Polymeric viologen systems	20
1.6. Conclusion	25
Chapter 2 Studies towards the synthesis of viologen containing polymers with fully conjugated main chains	26
2.1. Introduction and synthetic strategy	27
2.2. Results and Discussion	30
2.2.1. Verification of the structures of the products from initial polymerization reactions.	33
2.2.2. Investigations into the change in nucleophilicity of the amine residues in dianiline 2.9 during polymerization.	35
2.2.3. 2,5-Dimethoxybenzene-1,4-diamine 2.13 . ¹³⁰	37

2.3. Conclusion and Future work.....	38
--------------------------------------	----

Chapter 3 Efficient access to conjugated bipyridinium oligomers using the Zincke reaction: Synthesis, spectroscopic and electrochemical properties.....40

3.1. Introduction.....	41
3.2. Results and Discussion	44
3.2.1. Synthesis	44
3.2.2. Chemically reversible redox studies on 3.1 , 3.2 and 3.3	51
3.2.3. EPR Experiments.....	56
3.2.4. Cyclic voltammetry and Square wave voltammetry of 3.1 , 3.2 and 3.3	57
3.2.5 Spectroelectrochemistry (SEC) investigation of unimer 3.1 , dimer 3.2 and trimer 3.3 ..	61
3.2.5.1. IR-SEC study	61
3.2.5.2. Thin-layer UV-vis SEC study	62
3.3. Conclusion	69

Chapter 4 Synthesis, Characterization, and Electrochemical Behavior of.....71

Aromatic *N*-Substituted Viologens and Conjugated Oligo-Viologens71

4.1. Introduction.....	72
4.2. Results and Discussion	73
4.2.1. Design	73
4.2.2. Synthesis of a series of mono-viologen species with varying aromatic end groups.....	74
4.2.3. Synthesis of a series of di-viologen oligomers with varying aromatic end groups	76
4.2.4. Synthesis of tri-viologen oligomers with varying aromatic end groups.....	80
4.2.5 Synthesis of a di-viologen oligomer with 4,4'- (1,3,4- oxadiazole-2,5-diyl)dianiline as the central aromatic block.....	81
4.3. Cyclic voltammetry and Square wave voltammetry.....	82
4.3.1.1. CV data for monomeric and dimeric viologen species with varying numbers of ester residues on the end group	83
4.3.1.2. CV data for monomeric and dimeric viologen species with varying electron rich end groups.....	84

4.3.1.3 CV data for monomeric and dimeric viologen species with varying numbers of fused aromatic rings residues on the end group	86
4.3.1.4. Summary of half wave potentials for all of the monomeric and dimeric viologen species.	88
4.3.2. Correlation of pK_b values with half wave potentials ($E_{1/2}$) of viologen species having aromatic groups containing varying substituents.....	90
4.3.4 CV data trimeric viologen species with different end groups.....	93
4.3.5 CV data for trimeric viologen species with a different central, block unit.....	96
4.3. Conclusion	100

Chapter 5 Synthesis, and electrochemical behaviour of a [2] pseudo-rotaxane incorporating the novel cyclophane: cyclobis(paraquat-*p-m*-terphenylene).....102

5.1. Introduction.....	103
5.2. Results and Discussion	108
5.2.1. Binding studies of receptor 5.16 with π -electron rich 1,5-dioxynaphthalene derivatives.	111
5.2.1.1. Synthesis of 1,5-dialkoxy naphthalene 5.19	111
5.2.1.2. $^1\text{H-NMR}$ binding studies of 5.19 to macrocycle 5.16	112
5.2.1.3. $^1\text{H-NMR}$ binding studies of 5.22 to macrocycle 5.16	113
5.2.1.4. Binding properties of 5.16 and 5.22 in acetonitrile	114
5.2.2. Chemically reversible redox studies on macrocycle 5.16	116
5.2.3. Cyclic voltammetry and square wave voltammetry of 5.16	118
5.2.4. Electromechanical behaviour of 5.16 \supset 5.22	119
5.3. Conclusion	121

Chapter 6 Characterization of the solid-state electronic properties of viologen-containing compounds123

6.1. Introduction.....	124
6.1.1. Overview of conductive viologen-containing compounds	124
6.2. Results and Discussion	127

6.2.1. Preparation of the ITO substrate and thin films.....	127
6.2.2. Conductivity measurement	129
6.2.3. Dependence of the conductivity on the conjugation length.....	129
6.2.4. Dependence of the conductivity on the number of fused aromatic rings in the end group.	130
6.3. Photocurrent measurements on ether terminated monomeric, dimeric and trimeric viologens (4.10d , 4.13d and 4.16 , respectively).....	132
6.4. Conclusion	134
Chapter 7 Conclusion and Future Work	135
7.1. Review of Results	136
7.2. Future work.....	137
Experimental Techniques.....	138
Detailed synthetic procedures	142
References.....	168
Appendix 1.....	184
Appendix 2.....	187
Appendix 3.....	190

List of Figures

Figure 1.1. The structure of trans-polyacetylene.	3
Figure 1.2. A schematic representation of energy gaps in a conductor, semiconductor and insulator respectively.	5
Figure 1.3. Energy-band diagrams of n- type and p- type semiconductor.	5
Figure 1.4. Molecular structures of common p-type organic semiconductors.	6
Figure 1.5. Molecular structures of new n-type organic semiconductors.	7
Figure 1.6. Schematic of a light emitting diode.	8
Figure 1.7. PPV and its derivatives for LED applications. ⁶⁷	9
Figure 1.8. Model of photovoltaic cells.	11
Figure 1.9. Schematic energy diagram of two semiconductors with different LUMO levels. .	12
Figure 1.10. Chemical structures of three n-type conjugated polymers produced by Swager and co-workers. ⁹⁵	13
Figure 1.11. Basic schematic of a field-effect transistor. ¹⁰⁰	15
Figure 1.12. Structures of n-type semiconducting oligomeric materials which have been used in working OTFTs.	16
Figure 1.13. Structures of n-type semiconducting polymeric materials which have been used in working OTFTs.	17
Figure. 1.14. Schematic representation of the redox cycles (left) occurring within the Gentex's NVS mirror (right).	19
Figure 2.1. ¹ H-NMR spectrum of Zincke salt 1.65	31
Figure 2.2. ¹ H-NMR (D ₂ O, fully soluble) spectrum of the attempted synthesis of 2.8	32
Figure 2.3. Examples of proposed small molecules produced during the attempted synthesis of polymer 2.8	33
Figure 2.4. ¹ H NMR stack of "polymer 2.8 " with diamine 2.9 and Zincke salt 1.65	34
Figure 2.5. Comparison of nucleophilicity of 2.7 and 2.19	35
Figure 2.6. ¹ H-NMR spectra of the reaction between Zincke salt 1.65 and diamine 2.9 at time = 3 min (A) to time = 48 h (B).	36

Figure 2.7. The structure of the proposed decomposition product from the deprotection of 2.17 quinone type moiety.....	38
Figure 2.8. Structure of one of the commercially available aromatic diamines (2.19) with electron donating groups.....	39
Figure 2.9. Synthetic targets of unimer 3.1 , dimer 3.2 and trimer 3.3	39
Figure 3.1. Examples of "extended viologens": 3.4) <i>p</i> -phenylene extended Viologen, ¹⁶¹ 3.5), 4'- <i>(2,20</i> -bithiophene-5,5'-diyl)bis(1-decylpyridinium) ²⁺ , ¹⁶² 3.6) <i>p</i> -phenylene-bis-4,4'-(1-aryl-2,6-diphenylpyridinium) . ¹¹⁸	42
Figure 3.2. Structure of hexa-cationic trimer 3.3	43
Figure 3.3. ¹ H-NMR spectra of compound 3.1 (in acetone- <i>d</i> ₆ containing 1% of TFA).	44
Figure 3.4. ¹ H NMR spectrum of precursor 3.8 (D ₂ O).....	48
Figure 3.5. ¹ H NMR (acetone- <i>d</i> ₆ containing 1% of TFA) spectrum of compound 3.2	49
Figure 3.6. ¹ H NMR (acetone- <i>d</i> ₆ containing 1% of TFA) spectra of compound 3.3	51
Figure 3.7. UV-Vis spectra of compounds 3.1 , 3.2 and 3.3 in dimethylformamide (DMF, 0.2 mM) at 25 °C. Inset: Photograph of the compounds in DMF solution (0.2 mM).	52
Figure 3.11. EPR Spectra of radical species generated from 3.1 , 3.2 and 3.3 (1 mM) by addition of excess TEA in de-aerated acetone solution at room temperature.	57
Figure 3.13. Square wave voltammograms of 0.2 mM solutions of compounds 3.1 and 3.2 on a glassy carbon disc electrode in anhydrous DMF/0.1 M TBAPF ₆	60
Figure 3.14 Square wave voltammogram of 0.2 mM trimer 3.3 on a glassy carbon disc electrode in anhydrous DMF/0.1 M TBAPF ₆	60
Figure 3.15. IR spectral changes accompanying the stepwise one-electron reduction of dicationic unimer 3.1 (blue, 1 mM) to the corresponding radical cation (khaki) and then to the ultimate neutral form (purple) in anhydrous <i>n</i> -butyronitrile /0.1 M TABPF ₆ within an OTTLE cell ¹⁸⁷ . Solvent absorptions overload the detector between 1350 and 1500 cm ⁻¹	62
Figure 3.16. Reversible UV-vis spectral changes accompanying the stepwise 1e reduction of dicationic unimer 3.1 to the corresponding radical cation (spectrum A) and the neutral quinonoid form (spectrum B). Spectra recorded in anhydrous DMF/0.1M TABPF ₆ , using an OTTLE cell. ¹⁸⁷	63

Figure 3.17. Reversible UV-vis spectral changes accompanying the stepwise 1e reduction of tetracationic dimer 3.2 to the corresponding bis(radical cation) (spectrum A) and the neutral quinonoid form (spectrum B). Spectra recorded in anhydrous DMF/0.1M TABPF ₆ , using an OTTLE cell. ¹⁸⁷	64
Figure 3.18. Cathodic thin-layer cyclic voltammogram recorded in the course of the UV-Vis spectral monitoring of the three reductions (Table 1) of hexacationic trimer 3.3 (0.2 mM) in anhydrous DMF within an OTTLE cell ¹⁸⁷ at $v = 0.2 \text{ mV s}^{-1}$ at room temperature. The potential scale is arbitrary (Ag wire pseudoreference electrode was used).	65
Figure 3.19. Reversible UV-vis spectral changes accompanying the stepwise reduction of hexacationic 3.3 to the corresponding tris(radical cation) (spectrum A) and the mono(radical cation) (spectrum B) and the neutral quinoid form (spectrum C), recorded in anhydrous DMF/0.1M TABPF ₆ using an OTTLE cell. ¹⁸⁷	66
Figure 3.20. UV-vis spectral changes accompanying the stepwise reduction of hexacationic 3.3 to a neutral species. The change in intensity of the band at 515 nm associated with the formation of quinoidal bipyridinium residues occurs in the ratio 1:2 (arrows A and B respectively) during two-step reduction of the tris(radical cationic) form of 3.3 to the neutral species.	67
Figure 4.1. Schematic representation of target compounds: unimer, dimer and trimer.	73
Figure 4.2. Structures of mono-aromatic amine end groups and aromatic diamine mid-blocks.	74
Figure 4.4. ¹ H NMR spectrum of new dimer 4.12 in D ₂ O.	79
Figure 4.5. ¹ H NMR spectrum of dimer 4.17 in D ₂ O.	82
Figure 4.5. Cyclic voltammograms and squarewave voltammograms of 0.2 mM of unimer 3.1 and 4.10a ; dimer 3.2 and 4.13a at a glassy carbon disc (d = 2 mm) electrode in anhydrous DMF at $v = 500 \text{ mV s}^{-1}$	83
Figure 4.6. Cyclic voltammograms and squarewave voltammograms of 0.2 mM of unimer 4.10b , 4.10c , 4.10d and 4.10e ; dimer 4.13c and 4.13d at a glassy carbon disc (d = 2 mm) electrode in anhydrous DMF at $v = 500 \text{ mV s}^{-1}$	85
Figure 4.7. Cyclic voltammograms and squarewave voltammograms of 0.2 mM solutions of unimers 4.10f , 4.10g and 4.10h ; and dimers 4.13f , 4.10g and 4.13h at a glassy carbon disc (d =	

2 mm) electrode in anhydrous DMF at $v = 500 \text{ mV s}^{-1}$	87
Figure 4.8. Plot showing these two half wave potentials of unimers with various substituted end groups, obtained from CV experiments.	89
Figure 4.9. Plot showing two half wave potentials of dimers with various substituted end groups, obtained from CV experiments.....	90
Figure 4.10. Plot of the pK_b of N atom of each aromatic amine against the corresponding half wave potentials of unimers.	92
Figure 4.11. Plot of the average pK_b against the corresponding half wave potentials of dimers.	93
Figure 4.12. Structures of unimer 4.10d and dimer 4.13d and trimer 4.16	94
Figure 4.13. Cyclic voltammograms and squarewave voltammograms of 0.2 mM compounds 4.10d , 4.13d and 4.16 at a glassy carbon disc ($d = 2 \text{ mm}$) electrode in anhydrous DMF at $v = 500 \text{ mV s}^{-1}$	94
Figure 4.14. Structures of dimer 4.17 and dimer 3.2 with the central block units highlighted.	96
Figure 4.15. Structure of 2,5-diphenyl-1,3,4-oxadiazole (4.18).	97
Figure 4.14. Cyclic voltammograms of 0.2 mM 4.9 at a glassy carbon disc ($d = 2 \text{ mm}$) electrode in anhydrous DMF at $v = 500 \text{ mV s}^{-1}$	98
Figure 4.15. Cyclic voltammograms and square wave voltammograms of 0.2 mM compounds 4.17 and 3.2 at a glassy carbon disc ($d = 2 \text{ mm}$) electrode in anhydrous DMF at $v = 500 \text{ mV s}^{-1}$	98
Figure 5.1. Supramolecular polymers based on ureido-pyrimidinone (UPy) end-groups.	104
Figure 5.2. Schematic representation of a [2] pseudorotaxane, a [2] rotaxane and a [2] catenane.	105
Figure 5.3. MSTJ devices fabricated by Stoddard from the amphiphilic bistable [2] rotaxane 5.6 , the control dumb bell compound 5.7 , and the simple control, eicosanoic acid 5.8 , which consists of a molecule monolayer of the [2] rotaxane sandwiched between polycrystalline Si and metallic electrodes. This device can be switched reconfigurably and cycled repeatedly between ON and OFF states.....	105

Figure 5.4. Structures of four chemically stable macrocyclic diarylbipyridinium salts reported by Stoddart, Greenland and Colquhoun.....	106
Figure 5.5. Energy minimised structure with selected N to N bond length of <i>m</i> -terphenylene diamine 5.15 using ChemBio 3D.....	108
Figure 5.6. ¹ H-NMR spectrum (acetonitrile- <i>d</i> ₃) of macrocycle 5.16	110
Figure 5.7. Single-crystal X-ray structure of tetracationic macrocycle 5.16 4PF₆ in the solid state.....	111
Figure 5.8. ¹ H NMR (400 MHz) titration of guest species 5.19 against macrocycle 5.16 (2mM) in CD ₃ CN at 298 K. Molar ratios of host and guest are shown.....	113
Figure 5.9. ¹ H NMR (400 MHz) titration of guest species 5.22 against macrocycle 5.16 in CD ₃ CN at 298 K. Molar ratios of host and guest are shown.....	115
Figure 5.10. Chemical reduction of macrocycle 5.16 to the paramagnetic bis(radical cation) using TEA and reversible reoxidation with TFA monitored by ¹ H NMR spectroscopy and corresponding colour changes. The aromatic and heterocyclic rings highlighted in red indicate the region of the spin density in 5.16 ²⁺ (not bond order) (A) macrocycle 5.16 in acetone- <i>d</i> ₆ , (B) after addition of 20 equivs of TEA and (C) subsequent addition of an excess of TFA to B...	117
Figure 5.11. Cyclic voltammograms and square wave voltammogram of 0.2 mM compound 5.16 at a glassy carbon disc (d = 2 mm) electrode in anhydrous acetonitrile: A) 1 st reversible reaction at $v = 1.5 \text{ V s}^{-1}$, B) 2 nd not fully reversible reaction at $v = 0.5 \text{ V s}^{-1}$ and C) square wave voltammogram. The arrow indicates the scan direction from the initial potential.	118
Figure 5.12. Cyclic voltammograms of 0.2 mM compound 5.22 at a glassy carbon disc (d = 2 mm) electrode in anhydrous acetonitrile at $v = 500 \text{ mV s}^{-1}$. The arrow indicates the initial potential sweep.	120
Figure 5.13. Cyclic voltammograms and square wave voltammograms of 0.2 mM compound 5.16 and in the presence of 3NP (5.22) at a glassy carbon disc (d = 2 mm) electrode in anhydrous acetonitrile at $v = 500 \text{ mV s}^{-1}$	121
Figure 6.1. Structure of the TCNQ salts of diphenyl-4,4'-bipyridinium and its para-substituted congeners.	125
Figure 6.2. Structure of 1,1'-bis(p-cyanophenyl)-4,4'-bipyridinium with tetrafluoroborate salts.	

.....	125
Figure 6.3. Solid-state conductivities of the viologen-based species investigated by Port and Vaid. ^{168,179}	126
Figure 6.4a. Interdigitated ITO Substrates (Picture from Ossila: https://www.ossila.com/products/interdigitated-ito-ofet-substrates). The ITO channels are the paler areas in this image.....	127
Figure 6.4b. Photo of a coated ITO cell used in this work	127
Figure 6.5. The solid state conductivities of unimers (3.1 , 4.10d), dimers (3.2 , 4.13d) and trimers (3.3 , 4.16) containing ester or ether end groups respectively.	130
Figure 6.6. The conductivities of unimers 4.10f (phenyl), 4.10g (naphthyl) and 4.10h (pyrenyl) (mean of 4 results).	131
Figure 6.7. Photocurrent response of thin films of samples of 4.10d , 4.13d and 4.16 held at a constant applied potential 15 V as the wavelength of the incident radiation is varied from 300 to 800 nm.	132
Figure 6.8. Current response of thin films of 4.16 at constant applied potential of either +15 V or -15 V as the wavelength of incident radiation was varied between 300 and 800 nm.	133
Figure S1. Schematic diagram of the equipment used for current-voltage measurements.....	141
Figure S2. The I/V plot of unimer 3.1 , dimer 3.2 and trimer 3.3 containing ester end groups, respectively.	184
Figure S3. The I/V plot of unimer 4.10d , dimer 4.13d and trimers 4.16 containing ester end groups, respectively	185
Figure S4. The I/V plot of unimer 4.10f , 4.10g , 4.10h containing varying numbers of fused aromatic rings residues on the end group.	186

Chapter 1

Introduction

1.1. Introduction and aims of the thesis

Materials are characterised according to their physical properties, for example magnetic susceptibility, tensile modulus or elongation at break. Over the last 150 years controlling the electronic properties of materials has become one of the most exciting areas of research.

All materials can be defined as either a conductor, insulator or semiconductor.^{1,2} As will be discussed in more detail later, the precise electrical properties of a material are dependent on the positions of the electrons within their atomic or molecular structure.³ However, traditionally most conductors are metallic substances, semiconductors usually silicon based and insulators are frequently polymers and ceramics.⁴ Over recent years there has been great interest in producing polymeric materials with electrical properties as a consequence of their low cost, tunable mechanical properties and ease of fabrication.^{5,6} This chapter will briefly review the history of the fast moving field of polymer electronics. Towards the end of the review, the synthesis of pyridinium-containing electronic materials will be discussed as this is the focus of the experimental chapters of this thesis.

Polymers have become ubiquitous in the modern world.⁷ Their physical properties can be tuned by varying their chemical structure, chain length and dispersity.⁸ Through careful choice of monomer structure, polymers can be produced that are elastomeric in nature or are tough enough to construct the load bearing components of passenger aircraft.⁹ Despite these diverse mechanical properties, polymers have generally been considered to be electrical insulators.¹⁰ For example, they can be used as antistatic coating materials or to insulate copper wire.

The insulating properties of polymers were not challenged until the seminal work of Alan J. Heeger, Alan MacDiarmid and Hideki Shirakawa^{11,12} in 1977. They found that polyacetylene (Figure 1.1), a simple organic polymer comprising alternating single and double bonds, could exhibit conductive properties if subjected to a process known as doping. This occurs by

treatment of the material with oxidizing or reducing agents which results in the introduction of charge carriers into the material. The publication of this work on polyacetylene resulted in an explosion of research activity into conducting polymers. This is because compared to the traditional metallic conductors, polymers typically have a range of desirable attributes: lower raw material and production costs and more simple fabrication into large area devices. In addition, they are usually lower density and frequently exhibit excellent physical properties (such as flexibility). The importance of this first breakthrough in conducting polymers was acknowledged by the award of the Nobel Prize to Heeger, MacDiarmid and Shirakawa in 2000.

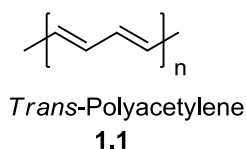


Figure 1.1. The structure of *trans*-polyacetylene.

More than 40 years of research and development has resulted in the synthesis and evaluation of a diverse range of organic small molecule and polymeric electronic materials. Each class has its own set of advantages and disadvantages.¹³ The advantages of electronically conductive small molecules include synthetic simplicity, mono-dispersity and ease of purification.¹⁴ On the other hand, compared to small molecules, polymers can exhibit intrinsic strength and flexibility which may make them easier to fabricate into working devices.¹⁵ Both small molecule and polymeric electronic materials have been shown to have great potential in many areas, including light-emitting diodes (LEDs),^{16,17} photovoltaic devices (PVDs),^{18,19} electrochromic devices (ECDs),²⁰⁻²² and field effect transistors (FETs).²³⁻²⁶

1.2. The electronic structure of organic semiconductors

In order to optimize device performance, it is important to understand how conjugated molecules conduct charge. Generally, charge transport can be thought of as an electron transfer

from a charged part of a polymer chain to neighboring region. Therefore, the material must contain an orbital system that allows the charge carriers to move. This can be achieved if the chemical structure of the material contains an unbroken region of overlapping of π -orbitals along the backbone (a conjugated or unsaturated system). This feature is clearly visible in polyacetylene as alternating single and double bonds (Figure 1.1). Extended conjugated systems provide a continuous region of π -electron density along the polymer backbone through which charge carriers can move unhindered.

As a consequence of their electronic structure, most conjugated polymers do not possess free electrons to act as charge carriers in their native state.²⁷ Therefore, as in the case of polyacetylene, the charge carriers are introduced through a doping process, either by the addition of electrons (n-doping) with electron donors (e.g. Na, K) or by the removal of electrons (p-doping) which creates a positively charged 'hole' through the addition of electron acceptors (e.g. I_2 , AsF_5).²⁸

Beyond the orbital structure and doping of a polymer, the electrical properties are also dependent on the relative and absolute energy of the orbitals.²⁹ The difference in energy between the highest energy molecular orbital occupied by electrons (HOMO or valence band) and the lowest unoccupied molecular orbital by electrons (LUMO or conduction band) is termed the band-gap (Figure 1.2).³⁰ The valence band and conduction band of metallic conductors overlap, therefore, electrons in metallic conductors are free to move. In contrast, in semiconductors and insulators, the conduction bands are empty and energetically separated from the valence bands. In both these cases, electrons must be promoted across the band gap to generate a conductive material. For insulating materials, the band gap between the conduction and valence band is too large to be crossed under typical environmental conditions, accounting for their lack of electrical conduction.

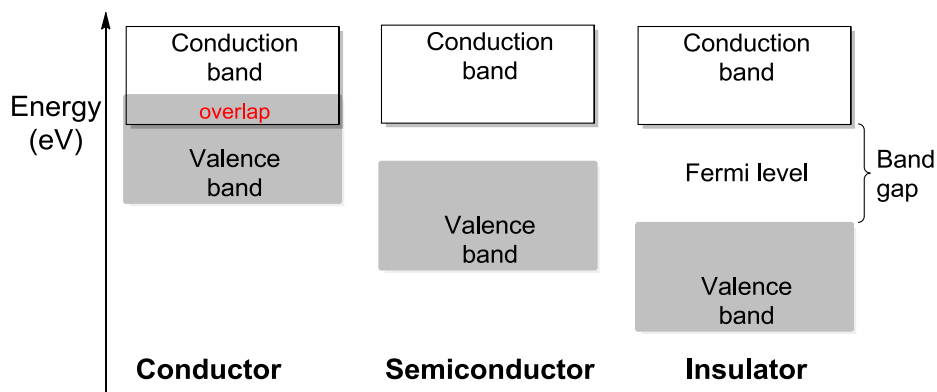


Figure 1.2. A schematic representation of energy gaps in a conductor, semiconductor and insulator respectively.

The energy levels of semiconductor materials can be tuned by the addition of dopants, as seen in the original work on polyacetylene (Figure 1.1). Figure 1.3 shows the energy level diagrams for a typical n-type and p-type semiconductor. In an n-type inorganic semiconductor, the addition of electron dopants results in the reduction in the energy level of the LUMO. This means that electrons from the valence band can be more easily excited into the conduction band. In contrast to n-type doping, p-type dopants increase the energy level of the HOMO. This also has the effect of reducing the HOMO-LUMO band gap.

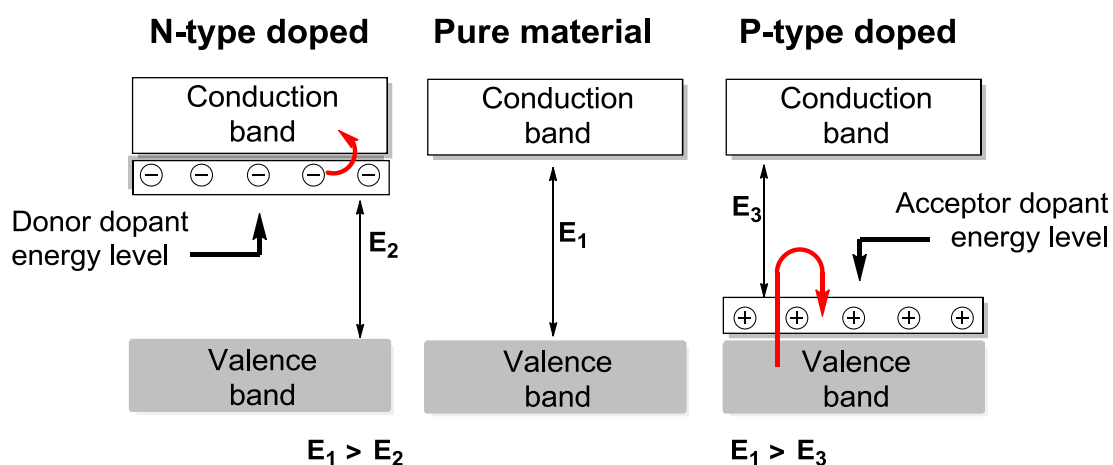


Figure 1.3. Energy-band diagrams of n-type and p-type semiconductor.

1.3. Electronic structures of p-type and n-type semiconductors

As with inorganic semiconductors, organic polymeric semiconductors can be defined as p-type (electron donor, hole transport) or n-type (electron acceptor, electron transport).³¹ P-type organic semiconductors have been studied most widely,^{32–36} with many hundreds produced with varying chemical structures over the past few decades. Figure 1.4 shows some of the most widely studied p-type organic semiconductors.

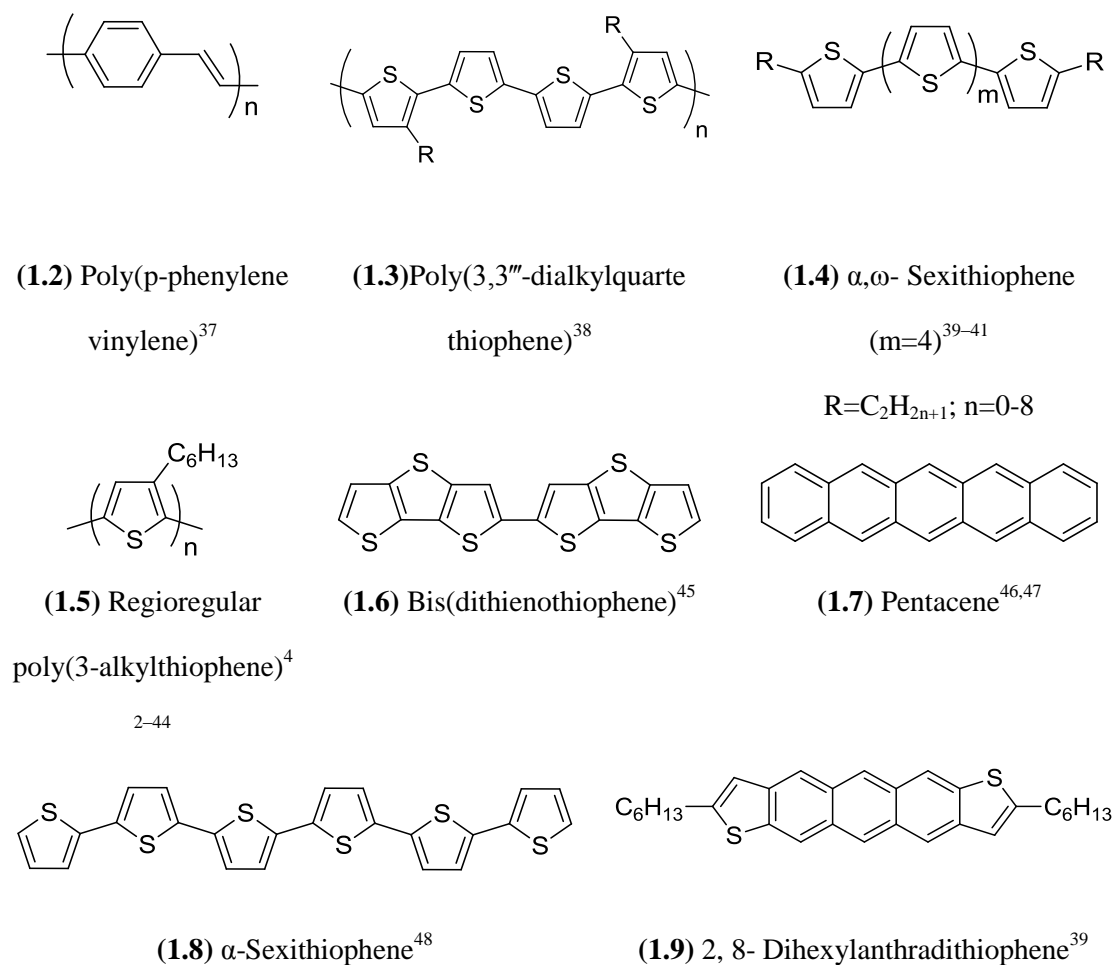


Figure 1.4. Molecular structures of common p-type organic semiconductors.

In contrast to the large number of p-type organic semiconductors, the number of n-type organic materials is limited to a very small number of oligomers and polymers.⁴⁹ This is because n-type organic materials can have significant drawbacks including complex synthesis, poor solubility and high susceptibility to oxidation. Despite this challenge, over recent years there

has been an intense interest in the design and synthesis of this class of small molecule and polymer as shown in Figure 1.5.

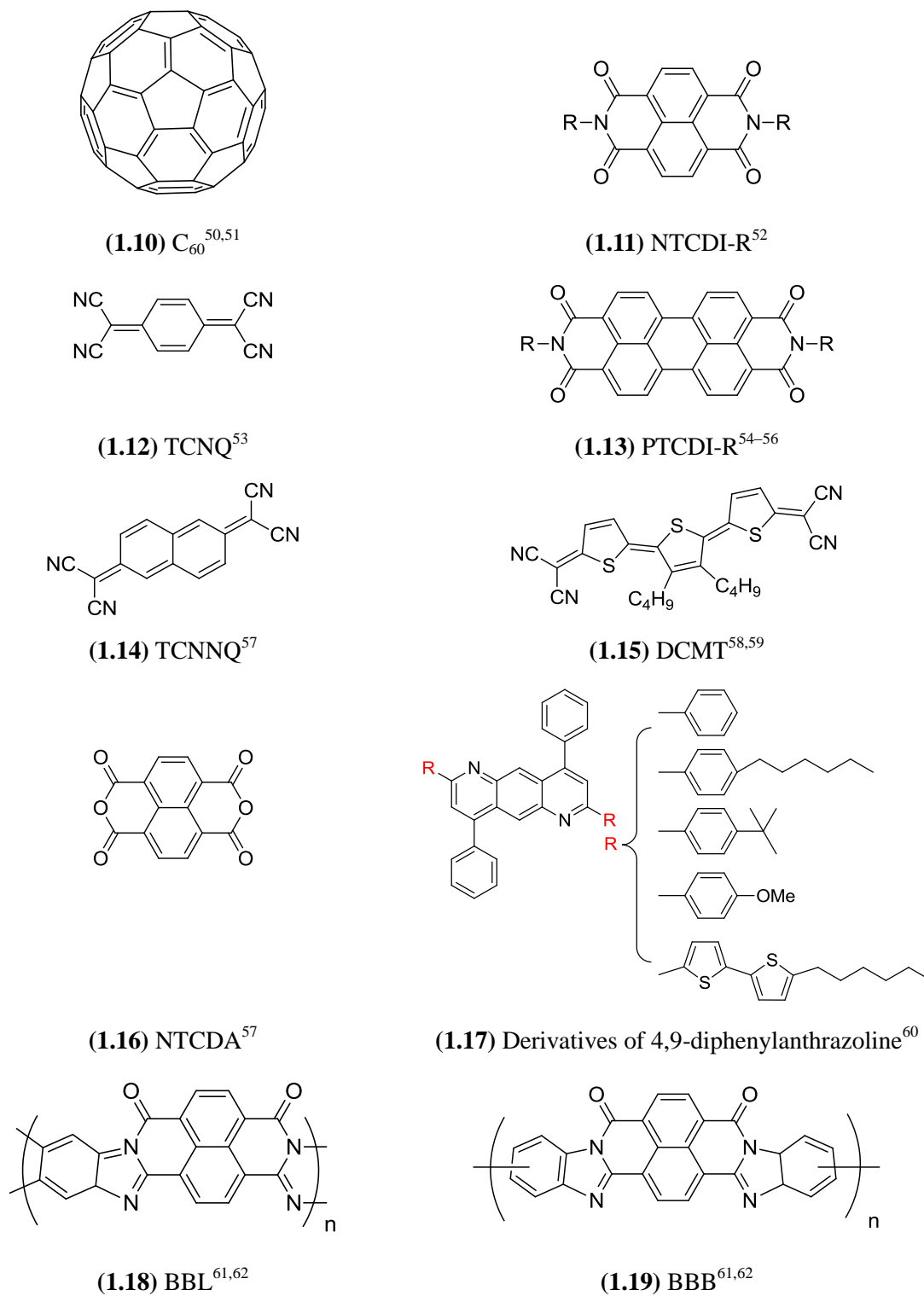


Figure 1.5. Molecular structures of new n-type organic semiconductors.

1.4. Applications of conjugated semiconductors

With a supply of organic conductors and semi-conductors at hand, increasing attention is now turning to their application in working electronic devices. Although many of these devices use similar physical principles they can have dramatically different uses. Over the following few sections the underlying concepts behind polymeric organic light emitting diodes (OLEDs), photovoltaic devices (PVDs) and thin film transistors (TFTs) will be briefly discussed.

1.4.1. Polymers for light-emitting diodes

One of the first commercial uses of conjugated polymers was in organic light emitting diodes (OLEDs) which emit light when electric current passes in one direction. OLEDs consist of two components: an n-type semiconductor which can accept electrons and a p-type semiconductor which readily lose electrons, creating a positively charged hole (Figure 1.6). The free electrons and holes are created by applying a voltage across the device. When the electrons in the n-type component and holes on the p-type component combine, a photon is released, generating light.

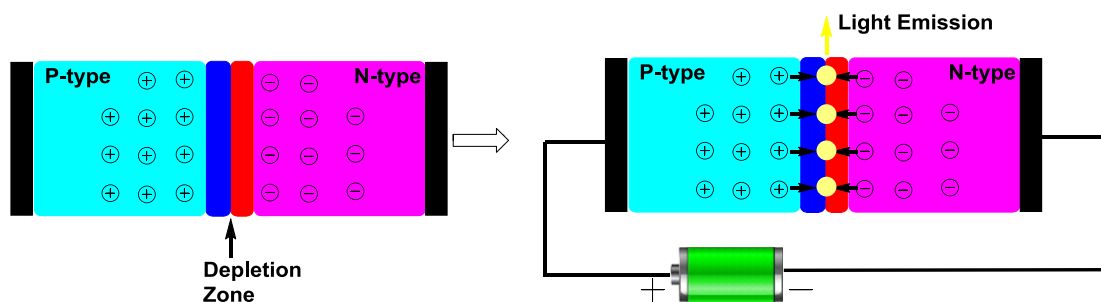


Figure 1.6. Schematic of a light emitting diode.

The colour of emitted light is related to the size of the n/p-type band gap energy.⁶³ Thus, finding materials with suitable band gaps to produce the primary colours of the visible spectrum is one of the main drivers in OLED research.

The frequency (colour) of the light emission can be tuned through chemical modification of the

macromolecules.⁶⁴ This was demonstrated in the first report of organic polymeric light-emitting diodes by Friend and co-workers⁶⁵ at University of Cambridge in 1990. The group reported the synthesis of π -conjugated poly(p-phenylene-vinylene)s (PPV) (Figure 1.7). PPV possesses many desirable properties, such as a small optical band gap, bright yellow fluorescence and high oxidative and thermal stability which makes it an excellent candidate in many electronic high-technology applications.⁶⁶ It is also the one of the few conjugated polymers that has been processed into a film with highly ordered crystallinity.⁶⁷ This morphology can create better percolation pathways for charges to move toward the corresponding electrode.⁶⁸

Despite these numerous valuable physical and electronic properties, PPVs still present processing problems, most notably an extremely low solubility in common solvents.⁶⁹ In order to overcome this, many studies have subsequently produced powerful synthetic strategies to synthesize structural variants with greater solubility.⁷⁰ The most successful derivatives contain flexible side groups along the polymer backbone or main chain.^{71–75} Over the last three decades of research, many promising electroluminescent conjugated polymers and their derivatives have been discovered as exemplified in Figure 1.7.

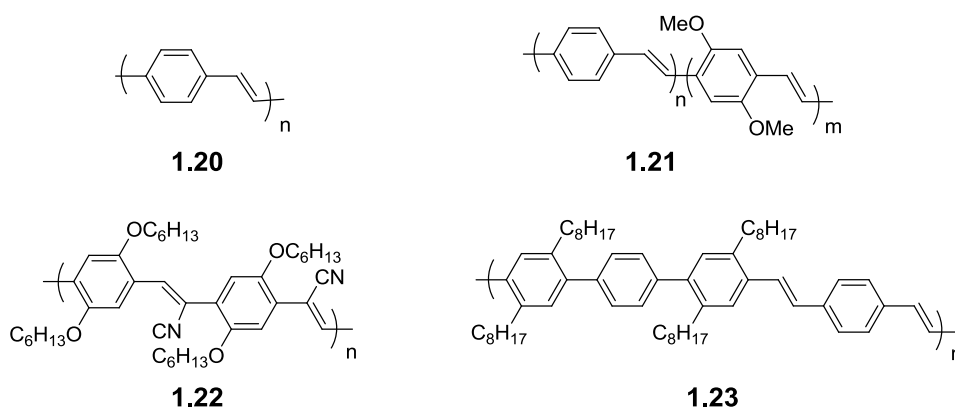


Figure 1.7. PPV and its derivatives for LED applications.⁶⁷

OLEDs have reached commercialization in recent years, for example, Pioneer had produced a car radio with an OLED Panel in 1997 with the first OLED TV released by Sony 10 years

later.⁷⁶

Due to the relatively high price of commercial OLEDs, research remains active in the conjugated polymers field to further improve the efficiency and fabrication of these products. In addition, the mode of action of OLEDs is closely related to that of photovoltaic (solar) cells which is briefly covered in the following section.

1.4.2. Polymers for photovoltaic cells (PV)

With an ever growing requirement to reduce the levels of Greenhouse Gas emissions, harnessing solar energy is one of the most promising renewable energy solutions. However, there are still many limitations which are related to the current silicon-based technology, such as the high costs of manufacturing the crystalline (inorganic) photovoltaic cells.

In 1954, Chapin and co-workers⁷⁷ produced the first inorganic p-n junction solar cell which converted solar radiation to electricity with 6% efficiency. Since this discovery, a continual improvement in crystalline silicon PVC design has resulted in devices that show up to a 25% conversion efficiency. However, crystalline silicon has poor mechanical properties when deposited on flexible substrates. Furthermore, raw material and production costs are still high, making them rather expensive.⁷⁸

Given the cost of crystalline silicon solar cells, scientists have attempted to exploit the potential of using organic materials in solar cells. There are three categories of organic photovoltaic cells, namely: small molecule,⁷⁹⁻⁸² dye-sensitized⁸³⁻⁸⁶ and polymer based solar cells.^{87,88} Given the immense depth of research in this area the following section will only cover the basics of PVC design and touch upon a small selection of polymers that are currently showing promise in this field.

A schematic of a basic bilayer type of PVC is shown in Figure 1.8. The cell is composed of two

thin films of semiconductor, n-type and p-type. When sunlight hits the p-type semiconductor, an electron is excited by the photon, which leads to the formation of an excited electron (exciton). If the exciton is in close proximity to the n/p type junction then the electron can move into the p-type region of the material, leaving a positively charged hole behind. Splitting the excitons into free electrons and holes results in a usable current being induced in the cell which can be used to do work.^{19,89,90}

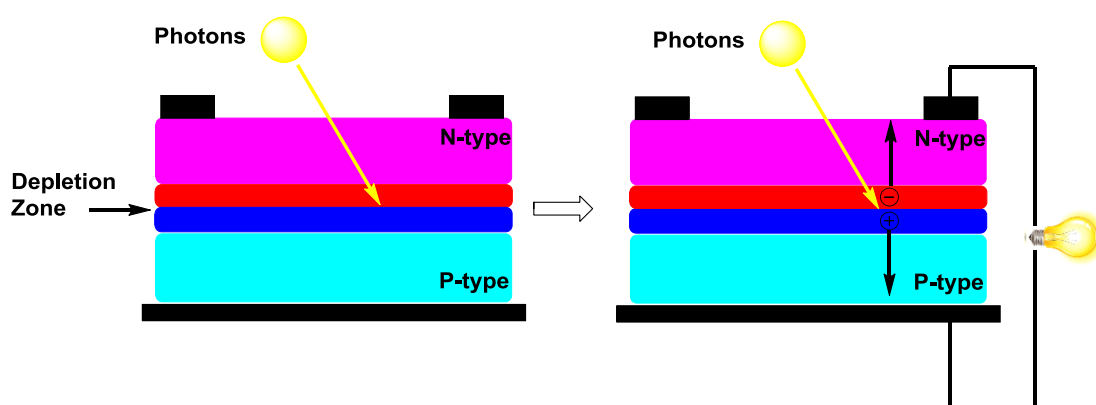


Figure 1.8. Model of photovoltaic cells.

One of the strategies for producing more efficient photovoltaic cells is to find a way to reduce the band gap between the n and p-type components of the cell. This can be achieved by different strategies.^{91,92} The material with highest LUMO level is called the donor and the semiconductor with the highest electron affinity the acceptor (Figure 1.6). After photo-excitation, the electron is transferred from the donor to the acceptor, as is shown schematically in Figure 1.9. By using this design rationale, in 1986, Tang and co-workers selected a phthalocyanine residue as an acceptor (n-type) and a perylene derivative as a donor (p-type) respectively and successfully demonstrated charge dissociation using non-silicon, organic materials.⁹³

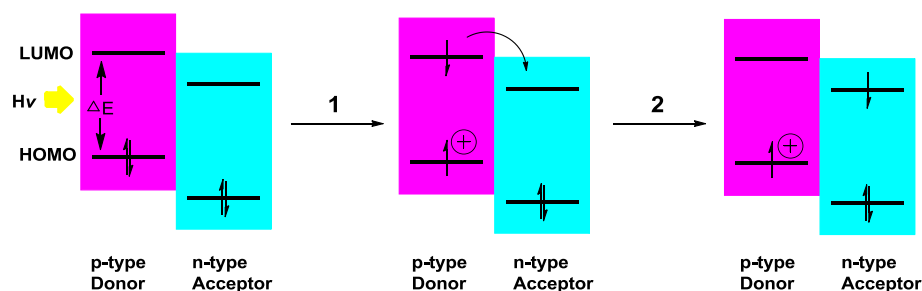


Figure 1.9. Schematic energy diagram of two semiconductors with different LUMO levels.

Partly due to the limited number of air-stable and soluble n-type (electron-transporting) polymeric semiconductors, the polymer photovoltaic field has primarily focused on combining p-type macromolecules with n-type small molecules such as fullerene derivatives.⁹⁴ However, compared to polymers, the drawback of small molecules is clear. For example, they cannot contribute to the intrinsic mechanical properties of the PVC, and they are difficult to solution cast into homogeneous films. Thus further study into the synthesis of n-type polymers remains extremely important.

One of the most interesting examples of n-type polymers used in PVCs was reported by Swager and co-workers.⁹⁵ The group developed a series of water-soluble electron-accepting (n-type) conjugated polymers which are shown in Figure 1.10. These three conjugated polymers (**1.24**, **1.25**, **1.26**) all exhibit high electron affinities (3.90-4.14 eV) as judged by their onset reduction potential using cyclic voltammetry. These values are comparable to the electron-affinity of both the fullerene derivative [6,6]-phenyl-C61-butyric acid methyl ester (PCBM) (4.2 eV) and polybenzimidazobenzophenanthroline (BBL) (4.0 eV) which have both found widespread use in prototype organic photovoltaic cells (OPVC). The pyridinium rings are highly electron-withdrawing in nature and are responsible for producing the extremely low LUMO energies. In addition, the optical band gaps and HOMO/LUMO levels can be further tuned by producing co-polymers where the pyridinium units are separated by acceptor residues such as thiophenes (e.g. **1.26**) resulting in a series of n-type polymers with varying electron affinities.⁹⁵

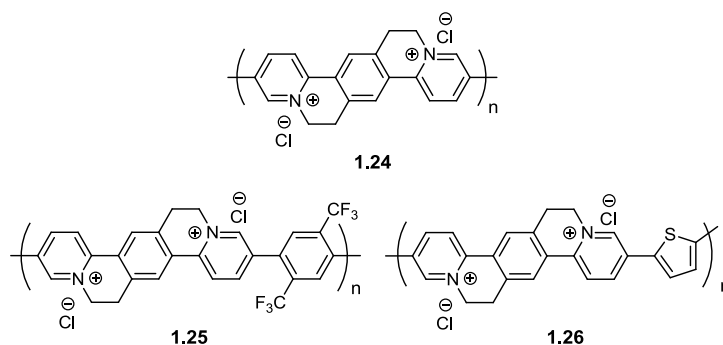
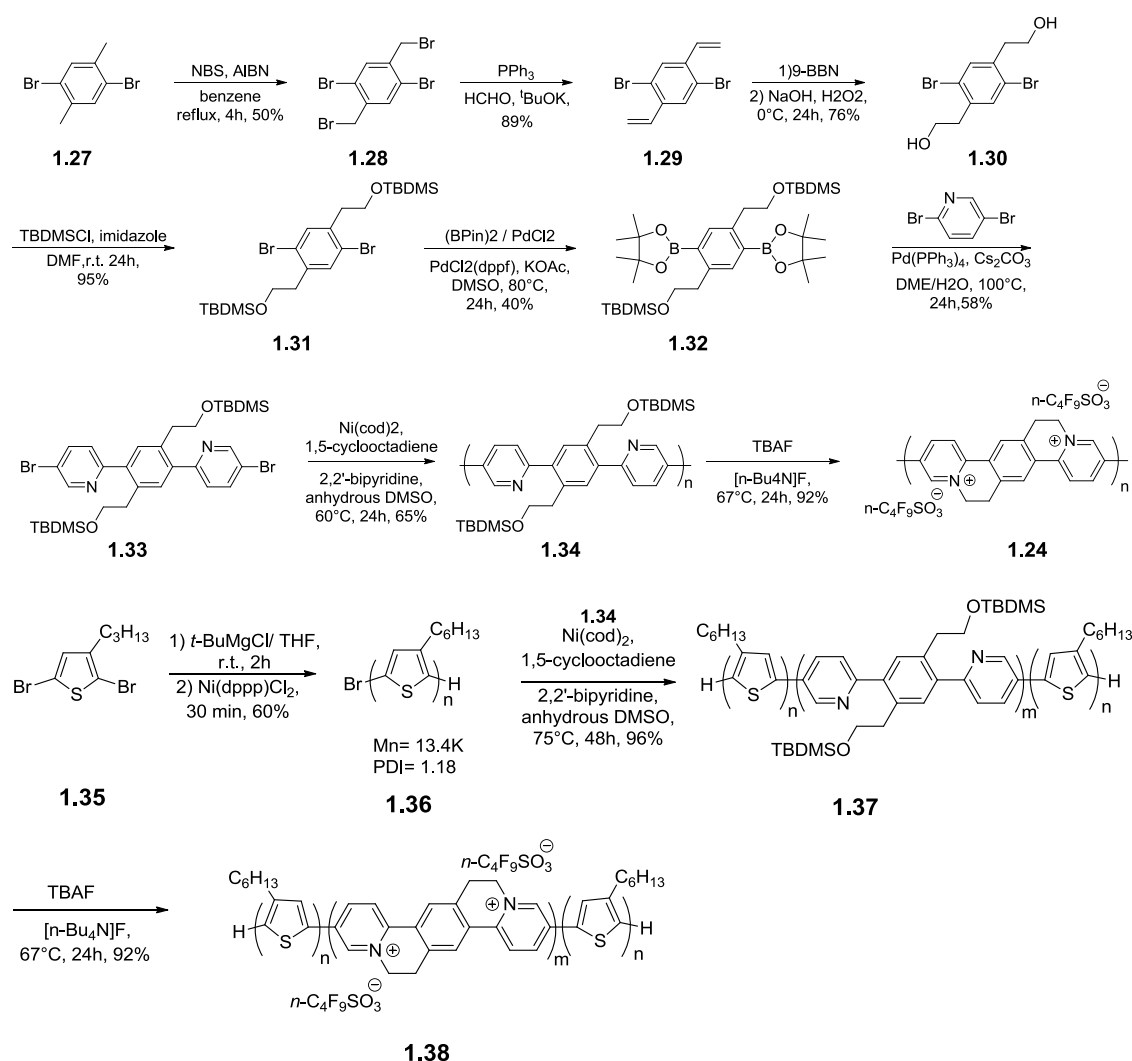


Figure 1.10. Chemical structures of three n-type conjugated polymers produced by Swager and co-workers.⁹⁵

Four years later, Swager and co-workers successfully synthesized and characterized new conjugated crystalline-crystalline donor-acceptor block copolymers (**1.38**) based on their previous methodology. In terms of structure, regioregular poly(3-hexylthiophene) segments are used as the electron donor in these block polymers, with the poly(pyridinium phenylene) segments acting as the electron acceptor. The LUMO energy level of this block polymer estimated from cyclic voltammetry was 3.8-4.0 eV and it exhibited an ionization potential (HOMO energy level) of 5.1 eV. Notably, all these conjugated block copolymers are soluble in aprotic polar solvents, such as DMF and DMSO. In addition, they also display broad optical absorption bands extending close to the near-infrared region. This makes them desirable candidates for photovoltaic materials as their absorption bands match the frequency range of the solar spectrum. The synthetic route to these conjugated block copolymers are outlined in Scheme 1.1. This lengthy linear synthesis results in an overall yield of approximately 1.3%. Therefore, although these materials exhibit interesting properties, they are clearly not suited to large-scale production without significant optimization.



Scheme 1.1. Synthetic route to P3HT-b-PPymPh **1.38**.^{95,96}

1.4.3. Organic Thin-Film Transistors (TFT)

Field-effect transistors (FET) are devices which can use an electric field to control the conductivity of a material.⁹⁷ This property is harnessed to produce the switches which are found in all electronic devices, for example, the Metal Oxide Semiconductor Field-Effect Transistor (MOSFET) the fast-acting switch which can be found in everything from radios to computers.⁹⁸ Since the invention of the first practical semiconducting transistor by John Bardeen, William Shockley, and Walter Brattain in 1947,⁹⁹ the FET has become a very widely used device within the semiconductor industry (Nobel Prize in physics, 1956). As discussed previously (sections 1.1 and 1.4.2), in contrast with silicon technology, some of the

benefits of organic thin film field-effect transistors (OTFTs) are lower material and fabrication costs.

A typical TFT is composed of several components as shown in Figure 1.11: three electrodes (i.e., gate, drain, and source electrodes), a dielectric layer and a semiconducting layer. The current flow between the source and drain is controlled by the gate electrode.

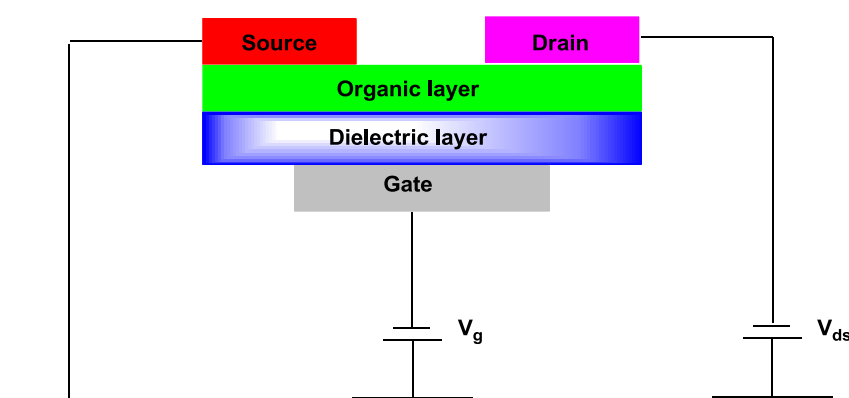


Figure 1.11. Basic schematic of a field-effect transistor.¹⁰⁰

One of the most significant parameters in characterizing a TFT is the efficiency of charge injection from the electrode, which is dependent on the fundamental characteristics of charge mobility and on/off ratio (the difference between the on-state current and off-state current).¹⁰¹

Since the first report concerning OTFTs in 1986,¹⁰² their performance has improved significantly. This improvement has mainly arisen due to the increasing number of suitable p-type materials that have been synthesized, particularly pentacene,^{46,103} α -sexithiophene⁴⁸ and poly-3-hexylthiophene (as shown in Figure 1.4).^{42-44,104}

The primary requirement of n-type materials in working OTFTs is that they must have an electron affinity high enough to allow efficient injection of electrons into their empty LUMO.

Therefore, as with PVC and OLEDs discussed previously, there is a particular requirement to develop air-stable n-type organic semiconductors. To achieve this, it has been found that the addition of electron withdrawing groups (cyano, perfluoroalkyl etc.) to known p-type molecules results in electronic structures suitable for use in OTFTs. In 1998, Bao and co-workers¹⁰⁵ produced an easily accessible n-type small molecule by introducing electron-withdrawing fluorine atoms to the perimeter of copper phthalocyanine. This small molecule exhibited an electron mobility of $0.03 \text{ cm}^2/\text{V}\cdot\text{s}$. Another example was reported by Facchetti et al,¹⁰⁶ who introduced perfluorohexyl groups (C_6F_{13}) to oligothiophenes generating a novel material. (Figure 1.12)

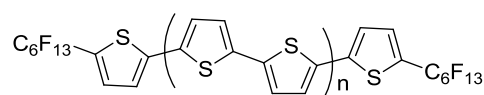
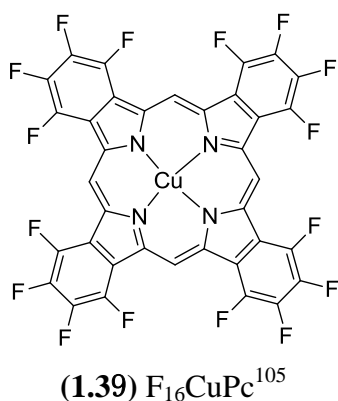


Figure 1.12. Structures of n-type semiconducting oligomeric materials which have been used in working OTFTs.

Compared to the quantity of literature concerning small molecules, the literature on n-type semiconducting polymers for TFT application is very limited. One of the few examples was reported by Babel and co-workers focusing on poly(benzobisimidazobenzophenanthroline) (**1.41**) and the corresponding poly(benzobisimidazobenzophenanthroline) (**1.42**) (Figure 1.13).⁶² It was demonstrated that the field-effect mobility of electron in the polymer **1.41** was as high as $0.1 \text{ cm}^2 \text{ V}^{-1} \text{ s}^{-1}$ in a solution cast film in air. However, the observed mobility of **1.42** in similarly fabricated films was only $10^{-6} \text{ cm}^2 \text{ V}^{-1} \text{ s}^{-1}$.

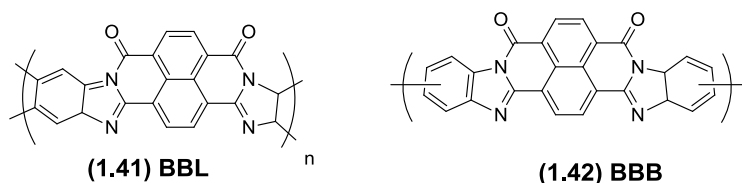


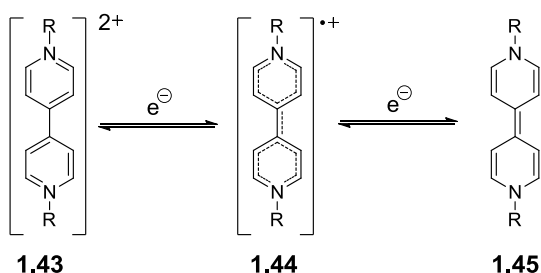
Figure 1.13. Structures of n-type semiconducting polymeric materials which have been used in working OTFTs.

1.4.4. Summary of organic semiconductor development

Many electronic devices are comprised of both n-type and p-type materials. Whilst there has been significant progress in the synthesis and structural optimization of p-type polymeric materials, much less work has focused on the production of n-type polymers. However, the recent work by Swager and co-workers⁹⁵ shows pyridinium based materials can act as n-type materials in working laboratory scale OLEDs and PVCs and therefore merit further attention. The following sections use selected examples from the literature to review the structure and properties of bipyridinium dications such as viologen and their introduction into the main chains of polymeric materials.

1.5. Structure and properties of viologens

Viologens (V) are disubstituted 4,4'-bipyridinium ions first reported by Michaelis 1933 (1.43, Scheme 1.2).¹⁰⁷ They can undergo two one-electron transfer reactions sequentially to form firstly a radical cation and secondly a neutral quinoidal species (Scheme 1.2).



Scheme 1.2. Electrochemical interconversion of 4,4'-bipyridinium units between dicationic (1.43), radical cationic (1.44) and neutral, quinoidal forms (1.45).

Viologen radical cations are generally intensely colored, with high molar absorption coefficients. This is as a consequence of an intramolecular optical charge transfer process.¹⁰⁸ Further reduction of $V^{•+}$ gives the neutral V^0 , which is weakly colored as there is no accessible assisted charge transfer or internal transition corresponding to the energy of light at a visible wavelength. The first reduction (V^{2+} to $V^{•+}$) is highly reversible and generally proceeds without significant side reactions. However, depending on the R group, the second reduction can sometimes be irreversible as a consequence of the poor solubility of the neutral species.¹⁰⁸ The color can be tuned by varying the substituents on the nitrogen atom in the heteroaromatic ring (Table 1.1).¹⁰⁹ This has resulted in the widespread use of viologen based structures in colour changing (electrochromic) devices.

R group	Native dication	Radical cation
Phenyl	Reddish black	Green
p-cyanophenyl	Olive	Green
alkyl	Blue or bluish purple	Green

Table 1.1. colour of viologens with different R substituents.¹⁰⁹

1.5.1. Viologens in electrochromic devices

Electrochromism (EC) is defined as an optical reversible colour change of a material by electrochemical oxidation and reduction in response to an electric field.¹¹⁰ The reversible redox properties and highly coloured oxidation states exhibited by viologen systems have made them prime candidates for use in electrochromic devices. Indeed, in 1973, the Philips Laboratories¹¹¹ created an E.C display (ECD) based upon the heptyl viologen which exhibited extremely fast on/off response times (~ 10 -50 ms) and could be cycled over 100,000 times between its coloured redox states.

Whilst not a display device, the best-selling ECD is an automatic dimming rear view mirror used in many cars world-wide.¹¹² Illustrated in Figure 1.14, this device contains an ITO-glass

front surface (anode) and a reflective rear metallic surface (cathode). These two layers are separated by a sub-millimeter gap, and form the two electrodes of the cell. The space between the electrodes is filled with a solvent containing a substituted viologen which serves as the cathodic-coloring electrochromic material and 9,10-dimethylphenazine (DMP) serves as the anodically coloring species. When a voltage is applied, the viologen undergoes a one-electron reduction to form the colored radical cationic species and migrates to the cathode. At the same time, the neutral electrochromic material DMP is oxidised at the anode. Once the dual electrochromic coloration process has started, each product diffuses away from their respective electrodes and recombine in solution to regenerate the original colourless species. As a consequence of the continued recombination of the coloured species in solution, a continuous current is needed to maintain the dimming effect.

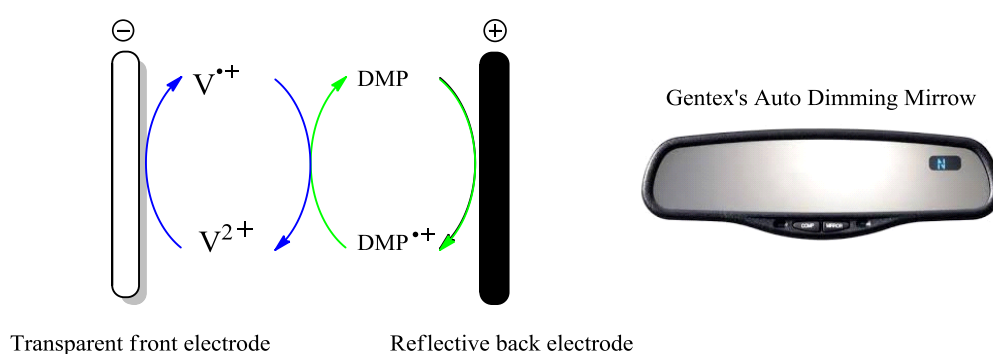
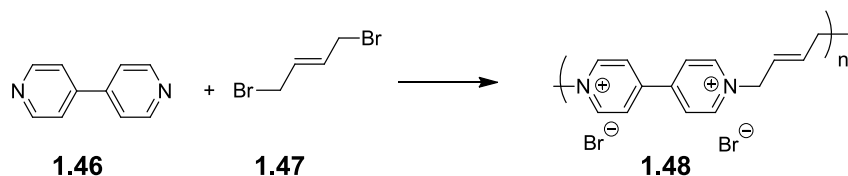


Figure. 1.14. Schematic representation of the redox cycles (left) occurring within the Gentex's NVS mirror (right).¹¹³

Polymers with viologen groups in the main chain or as pendant side groups have also been studied in electrochromic devices. Polymers may offer considerable advantages over the low molecular weight structures described above in that they have intrinsic strength and cannot diffuse away from the electrodes. Therefore, once the coloured redox state has been achieved, it is not necessary to maintain a constant current to retain the colour.¹¹⁴ This 'optical memory' could have significant advantages in designing low-power consumption mobile displays.

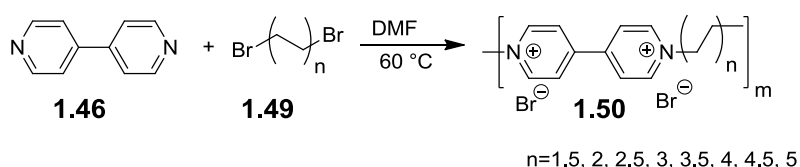
1.5.2. Polymeric viologen systems

The first known viologen containing polymer was reported by Heinsohn in 1971.¹¹⁵ The polymer was produced by addition of 4,4'-bipyridine to an equimolar amount of dibromobutene (the Menshutkin reaction, scheme 1.3).



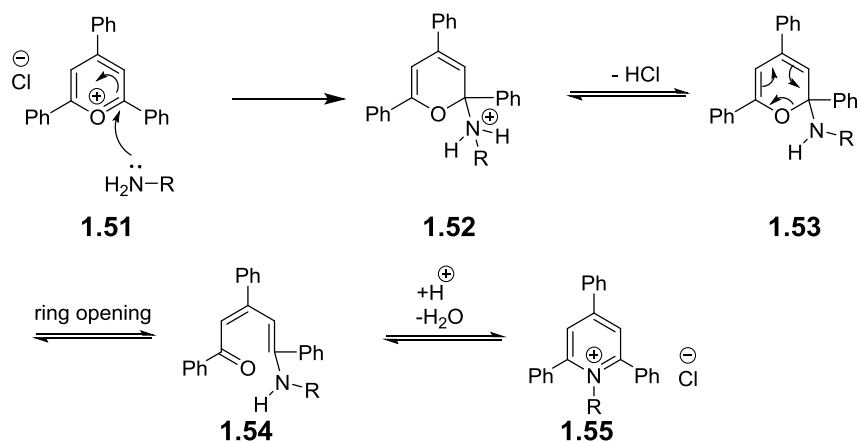
Scheme 1.3. Poly(viologen) synthesized by Heinsohn.¹¹⁵

Using a related method, Shimomura and co-workers¹¹⁶ have reported a series of poly(alkanediyl-viologen dibromide) by the addition of 4,4'-bipyridine to the corresponding dibromoalkane in DMF at 60 °C. (Scheme 1.4)



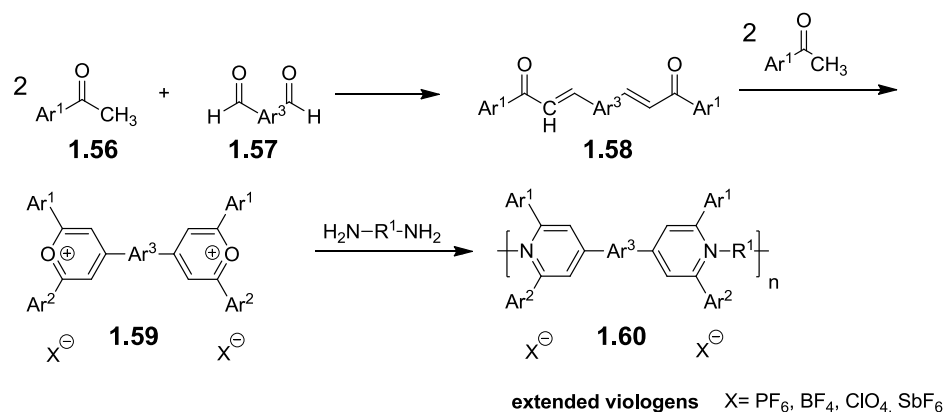
Scheme 1.4. The preparation of poly(alkanediyl-viologen dibromide).¹¹⁶

In each of the previous polymer syntheses (Schemes 1.3 and 1.4), the nitrogen on the pyridine ring acts as the nucleophile in the polymerization reaction. However, there have been several synthetic methodologies developed where the nitrogen that forms the pyridinium ring acts as the nucleophilic species during the reaction. This is exemplified in the reaction between pyrylium salts (e.g. **1.51**) and primary amines (Scheme 1.5). In this reaction, the pyrylium salt **1.51** can be converted to ketone **1.54** which slowly converts to the pyridinium cation **1.55** through loss of water.



Scheme 1.5. Mechanism of the synthesis of pyridinium salts from pyrylium salts and primary amines.¹¹⁷

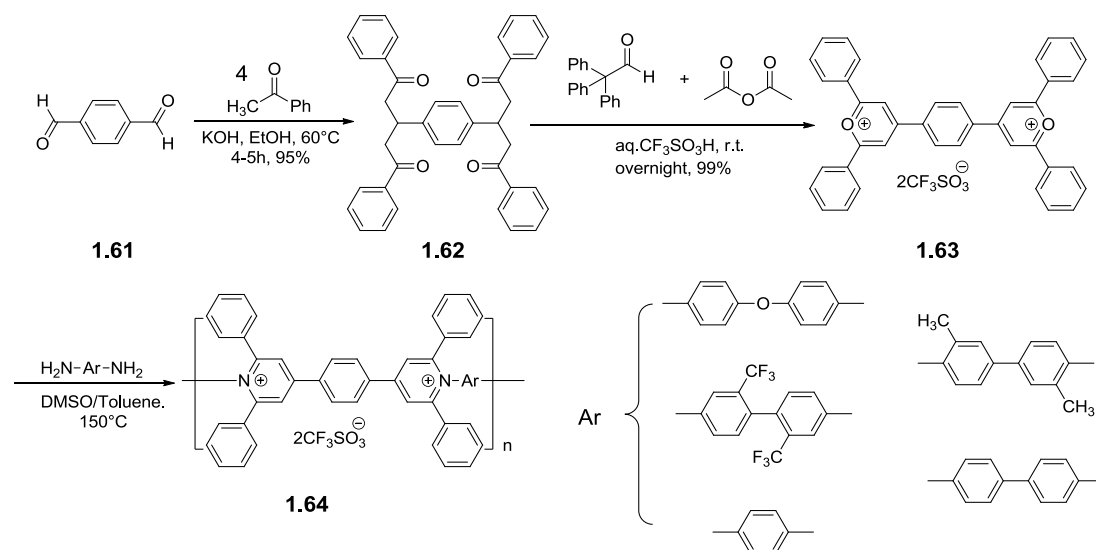
Conceptually, addition of diamines with a dipyrylium salt would produce an alternating co-polymer containing viologen salts. In practice, this reaction type has been shown to produce polymers containing ‘extended viologens’, in which the two pyridinium rings of a typical viologen are separated by at least one additional aromatic ring (**1.60**).



Scheme 1.6. Synthetic strategy of polypyridinium homopolymers.

Using this synthetic strategy, several groups have synthesized and studied polypyridinium species.^{118–121} One series of polymers based on the extended viologen units was reported by Harries in 1999.¹²² In this case, a novel monomer, *p*-bis[4-(2,6-diphenylpyrylium)]benzene ditriflate **1.63** was prepared by cyclisation of the tetraketone **1.62** with triphenylmethanol and fluoroboric acid. The tetraketone was obtained by treating terephthalaldehyde with 4

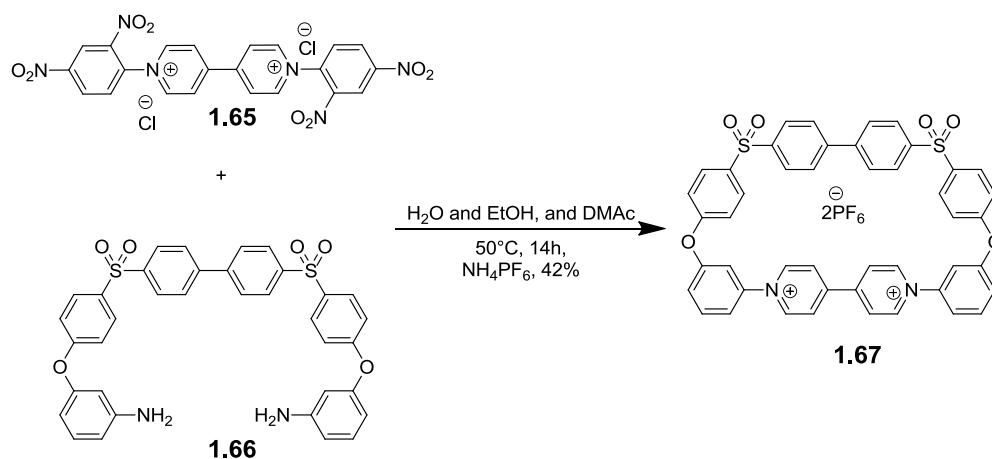
equivalents of acetophenone in the presence of base. This divalent pyrylium salt **1.63** was then used as a monomer in a condensation polymerisation by the reaction with a diamine (Scheme 1.7).



Scheme 1.7. Synthetic route to poly(pyridinium salts).¹²²

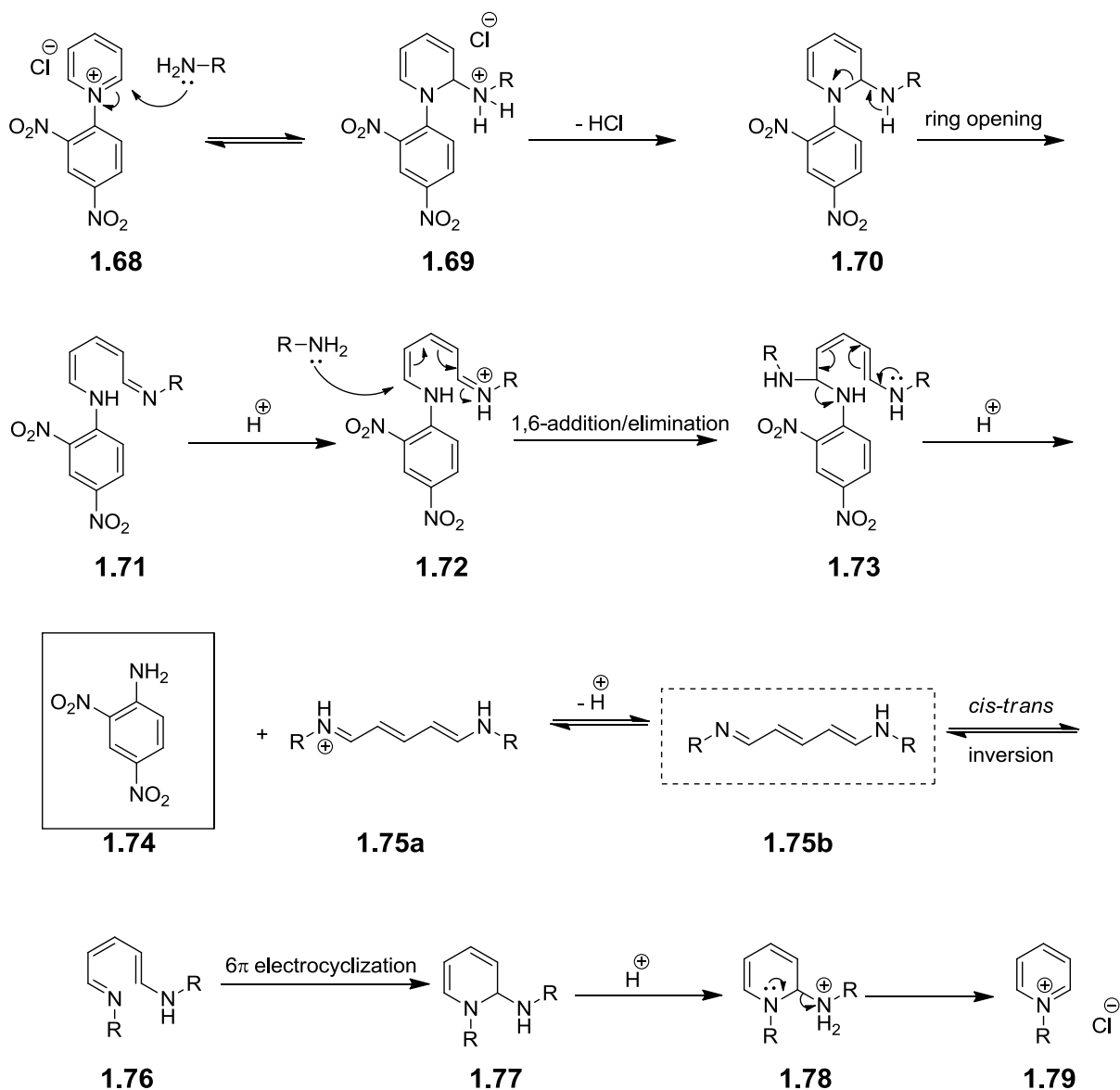
In the classic Menshutkin reaction (Scheme 1.3) the starting materials include the preformed pyridine ring. In contrast, the pyrylium reactions (Scheme 1.7) contains an activated monomer which undergoes nucleophilic attack by a nitrogen containing species. After loss of water, the pyridinium ion forms containing the nitrogen atom that originated in the nucleophilic species. In a related mechanism, it has long been established that substituted pyridinium containing species can be produced by the nucleophilic attack of an amine on pre-formed *N*-(2,4-dinitrophenyl) pyridinium salts. This class of reaction was first reported by Zincke in 1904,¹²³ and the *N*-(2,4-dinitrophenyl) pyridinium salts bear his name. The reaction can be considered as an amine exchange process that converts Zincke salts to another pyridinium species upon treatment with the appropriate aniline or alkyl amine. Although first reported well over 100 years ago, this versatile reaction is still undergoing extensive investigation to this day to improve the substrate scope and reaction yields.¹²⁴

A recent example of this reaction was reported by Greenland and Colquhoun *at al.*,¹²⁵ who used this reaction to produce a series of electron deficient viologen containing cyclophanes. In the selected example shown in the Scheme 1.8, macrocycle **1.67** was synthesised by treating the di(Zincke) salt **1.65** with aromatic diamine **1.66**.



Scheme 1.8. Synthesis of macrocycle **1.67**.

This unusual mechanism (Scheme 1.9) begins with nucleophilic attack of the primary amine on the *N*-2,4-dinitrophenyl-pyridinium salt **1.68**, leading to the opening of the pyridinium ring **1.71**. Then a second, intramolecular attack from the nitrogen atom expels 2,4-dinitroaniline **1.73** whilst simultaneously, the konig salt¹²⁶ (**1.75a** and **1.75b**) forms. Either of these salts (**1.75a** and **1.75b**) can be converted to the intermediate **1.76** with 6- π electrocyclization. Finally, the desired pyridinium ion will be formed after proton transfer and amine elimination.



Scheme 1.9. Mechanism of Zincke reaction.¹²⁷

As shown in Scheme 1.8, the use of aniline derivatives in this reaction results in products that contain a viologen in conjugation to an aromatic ring, however, this reaction has not yet been used to make polymers.

1.6. Conclusion

From the brief literature study present in this chapter it is clear that there is a pressing requirement to produce novel routes to n-type conducting polymers. The works by Swager^{95,96} and Harries¹²² have demonstrated that pyridinium containing polymers can be synthesized and used in opto-electronics applications. However, the paucity of reports in this area seems to indicate that there is much scope for improving the synthesis and properties of these materials. Building on the work reported by Stoddart, Colquhoun, Greenland *et al.*¹²⁵ (Scheme 1.8), this project will work towards the synthesis of novel, pyridinium-containing polymeric materials that contain all-aromatic, conjugated main chains.

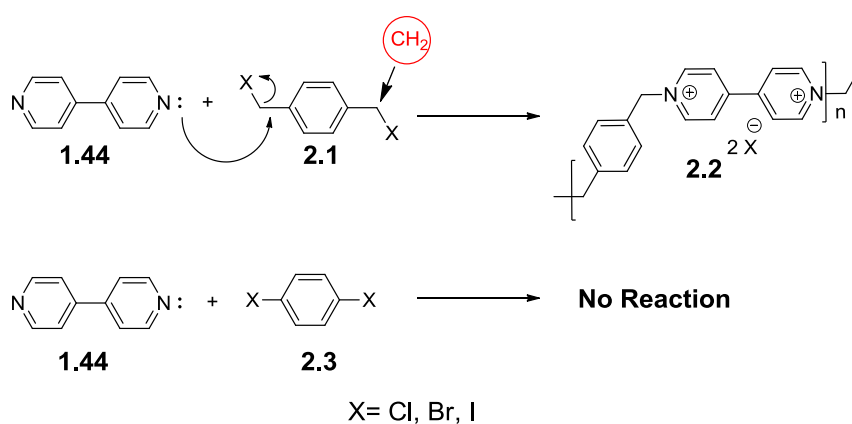
Chapter 2

Studies towards the synthesis of viologen containing polymers with fully conjugated main chains

2.1. Introduction and synthetic strategy

From the survey of the literature presented in chapter 1, it is clear that there is a pressing need to expand the range of electron accepting, n-type polymers for use in electronic devices such as OLEDs, PVCs and OTFTs. The work by Swager (Scheme 1.1) and Harries (Scheme 1.6) have demonstrated that pyridinium-containing fully conjugated polymers exhibit suitable electronic properties to form n-type materials which have been shown to have potential in photovoltaic devices.^{96,122}

It is interesting that the number of structural variants of these pyridinium containing polymers remains very low, suggesting that there is a large degree of molecular space to explore to optimise their properties. One of the reasons for this may be the complexity of their synthesis. The literature contains many examples of pyridinium containing polymers constructed using the Menshutkin reaction. Unfortunately, this method is unsuitable for the synthesis of polymers with fully aromatic mainchains as the mechanism requires an S_N2 type attack of the nitrogen in a pyridine ring on a methylene group α to a leaving group. This mechanism would not proceed if the reagent in the synthesis was an aryl or vinyl halide (Scheme 2.1).



Scheme 2.1. Top reaction: Menshutkin reaction of 4,4'-bipyridine 1.44 with halomethyl aromatic 2.1, lower reaction: Proposed attempted synthesis of conjugated polymer with 4,4'-bipyridine 1.44 and halide 2.3 which would not lead to product formation (X = Cl, Br or I).

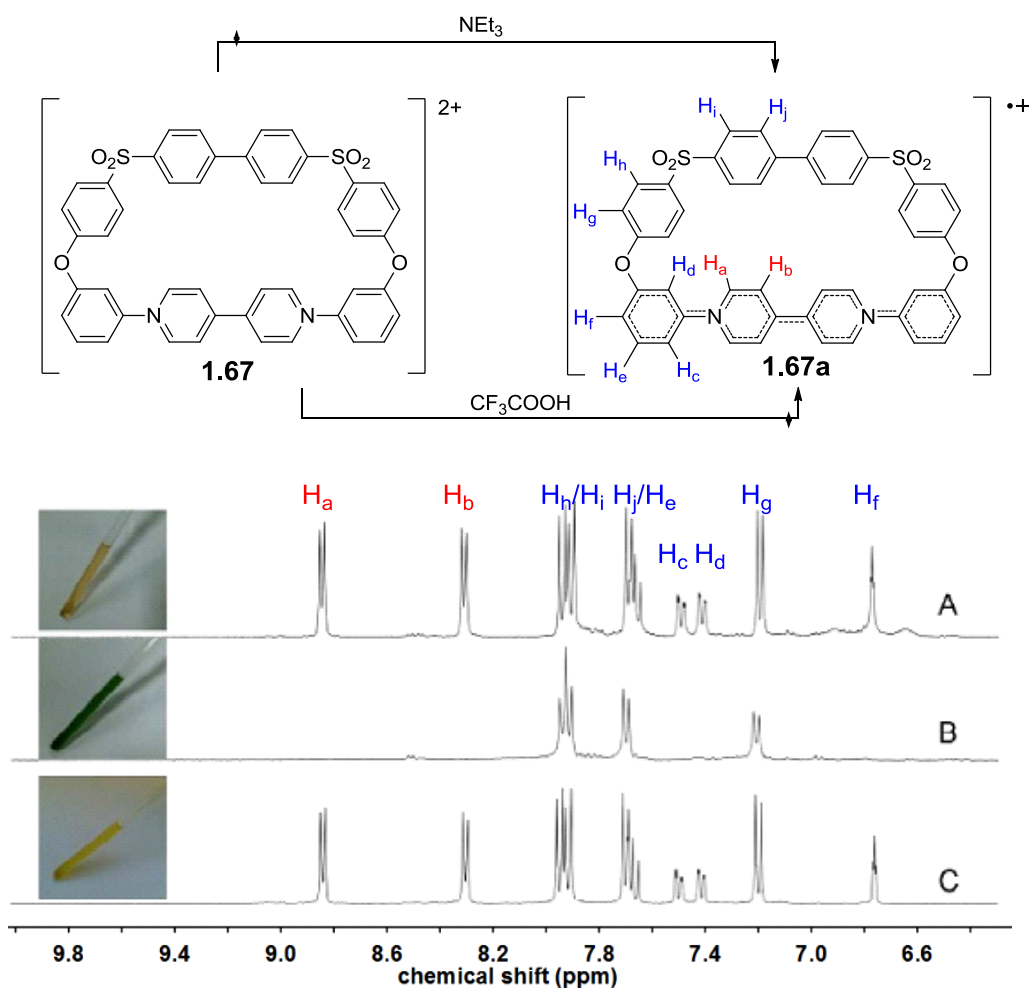
In the Swager synthesis of pyridinium containing polymers with fully conjugated mainchains, (Scheme 1.1) the key ring forming step is a late stage substitution reaction that occurs after the polymer is formed, and the total reaction scheme requires 8 steps. This methodology inherently not modular in nature and in order to produce a range of structural variants the entire synthetic route must be repeated.

In contrast to the Swager route, the Harries method, which starts from the pyriliium ion uses a more conventional A + B condensation co-polymerisation to produce the targeted pyridinium-based polymers (Scheme 1.6). This method allows the co-monomer to be varied and permits more rapid production of a structurally related family of materials to be synthesized and studied. However, the reaction still required the synthesis of the pyriliium monomer (**1.59**), which requires two steps.

There is an alternative methodology to create pyridinium-based systems that are directly connected to an aromatic residue through the use of the Zincke reaction, described in section **1.5.1** (Scheme 1.9). Based on this methodology, Stoddart, Greenland and Colquhoun have shown that it is possible to prepare viologen containing macrocycles from the reaction between Zincke salts and aromatic diamines.

In their work, it was found that the viologen-containing macrocycle **1.67** could undergo a one-electron reduction with various types of electron donors such as triethylamine (Scheme 2.2). The effect of this reduction could be seen in the ^1H NMR spectrum of the macrocycle and in the colour of the compound in solution. This is demonstrated in Scheme 2.2 (a) which shows the well-resolved ^1H -NMR spectrum and yellow colour of the starting macrocycle **1.67**. On addition of a small quantity of NEt_3 , the ^1H -NMR spectrum changes dramatically accompanied by a change in the colour of the solution to green (b). Addition of an electron to the viologen group generates a paramagnetic radical cation. Paramagnetic species typically exhibit extensive line broadening in their ^1H NMR spectra. In this instance the line

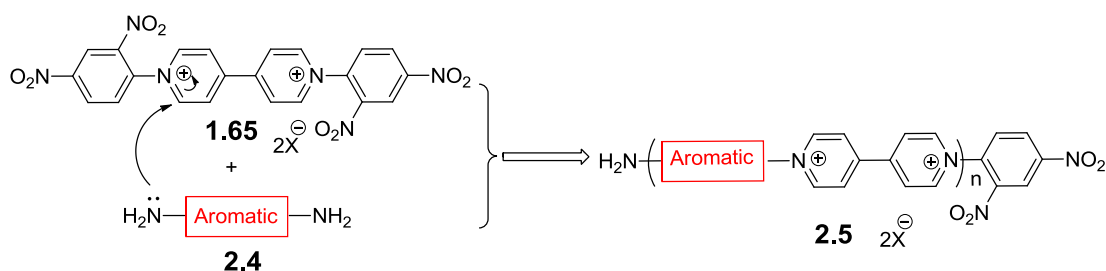
broadening occurs to such an extent that the proton signals for H_a to H_f are not observed. This shows that the single electron is delocalized over these 4 aromatic rings. However, the signals for H_g to H_j are still visible showing that the singlet electron is not able to delocalize over these rings, presumably as a consequence of the break in conjugation caused by the ether linkage. Addition of trifluoroacetic acid (TFA) essentially regenerates the ¹H-NMR spectrum of the starting material with the loss of green colour.



Scheme 2.2. ¹H NMR spectra (298 K) of (A) macrocycle **1.67** alone (3.8 mM in CD₃CN), (B) after addition of triethylamine (10 equiv), and (C) solution (B) after adding excess trifluoroacetic acid.¹²⁵

Using this work¹²⁵ as a starting point, it is clear that removing the break in conjugation caused by the ether linkages in macrocycle **1.67** (Scheme 2.2), would produce systems whereby delocalization was possible over a larger number of aromatic rings and ultimately along an

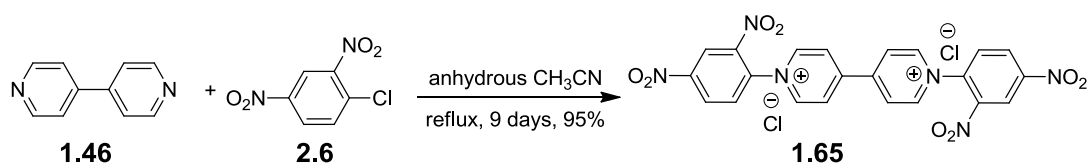
entire polymer backbone. In general, we proposed that the π -conjugated bipyridinium containing polymers could be synthesized by condensation of aromatic diamine **2.4** with Zincke salt **1.65**. (Scheme 2.3). The following sections show our initial efforts towards using the Zincke reaction to produce these fully conjugated polymers.



Scheme 2.3. approach to the synthesis of polymer (2.5) by the Zincke reaction.

2.2. Results and Discussion

Prior to commencing complex synthetic work it was necessary to produce the key intermediate and well-known di-Zincke salt **1.65**.¹⁰⁸ This was achieved by treating the commercially available reagent 4,4'-bipyridine **1.46** with 1-chloro-2,4-dinitrobenzene **2.6** in anhydrous acetonitrile. After 9 days, the Zincke salt **1.65** was collected by filtration from the reaction mixture and washed with absolute ethanol, dried *in vacuo* to afford a 95% yield of product as a pale grey powder, which can be readily prepared on a multigram scale.



Scheme 2.4. Synthesis of Zincke salt **1.65**.¹²⁸

The $^1\text{H-NMR}$ spectrum (Figure 2.1) of this material showed some coincidence of signals. Both the doublet at 9.40 ppm corresponding to proton H_b between the nitro groups on the

2,4-dinitrophenyl ring and the signal at 9.50 ppm indicative of the protons adjacent to the ammonium ions demonstrated the formation of Zincke salt **1.65**. The $^1\text{H-NMR}$ spectrum of the unpurified material showed it to be over 98% pure and it could therefore be used without further purification in the next reaction. A small quantity was purified *via* low temperature crystallization from acetonitrile with a drop of water to give yellow crystalline needles that exhibited a M.p. of 243-245 °C (Lit 250 °C).¹²⁸

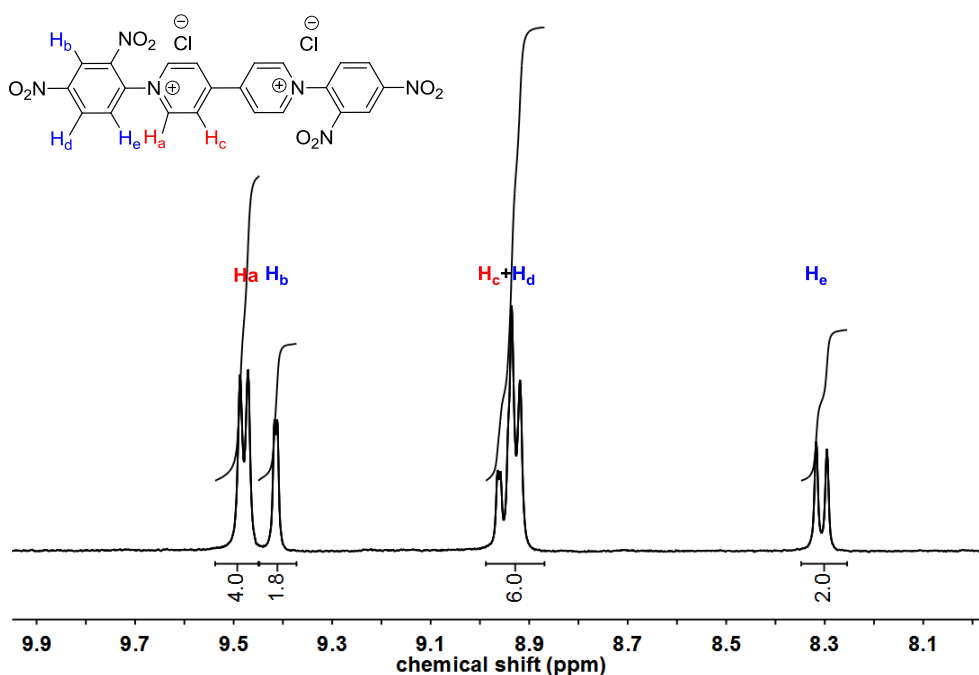
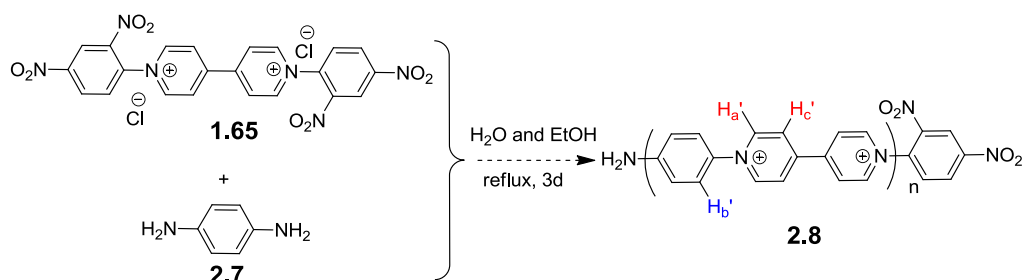


Figure 2.1. $^1\text{H-NMR}$ spectrum of Zincke salt **1.65**.

It was found that the structurally simplest and cheapest aromatic diamine that satisfies the criteria outlined in scheme 2.3 is benzene-1,4-diamine (**2.7**). Therefore, initial efforts to form conjugated polymers via the Zincke reaction were focused on the reaction of equimolar equivalents of di(Zincke) salt (**1.65**) and diamine (**2.7**) (Scheme 2.5) which yielded a black powder after work-up.



Scheme 2.5. Attempted to synthesis of polymer **2.8**.

Successful synthesis of high molecular weight polymer **2.8** would result in the formation of a highly symmetrical macromolecule with a very simple $^1\text{H-NMR}$ spectrum: in particular, the $^1\text{H-NMR}$ spectrum should be essentially three doublets (H_a' , H_b' and H_c' , see **2.8** in Scheme 2.5). However, the $^1\text{H-NMR}$ spectrum of the product, obtained (Figure 2.2) was very complex with multiple signals. From this evidence, it seemed likely that the targeted high molecular weight material had not been produced.

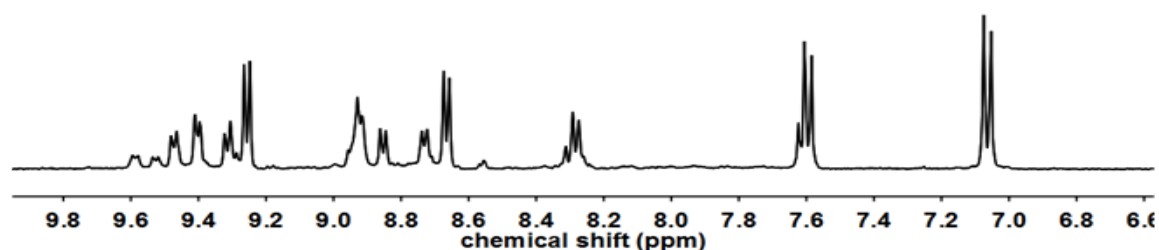


Figure 2.2. $^1\text{H-NMR}$ (D_2O , fully soluble) spectrum of the attempted synthesis of **2.8**.

It may be speculated that the attempted polymerization reaction did not go to completion. Therefore the isolated product would be a mixture of multiple small molecules such as those shown in Figure 2.3, From inspection of the structure for **2.9** it is clear that the protons on the terminal aromatic amine (H_h and H_j) are not chemically equivalent and may be expected to appear as doublets like those observed in the recorded spectrum (Figure 2.2).

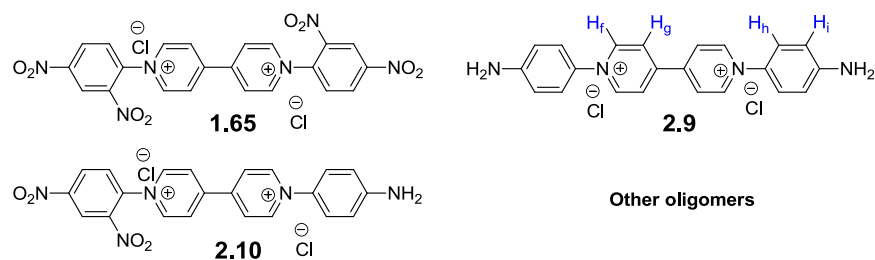
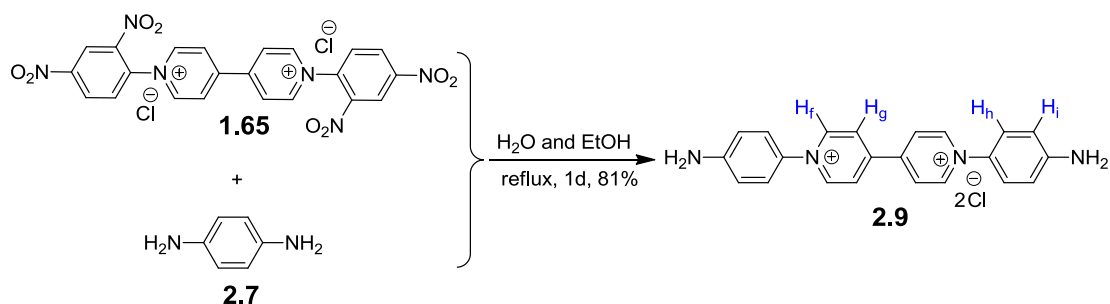


Figure 2.3. Examples of proposed small molecules produced during the attempted synthesis of polymer 2.8.

2.2.1. Verification of the structures of the products from initial polymerization reactions.¹²⁹

In order to test our hypothesis of incomplete reaction leading to multiple small molecules being produced during our initial polymerization reactions, it was decided to synthesize the simple and potentially useful diamine **2.9**. This would allow us to compare its spectrum with the complex spectra produced during the attempted synthesis of polymer **2.8**. Aromatic diamine **2.9** was synthesised by the procedure reported by Monk and Hodgkinson¹²⁹ in 1999. This synthesis was accomplished by heating the Zincke salt **1.65** to reflux with 6 equivalents of benzene-1,4-diamine **2.7** in a mixture of ethanol and water (v/v 1:2) for 24h which produced symmetrical diamine **2.9** as a black powder in 81% yield. (Scheme 2.6)



Scheme 2.6. Synthesis of 2.9

Comparison of the spectra of symmetrical diamine (**2.9**) and Zincke salt (**1.65**) with the

previous ^1H -NMR spectrum obtained from the failed polymerization reaction (Figure 2.2) showed that the polymerization product mixture contained at least **1.65** and **2.9**. The two doublet resonances at 9.26 ppm and 8.67 ppm shown in Figure 2.2 are in good agreement with the signals exhibited by diamine **2.9** in Figure 2.4. In addition, two doublet resonance peaks at 9.40 and 9.47 ppm in the spectrum of the attempted polymer synthesis correspond to the starting material, Zincke salt **1.65**. (Figure 2.4)

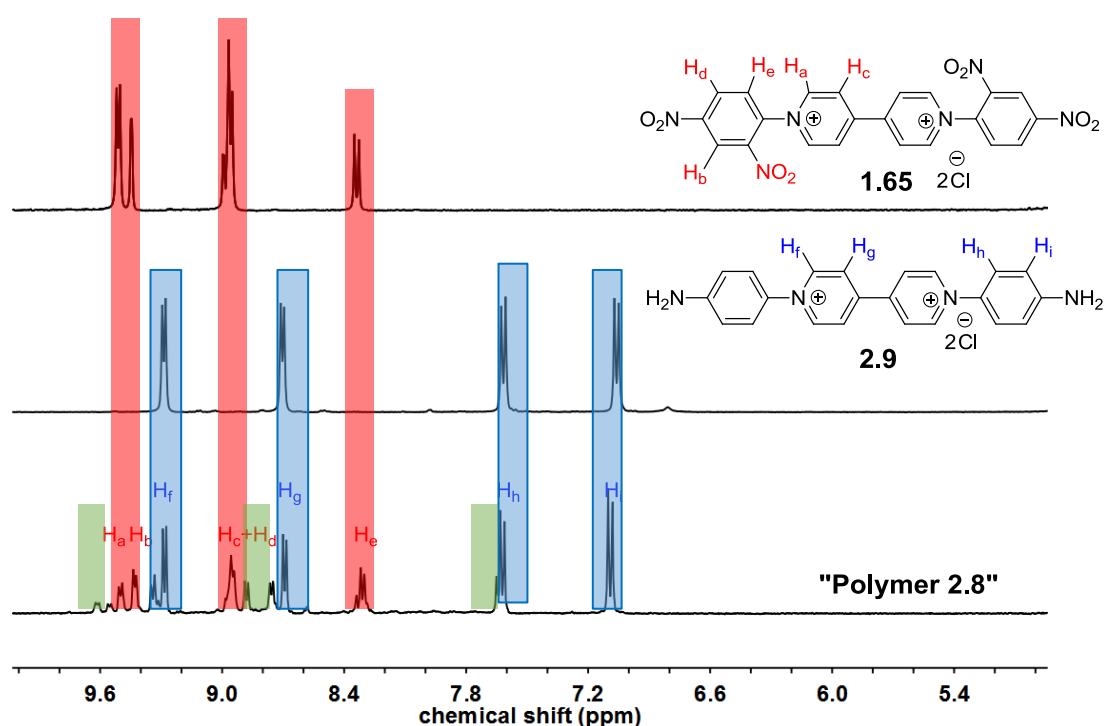


Figure 2.4. ^1H NMR stack of "polymer 2.8" with diamine **2.9** and Zincke salt **1.65**.

The identification of these two compounds (**1.65** ~ 31% and **2.9** ~ 43% of the total integral) in the spectrum of the attempted polymerization is important. It demonstrates that whilst **2.9** contains two free aniline functionalities these potentially nucleophilic species did not go on to react with the remaining Zincke salt **1.65**, even over the extended time periods used during the polymerization (3 days). This observation suggests the addition of one pyridinium unit to aromatic diamine reduces the nucleophilicity of the second NH_2 residue so that polymerization cannot proceed (Figure 2.5).

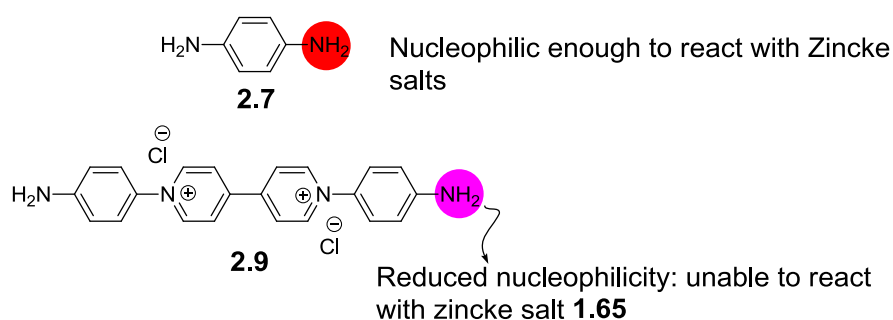
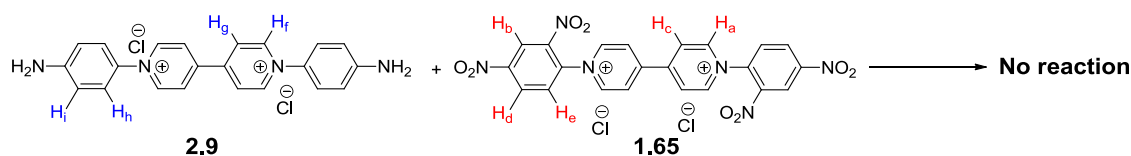


Figure 2.5. Comparison of nucleophilicity of 2.7 and 2.19.

This result would have significant impact on the design of our polymerization monomers so attempts were made to verify this conclusion experimentally. Indeed, very recent work by Zeghib and Thelliere¹²⁴ in 2016 has investigated the use of microwave assisted synthesis to increase the reaction rates of poorly nucleophilic amine residues in the Zincke reaction.

2.2.2. Investigations into the change in nucleophilicity of the amine residues in dianiline **2.9** during polymerization.

To investigate the potentially problematic reduction in nucleophilicity of amine residues in viologen containing diamine **2.9**, a control experiment was conducted whereby Zincke salt **1.65** was treated with 3 equivalents of diamine **2.9** for 2 days (ethanol, at reflux). Analysis of the ¹H-NMR spectrum of this reaction (Figure 2.6) showed that no reaction had occurred, conclusively demonstrating that addition of Zincke salts to aromatic diamines can completely inhibit the nucleophilic nature of the remaining amine residue under these conditions.



Scheme 2.7. Second exploratory experiment.

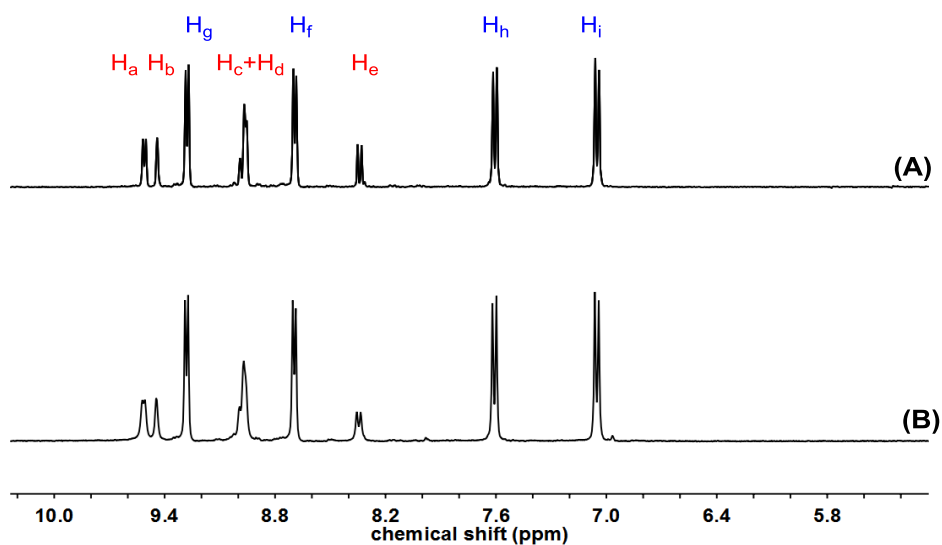
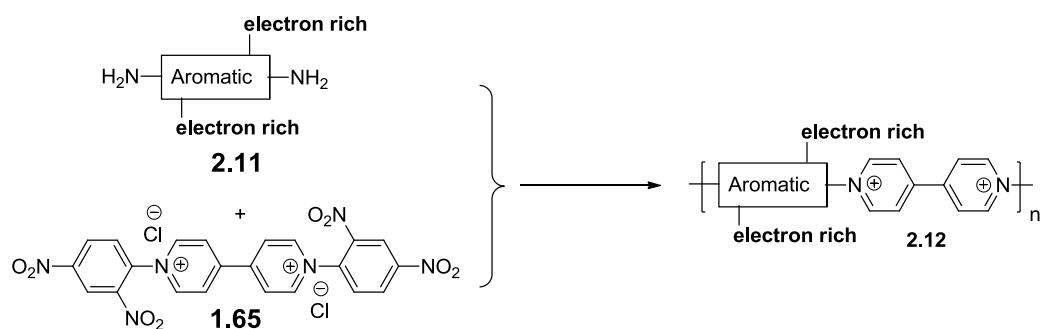


Figure 2.6. ^1H -NMR spectra of the reaction between Zincke salt **1.65** and diamine **2.9** at time = 3 min (A) to time = 48 h (B).

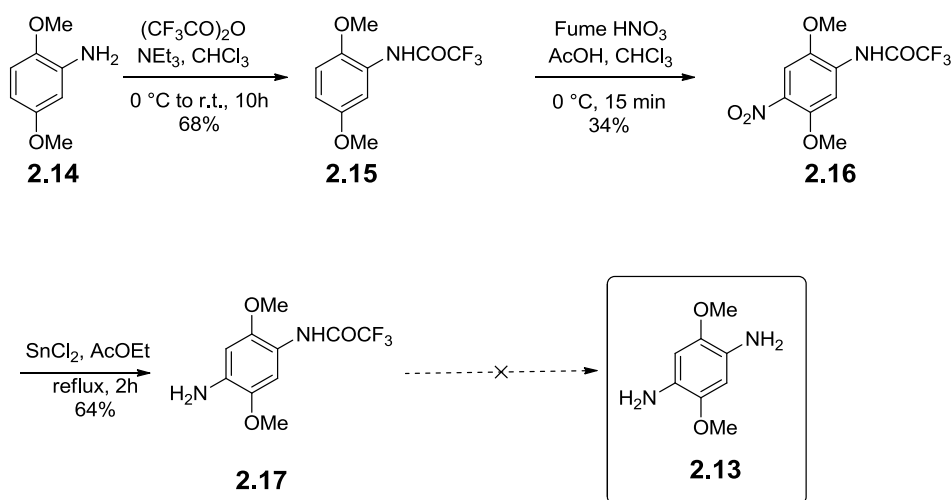
From the results of the previous two exploratory experiments concerning the change in reactivity of the amine residues in aromatic diamines, it was decided to investigate the potential of using a more electron rich aromatic diamine which it was hoped, would not suffer such a dramatic loss of reactivity during polymerization reactions.



Scheme 2.8. Schematic of the proposed structure of the 2nd generation of monomer **2.11** to be used to produce conjugated pyridinium containing polymers

2.2.3. 2,5-Dimethoxybenzene-1,4-diamine **2.13**.¹³⁰

A literature search revealed a seemingly straightforward synthesis of a dimethoxy substituted aromatic diamine (**2.13**, scheme 2.9) which would be expected to deliver an electron rich species suitable for polymerization. Thus, 2,5-dimethoxybenzene-1,4-diamine **2.13** was targeted for the next iteration of our synthesis of conjugated polymers. The synthetic strategy towards **2.13** is illustrated in Scheme 2.9.



Scheme 2.9. The route to synthesis of 2,5-dimethoxybenzene-1,4-diamine **2.13**.

This literature procedure started from commercially available dimethoxy aniline **2.14** which was protected as the trifluoroacetamide under standard conditions. Introduction of the nitro group (**2.16**) was somewhat hindered by a propensity of the aromatic ring to over-nitrate. In order to avoid this, the temperature was strictly maintained at $0\text{ }^\circ\text{C}$ for 15 min resulting in **2.16** with a low but acceptable yield of 34%. Reduction of the nitro group in **2.16** to the amine **2.17** proceeded well (64%) leaving the protecting group in place, which should be removed by treatment with NaBH_4 to deliver our target intermediate **2.17**. However, the deep purple product from the deprotection reaction did not have signals in its ^1H NMR spectrum that exhibited either the relative integral or splitting pattern consistent with the formation of **2.13**. On further reading, it appears that alkoxy substituted dianilines are unstable to oxidation even by air,¹³⁰ presumably decomposing to quinone type moieties (Figure 2.7) which are known to

be deep purple/black in colour.¹³¹

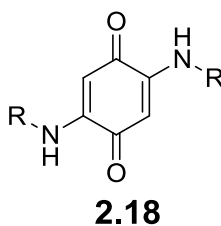


Figure 2.7. The structure of the proposed decomposition product from the deprotection of 2.17 quinone type moiety.

2.3. Conclusion and Future work

In this chapter, initial synthetic studies towards the synthesis of viologen containing polymers with fully conjugated main chains are reported. We describe an optimised multi-gram scale synthesis of the di-Zincke salt **1.65** which will be of key importance to this project. Investigations into the suitability of simple aromatic diamines such as benzene-1,4-diamine (**2.7**) to act as a co-monomer in the synthesis of the desired polymers were met with failure. This was demonstrated to be as a consequence of the initial addition of one of the amine groups on **2.7** to the Zincke salt resulting in a reduction of the nucleophilicity of the remaining amine residue which completely stopped the polymerization reaction. To overcome this limitation, diamine **2.13** which contained the electron rich methoxy substituents on the aromatic ring was investigated as a potential new co-monomer. Unfortunately, the synthesis of **2.13** proved to be non-trivial resulting in unstable products. Therefore it was decided to focus efforts on investigating the use of commercially available electron rich aromatic diamines as suitable co-monomers in the polymerization reaction. Moving away from unstable, non-commercial diamine residues as a starting material would greatly reduce the synthetic effort required to produce the targeted polymers.

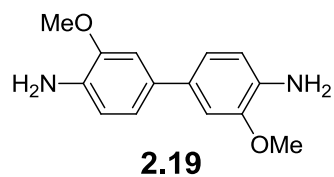


Figure 2.8. Structure of one of the commercially available aromatic diamines (**2.19**) with electron donating groups.

The following chapter details the use of diaromatic diamine **2.19** with Zincke salt **1.65** to produce a series of conjugated viologen containing oligomers (unimer **3.1**, dimer **3.2** and trimer **3.3**).

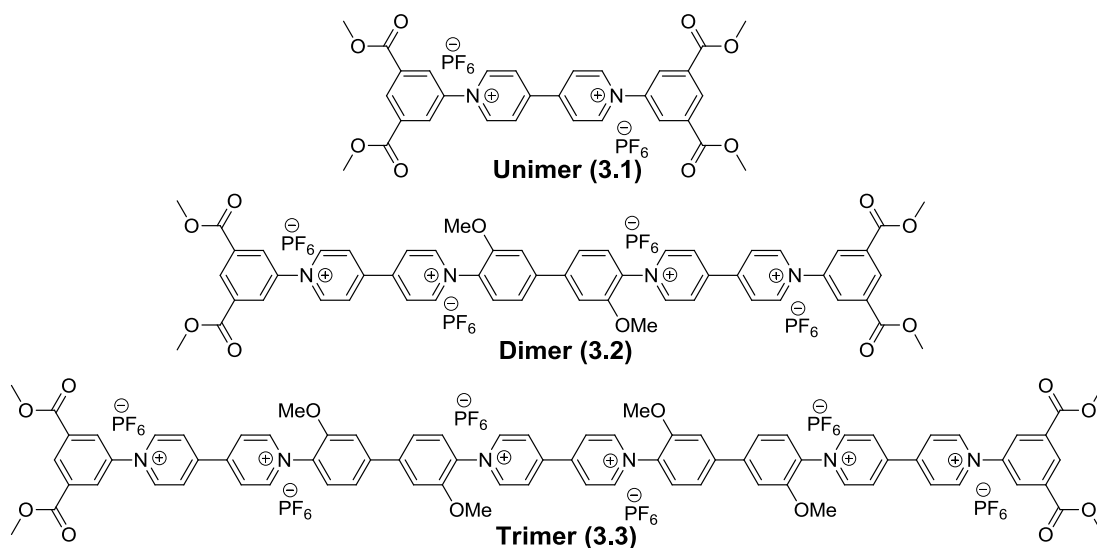


Figure 2.9. Synthetic targets of unimer **3.1**, dimer **3.2** and trimer **3.3**.

Chapter 3

Efficient access to conjugated bipyridinium oligomers using the Zincke reaction: Synthesis, spectroscopic and electrochemical properties.

This chapter is based on the following published work: (Chen, L.; Willcock, H.; Wedge, C. J.; Hartl, F.; Colquhoun, H. M.; Greenland, B. W. *Org. Biomol. Chem.* 2016, 14, 980.¹³²). I synthesised all the molecules presented in this chapter and obtained and analysed all the characterisation data except the electron paramagnetic resonance (EPR) spectra. The EPR spectra were kindly measured and analysed by Dr. Helen Wilcock (Loughborough) and Dr. Chris Wedge (Warwick).

3.1. Introduction

Bipyridinium residues are amongst the most intensively studied building blocks in supramolecular chemistry.^{91,133,134} They have found widespread application in molecular systems that exhibit controlled switching,^{135–139} rotational motion^{140–142} and potential for data storage.^{143–146} Many of these complex nanosystems harness the controllable electrochemical properties of 4,4'-bipyridinium ions ("viologens") in either their synthesis or application.¹⁴⁷ The reversible one- and two-electron reduction of 4,4'-bipyridinium derivatives are accompanied by a dramatic change in the UV-vis absorption spectra of the materials, an effect which has been widely studied in the context of electrochromic devices.^{135,148–150} The colour of cationic bipyridinium residues is highly dependent on the electronic ground state energy of the molecule, which can be finely tuned by varying the substituents (Table 1.1).^{108,109,151–153}

There have been a number of studies concerning the synthesis of oligomers and polymeric materials containing 4,4'-bipyridine units in the backbone. Typically, the electroactive 4,4'-bipyridinium groups are separated by at least one methylene residue.^{154–157} This structural arrangement precludes electronic communication between the bipyridine groups.¹⁵⁸ In addition, there have been several reports of the synthesis of so-called "*extended viologens*", whereby two pyridinium residues are separated by increasing numbers of aromatic rings (Figure 3.1).^{118,159–168} These have rapidly found widespread application in the construction of supramolecular complexes.^{169–174}

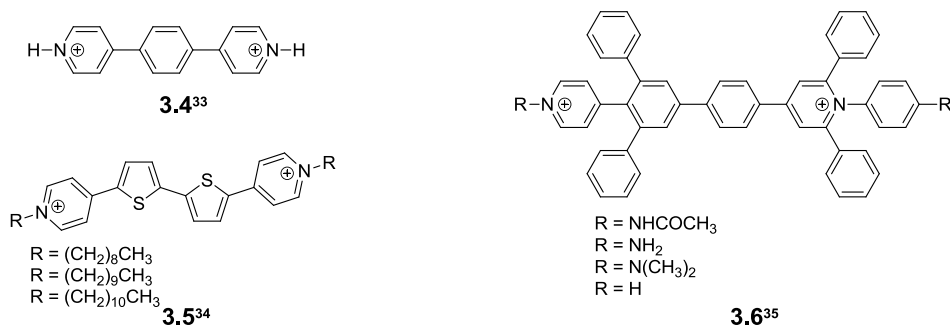
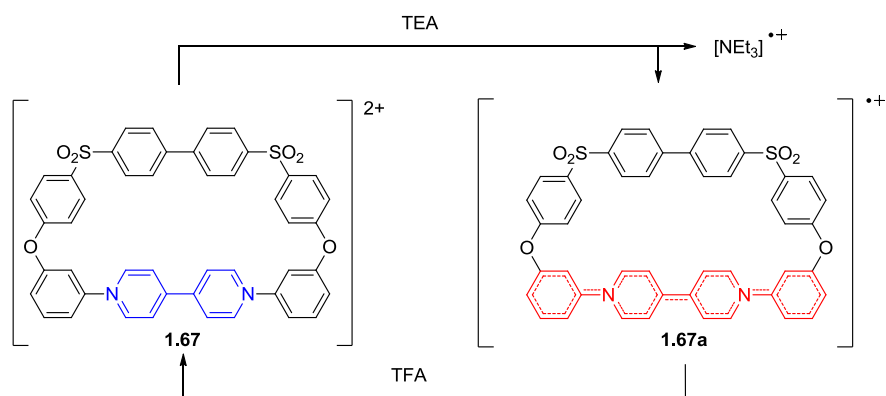


Figure 3.1. Examples of "extended viologens": 3.4) *p*-phenylene extended Viologen,¹⁶¹ 3.5), 4'-(2,20-bithiophene-5,5'-diyl)bis(1-decylpyridinium)²⁺,¹⁶² 3.6) *p*-phenylene-bis-4,4'-(1-aryl-2,6-diphenylpyridinium).¹¹⁸

There are also examples of (di)phenyl viologen structures in which the conjugation length has been extended by the addition of an aromatic residue to the *N*-termini of the viologen (Scheme 1.2, Table 1.1). Small molecules containing 4,4'- or 3,3'-bipyridinium units,^{95,96,121,158,165,175–180} and polymers¹⁸¹ with 3,3'-bipyridine residues have been shown to exhibit interesting conductivity properties in the solid state. (Figure 1.11)

Previous work from the Colquhoun/Greenland team in this area has concentrated on the synthesis of 4,4'-bipyridinium-containing macrocycles such as (**1.67**) (Scheme 3.1). A family of related compounds was synthesised by exploiting the Zincke reaction, in which the condensation of nucleophilic amines with *N*-(2,4-dinitrophenyl)pyridinium salts resulted in efficient access to *N*-substituted pyridinium residues.¹²⁵ These macrocycles underwent one-electron reduction both chemically [e.g. by triethylamine (TEA)] and electrochemically, to yield the corresponding radical cations (**1.67a**).¹²⁵ The unpaired spin density was found to be delocalized over four aromatic/heterocyclic rings, but was prevented from more extensive delocalization by the break in conjugation as a consequence of the ether linkages in these macrocyclic systems.



Scheme 3.1. Reduction of dicationic macrocycle (1.67) to the radical mono-cation (1.67a) in which the unpaired electron is delocalized over the four aromatic rings highlighted in red.

In this chapter, I report the syntheses and spectroelectrochemical analysis of a series of redox-active oligomers containing progressively increasing numbers of 4,4'-bipyridinium units, culminating in the synthesis of a hexa-cationic trimer containing twelve aromatic/heterocyclic residues.

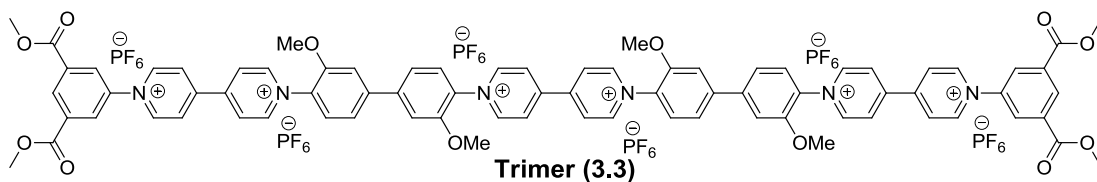
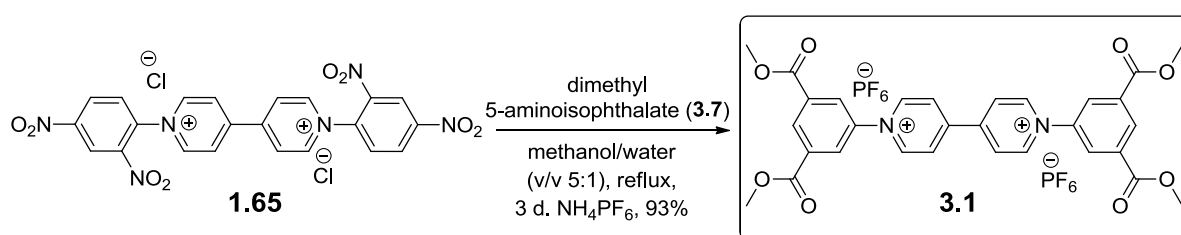


Figure 3.2. Structure of hexa-cationic trimer 3.3.

3.2. Results and Discussion

3.2.1. Synthesis

The synthetic route to the targeted oligomers started from Zincke salt **1.65**, which can be readily prepared on a multigram scale as described previously (Scheme 2.4).¹⁸² As an example of the efficiency of the Zincke reaction, the reaction of Zincke salt **1.65** with dimethyl 5-aminoisophthalate **3.7** afforded unimer **3.1** in 93% (isolated) yield.



Scheme 3.2. Synthesis of conjugated unimer **3.1**.

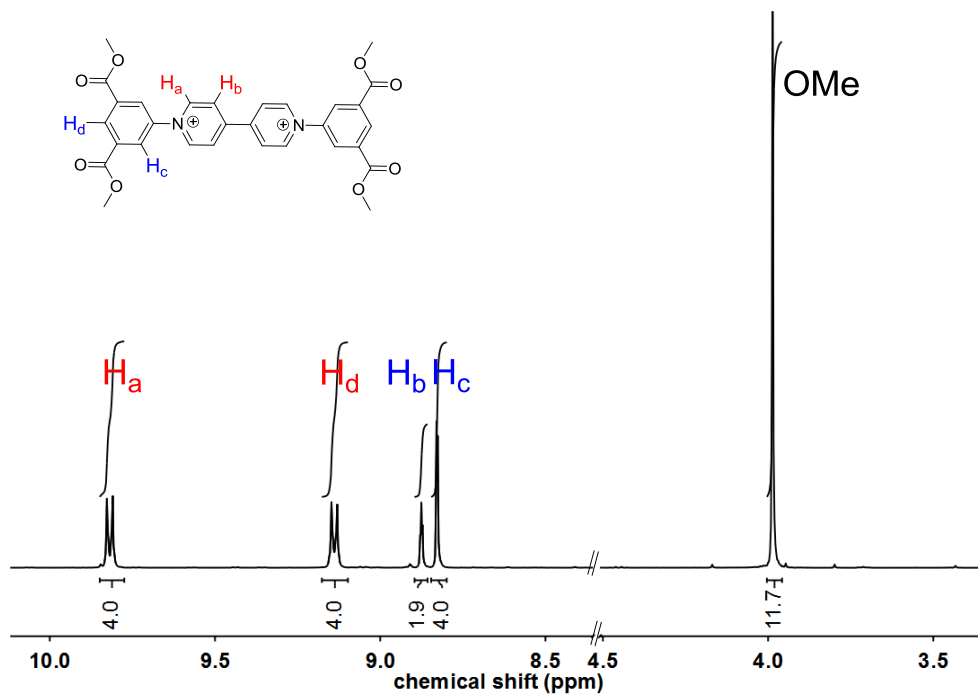
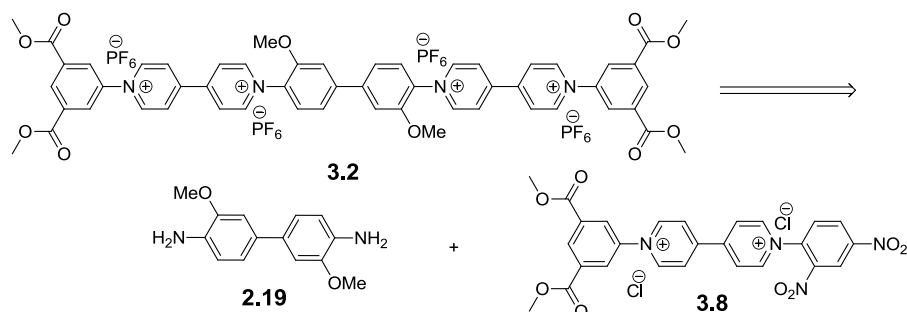


Figure 3.3. $^1\text{H-NMR}$ spectra of compound **3.1** (in acetone- d_6 containing 1% of TFA).

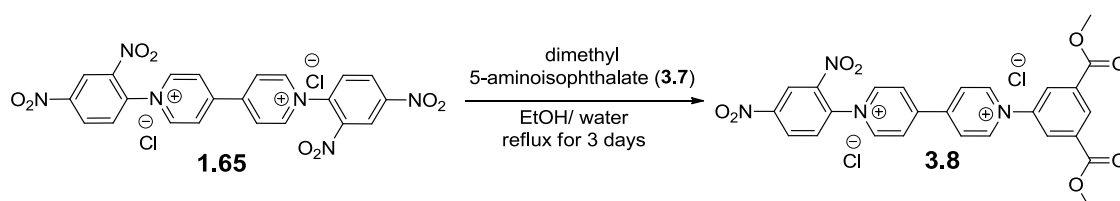
In comparison with the $^1\text{H-NMR}$ spectrum of Zincke salt **1.65**, the spectrum of **3.1** (Figure 3.3) lacks the doublet resonance peaks at 8.30 ppm corresponding to the 2,4-dinitrophenyl group (Figure 2.1) and contains the diagnostic singlet peak at 4.02 ppm of the methoxy groups. In addition, the ^{13}C NMR spectrum of **3.1** shows a resonance at 166 ppm corresponding to the sp^2 hybridised carbon in the ester groups.

Having prepared the unimer **3.1**, the next objective was the synthesis of the dimer **3.2**. It was envisaged that this could be produced by the addition of mono-Zincke salt **3.8** to diamine **2.19** as shown retrosynthetically in Scheme 3.3.



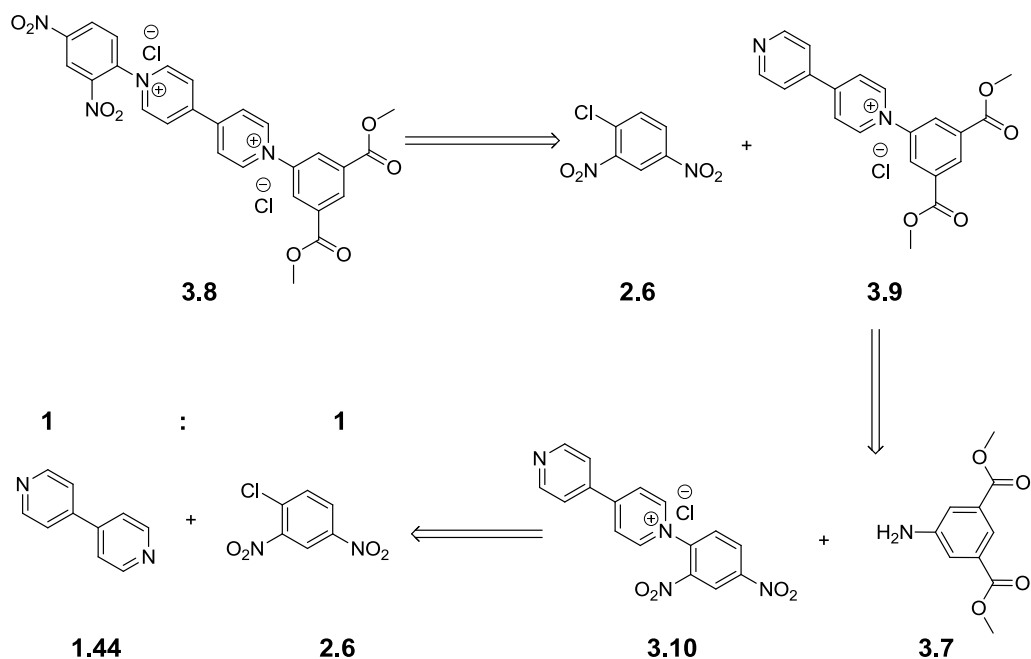
Scheme 3.3. Retrosynthetic approach to dimer **3.2**.

In the forwards synthetic direction, the first step towards the formation of dimer **3.2** consisted of the formation of intermediate **3.8** (Scheme 3.4). The initial attempts to produce this compound (**3.8**) by treatment of Zincke salt **1.65** with dimethyl 5-aminoisophthalate **3.7** in a 1:1 ratio produced poor results. Even after extensive purification by column chromatography and several recrystallizations, precursor **3.8** was obtained in a yield of only 3%. However, the $^1\text{H-NMR}$ of the crude reaction mix suggested very good conversion to the desired product and therefore it appears that the poor yield was in a consequence of inefficient purification.



Scheme 3.4. One step of the synthesis of precursor **3.8**.

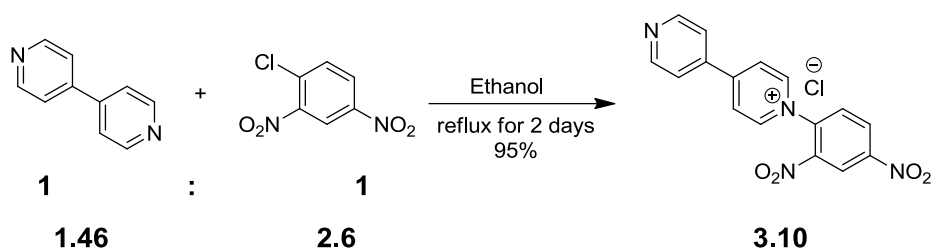
Due to the significant drawbacks of this ‘one pot’ route to **3.8** (Scheme 3.4), efforts focused on attempting to find a higher yielding synthesis. In 2006, Harries, Helliwell *et al.*,¹⁸³ reported the efficient synthesis (82%) of **3.10** (Scheme 3.5) by treatment of 4,4'-bipyridine with one equivalent of 1-chloro-2,4-dinitrobenzene. Inspired by this reaction, a new synthetic strategy was developed which is outlined in Scheme 3.5.



Scheme 3.5. A second generation retrosynthetic approach to precursor **3.9**.

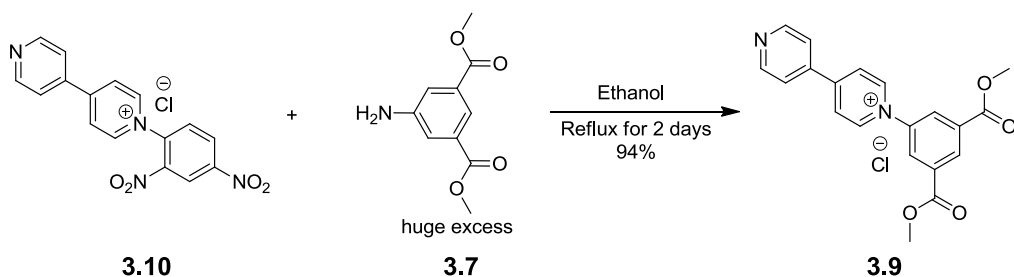
In the forward reaction scheme we planned to use the high yielding Harries¹⁸³ synthesis to make the mono-substituted bipyridinium salt **3.10**. Subsequent addition of 2.5 equivalents of dimethyl 5-aminoisophthalate would furnish **3.9** prior to addition of a single dinitrophenyl group to give the target compound **3.8**. Whilst clearly a more lengthy synthesis than attempted previously (Scheme 3.4), it was hoped that the intermediates would prove to be more readily purified and therefore produce a higher overall yield of **3.8**.

Reaction of equimolar equivalents of 4,4'-bipyridine and 1-chloro-2,4-dinitrobenzene successfully give the pyridinium salt **3.10** in an excellent yield of 95% (Scheme 3.6).



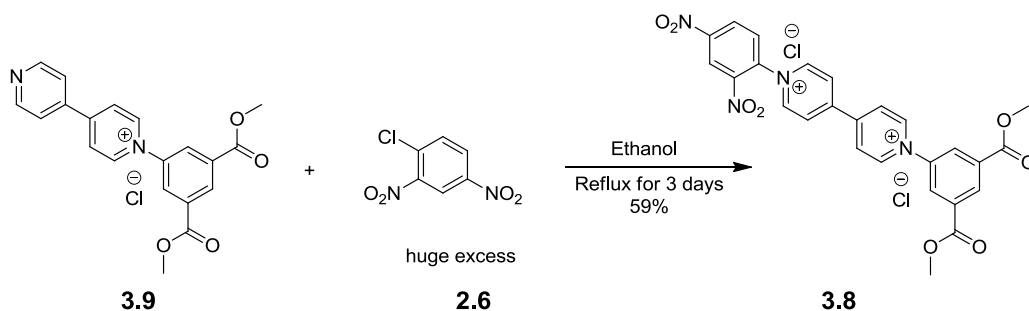
Scheme 3.6. Synthesis of mono-substituted Zincke salt **3.10**.

After the successful synthesis of compound **3.10**, our strategy required the substitution of the 2,4-dinitrophenyl leaving group with the dimethyl 5-aminoisophthalate **3.7** stopper group. The diester **3.9** was obtained by reaction of compound **3.10** with a 14-fold excess of aromatic amine **3.7** using the conditions developed previously (Scheme 3.2). After recrystallization from water to THF, a light yellow powder was isolated in a very good yield of 94%.



Scheme 3.7. Synthesis of diester **3.9** from **3.10**.

Subsequently, the mono Zincke salt, precursor **3.8**, was produced through addition of 10 equivalents of 1-chloro-2,4-dinitrobenzene to **3.9** under reflux in ethanol for 3 days at very high concentration (1.42 g/mL, Scheme 3.8). After cooling to room temperature, the precipitate was filtered and washed with 100 mL of THF to give the unsymmetrical target compound **3.8** in 59% yield and excellent purity (> 99% by ^1H NMR).



Scheme 3.8. Synthesis of precursor **3.8**.

The success of this reaction was verified from analysis of the $^1\text{H-NMR}$ and COSY spectra. Figure 3.4 shows the double doublet at 8.86 ppm that correspond to proton H_c between the nitro groups on the newly installed 2,4-dinitrophenyl group. In addition, the integral ratio between this double doublet (8.86 ppm) and the singlet for the methoxy group at 3.93 ppm was 1:6, which confirmed the successful synthesis of the precursor.

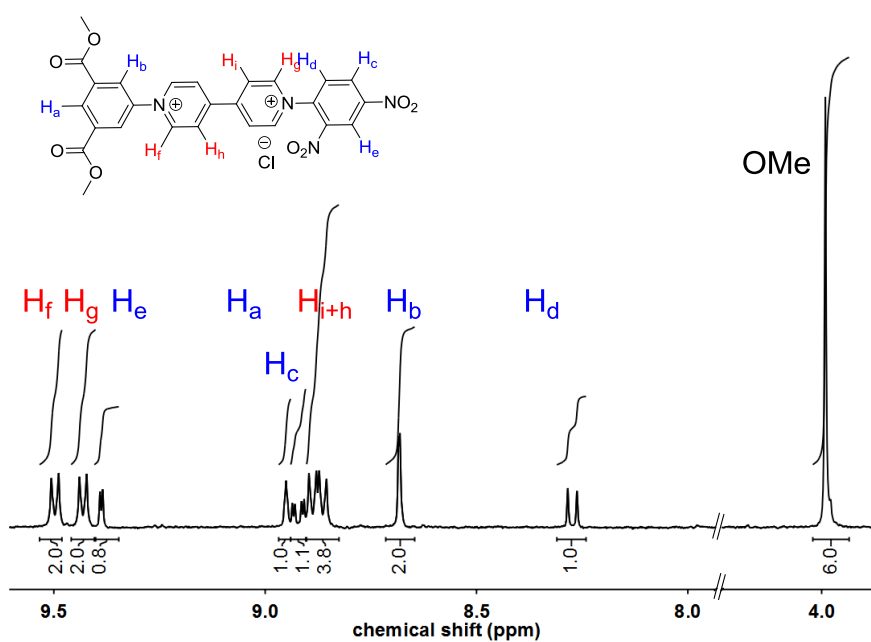
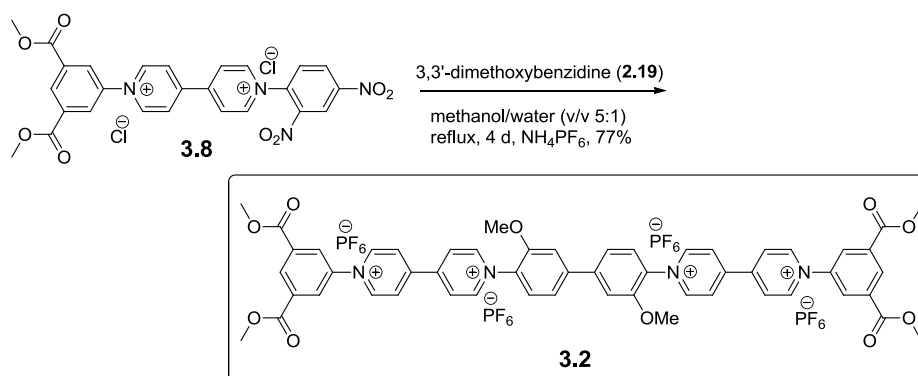


Figure 3.4. ^1H NMR spectrum of precursor **3.8** (D_2O).

The overall yield of this three step route (Scheme 3.5) to precursor **3.8** was 55 %, which is a very significant increase compared with the 3% yield achieved via the shorter route described

in Scheme 3.2. In addition, due to the straightforward purification and excellent purity of each compound, this multistep synthesis could reproducibly produce 10 g of the key intermediate **3.8**.

The second oligomer in our series was then accessed through the condensation of two equivalents of **3.8** with the electron-rich aromatic diamine **2.19** to give dimer **3.2** in 77% yield after ion exchange to form the tetrakis hexafluorophosphate salt (Scheme 3.9).



Scheme 3.9. Synthesis of conjugated dimer **3.2**.

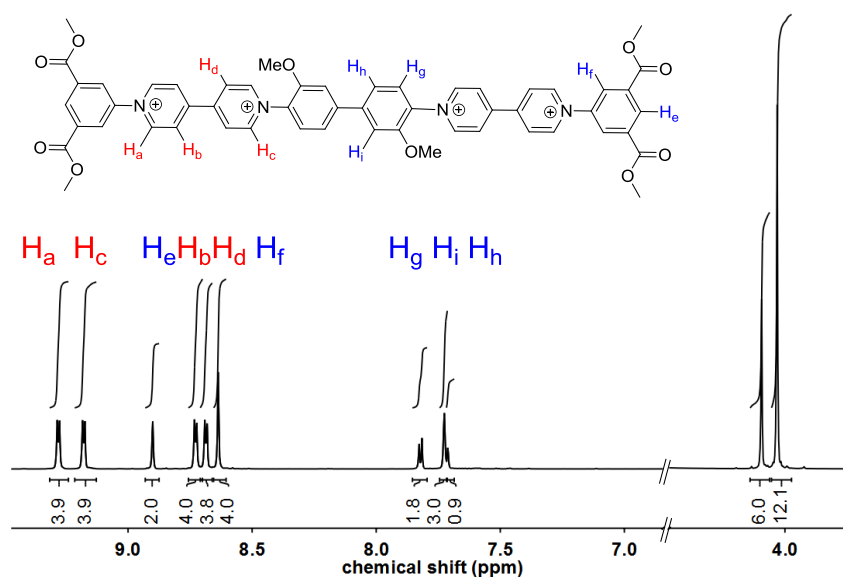
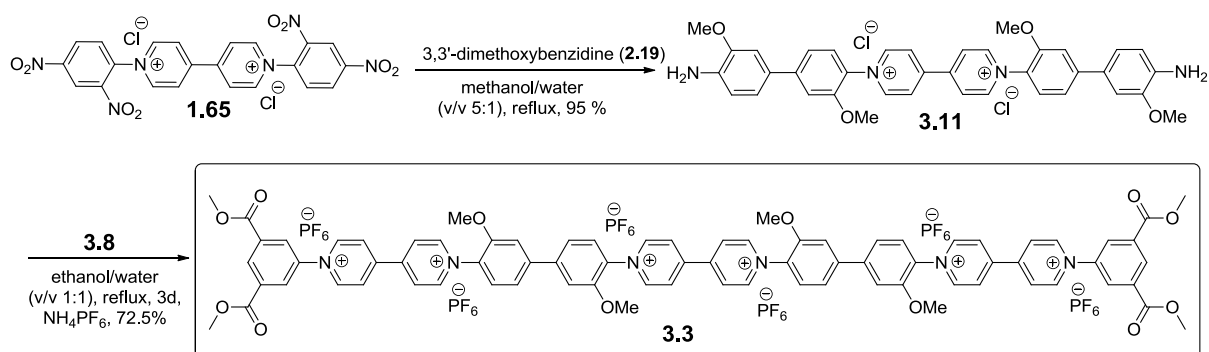


Figure 3.5. ^1H NMR (acetone- d_6 containing 1% of TFA) spectrum of compound **3.2**.

In contrast to unimer **3.1**, each viologen moiety in **3.2** is in an asymmetric environment. Each viologen is attached to an electron poor diester substitute aromatic through one ammonium ion with an electron rich methoxy substituted aromatic at the other. Therefore, each viologen contains 4 distinct proton environments which are readily resolved by ^1H NMR spectroscopy (H_a , H_b , H_c and H_d , Figure 3.5). In addition, the relative integral ratio of the 4 methoxy groups of the esters (4.0 ppm) and the two methoxy groups on the benzidine rings (4.03 ppm) is two to one as expected for the proposed structure of **3.2**. In the electrospray mass spectrum of **3.2**, the target species was observed as the doubly charged ion $[(\text{C}_{54}\text{H}_{46}\text{N}_4\text{O}_{10})^{2+}]$ at $m/z = 454.1519$ Da, in good agreement with the expected value of 454.1523 Da.

With significant quantities of the mono-Zincke salt **3.8** in hand, the targeted trimeric viologen containing oligomer was produced in just two further synthetic steps (Scheme 3.10). Initially, the reaction of three equivalents of diamine **2.17** with **1.65** gave diamine **3.11** (95%) which was converted smoothly to trimer **3.3** (72%) by reaction with two equivalents of the mono Zincke salt **3.9** which was isolated as its hexafluorophosphate salt after column chromatography.



Scheme 3.10. Synthesis of conjugated trimer **3.3**.

The successful formation of **3.3** was confirmed by analysis of its ^1H NMR spectrum and by ESI mass spectrometry. As expected, in comparison with the ^1H -NMR spectrum of dimer **3.2**, the spectrum of **3.3** (Figure 3.6) shows similar resonances. Crucially, the resonances at 4.02

corresponding to the 4 methoxy groups attached to the 2 benzidine residues and at 4.13 ppm for the 4 methoxy esters on the two end groups exhibit the same integral. The formation of trimer **3.3** also can be determined by mass spectrum, its parent-ion peak ($C_{78}H_{62}N_6O_{12}$)²⁺ observed at $m/z = 637.2210$ (calculated for 637.2207).

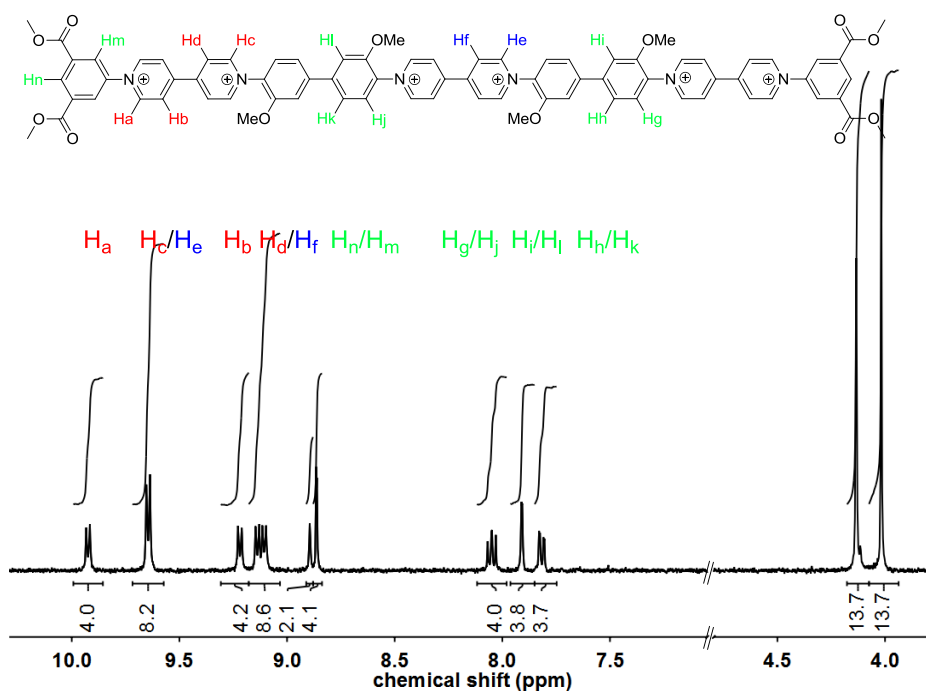


Figure 3.6. ¹H NMR (acetone-*d*₆ containing 1% of TFA) spectra of compound **3.3**.

With the successful synthesis of this series of compounds, attention was then turned to the investigation of their electrochemical properties.

3.2.2. Chemically reversible redox studies on **3.1**, **3.2** and **3.3**

Electronic absorption spectra of **3.1**, **3.2** and **3.3** in dimethylformamide (DMF) are presented in Figure 3.7. The most significant difference between the spectra of **3.1**, **3.2** and **3.3** is the new absorption band of the dimer at ca. 380 nm, tailing into the visible region. The intensity of this band increases markedly with oligomer length.

Concurrently, the dominant UV absorption at ca. 300 nm shifts slightly to higher energy, as the absorbance maximum tends to shorter wavelengths with increasing length of the conjugation system.

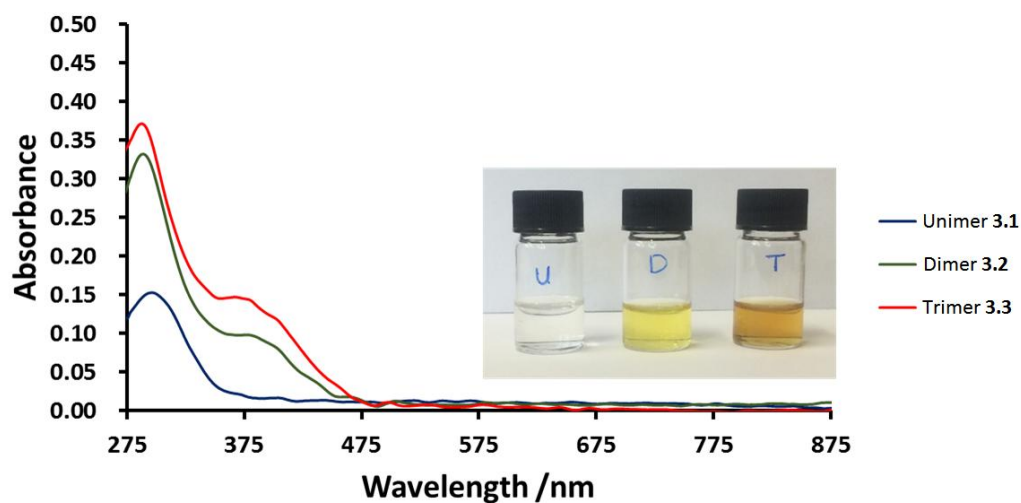


Figure 3.7. UV-Vis spectra of compounds 3.1, 3.2 and 3.3 in dimethylformamide (DMF, 0.2 mM) at 25 °C. Inset: Photograph of the compounds in DMF solution (0.2 mM).

During our group's previous work on macrocyclic systems (Schemes 2.2 and 3.1) we had shown its ability to accept an electron from TEA which was then quenched by the addition of TFA. This redox cycling study was repeated on unimer **3.1** to gain an initial insight into the redox properties of this new family of oligomers.¹²⁵

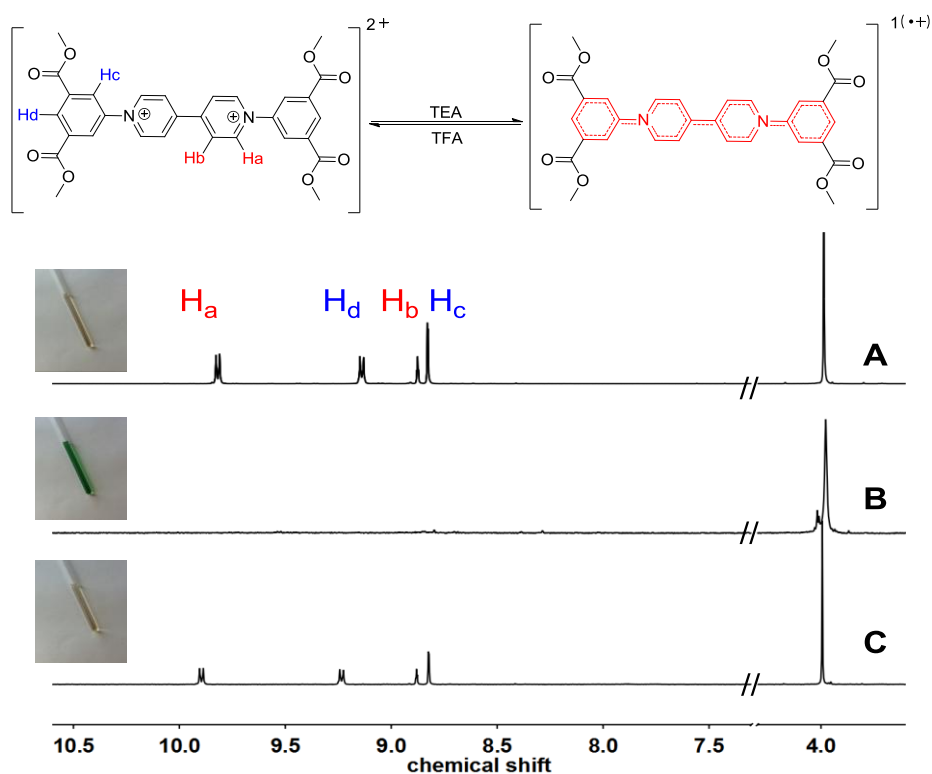


Figure 3.8. Chemical reduction (one-electron) and reoxidation of unimer **3.1** using TEA and TFA, respectively. The aromatic and heterocyclic rings highlighted in red indicate the region of unpaired spin density (not bond order). ^1H NMR spectra and photographs of the samples: (A) unimer **3.1** in acetone- d_6 , (B) after addition of 10 equivs of TEA and (C) subsequent to addition of an excess of TFA to B.

Figure 3.8(A) shows the ^1H NMR spectrum of **3.1** and a photograph showing a colourless solution of the unimer in its native dicationic state. On addition of a small quantity of TEA, all the signals corresponding to the protons of the aromatic and heterocyclic rings disappear, as a consequence of the formation of a paramagnetic radical cation. The change in the ^1H NMR spectrum is accompanied by a change in the colour of solution to green (B), which is characteristic of the formation of a radical cationic chromophore. Addition of a proton source (TFA), essentially regenerates the ^1H -NMR spectrum of the starting material with the loss of green colour.

As expected, the other two oligomers also exhibit excellent one-electron chemical reversibility. Figure 3.9 and Figure 3.10 shows the changes in colour of ^1H NMR spectra of dimer **3.2** and trimer **3.3**, respectively.

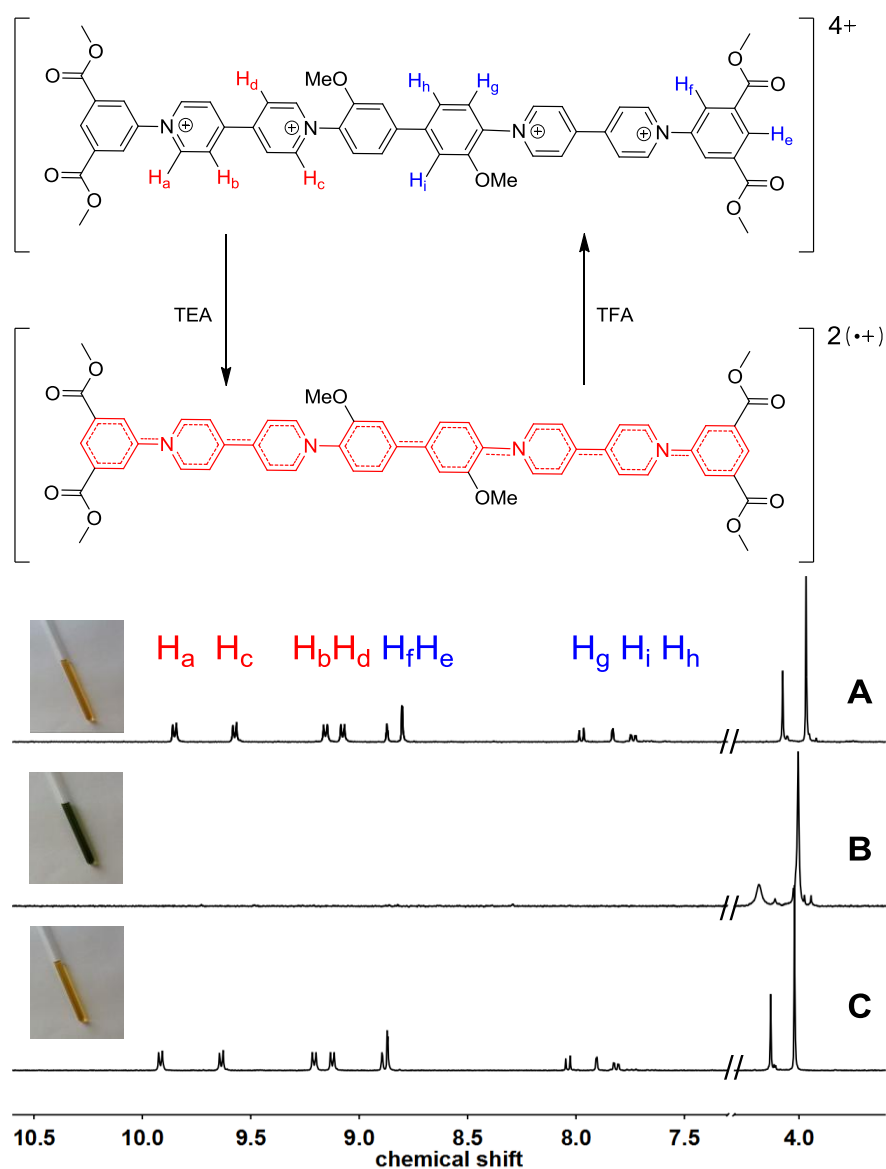


Figure 3.9. Chemical reduction ($2 \times$ one-electron) and reoxidation of dimer **3.2** using TEA and TFA, respectively. The aromatic and heterocyclic rings highlighted in red indicate the region of unpaired spin density (not bond order). ^1H NMR spectra and photographs of the samples: (A) dimer **3.2** in acetone- d_6 , (B) after addition of 10 equivs of TEA and (C) subsequent to addition of an excess of TFA to B.

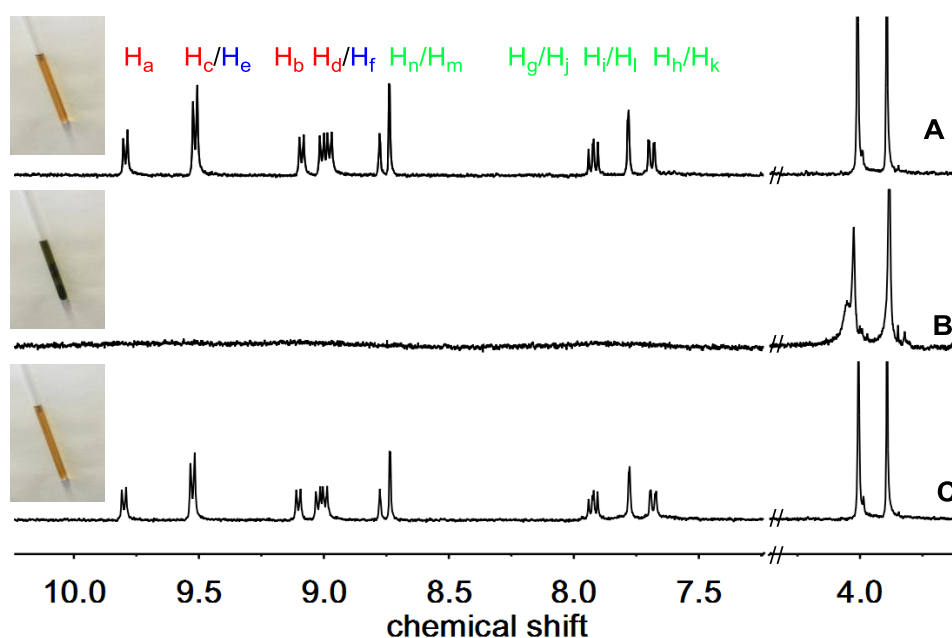
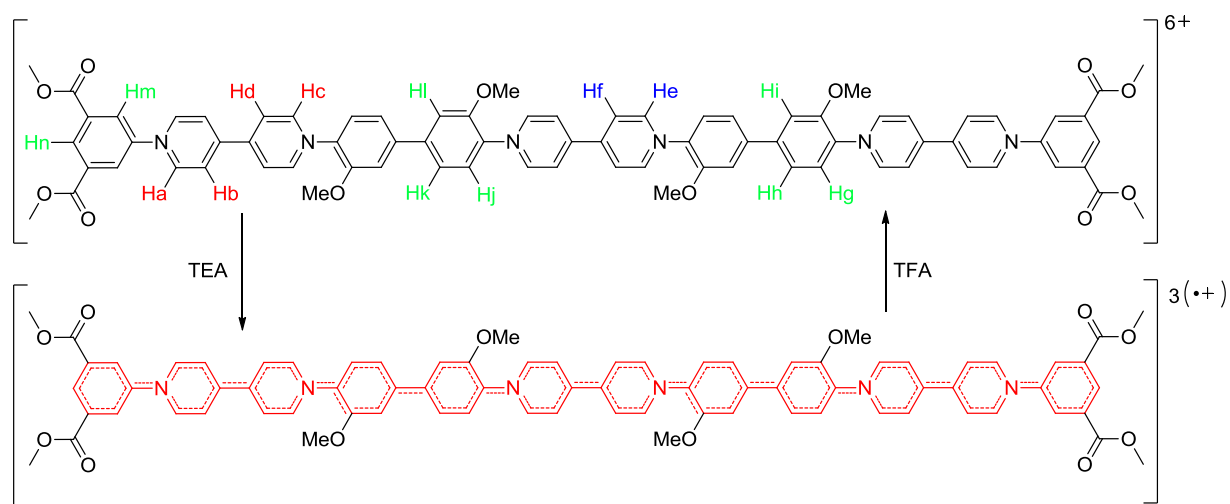


Figure 3.10. Chemical reduction (3 × one-electron) and reoxidation of trimer 3.3 using TEA and TFA, respectively. The aromatic and heterocyclic rings highlighted in red indicate the region of unpaired spin density (not bond order). ^1H NMR spectra and photographs of the samples: (A) trimer 3.3 in acetone- d_6 , (B) after addition of 20 equivs of TEA and (C) subsequent to addition of an excess of TFA to B.

In the case of the trimeric species, upon addition of excess triethylamine, all the signals corresponding to the protons of the aromatic and heterocyclic rings disappear, as a consequence of the formation of a paramagnetic tris(radical cation) (Figure 3.10B). This change in the ^1H NMR spectrum is accompanied by a transformation in the color

of the solution to a deep green, which is characteristic of the formation of radical cationic chromophores of this type.²⁷ However, the ¹H NMR signals corresponding to the non-conjugated methoxy groups remain visible at *ca.* 3.8 and 4.0 ppm. Addition of TFA to the tris(radical cation), not only regenerates the original colour of the solution but also restores the missing signals in the aromatic region of the ¹H NMR spectrum (Figure 3.10C).

3.2.3. EPR Experiments

The radical-cationic redox states of compounds **3.1**, **3.2** and **3.3** were investigated by electron paramagnetic resonance (EPR) spectroscopy in acetone at room temperature. The EPR spectrum of **3.1**^{•+} centred at $g = 2.0034(3)$ is characteristic of a viologen radical cation, showing well-resolved hyperfine splittings arising from a pair of equivalent ¹⁴N nuclei and multiple groups of equivalent ¹H nuclei (Figure 3.11).^{184,185} The bis(radical cationic) form of dimer **3.2** and the tris(radical cationic) form of trimer **3.3** are also EPR-active. This indicates that the electron spins of the dimer biradical do not exclusively pair to form a diamagnetic singlet state, though a half-field transition characteristic of a triplet state was not observed. The EPR signal of **3.2**^{2(•+)} exhibits the same broad envelope as **3.1**^{•+}, but the hyperfine structure is apparent only through weak shoulders. The EPR spectrum of **3.3**^{3(•+)} also has unresolved hyperfine shoulders, though the peak-to-peak linewidth has narrowed. The changes in spectral shape from unimer to dimer to trimer are characteristic of successive broadening of the hyperfine spectrum as may arise from increasingly rapid Heisenberg spin exchange or electron transfer processes.¹⁸⁶

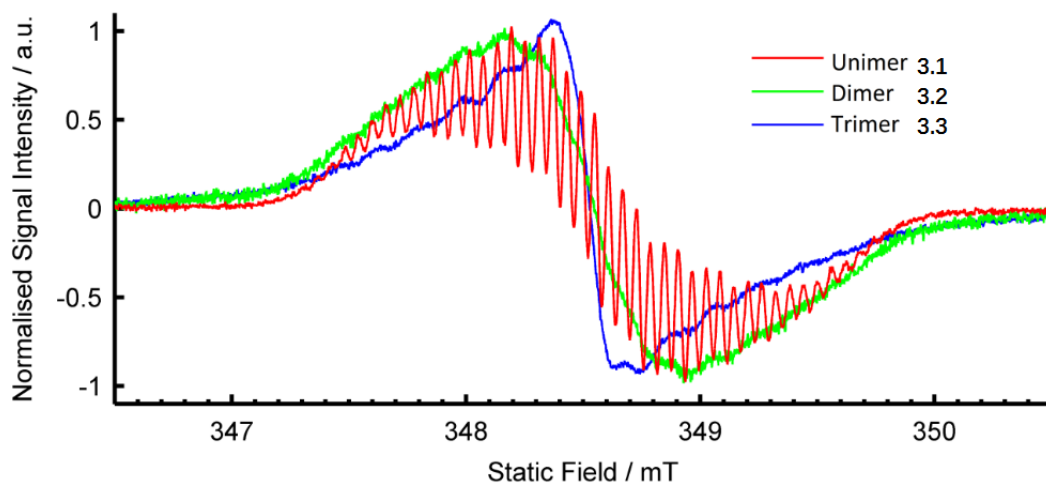


Figure 3.11. EPR Spectra of radical species generated from 3.1, 3.2 and 3.3 (1 mM) by addition of excess TEA in de-aerated acetone solution at room temperature.

3.2.4. Cyclic voltammetry and Square wave voltammetry of 3.1, 3.2 and 3.3

The electrochemical reductions of 3.1, 3.2 and 3.3 were studied by cyclic voltammetry (CV) at a polished glassy carbon disc electrode, using anhydrous DMF as solvent, containing 0.1 M tetrabutylammonium hexafluorophosphate (TBAPF₆) as supporting electrolyte. Ferrocene was selected as internal reference (set to 0.0 V). Cyclic voltammograms for compounds 3.1, 3.2 and 3.3 are shown in Figure 3.12 and Table 3.1.

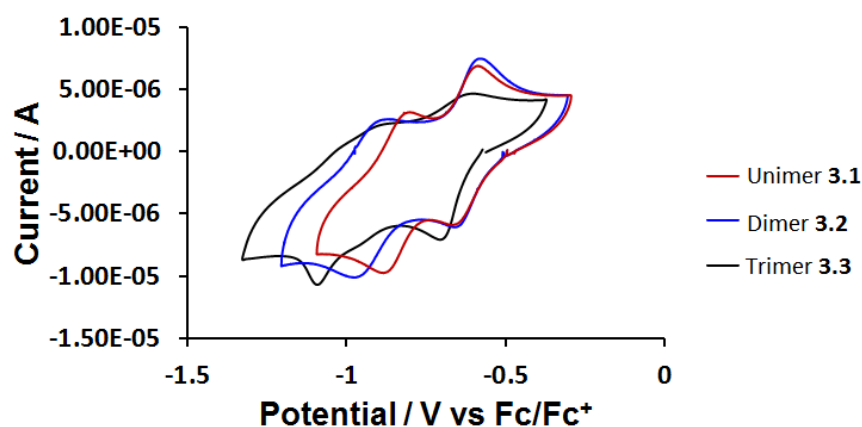


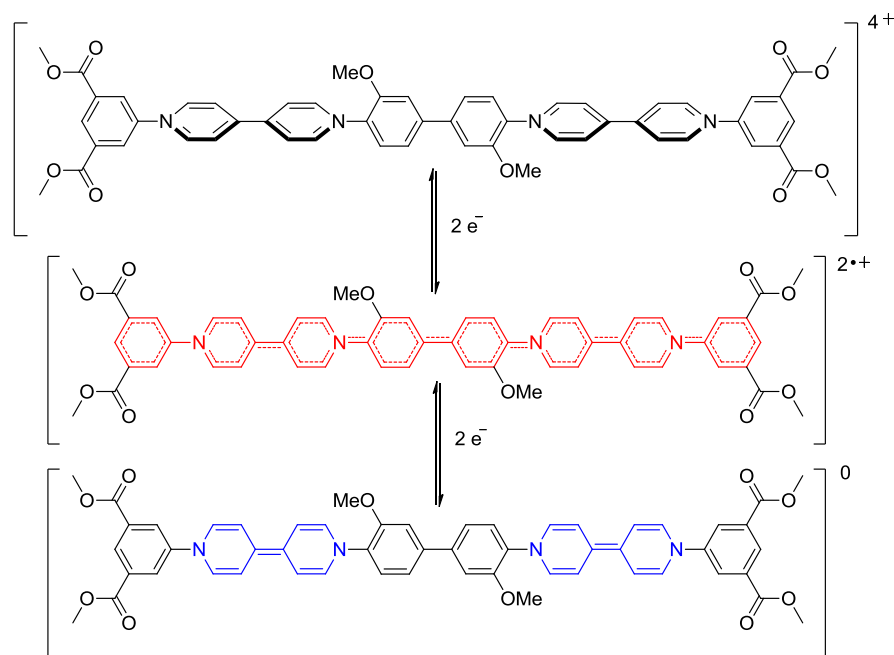
Figure 3.12 Cyclic voltammograms of 0.2 mM solutions of compounds 3.1, 3.2 and 3.3 at a glassy carbon disc ($d = 2$ mm) electrode in anhydrous DMF at $\nu = 500$ mV s⁻¹.

Table 3.1 Cyclic voltammetric half wave potentials observed on a glassy carbon disc ($d = 2$ mm) electrode in anhydrous DMF at $v = 500$ mV s⁻¹.

	CV = 0.5 Vs ⁻¹ $E_{1/2}^1$ (V) vs Fc/Fc ⁺	CV = 0.5 Vs ⁻¹ $E_{1/2}^2$ (V) vs Fc/Fc ⁺
Unimer 3.1	-0.63	-0.84
Dimer 3.2	-0.63	-0.92
Trimer 3.3	-0.66	-1.06

Two reversible one-electron cathodic waves for unimer **3.1** occur at $E_{1/2} = -0.63$ and -0.84 V vs Fc/Fc⁺.

For dimer **3.2**, two reduction waves was found at $E_{1/2} = -0.63$ and -0.92 V. The first reduction occurs at essentially the same potential as seen in the unimer **3.1** which indicates that the two viologen moieties in tetracationic dimer **3.2** are electronically independent. This may be as a result of a break in conjugation along the oligomer backbone caused by the presence of a twist between the central biphenyl rings and the viologen residues (Scheme 3.11) precluding efficient orbital overlap. In contrast, the second reduction potential of **3.2** is shifted significantly to a more negative value compared to that of **3.1** ($\Delta E_p = 80$ mV). This difference can be attributed to increased electronic conjugation in the more planar bis(radical cationic) form of **3.2** generated at the first cathodic wave.



Scheme 3.11. The structures of the stable intermediates observed during the electrochemical interconversions of dimer **3.2**: bis(dicationic) - twist, bis(radical cationic)-plannar, and neutral, quinoidal forms (top to bottom respectively).

Hexacationic compound **3.3** is reduced at only a slightly more negative potential than in **3.1** or **3.2** ($E_{1/2} = -0.66$ V, $\Delta E_p = 100$ mV). As observed for **3.2**, all three viologen units in **3.3** are reduced to their corresponding radical cations at the same electrode potential, suggesting that the viologens are twisted with respect to the chain direction and are therefore electronically independent (Scheme 3.11). The cyclic voltammogram of **3.3** indicates a strong influence of adsorption phenomena at this scan rate (poorly resolved cathodic waves and diminished anodic counter-waves). The rather unusual second cathodic step which ultimately converts the tris(radical cationic) form of **3.3** to the neutral species, remains indistinct.

Thus, to further investigate the electrochemical properties of these series of compounds, a set of square wave voltammograms (SWV) was acquired. For **3.1** and **3.2**, under the same condition as CV measurement, the SWV for both compounds showed two reduction events with their E_p values also in agreement with their $E_{1/2}$ values calculated by conventional CV (Figure 3.13).

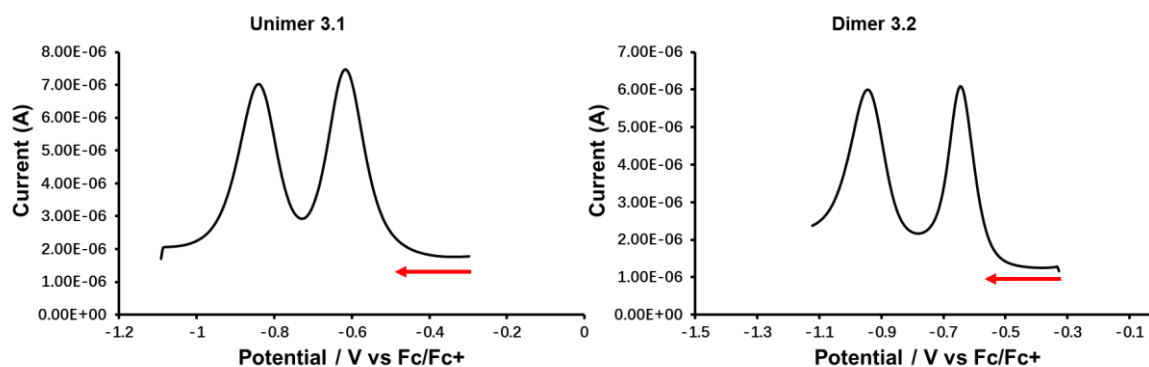


Figure 3.13. Square wave voltammograms of 0.2 mM solutions of compounds 3.1 and 3.2 on a glassy carbon disc electrode in anhydrous DMF/0.1 M TBAPF₆.

However, under these conditions the SWV trimer **3.3** exhibited three distinct reduction events (signals A, B and C in Figure 3.14 and Table 3.2). Although the peak current of square wave voltammetry (SWV) signals can be influenced by solubility effects and molecular re-organisation during reduction, it would appear that reduction for the single central (signal b, Figure 3.14) and two terminal bipyridinium units (signal C, Figure 3.14) to the neutral, quinoidal species can, nevertheless, be resolved in this experiment.

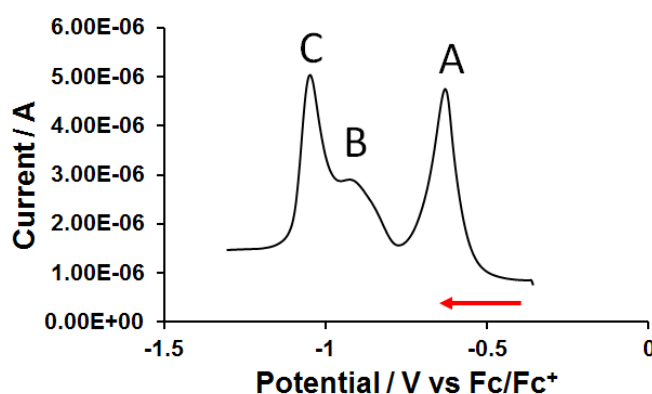


Figure 3.14 Square wave voltammogram of 0.2 mM trimer 3.3 on a glassy carbon disc electrode in anhydrous DMF/0.1 M TBAPF₆.

Table 3.2 Square wave voltammetric peak and cyclic voltammetric half wave potentials of trimer **3.3** observed on a glassy carbon disc ($d = 2$ mm) electrode in anhydrous DMF.

SQW, $f = 10$ Hz E_p (V) vs Fc/Fc ⁺	CV, $v = 0.5$ V s ⁻¹ $E_{1/2}$ (V) vs Fc/Fc ⁺
-0.65	-0.66
-0.93	-
-1.05	-1.06

3.2.5 Spectroelectrochemistry (SEC) investigation of unimer **3.1**, dimer **3.2** and trimer **3.3**

3.2.5.1. IR-SEC study

In order to try to investigate the changes in the conjugated structure of these viologen-based molecules throughout the redox cycle infra-red spectroelectrochemistry (IR-SEC) was carried out on simple mono-viologen unimer **3.1** within an OTTLE cell¹⁸⁷ (Figure 3.15). The voltage applied during the spectroelectrochemical experiment was monitored by thin-layer cyclic voltammetry and multiple IR spectra acquired over the course of the CV cycle.

The IR spectra of the sample when the applied voltage would result in the predominance of the dicationic, cationic and neutral versions of **3.1** are shown in Figure 3.16. Formation of the viologen radical cation was accompanied by the appearance of a strong $\nu(\text{C}=\text{C})$ band at 1639 cm^{-1} associated with this species.¹⁸⁸ There was, however, negligible change in the wavenumber of the $\nu(\text{C}=\text{O})$ band at 1734 cm^{-1} arising from the terminal ester groups. This observation suggests that the ester groups are not significantly conjugated with the aromatic system (Figure 3.15), so that their influence on the reduction potential is only minor. Unfortunately, IR-SEC experiments with **3.2** and **3.3** were precluded by poor solubility of the reduced species in DMF at the high concentrations required to give reasonable absorbance values.

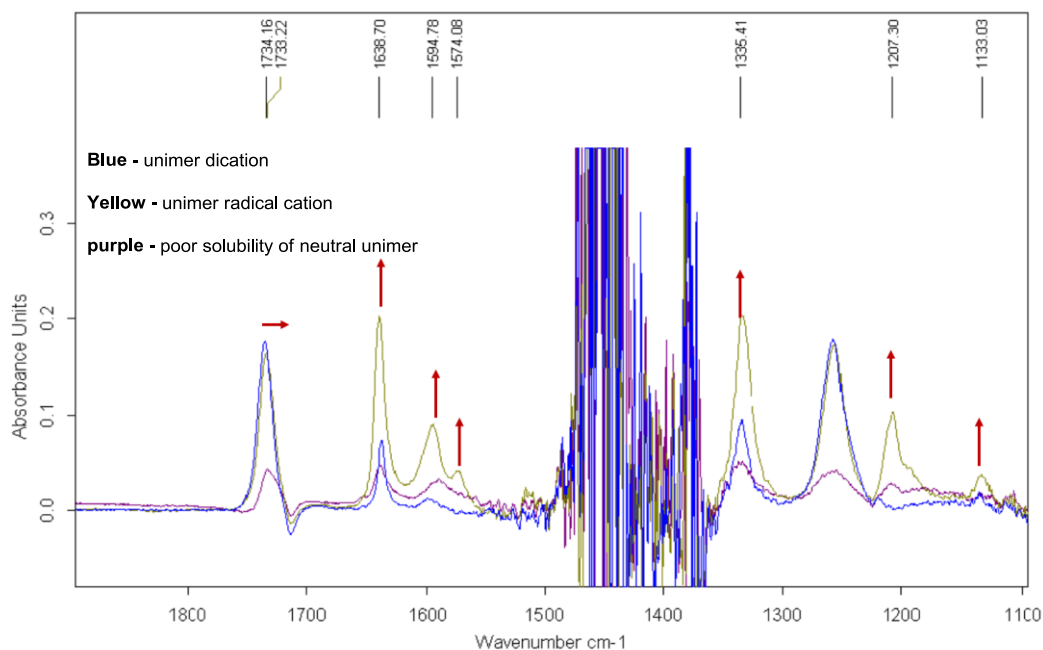
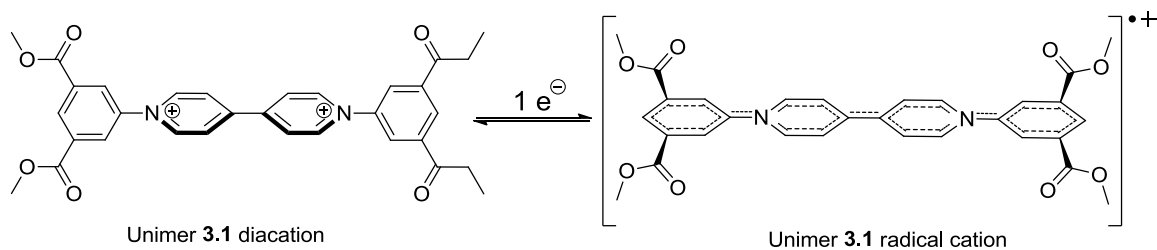


Figure 3.15. IR spectral changes accompanying the stepwise one-electron reduction of dicationic unimer **3.1** (blue, 1 mM) to the corresponding radical cation (khaki) and then to the ultimate neutral form (purple) in anhydrous *n*-butyronitrile /0.1 M TABPF₆ within an OTTLE cell¹⁸⁷. Solvent absorptions overload the detector between 1350 and 1500 cm⁻¹.

3.2.5.2. Thin-layer UV-vis SEC study

In order to study the redox-induced changes in electronic spectra of these systems (**3.1**, **3.2** and **3.3**), thin-layer ultraviolet-visible spectroelectrochemical (UV-vis SEC) measurements were carried out at 293 K with 0.2 mM **3.1**, **3.2** or **3.3** in DMF/0.1 M TBAPF₆. The observed spectral changes for all three species exhibit isosbestic points, excluding the possibility of side-reactions on the timescale of the experiment. All cathodic steps were fully reversible and the parent electronic absorption spectra were recovered upon reoxidation.

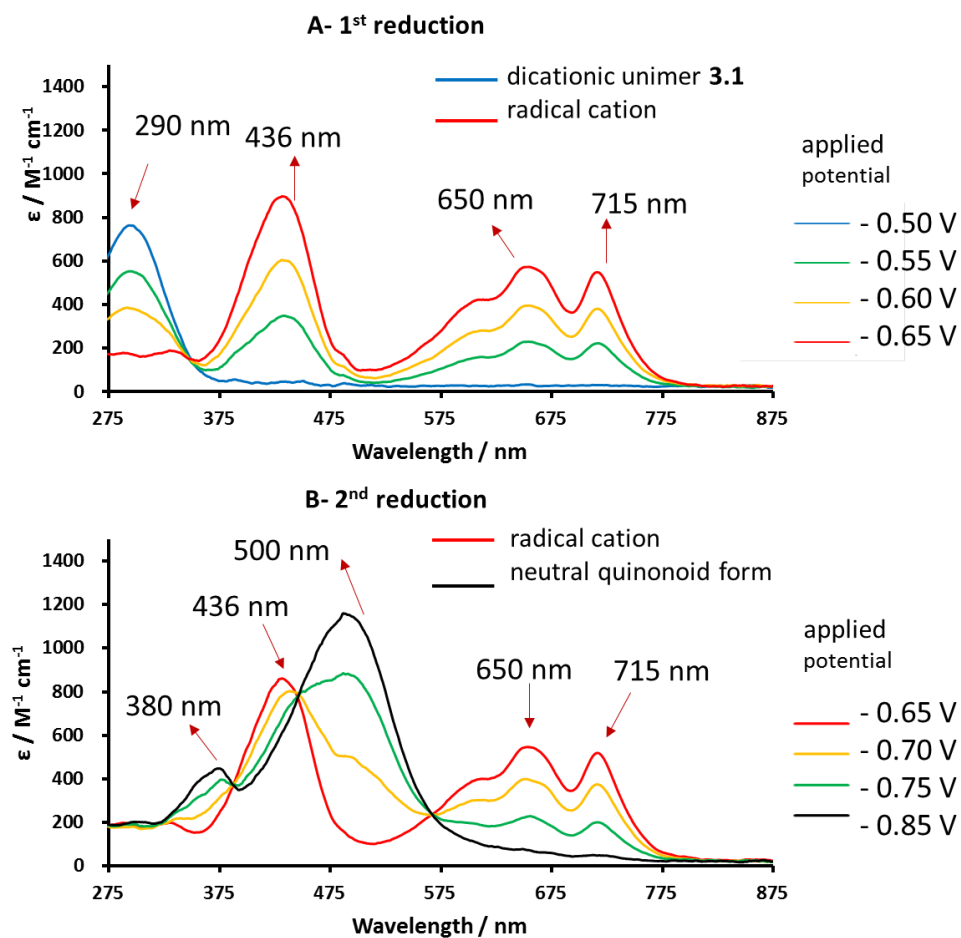


Figure 3.16. Reversible UV-vis spectral changes accompanying the stepwise 1e reduction of dicationic unimer 3.1 to the corresponding radical cation (spectrum A) and the neutral quinonoid form (spectrum B). Spectra recorded in anhydrous DMF/0.1M TABPF₆, using an OTTLE cell.¹⁸⁷

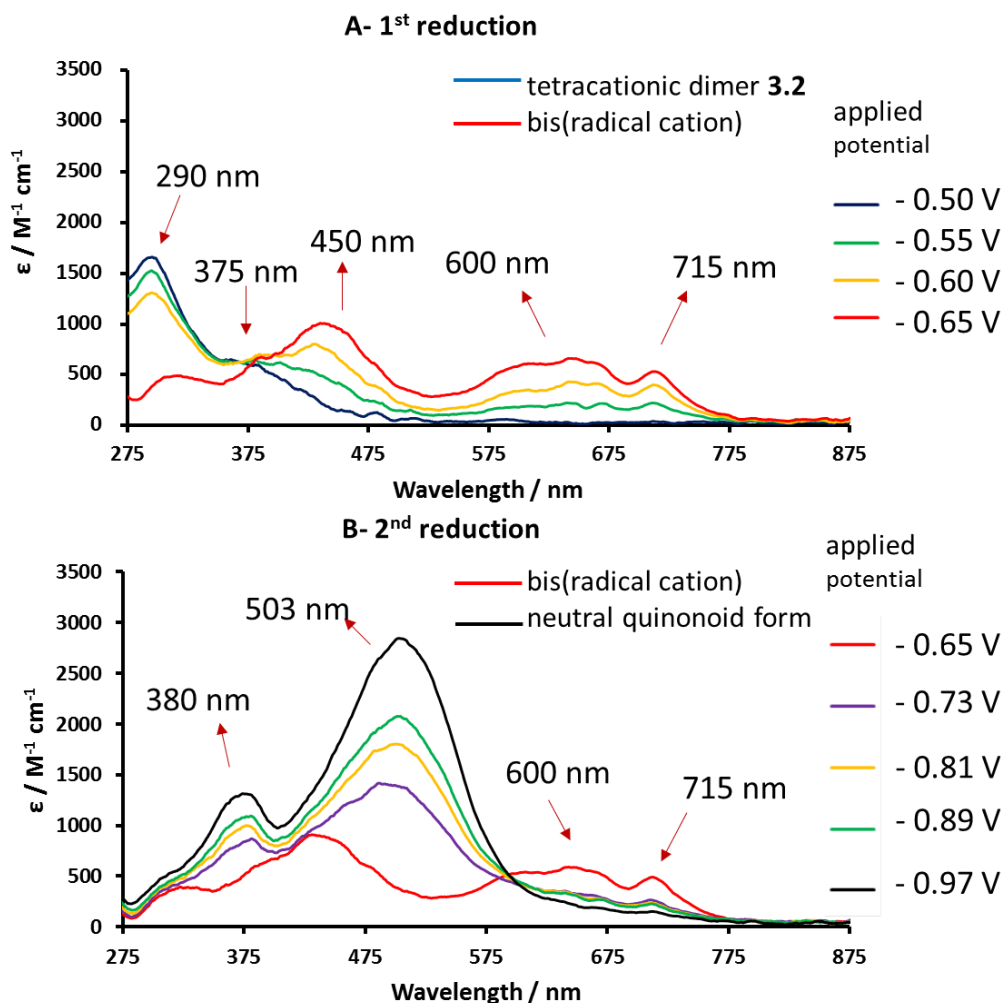


Figure 3.17. Reversible UV-vis spectral changes accompanying the stepwise 1e reduction of tetracationic dimer **3.2** to the corresponding bis(radical cation) (spectrum A) and the neutral quinonoid form (spectrum B). Spectra recorded in anhydrous DMF/0.1M TABPF₆, using an OTTLE cell.¹⁸⁷

Figures 3.16 and 3.17 show the UV-Vis spectral monitoring of the electrochemical reduction of unimer **3.1** and dimer **3.2** at the two well-defined cathodic waves shown in Figure 3.12. Similar to the UV-SEC of its unimer homologue, the tetracationic species shows two absorption bands at 290 and 375 nm (Figure 3.17A). After completion of the first reduction step, the new absorption bands at 450, 600 and 715 nm are indicative of the bis(radical cation) (Figures 3.17A and 3.17B).¹⁴⁹ Continuation of the cathodic sweep results in a second transformation in the electronic absorption spectrum due to formation of the neutral quinonoid form absorbing at 380 and 503 nm (Figure 3.17B).

Compared to unimer **3.1** and dimer **3.2**, the spectrochemical response of trimer **3.3** is more complex, as might be expected from SWV data (Figure 3.14). Using a continuous scan process (Figure 3.18), the voltammogram exhibits the same three stable states as observed in the SWV (Figure 3.14). Therefore, we attempted to analyse the UV/vis spectra of each state in order to further understand the electronic structure of each.

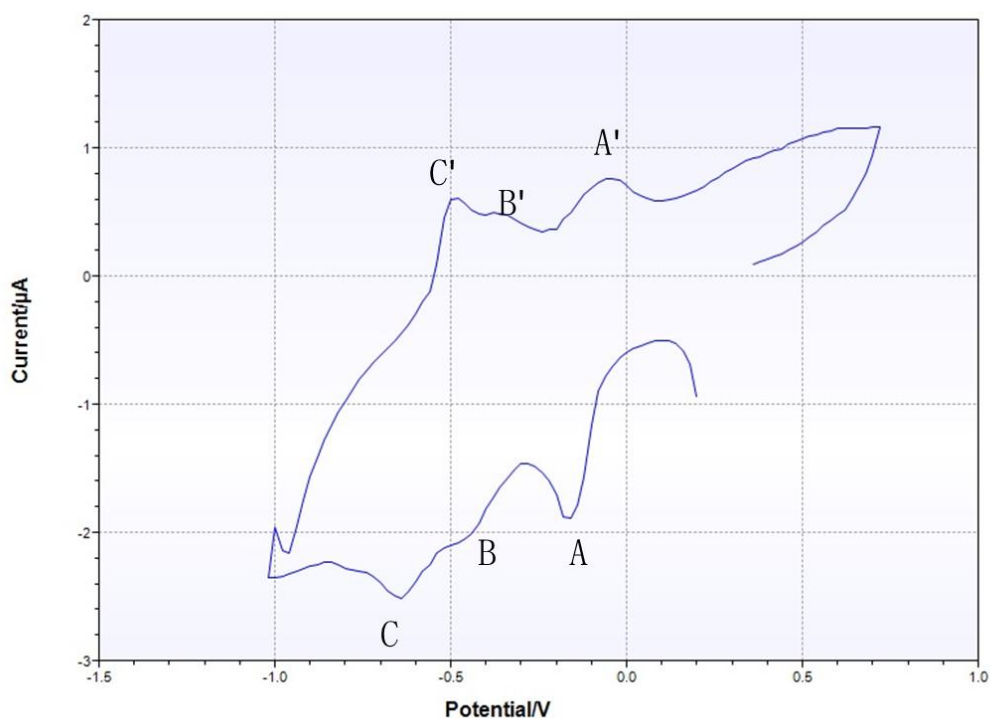


Figure 3.18. Cathodic thin-layer cyclic voltammogram recorded in the course of the UV-Vis spectral monitoring of the three reductions (Table 1) of hexacationic trimer **3.3** (0.2 mM) in anhydrous DMF within an OTTLE cell¹⁸⁷ at $\nu = 0.2$ mV s⁻¹ at room temperature. The potential scale is arbitrary (Ag wire pseudoreference electrode was used).

Spectroelectrochemical (UV-vis) data for the four stable redox forms of trimeric species **3.3** were recorded at the reduction potentials corresponding to the three cathodic waves measured previously (Table 3.2).

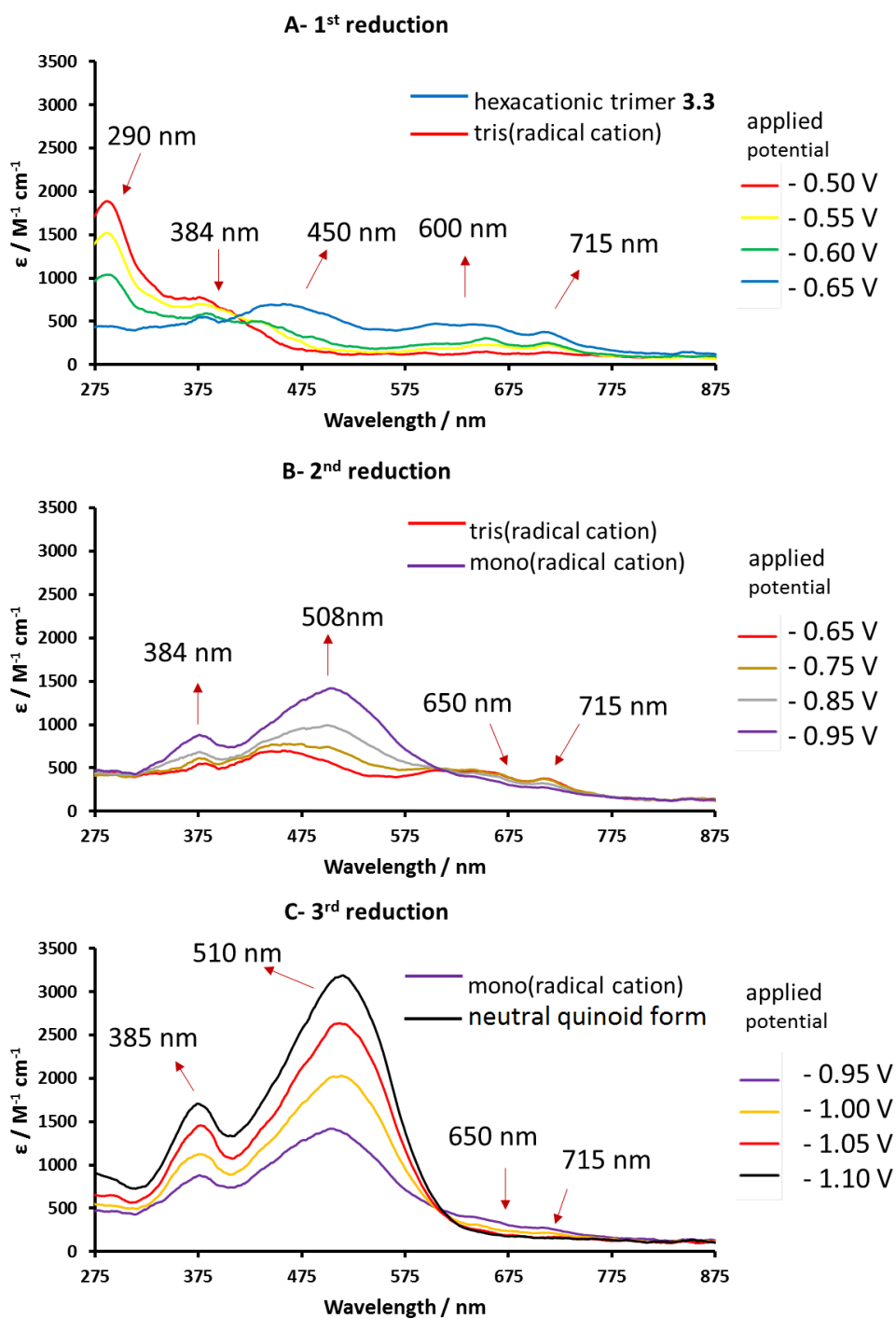


Figure 3.19. Reversible UV-vis spectral changes accompanying the stepwise reduction of hexacationic **3.3** to the corresponding tris(radical cation) (spectrum A) and the mono(radical cation) (spectrum B) and the neutral quinoid form (spectrum C), recorded in anhydrous DMF/0.1M TABPF₆ using an OTTLE cell.¹⁸⁷

Conversion of the hexa-cationic species to the tris(radical cation) results in a spectrum similar to that observed for the analogous radical cation of **3.1** and bis(radical cation)

of **3.2**, with absorption maxima at 450, 600, 650 and 715 nm (Figure 3.19A). Continued decrease in the applied cathodic potential results in the formation of a second stable species associated with absorption bands at 384 and 508 nm, which confirm the formation of fully reduced, quinoidal heterocycles. The absorption bands of the radical cation above 600 nm are diminished but still evident (Figure 3.19B). This spectrum is consistent with a mixed oxidation state species containing both radical cationic and quinoidal heterocyclic species. Further lowering of the applied potential delivers the final species with intense absorption bands and 385 and 510 nm and no significant absorption bands above 600 nm (Figure 3.19C), indicative of a fully reduced, neutral species.

Figure 3.20 shows an overlaid plot of the UV/vis spectra of the four stable, spectroscopically distinct species in the redox cycle of **3.3**.

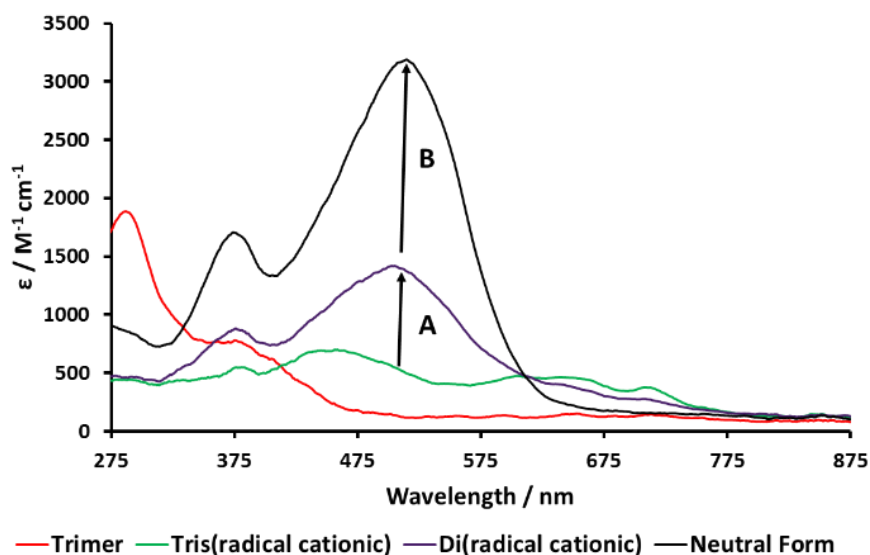
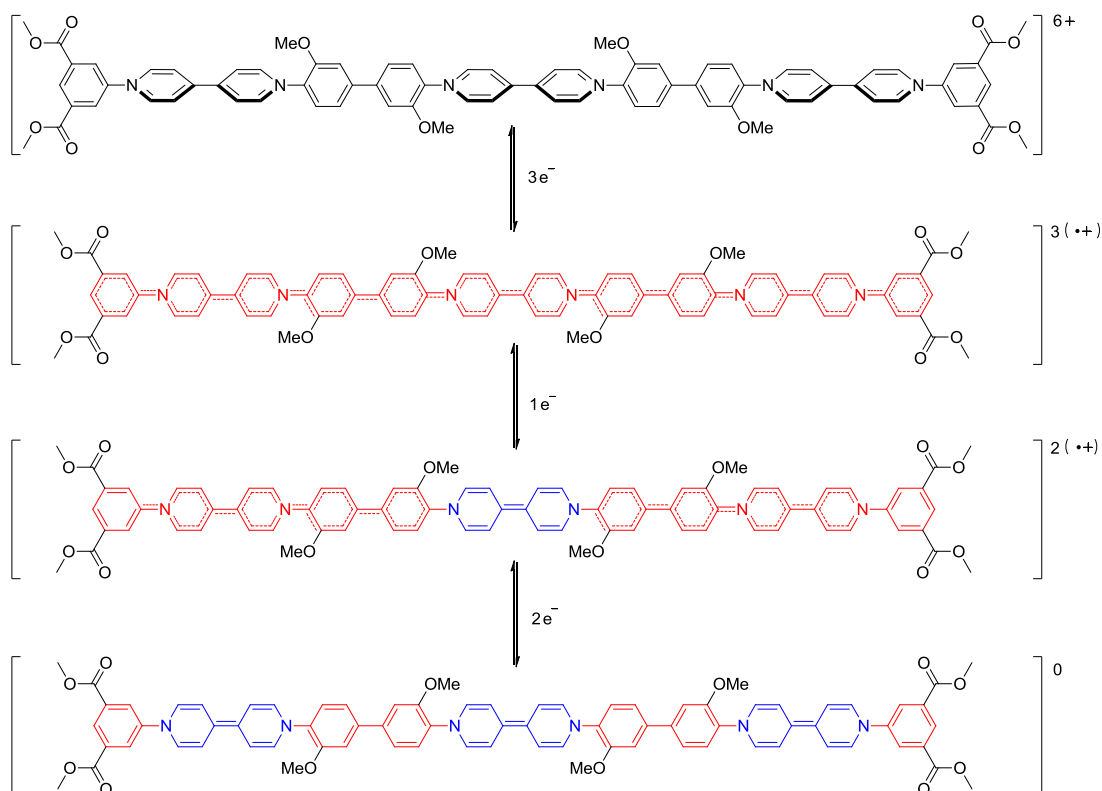


Figure 3.20. UV-vis spectral changes accompanying the stepwise reduction of hexacationic **3.3** to a neutral species. The change in intensity of the band at 515 nm associated with the formation of quinoidal bipyridinium residues occurs in the ratio 1:2 (arrows A and B respectively) during two-step reduction of the tris(radical cationic) form of **3.3** to the neutral species.

The most striking difference between the four spectra is the increase in the absorption band at 515 nm. When the molecule becomes reduced from the tris(radical cation) (green curve) to the mixed oxidation state (purple curve) system, the change of molar extinction coefficient (ϵ) between these two states is $870 \text{ M}^{-1}\text{cm}^{-1}$ (Arrow A). This compares to a change in intensity of $1800 \text{ M}^{-1}\text{cm}^{-1}$ (Arrow B) when moving from the mixed oxidation state species (purple curve) to the fully reduced, neutral trimer (black curve). The ratio of the difference in ϵ values is 1:2 respectively. These data suggest that the intermediate species, which is formed at approximately -0.9 V (Table 3.2), contains a single quinoidal bipyridinium species compared to the three quinoidal species present in the ultimate, neutral form of **3.3**. Data from the SWV (Figure 3.14) and the UV-vis SEC (Figure 3.19 & 3.20) of **3.3**, supported by thin-layer cyclic voltammetry carried out during the latter experiment (see Figure 3.18), prove that the reduction of all these bipyridinium groups to give the tris(radical cation), occurs by the addition of three electrons at the same potential (-0.65 V). However, the subsequent reduction of the tris(radical cation) to the neutral species occurs in a stepwise manner, by the addition of a single electron (at -0.93 V) followed by two electrons (at -1.05 V). This can be accounted for if the central bipyridinium radical cation is reduced first, followed by the two terminal radical cations (Scheme 3.12).



Scheme 3.12. The structures of the stable intermediates observed during the electrochemical interconversions of trimer **3.3**: tris(dicationic), tris(radical cationic), di(radical cationic) and neutral, quinoidal forms (top to bottom respectively).

3.3. Conclusion

This chapter has reported an efficient synthesis of 4,4'-bipyridinium-based aromatic oligomers (**3.1-3.3**) and their spectro-electrochemical properties. Specifically, a controlled stepwise synthesis to produce single molecules with three 4,4'-bipyridinium residues containing twelve conjugated aromatic/heterocyclic rings has been developed for the first time. All the compounds undergo reversible stepwise two-electron reduction of each viologen residue.

Combined results from CV and UV-vis SEC demonstrate that, in these three oligomers, their ground states are not planar, but the phenyl groups and viologen residues are likely to be out of plane (twisted) with respect to each other. During reduction to the radical cationic state, the second $E_{1/2}$ tends to a slightly more negative value as the conjugation length increases.

Spectroscopically, the UV-vis SEC results for **3.3** demonstrated that the apparently more electron rich, central radical cationic bipyridinium moiety is reduced to a quinoidal, neutral form before the two terminal bipyridinium units which appear comparatively electron poor. In support of this computational studies of related conjugated oligomers and polymers have also shown that those maxima for their HOMO/LUMO coefficients are found at the centre of the molecule.^{189,190} If then the highest occupied spin orbital (HOSO) of the tris(radical cation) form of **3.3** is also localised in the centre of the molecule then the central 4,4'-bipyridinium would be reduced prior to the higher energy terminal radical cationic units. In addition, the UV-vis SEC measurements have highlighted the potential of those new molecules to find application in display technologies where dramatic and reversible colour changes are required.

Chapter 4

Synthesis, Characterization, and Electrochemical Behavior of Aromatic *N*-Substituted Viologens and Conjugated Oligo-Viologens

4.1. Introduction

From the results presented in the previous chapter, it is clear that the Zincke reaction is an efficient way to synthesise 4,4'-bipyridinium-based aromatic oligomers with up to 12 conjugated aromatic rings (**3.3**). In each of the oligomers studied, the viologen residues were clearly observed to undergo two reversible reduction events. Within a functioning nano-machine (for examples see Figure 5.3 in chapter 5) or electrochromic device, it is the precise potential at which the systems exhibit redox switching that would be a key performance parameter.

Within the extensive number of viologen species reported to date, there has been some attempt to investigate how the structure of the *N*-substituent affects the redox properties of the viologen. For example Arihara and co-workers studied a series of alkyl substituted viologens (i.e. Me, Et and Pr).¹⁹¹ They found slight negative shifts in the first and second reduction half-wave potentials of the viologen as the length of the alkyl chain increased. It was proposed that this was due to an increase in electron donating ability of the substituents as the alkyl chain lengthened.¹⁴⁸ Perhaps as a consequence of the lack of efficient synthetic routes to aromatic *N*, *N'*-substituted viologen, there has not been a systematic structure/redox potential study produced concerning these materials. Such an investigation is important as these species are becoming more prevalent in a multitude of applications (see sections 1.51 and 5.1).

Herein, we report the synthesis of a series of π conjugated viologen containing oligomers which contain aromatic residues with varying functional groups and substitution patterns (see below). The redox properties of this structurally related series of viologens are compared to evaluate the effect of substituents on electronic properties.

4.2. Results and Discussion

4.2.1. Design

Despite the huge number of different viologen-containing molecules studied, a systematic investigation concerning viologens with different end groups and oligomer length has not been made. The target viologen containing species are illustrated schematically in Figure 4.1.

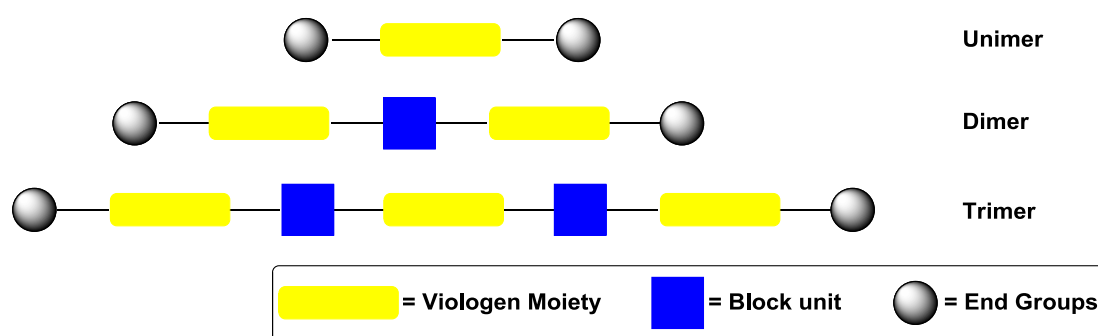


Figure 4.1. Schematic representation of target compounds: unimer, dimer and trimer.

The design of these viologen species with different redox potentials requires ready access to mono-aromatic amines with varying electronic properties (e.g. containing electron withdrawing/donating groups or varying numbers of fused aromatic rings), which could be used as end groups (see Figure 4.2). The central, linking block unit must clearly be an aromatic diamine. It was known from our previous investigations (chapters 2 and 3) that electron rich aromatic diamines (like 3,3'-dimethoxybenzidine **2.19**) or spatially separated amine groups (like 4,4'-(1,3,4-oxadiazole-2,5-diyl)dianiline) are likely to be best suited to the construction of dimeric and trimeric viologen oligomers. With these design criteria in mind, a table of suitable starting materials was assembled which were all inexpensive and readily commercially available (Figure 4.2).

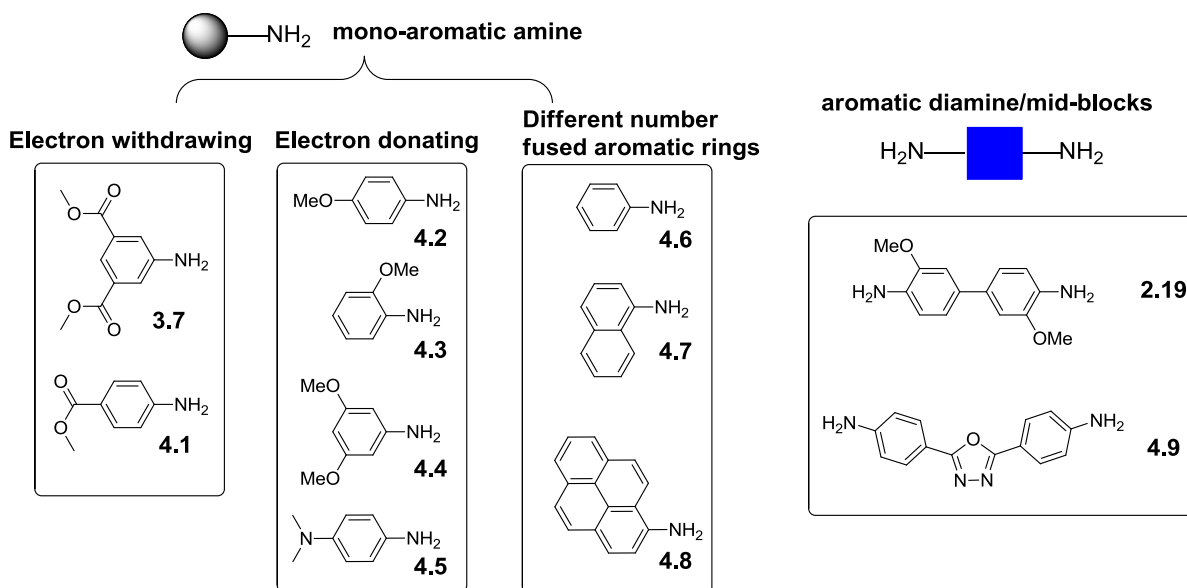
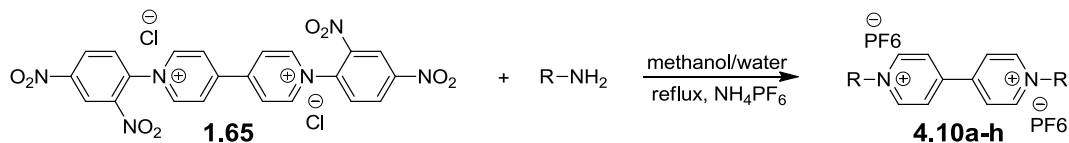


Figure 4.2. Structures of mono-aromatic amine end groups and aromatic diamine mid-blocks.

4.2.2. Synthesis of a series of mono-viologen species with varying aromatic end groups

Building on the synthetic strategy from the previous chapter, the synthesis of unimers **4.10a-4.10h** (Scheme 4.1, Table 4.1). started with Zincke salt **1.65** which was reacted with an excess of mono amine to deliver a series of structurally related aromatic *N*, *N'*-substituted viologens. Five of these viologens (**4.10a, b, f, g**) have been reported previously in the literature.

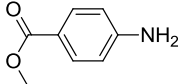

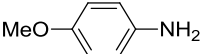
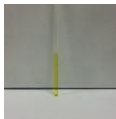
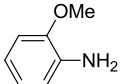
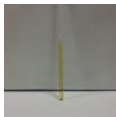
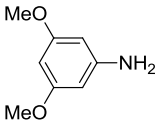
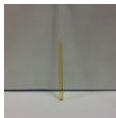
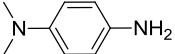

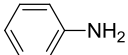

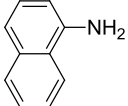

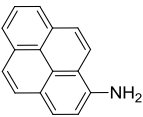



Scheme 4.1. Synthetic strategy for unimers (**4.10a-4.10h**).

Each monomer (**4.10a** to **4.10h**) was synthesized in good yield (79-86%) under the same conditions demonstrating the utility of the reaction. Most products were pale yellow or orange in colour except the *N,N*-dimethylamino substituted viologen (**4.10e**) which was dark purple/black in solution. This is perhaps indicative of the extremely strong electron donating

ability of the N,N-dimethyl functional group.¹⁹²

Table 4.1. Table showing the colour of the di-substituted viologens in acetonitrile-*d*₃ (c. 5 mg/mL) and the yield of the unimers from 4.10a to 4.10h.

Compound number	Aromatic amine	Colour of 4.10x	Isolated yield
4.10a ¹⁹³	 4.1		93%
4.10b ¹⁹⁴	 4.2		95%
4.10c	 4.3		92%
4.10d	 4.4		79%
4.10e	 4.5		81%
4.10ff ¹⁹⁴	 4.6		96%
4.10g ¹²⁸	 4.7		87%
4.10h	 4.8		85%

4.2.3. Synthesis of a series of di-viologen oligomers with varying aromatic end groups

Previously, dimer **3.2** was prepared by the reaction between two equivalents of the asymmetric viologen intermediate **3.8** (Figure 4.2) and one equivalent of 3,3'-dimethoxybenzidine. However, to repeat this method to produce multiple diviologen oligomers with different endgroups would require the 3-step synthesis of an intermediate analogous to **3.8**, each containing a different endgroup (see **3.8a** where R = end groups **4.1** to **4.8**).

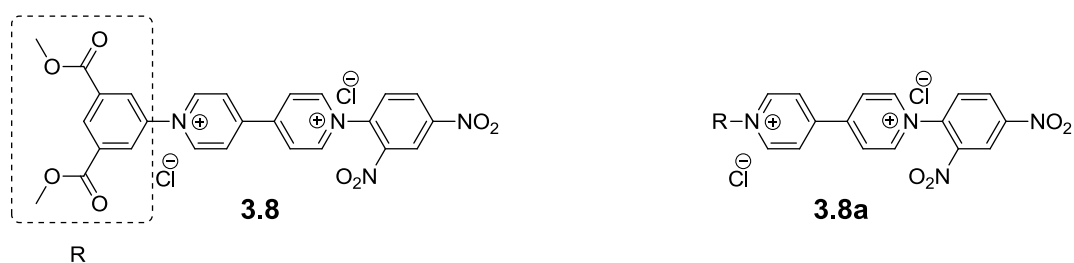
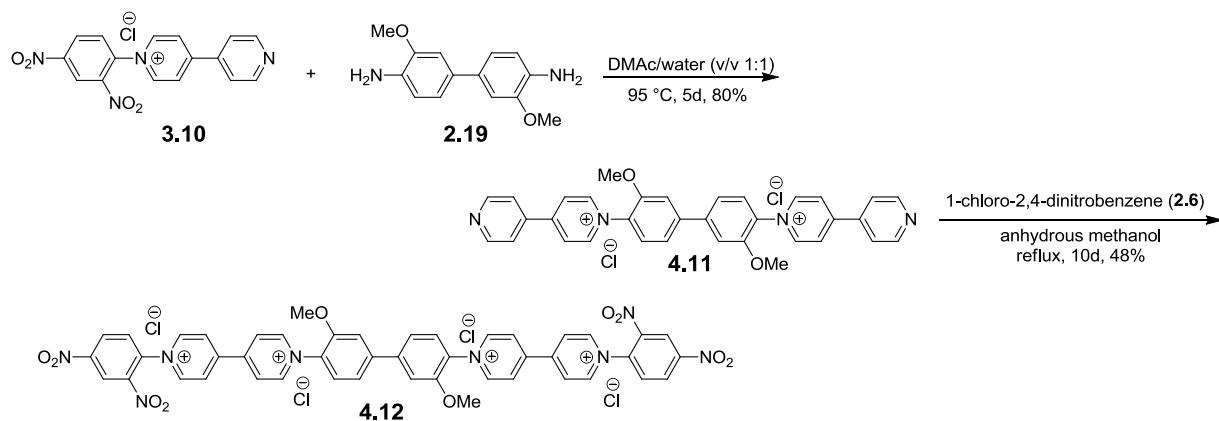


Figure 4.2. Structure of viologen intermediate compound **3.8** used to synthesis dimer **3.2** and the generic structure of intermediate analogous **3.8a** R = a to h (see Table 4.1).

This non-modular synthesis would clearly be extremely time consuming, and so to speed the production of multiple dimers, the diZincke salt **4.12** was identified as a new intermediate, which could serve as the basis for the addition of multiple endgroups. The synthesis of **4.12** started with the preparation of mono-Zincke salt **3.10** according to the method of Harries, Helliwell et al in 2006 (Scheme 3.6).¹⁸³Compound **3.10** was then used in a double Zincke reaction with 3,3'-dimethoxybenzidine **2.19** in DMAc/water to yield **4.11** containing a central diphenyl unit and two terminal viologen residues in 80% yield as a yellow solid. Finally, treatment of **4.11** with an excess of 1-chloro-2,4-dinitrobenzene **2.6** in anhydrous methanol under nitrogen for 10 days gave the target compound **4.12**. Gratifyingly, this key intermediate could be routinely produced on a 5 gram scale in just 3 steps without column chromatography.



Scheme 4.2. Synthesis of the key intermediate **4.12**.

The successful formation of **4.12** was confirmed by analysis of its ^1H NMR spectrum in D_2O (Figure 4.3). In comparison with the ^1H -NMR spectrum of Zincke salt **1.68** (Figure 2.1), **4.12** also exhibits the same characteristic double doublet at 9.42 ppm which corresponds to proton H_g between the nitro groups. This spectrum also contains the diagnostic singlet peak at 4.03 ppm of the methoxy ethers in the core diphenyl group. The integral ratio between the double doublet (H_f) and signal for the methoxy group is 1:3, confirms the successful synthesis of the intermediate.

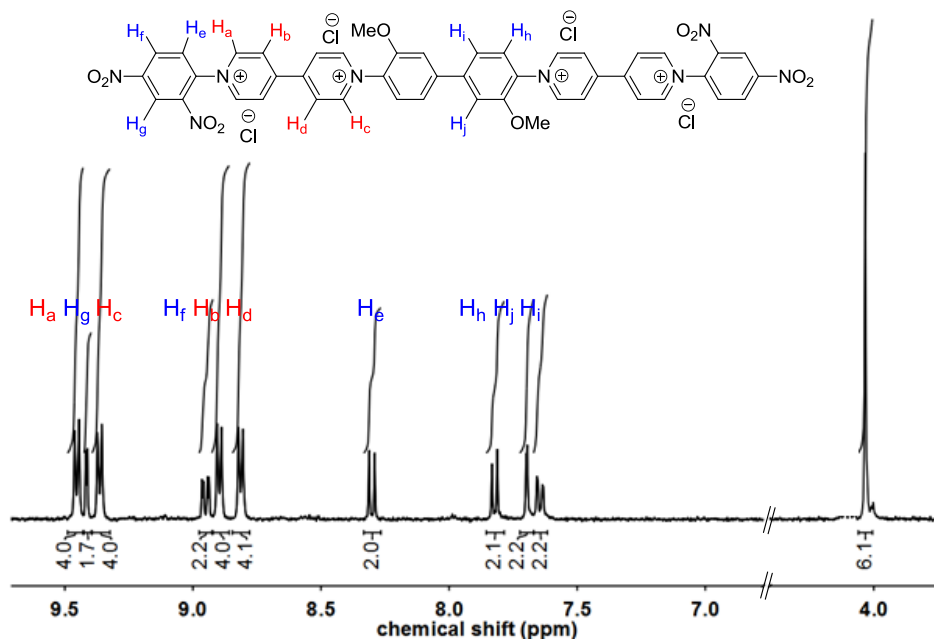
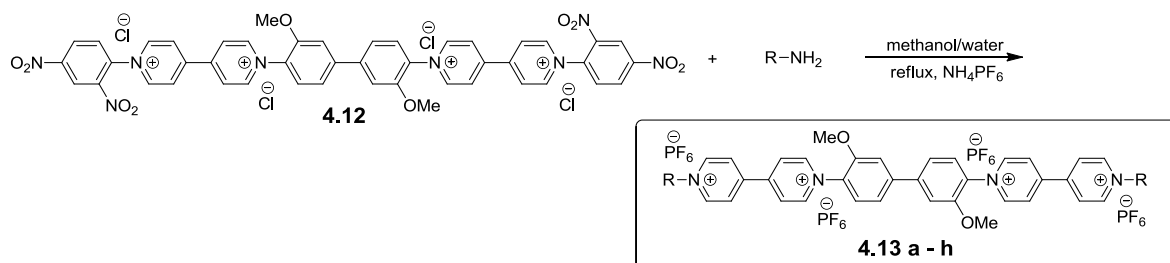


Figure 4.3. ^1H NMR spectrum of new intermediate **4.12** in D_2O .

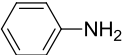

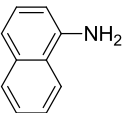

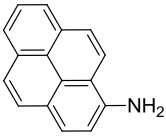

With multiple grams of **4.12** easily accessible, a series of dimeric viologen species (**4.13a**–**4.13h**) were obtained in one step by treatment with excess aromatic amines in water/ethanol at reflux (**4.1–4.8**, table 4.2, Scheme 4.3).



Scheme 4.3. Synthesis of the series of dimers from **4.13a** to **4.13h**.

Table 4.2. Table showing the colour of the di-substituted viologens in acetonitrile- d_3 and the yield of the dimers from **4.13a** to **4.13h**.

Entry	Aromatic amine	Colour of 4.13x	Isolated yield
4.13a	 4.1		95%
4.13b*	 4.2	n/d	n/d
4.13c	 4.3		85%
4.13d	 4.4		90%
4.13e*	 4.5	n/d	n/d

4.13f	 4.6		87%
4.13g	 4.7		92%
4.13h	 4.8		95%

*4.13b and *4.13e could not be isolated cleanly. n/d: not determined

Each dimer could be isolated in good yield (>85%) by precipitation into EtOAc without need for further purification. This is exemplified for **4.13a** for which the ^1H NMR spectra of the precipitated material shows the singlets at 4.14 and 4.00 ppm of equal intensity which are indicative of the methoxy protons on the central core and terminal end groups respectively.

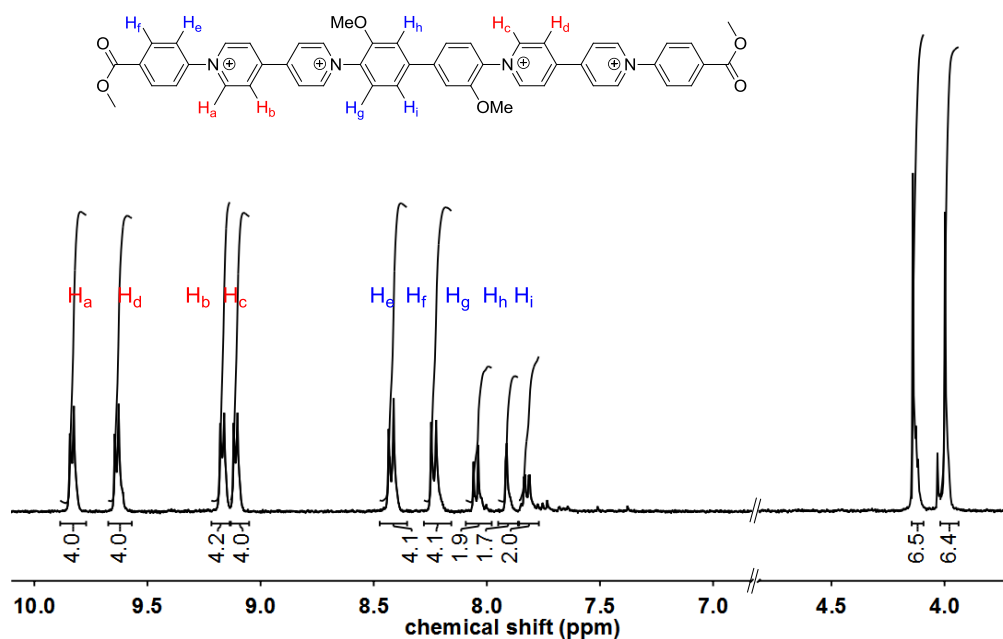
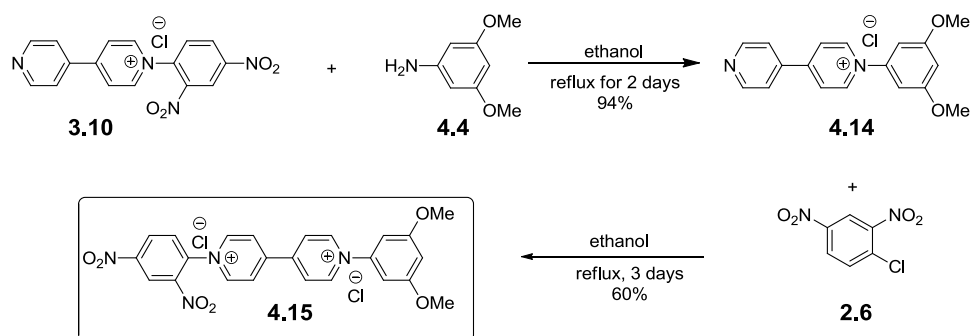


Figure 4.4. ^1H NMR spectrum of new dimer 4.12 in D_2O .

4.2.4. Synthesis of tri-viologen oligomers with varying aromatic end groups

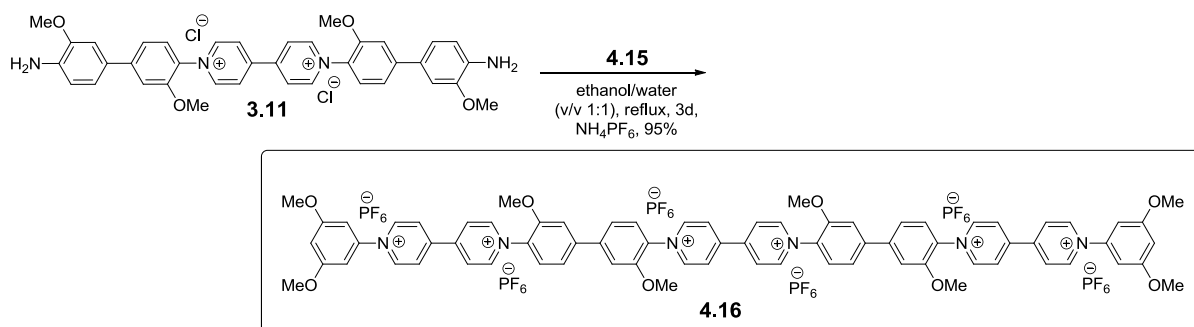
Time constraints did not permit the synthesis of the full series of trimers containing each different class of endgroup (Figure 4.2). Therefore, it was decided to synthesise just the trimer containing electron donating dimethoxy-substituted endgroups (**4.4**, Figure 4.2). It was thought that this new trimer (**4.16**, Scheme 4.6) would serve as a good comparator to our previously synthesized trimer (**3.3**) which contained two ester (electron withdrawing) endgroups.

Trimer **4.16** can be obtained using the same method used to produce **3.3** (Scheme 4.4 and 4.5). To achieve this, the asymmetric viologen compound **4.15** was synthesised over two steps from **3.10**.



Scheme 4.4. Synthesis of intermediate **4.15**.

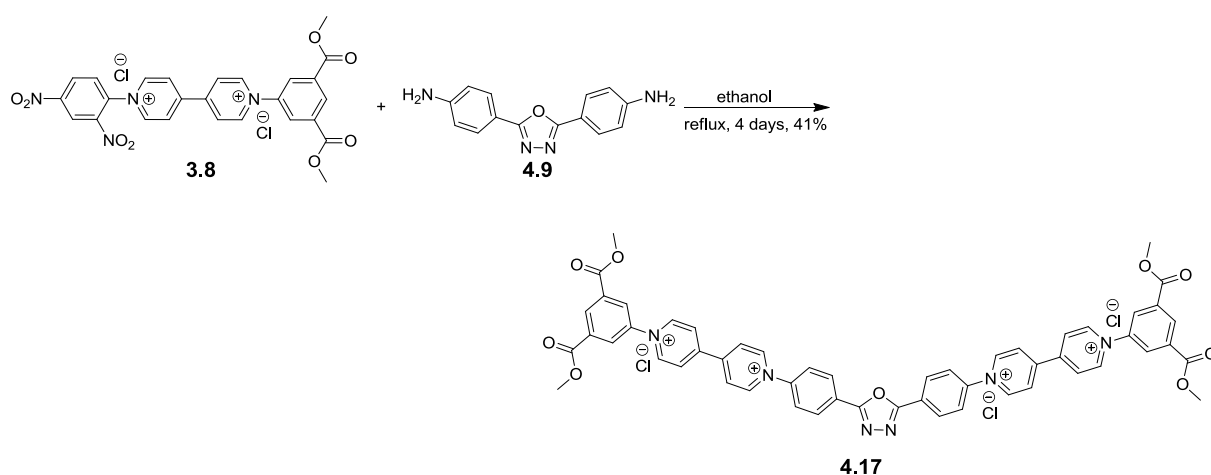
Addition of **4.15** to the monoviologen, diamine core **3.11** resulted in the formation of the novel trimer **4.16** in 95% yield after 10 days reaction time.



Scheme 4.5. Synthesis of trimer **4.16**.

4.2.5 Synthesis of a di-viologen oligomer with 4,4'-(1,3,4-oxadiazole-2,5-diyl)dianiline as the central aromatic block.

As a final challenge to our established synthetic methodology it was necessary to synthesise materials with a different central block unit (Figure 4.1 & 4.2). This would also allow the measurement of redox potentials for oligomeric species that did not include 3,3'-dimethoxybenzidine (**2.19**) for the first time. As noted previously, 4,4'-(1,3,4-oxadiazole-2,5-diyl)dianiline was identified as a suitable electron rich diamine to construct viologen oligomers. Gratifyingly, the synthesis of viologen dimer **4.17** proceeded smoothly by the addition of two equivalents of **3.8** and one equivalent of aromatic diamine **4.9** to give the product in 41% yield after a single recrystallization from water.



Scheme 4.6. Synthesis of dimer **4.17**.

The success of this reaction was verified from analysis of the $^1\text{H-NMR}$ spectrum (Figure 4.5). This did not contain the signals which correspond to the 2,4-dinitrophenyl group at 8.21 ppm in the starting material (**3.8**). In addition, the observed 1:1 integral ratio between the doublet corresponding to the proton H_f 8.59 ppm and singlet H_g at 8.73 ppm is as expected for the target molecule.

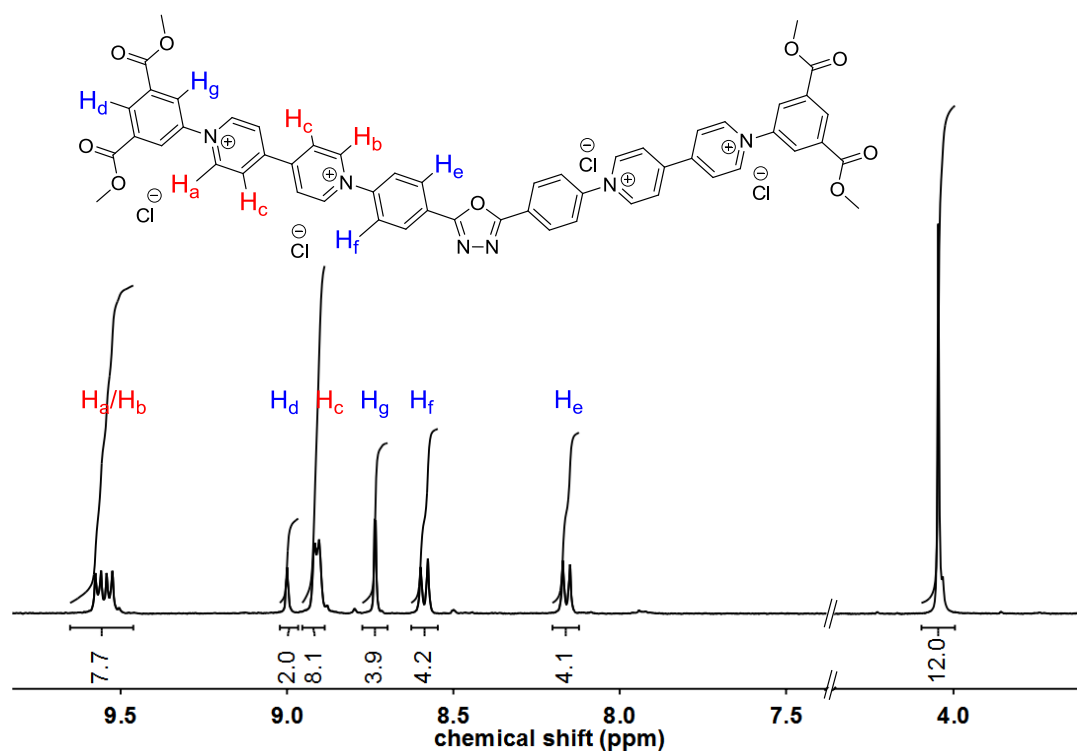


Figure 4.5. ¹H NMR spectrum of dimer 4.17 in D₂O.

4.3. Cyclic voltammetry and Square wave voltammetry

The CV data for all the newly synthesized systems were obtained using the same conditions as described in chapter 3. The data for the monomeric and dimeric series of viologen compounds are presented first. The data is split into three sections to allow for the qualitative comparison between members of each series which vary by: i) the number of electron withdrawing residues on the end group, ii) the number of electron donating residues on the end group, iii) the number of fused aromatic rings; as set out in figure 4.2. This section concludes by combining all this CV data to produce a model for predicting the half wave potentials of viologen species with aromatic substituents containing varying substituents and substitution patterns.

4.3.1.1. CV data for monomeric and dimeric viologen species with varying numbers of ester residues on the end group

Figure 4.5 presents CV and SWV voltammograms for monomeric and dimeric viologen species with varying numbers of ester residues on the end groups. Each of these molecules exhibit two distinct reversible redox events. The $E_{1/2}$ values were measured by taking the average of the forward and reverse peak potential, and are listed in Table 4.3.

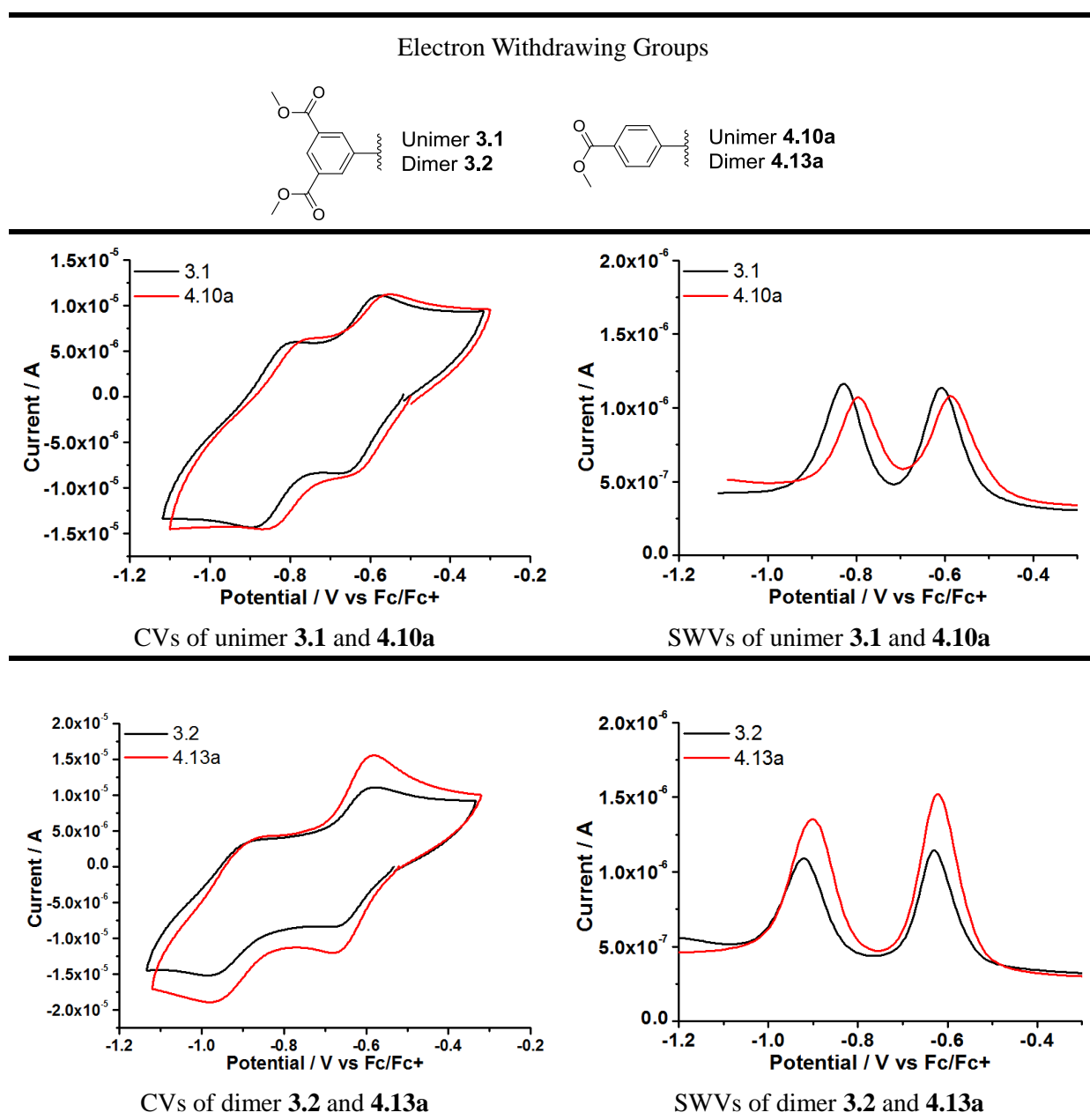


Figure 4.5. Cyclic voltammograms and squarewave voltammograms of 0.2 mM of unimer 3.1 and 4.10a; dimer 3.2 and 4.13a at a glassy carbon disc ($d = 2$ mm) electrode in anhydrous DMF at $\nu = 500$ mV s⁻¹.

Table 4.3. Cyclic voltammetric halfwave potentials observed on a glassy carbon disc (d = 2 mm) electrode in anhydrous DMF at $\nu = 500 \text{ mV s}^{-1}$.

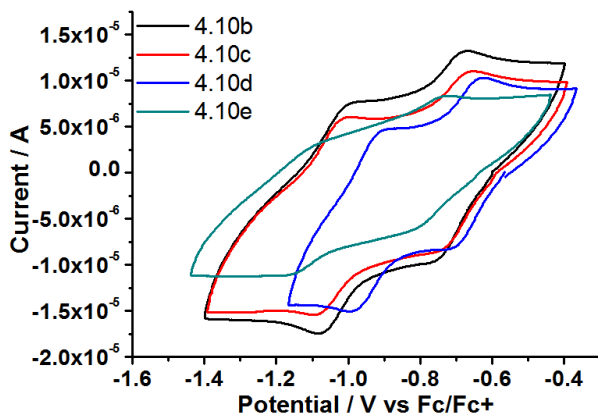
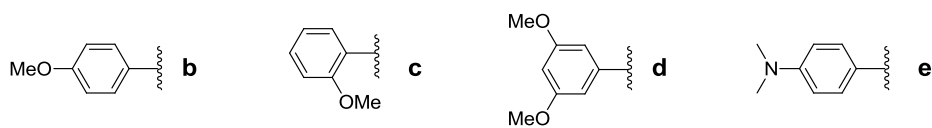
	CV = 0.5 V s^{-1} $E_{1/2}^1$ (V) vs Fc/Fc ⁺	CV = 0.5 V s^{-1} $E_{1/2}^2$ (V) vs Fc/Fc ⁺
Unimer 3.1	-0.630	-0.840
Unimer 4.10a	-0.583	-0.794
Dimer 3.2	-0.629	-0.921
Dimer 4.13a	-0.619	-0.900

The unimers and dimers containing a single ester on the endgroups (**4.10a** and **4.13a**, respectively) underwent each reduction step at less cathodic potentials than the corresponding monomer and dimer which contained two ester residues on their endgroups (**3.1** and **3.2** respectively). From inspection of the half wave values, this cannot simply be rationalised by the number of electron-withdrawing substituents on the molecule, but it is also dependent on the substitution positions of the ester on the aromatic endgroups.

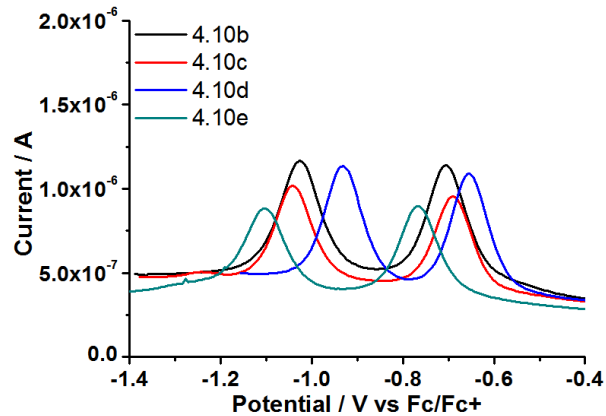
4.3.1.2. CV data for monomeric and dimeric viologen species with varying electron rich end groups

Figure 4.6 summarises the CV and SWV data for the monomers **4.10b-e** and dimers **4.13c** and **4.13d**. Each of these contains endgroups with varying degrees of electron-rich substituents.

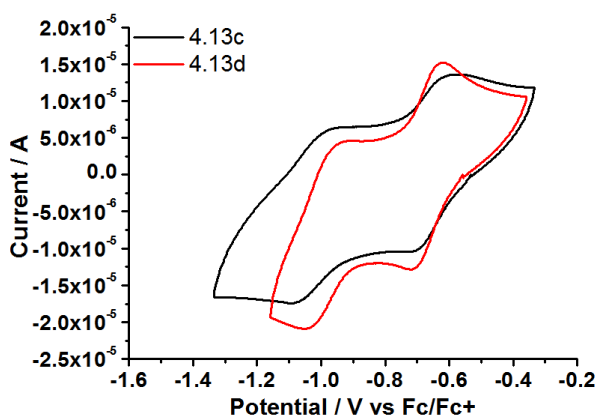
Electron Donating Groups



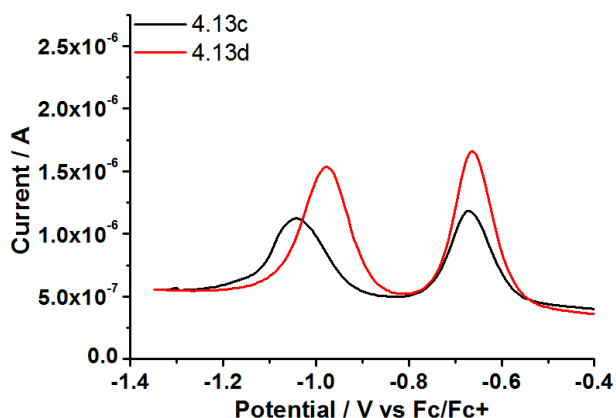
CVs of unimer **4.10b**, **4.10c**, **4.10d** and **4.10e**



SWVs of unimer **4.10b**, **4.10c**, **4.10d** and **4.10e**



CVs of dimer **4.13c** and **4.13d**



SWVs of dimer **4.13c** and **4.13d**

Figure 4.6. Cyclic voltammograms and squarewave voltammograms of 0.2 mM of unimer **4.10b**, **4.10c**, **4.10d** and **4.10e**; dimer **4.13c** and **4.13d** at a glassy carbon disc ($d = 2$ mm) electrode in anhydrous DMF at $v = 500$ mV s^{-1} .

Table 4.4. Cyclic voltammetric half-wave potentials observed on a glassy carbon disc (d = 2 mm) electrode in anhydrous DMF at $v = 500 \text{ mV s}^{-1}$.

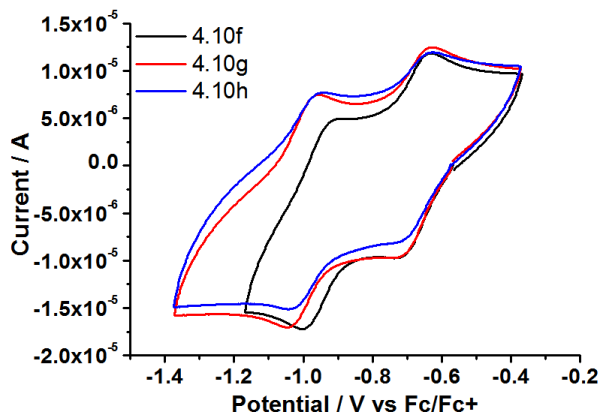
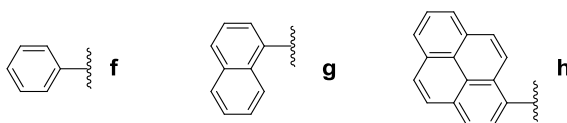
	CV = 0.5 V s^{-1} $E_{1/2}^1$ (V) vs Fc/Fc ⁺	CV = 0.5 V s^{-1} $E_{1/2}^2$ (V) vs Fc/Fc ⁺
Unimer 4.10b	-0.705	-1.026
Unimer 4.10c	-0.689	-1.041
Unimer 4.10d	-0.654	-0.931
Unimer 4.10e	-0.770	-1.107
Dimer 4.13c	-0.669	-1.046
Dimer 4.13d	-0.660	-0.976

As expected, all the monomeric and dimeric viologen species within this series exhibited two distinct reversible redox behaviours. The first and second half wave potentials of these monomers and dimers (**4.10b-e** and **4.13c-d**) all occur at more cathodic potentials than observed for the systems containing electron withdrawing groups (Table 4.3). This demonstrates that the presence of the electron donating endgroups serves to increase the energy required to reduce the viologen species when compared to the energy required to reduce the ester containing compounds. However, within the series of methoxy substituted viologen molecules, the molecule containing two methoxy groups (**4.10d**) is *easier* to reduce than either of the monomethoxy species (**4.10b** and **4.10c**). Therefore, the reduction potential trend is not simply related to the number of electron withdrawing/donating groups, but clearly also dependent on the substitution pattern of the endgroups.

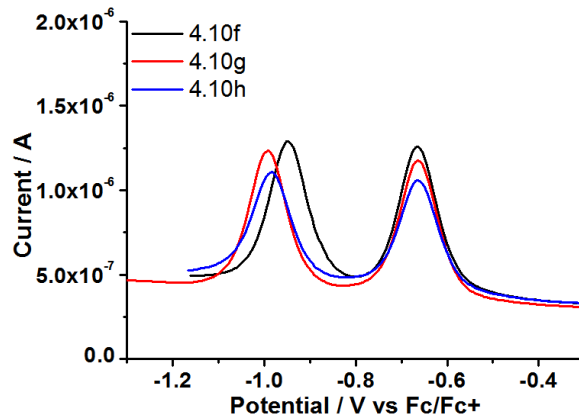
4.3.1.3 CV data for monomeric and dimeric viologen species with varying numbers of fused aromatic rings residues on the end group

CV data for the third series of monomeric and dimeric viologen containing endgroups with varying numbers of fused aromatic rings is presented in Figure 4.7 and Table 4.5.

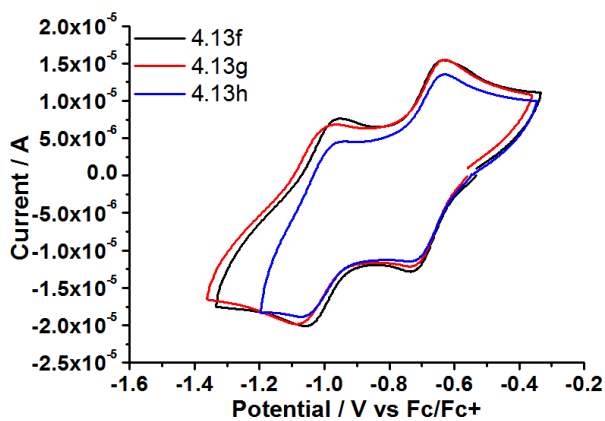
Number of Benzene rings



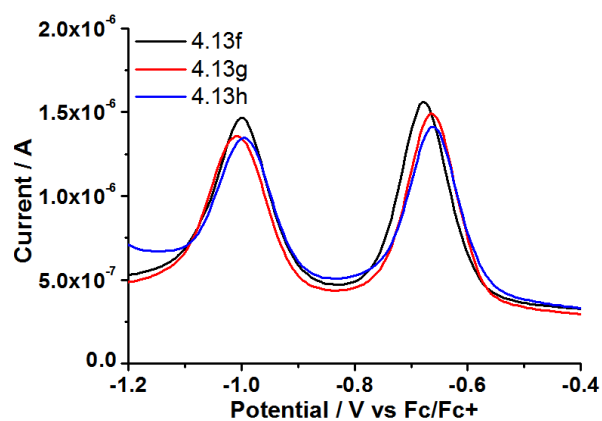
CVs of unimer **4.10f**, **4.10g** and **4.10h**



SWV of unimer **4.10f**, **4.10g** and **4.10h**



CVs of dimer **4.13f**, **4.13g** and **4.13h**



SWV of dimer **4.10f**, **4.10g** and **4.10h**

Figure 4.7. Cyclic voltammograms and squarewave voltammograms of 0.2 mM solutions of unimers **4.10f**, **4.10g** and **4.10h**; and dimers **4.13f**, **4.10g** and **4.13h** at a glassy carbon disc ($d = 2$ mm) electrode in anhydrous DMF at $v = 500$ mV s^{-1} .

Table 4.5. Cyclic voltammetric halfwave potentials observed on a glassy carbon disc (d = 2 mm) electrode in anhydrous DMF at $v = 500 \text{ mV s}^{-1}$.

	CV = 0.5 V s^{-1} $E_{1/2}^1$ (V) vs Fc/Fc ⁺	CV = 0.5 V s^{-1} $E_{1/2}^2$ (V) vs Fc/Fc ⁺
Unimer 4.10f	-0.664	-0.946
Unimer 4.10g	-0.664	-0.991
Unimer 4.10h	-0.664	-0.981
Dimer 4.13f	-0.679	-0.996
Dimer 4.13g	-0.664	-1.007
Dimer 4.13h	-0.659	-0.996

As can be seen in Table 4.5, the first reduction potential for each of these species (**4.10f-h** and **4.13f-h**) is relatively invariant (approximately -0.66V) and falls approximately between the average of the first half wave potential for the electron-withdrawing (-0.61 V) and electron-donating series of molecules (-0.70 V).

4.3.1.4. Summary of half wave potentials for all of the monomeric and dimeric viologen species.

Figure 4.8 summarizes the first and second $E_{1/2}$ values measured for the 9 unimers. There is a considerable change in first (-0.583 to -0.770 V) and second (-0.794 to -1.107 V) reduction potentials across the series approximately progressing from systems with highly electron withdrawing substituents to those with more electron donating substituents. It is clear, therefore, that there is qualitative relationship between the nature of the endgroups and the half wave potential of the viologen reduction potentials. This is explored in more detail in the next section.

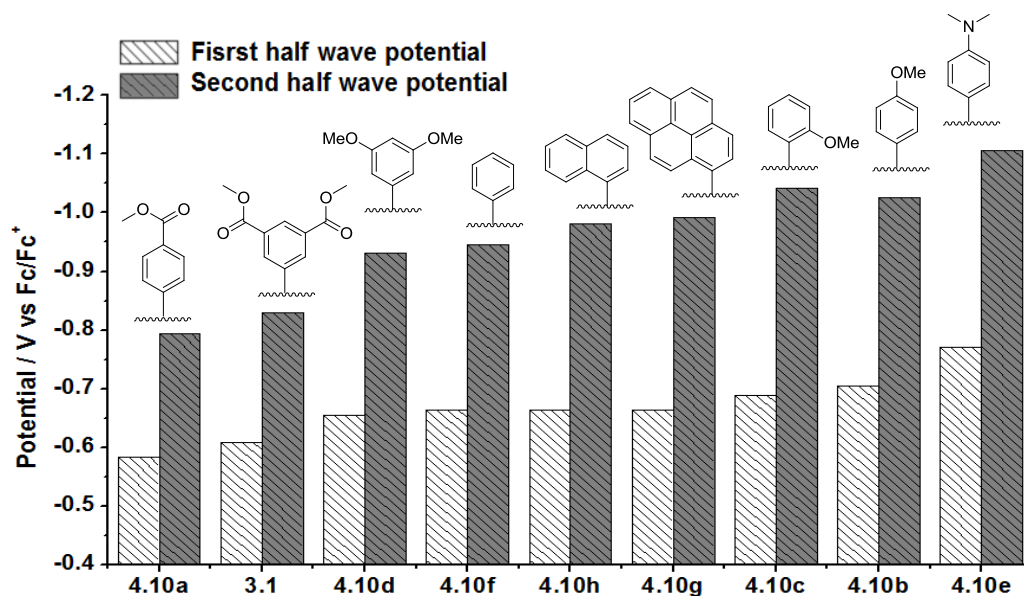


Figure 4.8. Plot showing these two half wave potentials of unimers with various substituted end groups, obtained from CV experiments.

Figure 4.9 summarizes the first and second $E_{1/2}$ values shown for the dimers. There is a relatively small change in first reduction potentials (-0.619 to -0.679 V). However, the observed redox properties of this system exhibit a slightly different trend when compared to the relationship in the monomeric system (Figure 4.8). From inspection of the dimeric structures, this may be rationalised by considering that the central block unit also affects the redox potentials in the dimeric species. Therefore, the reduction potential trend in the dimeric system is not simply related to the nature of the endgroups, but also depends on the central block units.

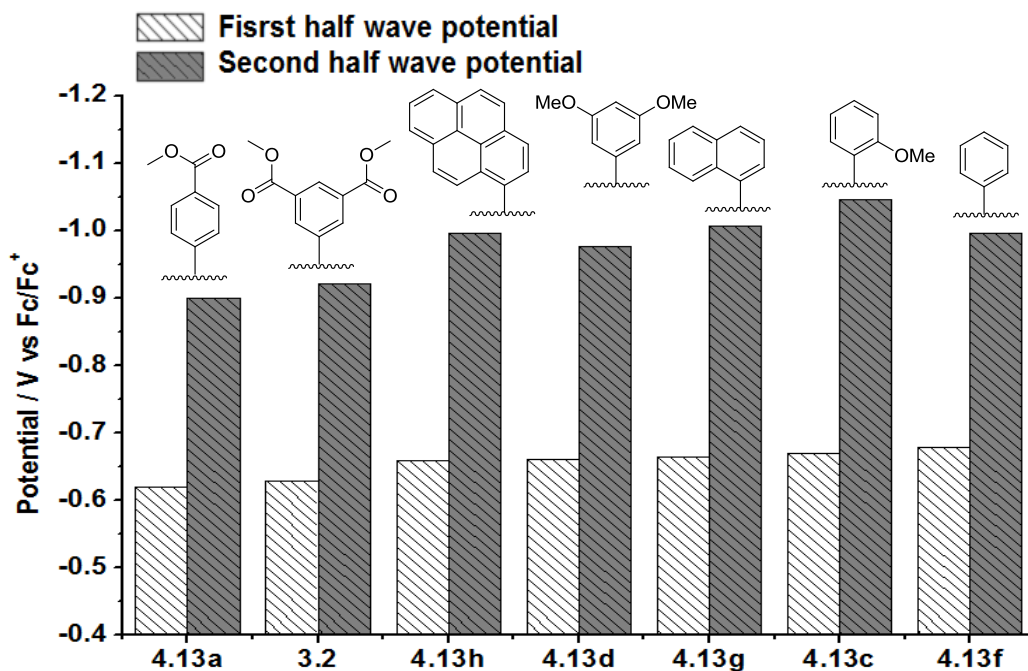


Figure 4.9. Plot showing two half wave potentials of dimers with various substituted end groups, obtained from CV experiments

4.3.2. Correlation of pK_b values with half wave potentials ($E_{1/2}$) of viologen species having aromatic groups containing varying substituents.

Estimates for the reduction potentials of viologen based species have been made using data from SEC-UV/vis spectra used in conjunction with the Nernst equation.^{195,196} However, these methods are frequently experimentally complex and time-consuming. Therefore, we were keen to explore the possibility of using easy and non-computationally intensive methods to estimate the electron donating ability of the endgroups and mid-blocks. This may also enable the prediction of the reduction potentials of these aromatic substituted viologen species. For substituted aromatic systems, the electron-donor character of the structure can be estimated using Hammett parameters. However, these empirical values do not work for *ortho* substituted aromatic species, and therefore cannot be used to approximate all of our systems (e.g. **4.10c** and **4.13c**).

In contrast to Hammett parameters, pK_b values could be used to give an approximate value for

the electron donating ability of the starting aromatic amines. Fortunately, pK_b values can now be easily estimated using one of many online tools, for example, the ACE and JChem acidity and basicity calculator. (<https://epoch.uky.edu/ace/public/pKa.jsp>) This tool has been validated and used by many researchers to estimate the pK_a and pK_b values of molecules.^{197–199} Using this program, the pK_b values of the nitrogen of the aniline (shown in Figure 4.2) were calculated and are presented in Table 4.6.

Table 4.6. pK_b values of N atom in each starting aromatic amine calculated using the ACE and JChem acidity and basicity calculator.

Aromatic amine	pK_b values (ACE and JChem acidity and basicity calculator)
3.7	1.30
4.1	2.70
4.2	5.10
4.3	4.40
4.4	3.50
4.5	6.10
4.6	4.60
4.7	4.10
4.8	4.00

The half wave potentials for each monomeric viologen (Figure 4.8) were plotted as a function of the calculated pK_b value (Table 4.10). It can be seen that the correlation is essentially linear ($R^2 = 0.8$). The negative slope of the plot shows that monomers containing more basic (electron-donating) amine endgroups are more difficult to reduce.

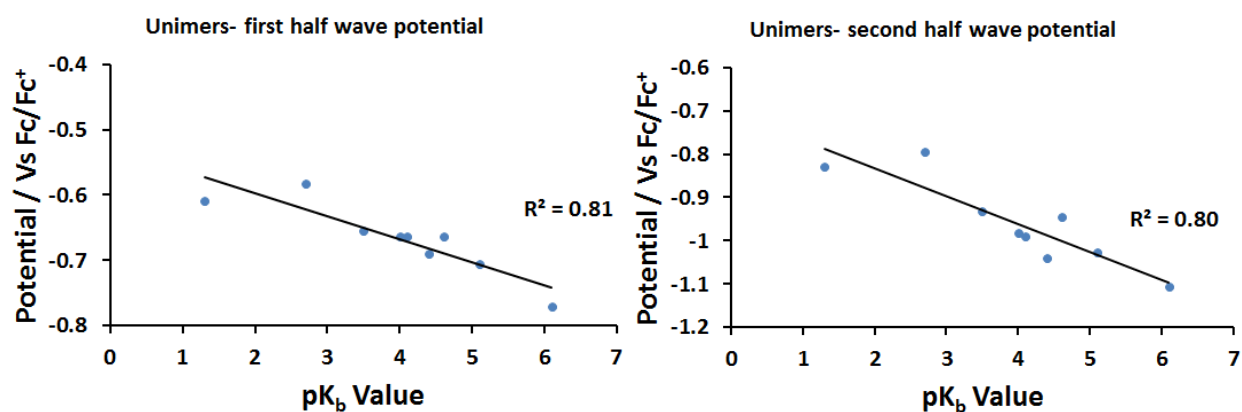


Figure 4.10. Plot of the pK_b of N atom of each aromatic amine against the corresponding half wave potentials of unimers.

Although there is a smaller variation in $E_{1/2}$ values across the series of dimers produced, we were interested to see if the relationship between pK_b and $E_{1/2}$ values extended to these more complex molecules. Inspection of the dimer structures shows that the viologen in each dimer is connected to the midblock through one pyridinium nitrogen and to the end group through the outermost pyridinium ion. Therefore we decided to average the pK_b for the amine on the midblock (pK_b = 4.3) and end group (Table 4.6) to provide an estimate for the combined electron donating ability of the substituents at either end of the viologen (Table 4.7).

Table 4.7. The average pK_b values of N atom in each starting aromatic amine and central block unit which were calculated by ACE and JChem acidity and basicity calculator.

Dimer	Aromatic amine	Average pK _b values of central and terminal units (ACE and JChem acidity and basicity calculator)
3.2	3.7	2.85
4.13a	4.1	3.55
4.13c	4.3	4.40
4.13d	4.4	3.95
4.13f	4.6	4.50
4.13g	4.7	4.25
4.13h	4.8	4.20

Plots of experimentally determined first and second $E_{1/2}$ values for the dimers as a function of the average pK_b value are shown in Figure 4.11. In this case, a weaker ($R^2 \approx 0.72$) but still linear correlation was observed for both the two $E_{1/2}$ values against the pK_b . This correlation shows the same relationship between pK_b values with $E_{1/2}$ values as unimers, where lower average pK_b values result in less cathodic $E_{1/2}$ values.

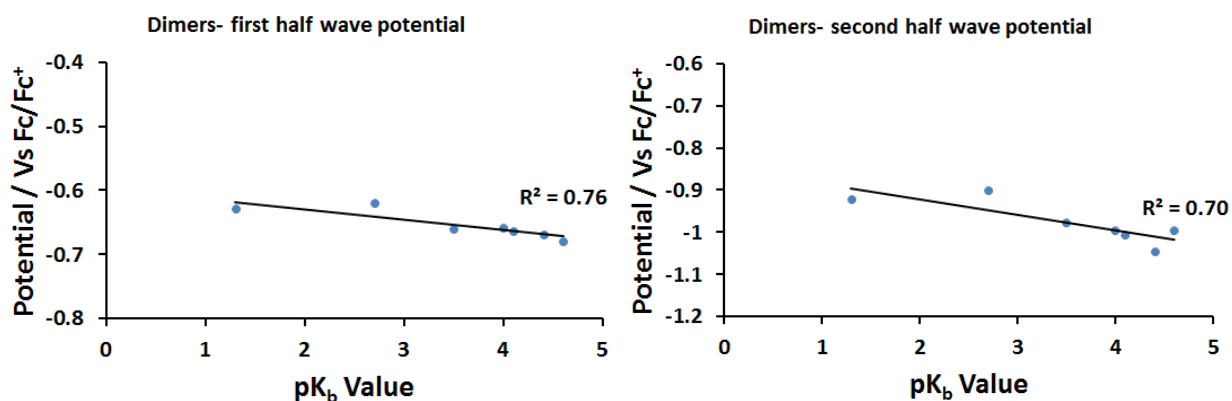


Figure 4.11. Plot of the average pK_b against the corresponding half wave potentials of dimers.

Although not exact, the correlation between pK_b (or average pK_b) values and $E_{1/2}$ potentials holds for even structurally complex systems. Therefore this result will enable the prediction of $E_{1/2}$ values for viologen species prior to their synthesis. This could be of great use in designing systems that are to be used in nano-machines,^{200,201} ECD^{135,149,150} and in catalysis.^{202–205}

4.3.4 CV data trimeric viologen species with different end groups

To provide a structural contrast to the ester terminated series of viologens presented in chapter 3, unimer **4.10d** and dimer **4.13d** and trimer **4.16** are terminated with electron-donating functionalised aromatic rings, as shown in Figure **4.12**.

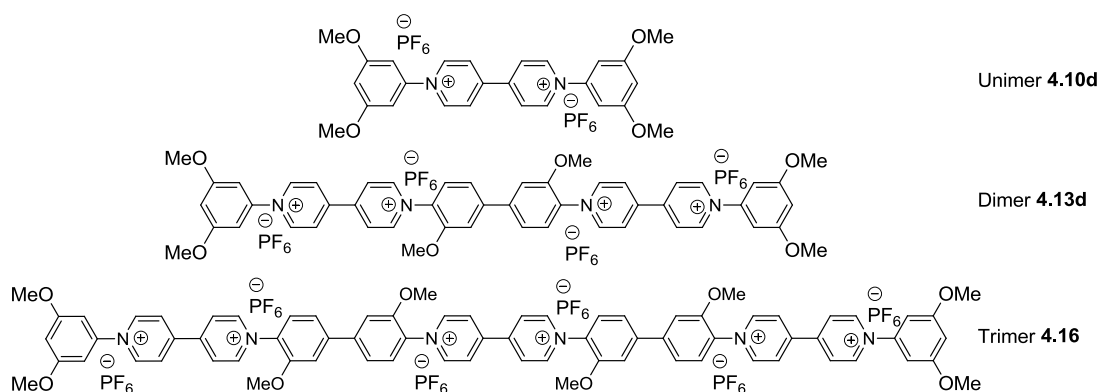


Figure 4.12. Structures of unimer **4.10d** and dimer **4.13d** and trimer **4.16**.

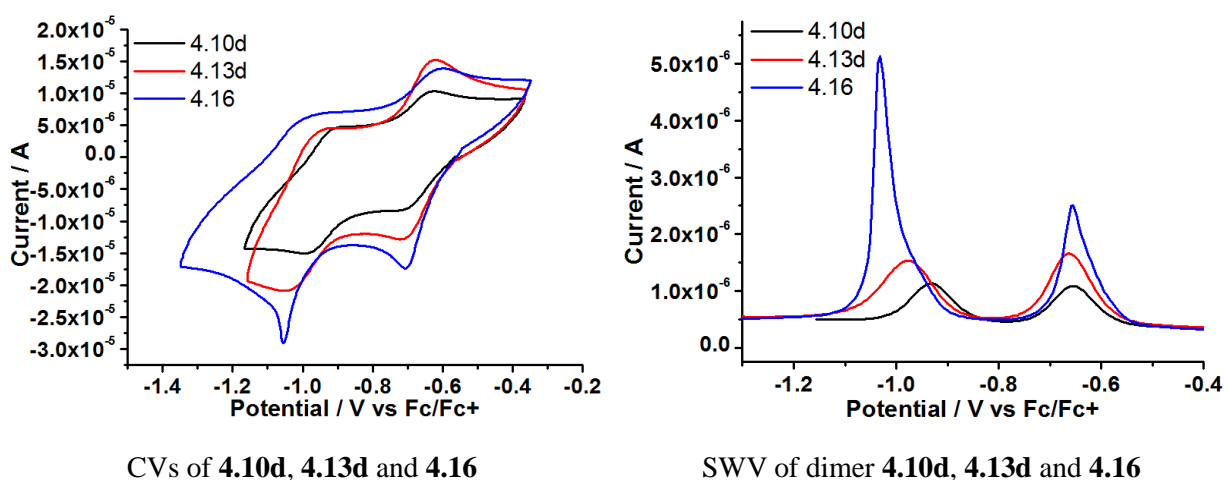


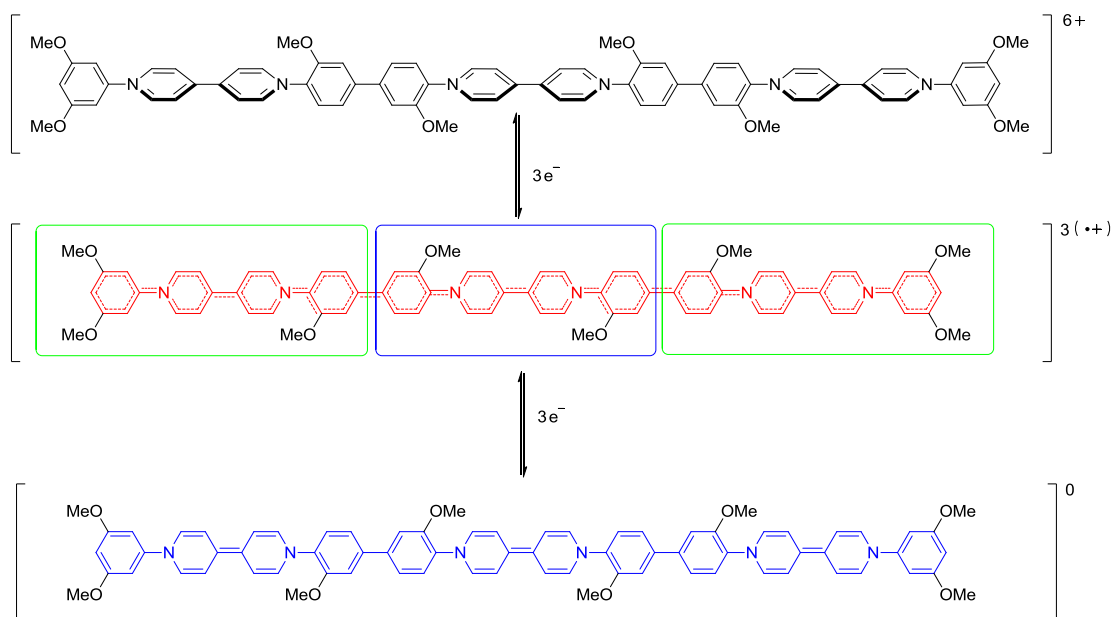
Figure 4.13. Cyclic voltammograms and squarewave voltammograms of 0.2 mM compounds **4.10d**, **4.13d** and **4.16** at a glassy carbon disc ($d = 2$ mm) electrode in anhydrous DMF at $v = 500$ mV s⁻¹.

Table 4.8 Cyclic voltammetric half wave potentials observed on a glassy carbon disc ($d = 2$ mm) electrode in anhydrous DMF at $v = 500$ mV s⁻¹.

	CV = 0.5 V s ⁻¹ $E_{1/2}^1$ (V) vs Fc/Fc ⁺	CV = 0.5 V s ⁻¹ $E_{1/2}^2$ (V) vs Fc/Fc ⁺
Unimer 4.10d	-0.654	-0.936
Unimer 3.1	-0.630	-0.840
Dimer 4.13d	-0.664	-0.981
Dimer 3.2	-0.629	-0.921
Trimer 4.16	-0.674	-1.051
Trimer 3.3	-0.660	-1.060

Figure 4.13 shows the CVs and SWVs of the series of compounds containing two electron donating methoxy residues on the terminal endgroups (**4.10d**, **4.13d** and **4.16**, respectively). A similar trend was observed during the reduction from the radical cationic species to quinoidal forms as was seen in the series **3.1**, **3.2**, **3.3** (chapter3): as the oligomer chain length increases, the second $E_{1/2}$ tends to move to a more negative value (Table 4.8). Comparison of the first and second $E_{1/2}$ for each unimer (**4.10d** and **3.1**), dimer (**4.13d** and **3.2**) and trimer (**4.16**, **3.3**) shows that the oligomer that contained electron withdrawing ester groups underwent each reduction step at less cathodic potentials than the corresponding oligomers which contained two electron donating methoxy residues. This may be accounted for by considering the pK_b values of the amine endgroups. The pK_b for **3.7** (diester) was calculated to be 1.3 in comparison to **4.4** (dimethoxy) which was calculated to be 3.5. Even within these structurally large systems, the clear, if qualitative relationship between pK_b and $E_{1/2}$ still holds.

Notably, the redox behaviour of trimer **4.16** is different to that observed for trimer **3.3** (with ester endgroups). In trimer **3.3** (Section 3.2.5.2) the tris(radical cation) is reduced to the neutral species in two discrete steps. In contrast, the three radical cationic viologens in the tris(radical cationic) trimer **4.16** are reduced to their neutral forms at essentially the same potential. This may be attributed to the similar pK_b values of the aniline residues on the midblock ($pK_b = 4.3$) and end block ($pK_b = 3.5$). This results in the two terminal viologens and the central viologen species being in very similar electronic environments. (Scheme 4.7).



Scheme 4.7. The structures of the stable intermediates observed during the electrochemical interconversions of trimer **4.16**.

4.3.5 CV data for trimeric viologen species with a different central, block unit

As a final investigation in our series of oligomers, it was important to study the effect of changing the central unit, by measuring the redox potentials of viologen dimer **4.17**.

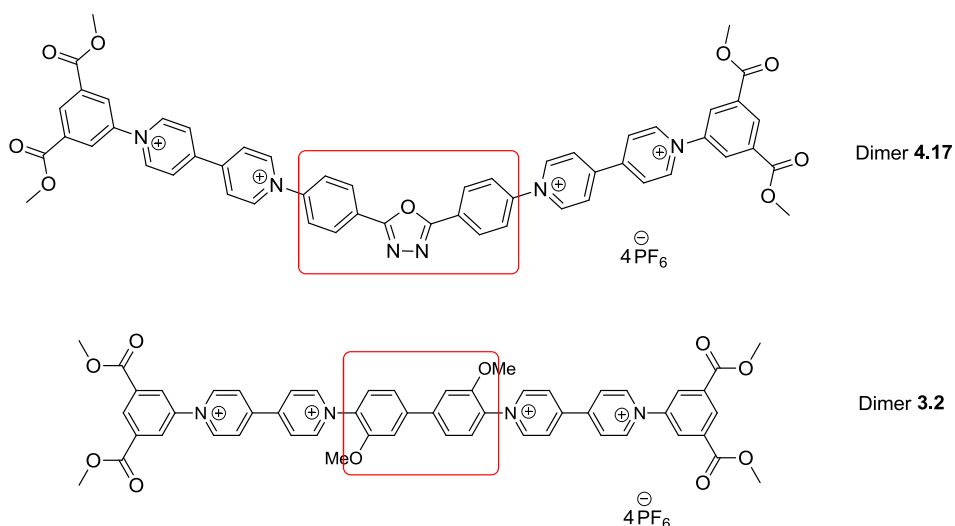


Figure 4.14. Structures of dimer **4.17** and dimer **3.2** with the central block units highlighted.

Prior to investigating the properties of the novel dimer, it was important to understand the electrochemical properties of the central block unit (Figure 4.14). 1,3,4-Oxadiazoles have been widely used as an electron transport materials or in the emitting layers of electro-luminescent devices. Therefore, structures of this type have been thoroughly studied during the last few decades. In 1996, the electrochemistry of 2,5-diphenyl-1,3,4-oxadiazole (**4.18**) was investigated by spectroelectrochemistry, cyclic voltammetry and EPR-spectroscopy. It was found that the first reduction is reversible, whereas the second reduction is irreversible due to decomposition of the central heteroaromatic ring.²⁰⁶

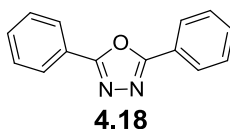
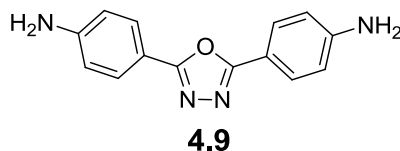


Figure 4.15. Structure of 2,5-diphenyl-1,3,4-oxadiazole (**4.18**).

Figure 4.14 shows the CV of 2,5-bis(4-aminophenyl)-1,3,4-oxadiazole **4.9**. In agreement with the electrochemical data reported for related compounds (see above), the first reduction is reversible. However, the second, irreversible reduction occurs at a significantly more negative value (- 2.5 V) than that of the second reduction potential of a typical viologen residue (c. -0.9 V see Figures 4.8 and 4.9), therefore the decomposition of the central block should not be a problem when investigating the dimer **4.17**.



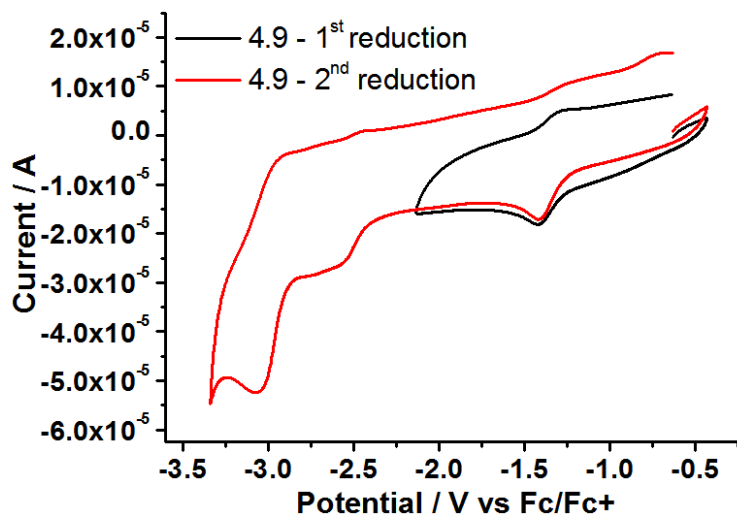


Figure 4.14. Cyclic voltammograms of 0.2 mM 4.9 at a glassy carbon disc ($d = 2$ mm) electrode in anhydrous DMF at $v = 500$ mV s^{-1} .

Figure 4.15 shows the CVs and SWVs of dimers 4.17 and 3.2; their half wave potentials are presented in Table 4.10.

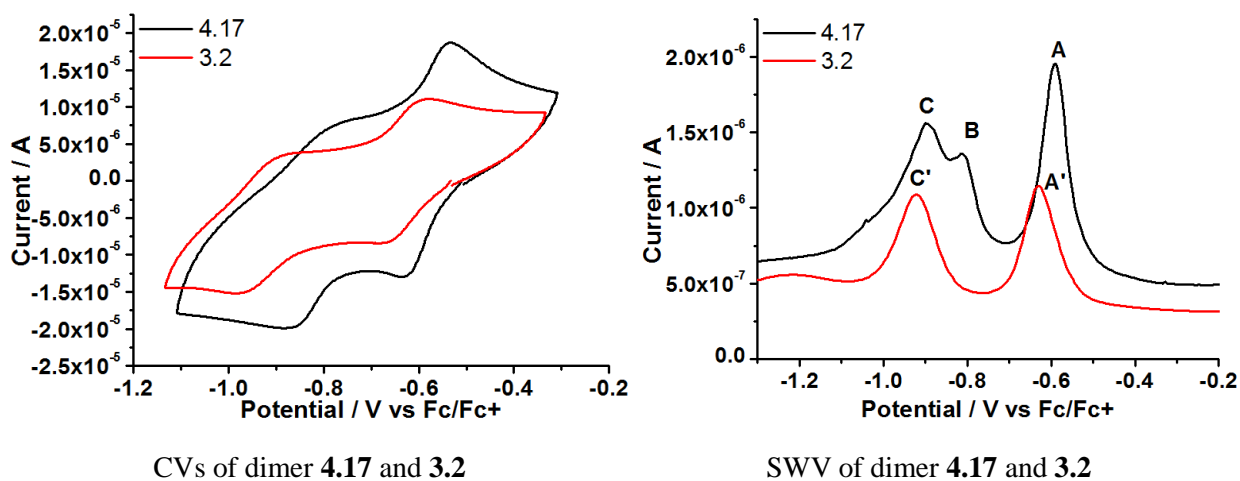
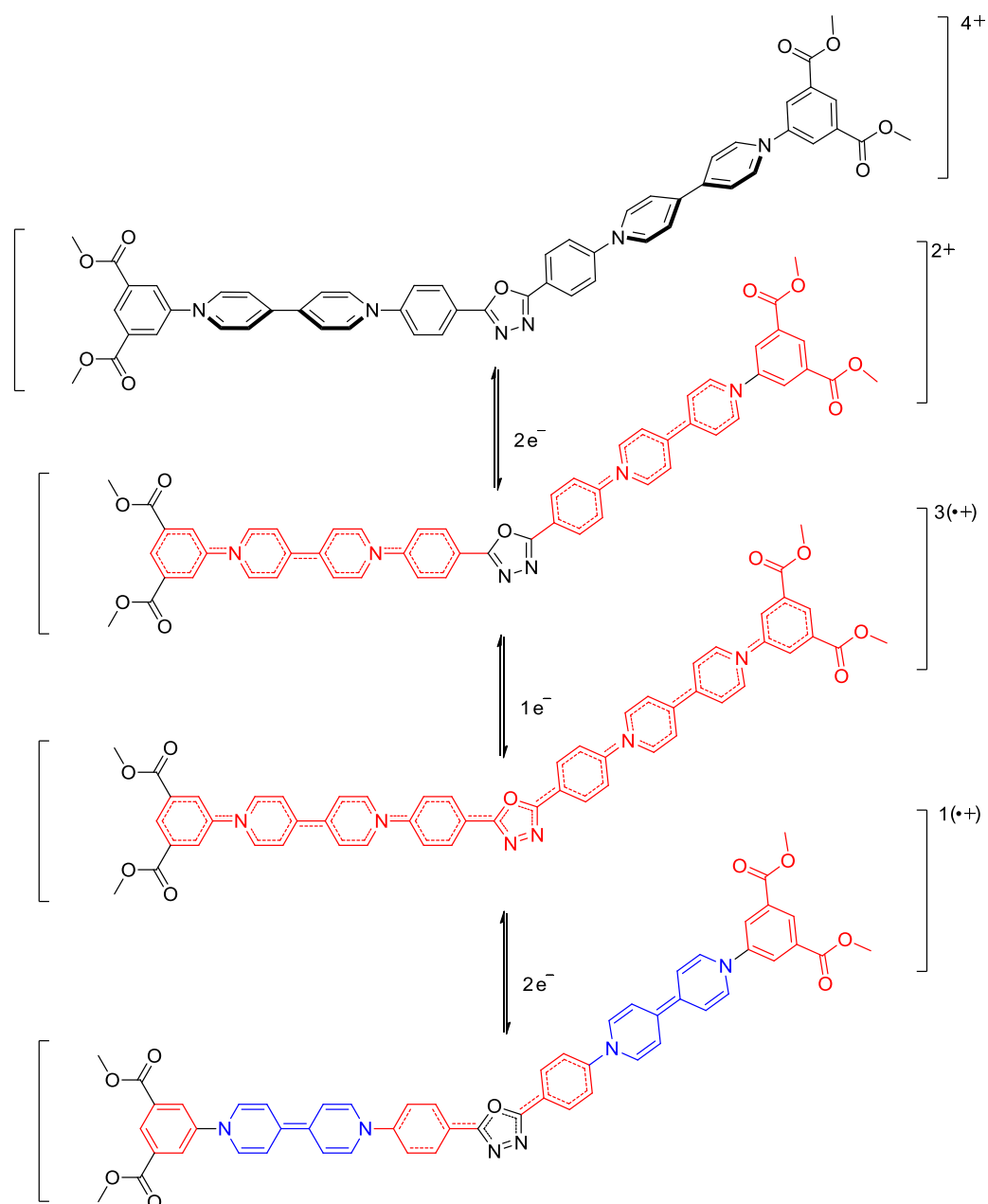


Figure 4.15. Cyclic voltammograms and square wave voltammograms of 0.2 mM compounds 4.17 and 3.2 at a glassy carbon disc ($d = 2$ mm) electrode in anhydrous DMF at $v = 500$ mV s^{-1} .

Table 4.10. Cyclic voltammetric halfwave potentials observed on a glassy carbon disc ($d = 2$ mm) electrode in anhydrous DMF at $v = 500$ mV s⁻¹.

Dimer 4.17 , SQW, $f = 10$ Hz E_p (V) vs Fc/Fc ⁺	Dimer 3.2 , SQW, $f = 10$ Hz E_p (V) vs Fc/Fc ⁺
-0.590	-0.630
-0.810	-
-0.900	-0.920

Under the same conditions, a square wave voltammogram of dimer **4.17** was acquired. Three distinct reduction events were resolved (signals A, B and C in Figure 4.15 and Table 4.10). Comparison of the E_p values of dimer **3.2** and **4.17** suggests the sequence of reduction steps for dimer **4.17** begins with the one-electron reduction for both viologen moieties (-0.59). The second process may be followed by the reduction of the mid-block unit (-0.81 V) before the final reduction of bis(radical cationic) viologens residues at -0.90 V to generate an ionic species that contains a negative charge (Scheme 4.8).



Scheme 4.8. The structures of the stable intermediates observed during the electrochemical interconversions of dimer 4.17.

4.3. Conclusion

In this chapter, a series of 4,4'-bipyridinium-based aromatic oligomers with different end groups or core groups have been synthesised and their electrochemical properties were investigated. As expected, all the compounds undergo reversible stepwise

two-electron reductions of each viologen moiety. Comparison of all of the unimers and dimers (Figure 4.8 and 4.9) shows a strong correlation between the half wave potentials and pK_b values of the amine residues of the endgroups: higher endgroup pK_b values increase the energy required to reduce the viologen species. The identification of this correlation over a broad range of aromatic end groups will allow the $E_{1/2}$ value of unmade systems to be predicted before synthesis.

In addition, this work has shown that the Zincke reaction can be used to synthesise dimers with different mid-blocks (e.g **4.17**). CV and SWV data for this dimer **4.17**, reveal three reversible redox processes. We propose that the first reduction occurs at the viologen residues forming the bis(radical cationic) state. The second event may be followed by the reduction of the middle block unit before the final reduction of bis(radical cationic) viologen residues to generate an ionic species that contains a negative charge.

Chapter 5

Synthesis, and electrochemical behaviour of a [2] pseudo-rotaxane incorporating the novel cyclophane: cyclobis(paraquat-*p-m*-terphenylene)

5.1. Introduction

Supramolecular chemistry harnesses non-covalent interactions between multiple molecules to assemble them in specific orientations in 3 dimensional space.^{207–210} A key feature of supramolecular interactions is that they are reversible in nature. They can assemble and disassemble multiple times without damaging the molecules that compose them.^{211,212} This property means that they can respond to an external stimulus e.g. heat or light.^{213,214} By altering the strength and orientation of the supramolecular interactions it is possible to change the properties of the material.²¹⁵ This process can produce materials with high value properties that cannot be easily made with conventional, covalently assembled materials.²¹⁶

One of the most well studied supramolecular interactions in supramolecular chemistry is hydrogen bonding,²¹⁷ which can bring smaller molecules together to generate self-assembled polymers.^{218–221} Typically, single hydrogen bonds are not strong enough to yield thermally stable self-assembled structures.^{222,223} To overcome this deficiency, significant effort has been focussed on increasing the binding strength between residues by producing systems with multiple complementary hydrogen bonds.^{224–235} Based on this design, in 1997, the Meijer group synthesised 2-ureido-4[1H]-pyrimidinone (UPy) (Figure 5.1).²³⁶ The UPy residue contains 4 complementary hydrogen bonds, and has become one of the most widely studied supramolecular systems developed to date. This self-complementary, quadruply hydrogen bonded system exhibits a binding energy of 42 kJ mol^{-1} , which means it self-associates at room temperature to form a dimeric system in solution (Figure 5.1).²³⁷

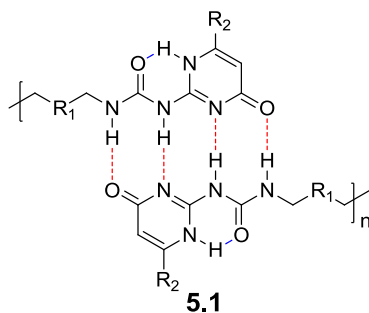
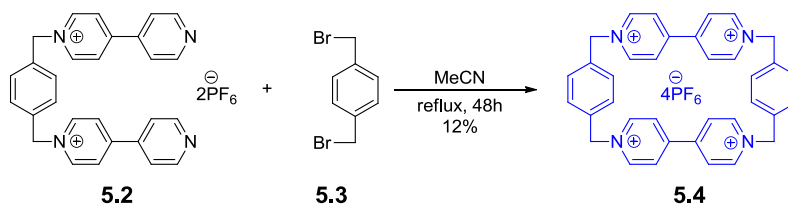
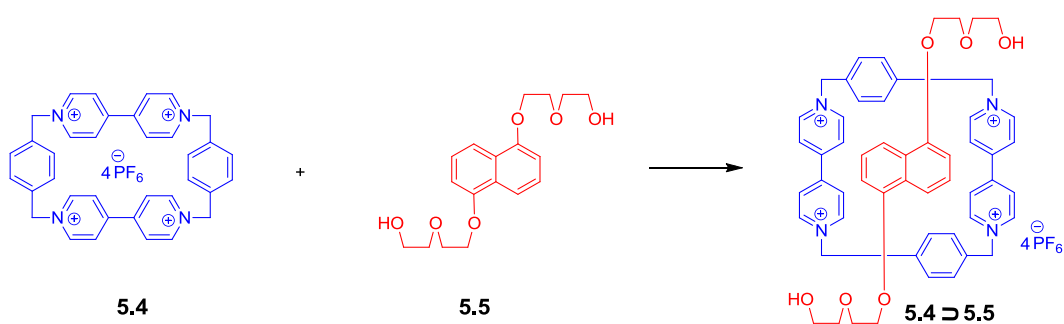


Figure 5.1. Supramolecular polymers based on ureido-pyrimidinone (UPy) end-groups.

Over recent years, numerous other non-covalent interactions have been built into supramolecular systems, such as cation- π interactions,²³⁸ anion- π interactions,²³⁹ π - π interactions,²⁴⁰ etc. Of particular importance to this chapter is the π - π interaction which occurs between aromatic rings where one is relatively electron rich and one is electron poor. The classic example of this is the complex formed between cyclobis(paraquat-*p*-phenylene) (CBPQT⁴⁺) **5.4**²⁴¹ and 1,5-dialkoxy naphthalenes **5.5** (Scheme 5.2).



Scheme 5.1. Synthesis of cyclobis(paraquat-*p*-phenylene) **5.4**.²⁴¹



Scheme 5.2. π - π interactions between cyclobis(paraquat-*p*-phenylene) **5.4** and 1,5-dialkoxy naphthalene **5.5**.²⁴²

This system has been thoroughly investigated by the Stoddart group, amongst others.²⁴² Their work has primarily focused on the construction of mechanically bonded systems including pseudorotaxanes,²⁴² rotaxanes,^{243–246} catenanes^{247–249} which have distinct features and topology as shown in Figure 5.2.



Figure 5.2. Schematic representation of a [2] pseudorotaxane, a [2] rotaxane and a [2] catenane.

As the synthesis of mechanically interlocked systems has progressed, it has been possible to produce supramolecular systems with two (or more) stable states (Figure 5.3). Through careful design it is possible to switch the system between these two stages in response to an external stimulus.

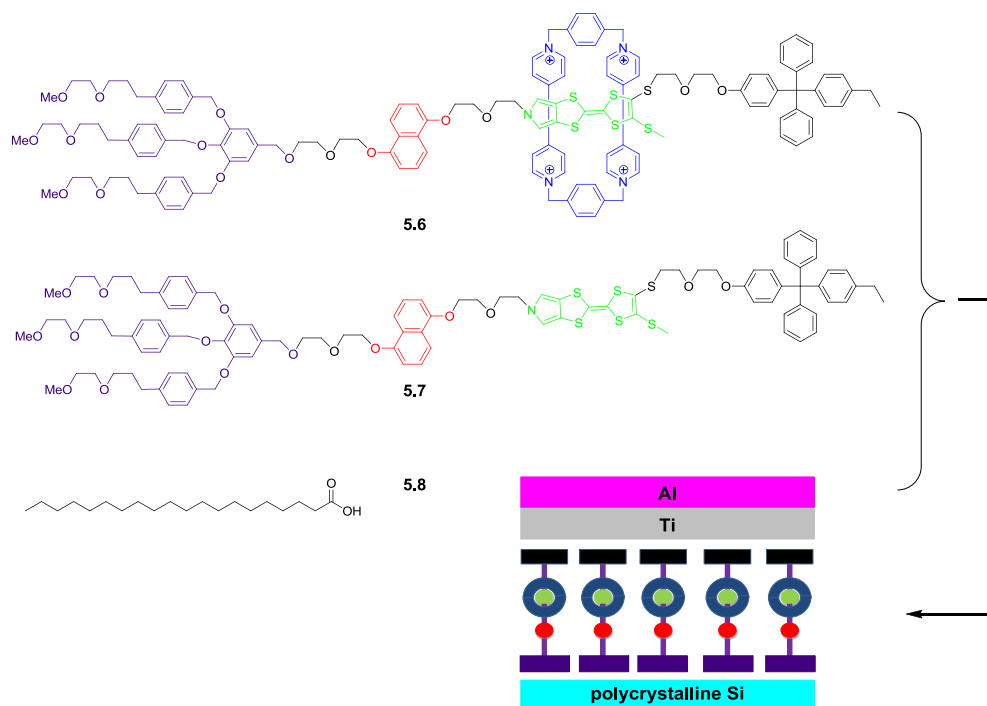


Figure 5.3. MSTJ devices fabricated by Stoddard from the amphiphilic bistable [2] rotaxane 5.6, the control dumb bell compound 5.7, and the simple control, eicosanoic acid 5.8, which consists of a molecule monolayer of the [2] rotaxane sandwiched between polycrystalline Si and metallic electrodes. This device can be switched reconfigurably and cycled repeatedly between ON and OFF states.²⁵⁰

This results in a molecular-level system that can be thought of as being in an ‘ON’ (1) or ‘OFF’ (0) state. The group have used this concept to produce systems that have the potential to act as molecular memory. Indeed, the Stoddart group developed a family of “molecular electronic devices” by using bistable rotaxanes. This work contributed towards the award of the Nobel Prize in 2016.

Although CBPQT⁴⁺ **5.4** has become one of the most widely studied cyclophanes in supramolecular chemistry it is susceptible to degradation from many common reagents. For example, under basic conditions, or in the presence of a multitude of nucleophiles, deprotonation of, or nucleophilic attack on, the benzylic methylene group leads to a number of rearranged and ring-opened products.^{251,252} This hinders the range of chemistries that can be carried out on systems containing **5.4**.

In an effort to produce more chemically stable viologen-containing cyclophanes, previous work by Stoddart, Greenland and Colquhoun has concentrated on the synthesis of 4,4'-bipyridinium-containing macrocycles such as **1.67**, **5.9**, **5.10** and **5.11** (Figure 5.4) which were all synthesised by exploiting the Zincke reaction (Scheme 1.8).

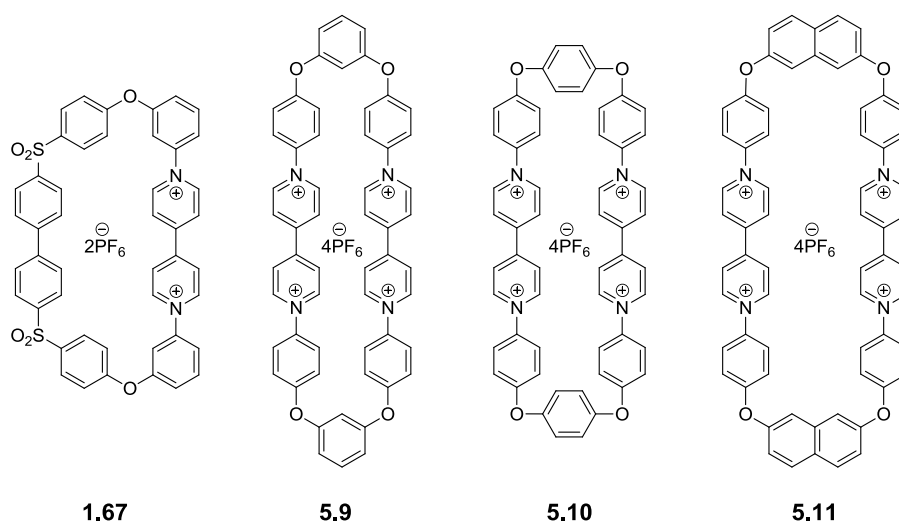
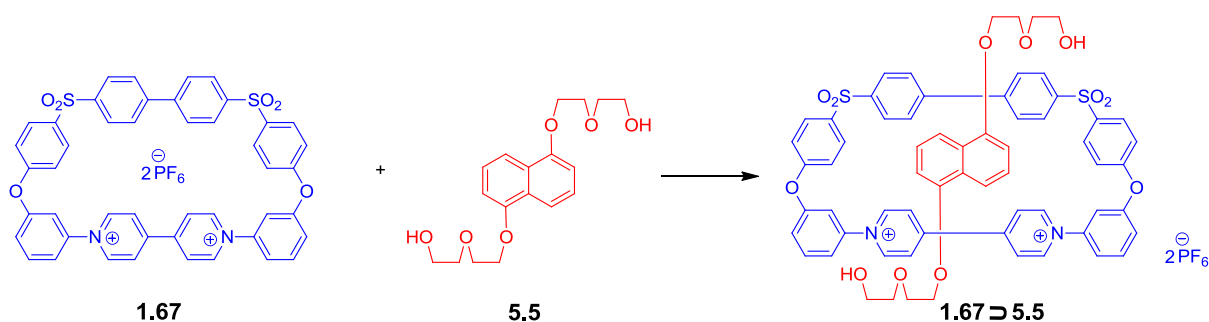


Figure 5.4. Structures of four chemically stable macrocyclic diarylbipyridinium salts reported by Stoddart, Greenland and Colquhoun.¹²⁵

The macrocycles were shown to be stable to a range of common bases and nucleophiles including pyridine, sodium methoxide, triphenylphosphine, and tetra-*N*-butylammonium iodide.¹²⁵

Macrocycle **1.67** was also shown to bind the electron-rich guest molecule **5.5**, (Scheme 5.3) as revealed by the significant upfield complexation shifts of the proton resonances corresponding to the 4,4'-bipyridinium unit in the macrocycle (up to 0.22 ppm).



Scheme 5.3. Assembly of a [2] pseudorotaxane based on macrocycle **1.67** and guest species **5.5**.¹²⁵

The binding properties of the complex **1.67**⊃**5.5** were investigated by ¹H NMR spectroscopy. It was found that the binding constant of this 1:1 complex in CD₃CN is 17 ± 1 M⁻¹, which is approximately 130 times lower than the 1:1 complex of bis-viologen containing receptor CBPQT⁴⁺ **5.4** with the same electron rich guest species **5.5** (2220 ± 240 M⁻¹).^{125,242} It was proposed that the difference in binding properties of **5.4** and **5.5** could be related to the number of viologen groups in the macrocycle and subtle changes in cavity diameter (**5.4**: 6.8 Å, **1.67**: 8.2 Å).

This previous work by Colquhoun and co-workers has shown that di-viologen type cyclophanes can be synthesized which do not contain the sp³ hybridised carbon, resulting in more chemically stable systems than **5.4**. However in each example produced to date the macrocycle contained ether linkages (Figure 5.4) resulting in a break of conjugation in the reduced, radical-cationic ring systems. Synthesising macrocycles that are fully conjugated in this state may open prospects for new and exciting redox responsive electronic properties.

This chapter reports the syntheses of a new fully π conjugated receptor containing two viologens and details its electrochemical and binding properties with electron rich 1,5-dialkoxy naphthalenes.

5.2. Results and Discussion

To meet the above criteria it was first necessary to design the aromatic diamine that would link the two viologens in the macrocycle. Previous computational design in the Colquhoun group has shown that the *m*-terphenylene diamine **5.17** has the correct nitrogen to nitrogen separation (c. 7.3 Å) to produce a cavity suitable for the inclusion of electron rich aromatic species. (Figure 5.5)

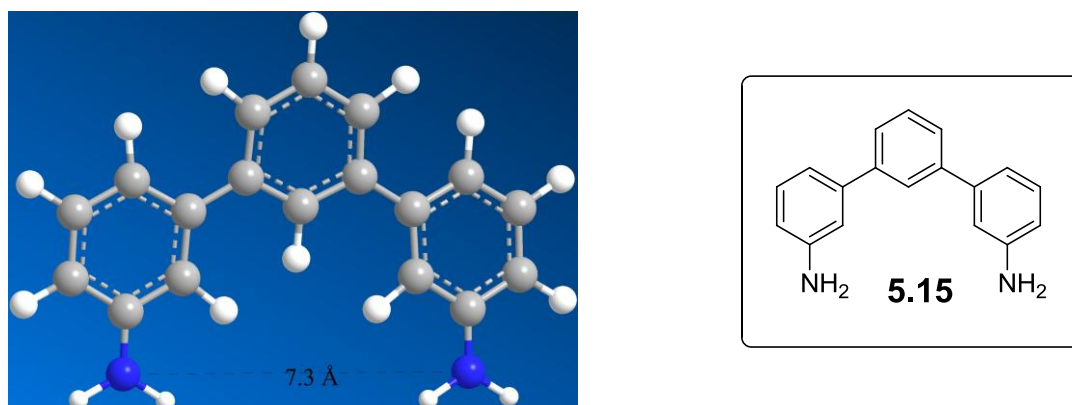
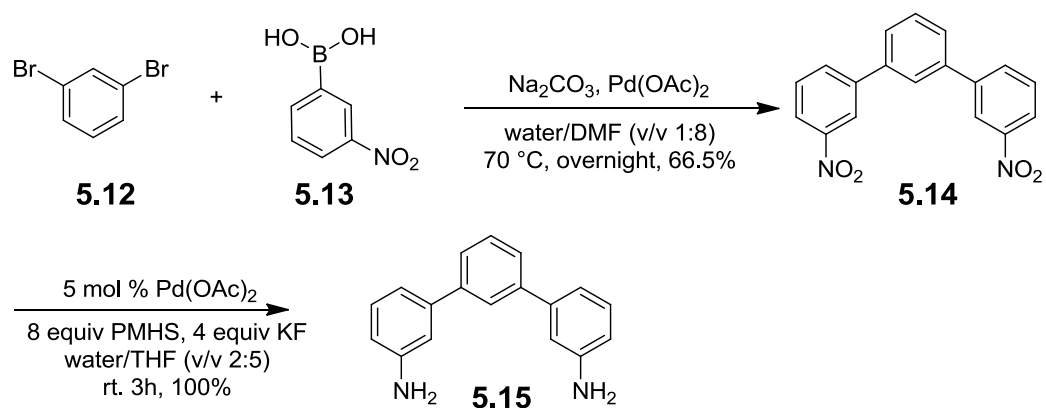


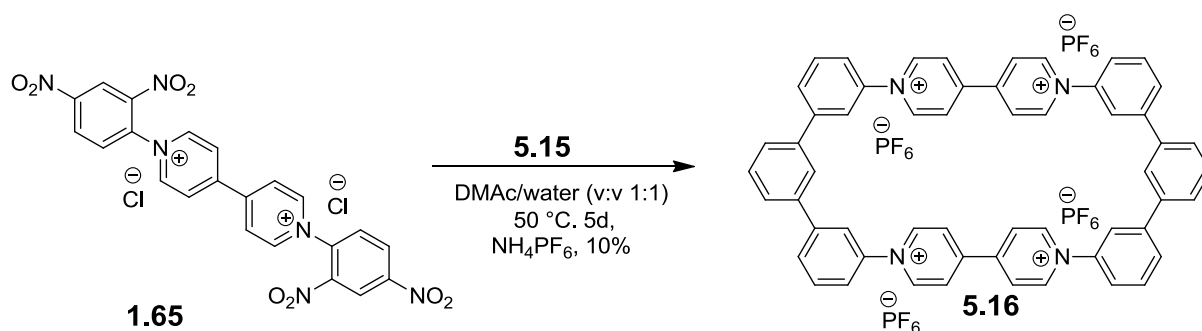
Figure 5.5. Energy minimised structure with selected N to N bond length of *m*-terphenylene diamine **5.15** using ChemBio 3D.

Synthesis of the aromatic diamine **5.15** was achieved by two steps in good overall yield (ca. 66%). Firstly, a dinitro intermediate (**5.14**) was synthesised by the reaction between one equivalent of 1,3-dibromobenzene **5.12** and two equivalents of 3-nitrophenyl boronic acid **5.15** under typical Suzuki conditions.²⁵³ Subsequently, the nitro groups were reduced to amino (**5.15**) using polymethylhydrosiloxane (PHMS) as the hydrogen source according to the procedure outlined by Rahaim, and Maleczka in 2005 (Scheme 5.4).²⁵⁴



Scheme 5.4. Synthesis of aromatic diamine **5.15** over two steps.^{253,254}

A four-component macrocyclization reaction was then carried out by condensation of Zincke salt **1.65** with **5.15** in a 1:1 ratio under high dilution conditions at 45 °C for 5 days (Scheme 5.5). After ion exchange with NH_4PF_6 , the product **5.16** was isolated by precipitating into a mixture of acetonitrile: acetone (10:90, v/v) in modest yield (10%) but excellent purity (over 99% by ^1H NMR, Figure 5.6).



Scheme 5.5. Synthesis of fully conjugated π -conjugated macrocycle **5.16**.

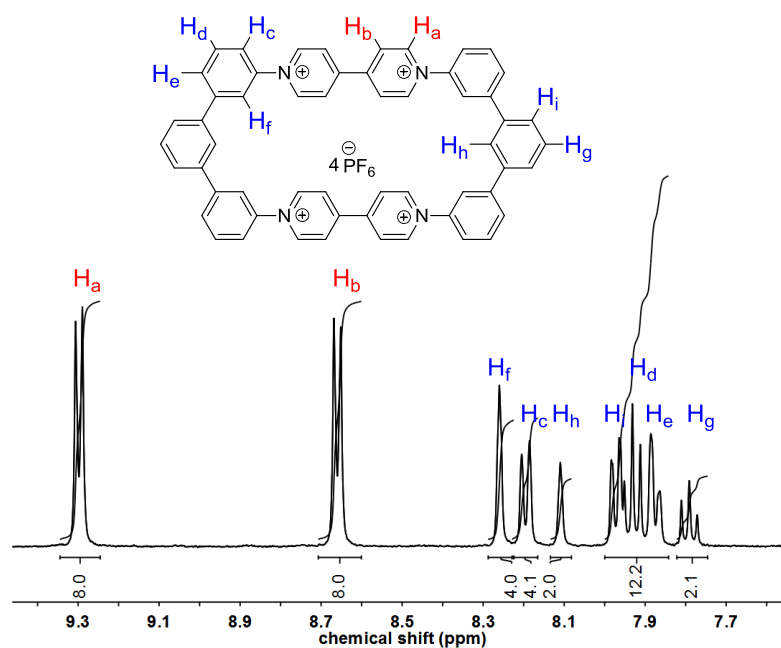


Figure 5.6. $^1\text{H-NMR}$ spectrum (acetone- d_3) of macrocycle **5.16**.

Crystals of **5.16** suitable for X-ray analysis were grown by slow vapour diffusion of acetone into acetonitrile solution. The solid state structure (Figure 5.7) shows a box-like conformation with two viologen units and two *m*-terphenyl residues. There is a 57.8° torsional twist angle between the two pyridinium rings of each viologen units, the bond angle of viologens with their associated *m*-terphenyl units is 53.4° whilst the torsion angle between the central and outer rings in the *m*-terphenyl units are both 33.6° (crystallographic mirror plane). In addition, the internal cavity of tetracationic macrocycle **5.16** (ca. 7.4 \AA) is in good agreement with that predicted (Figure 5.5) and therefore the new macrocycle should be suitable to bind to electron rich aromatic derivatives.

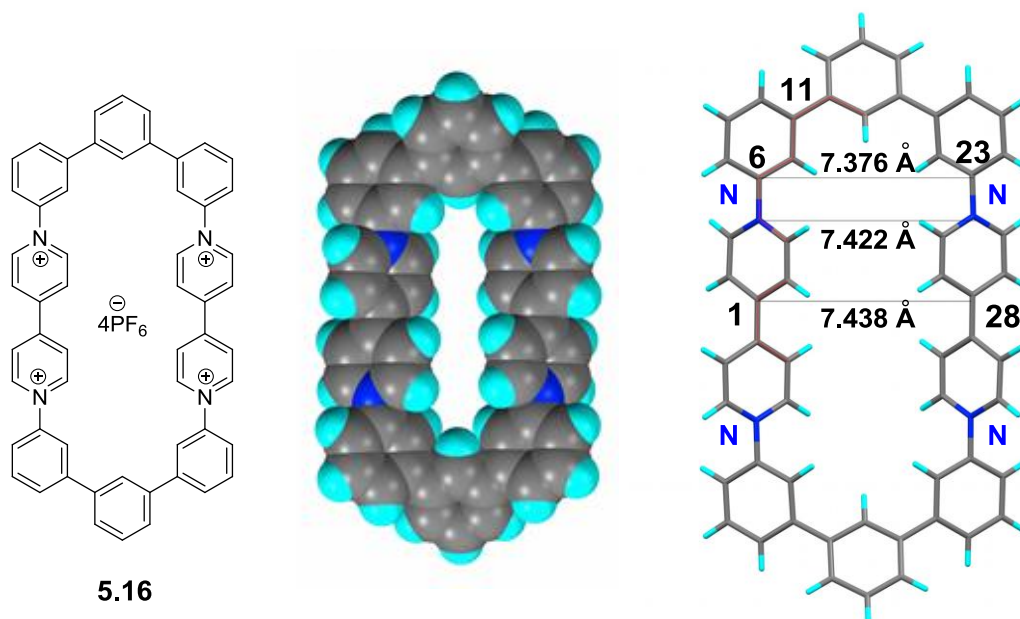


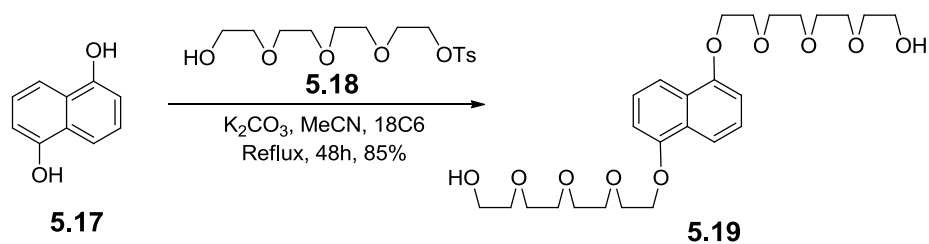
Figure 5.7. Single-crystal X-ray structure of tetracationic macrocycle **5.16** 4PF_6 in the solid state.

5.2.1. Binding studies of receptor **5.16** with π -electron rich 1,5-dioxynaphthalene derivatives.

The binding between viologen containing macrocycles and π -electron rich systems has formed the basis of supramolecular molecular chemistry for several decades. As a demonstration of the utility of our new macrocycle we selected the known dialkoxy naphthalene **5.19**²⁵⁵ as a simple starting point for our complexation studies. In addition to increasing the solubility of the naphthalene residues, it has been suggested that the oligoether groups can form hydrogen bonds with the relatively acidic protons on the pyridinium rings which assists complex formation.^{256,257}

5.2.1.1. Synthesis of 1,5-dialkoxy naphthalene **5.19**.

Following the procedure described by Basu and Stoddart *et al.* in 2011,²⁵⁵ reaction of 3 equivalents of monotosylated tetraethylene glycol **5.18** with 1 equivalent of 1,5-dihydroxynaphthalene **5.17** successfully generates the simple 1,5-dialkoxy naphthalene **5.19** in an excellent yield 85% (Scheme 5.6).



Scheme 5.6. Synthesis of 1,5-dialkoxy naphthalene **5.19**.²⁵⁵

5.2.1.2. ¹H-NMR binding studies of **5.19** to macrocycle **5.16**.

In order to study the host/guest binding, it was decided to assume the stoichiometry of this complex is 1:1, so the association constant of dialkoxy naphthalene **5.19** to receptor **5.16** could be determined by a ¹H NMR titration (Figure 5.8). This was achieved by the addition of increasing quantities of dialkoxy naphthalene **5.19** to a fixed concentration tetracationic macrocycle **5.16** in CD₃CN. As the concentration of the guest (**5.19**) increased there was a small but discernable upfield shift in the position of the resonances for the protons on the bipyridinium units. This suggests complex formation between the macrocycle and the guest. As shown in Figure 5.8, the protons on the viologens (H_a and H_b) shift downfield at low concentrations of guest, but then move upfield as the concentration of the guest increases further. These changes in chemical shift position with concentration of guest are not typical of the behaviour observed in related π - π stacked complexes.^{125,242} Although the reason for this is not clear, perhaps the macrocycle is undergoing as form of self-association in the absences of guest molecules, which is disrupted when the guest is added. However, protons H_f and H_h did exhibit a continuous downfield change in chemical shift value as a function of guest concentration and by fitting this data with “Bindfit”, (<http://app.supramolecular.org/bindfit/>) the binding constant was determined to be $140 \pm 34 \text{ M}^{-1}$.

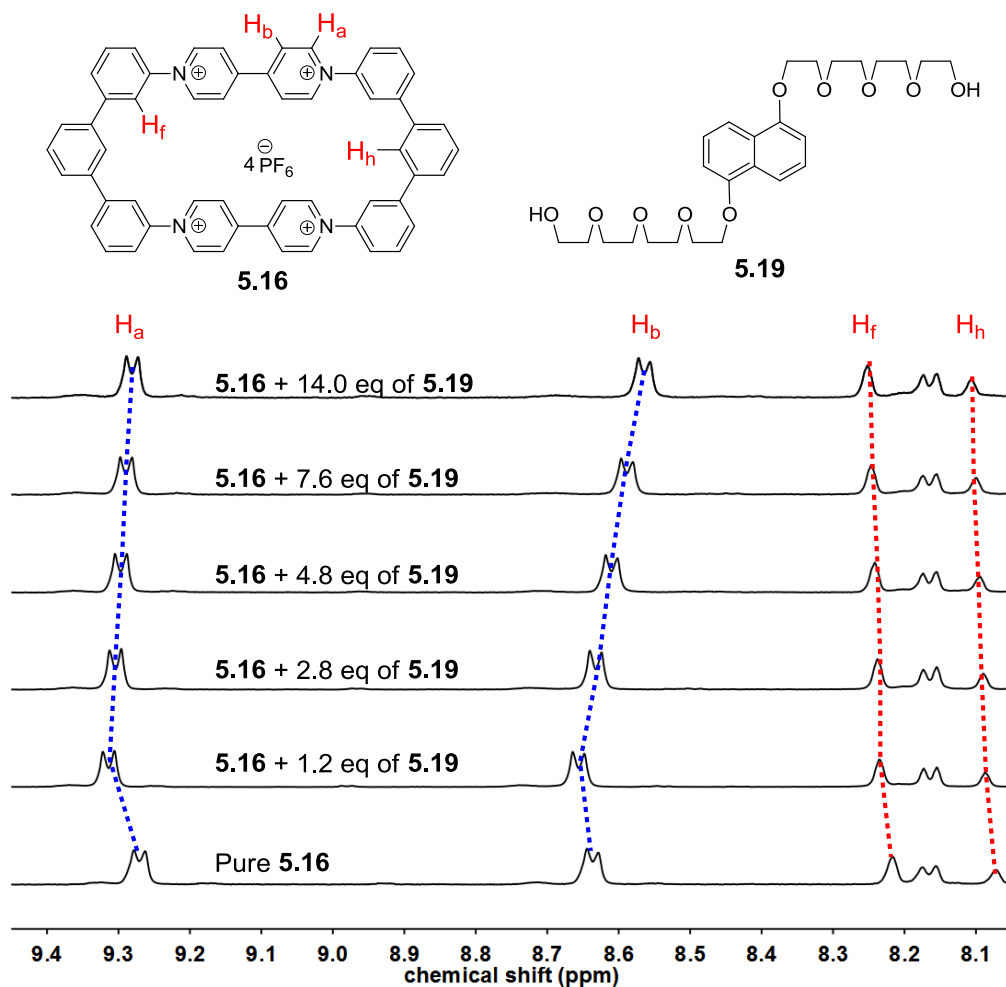
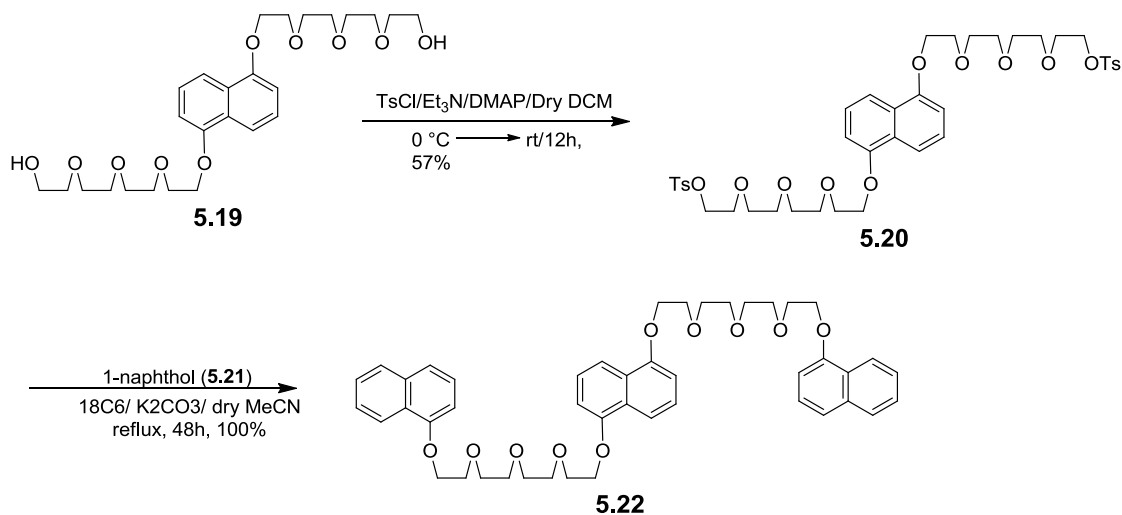


Figure 5.8. ^1H NMR (400 MHz) titration of guest species **5.19** against macrocycle **5.16** (2mM) in CD_3CN at 298 K. Molar ratios of host and guest are shown.

5.2.1.3. ^1H -NMR binding studies of **5.22** to macrocycle **5.16**.

As the binding between tetracationic macrocycle **5.16** and the diol 1NP **5.19** was relatively weak, it was decided to try to design a more strongly bound complex. It is a well-studied phenomenon in supramolecular chemistry that increasing the number of complementary binding interactions in a single complex increases the association constant (Figure 5.1). To achieve this for the macrocycle **5.16** required the design and synthesis of molecule containing multiple π -electron rich residues. Inspired by the synthesis of previous oligomers of this type the new trimer, 3NP, (**5.22** in scheme 5.7) was produced in two steps from the previously obtained guest **5.19**.²⁵⁵



Scheme 5.7. Synthesis of the π -electron rich trimer 3NP **5.22** from precursor **5.19**.

5.2.1.4. Binding properties of **5.16** and **5.22** in acetonitrile

The properties of the new complex were investigated by ^1H NMR spectroscopic studies to establish the binding constant. This was done using the same titration methodology as used to determine K_a for **5.16** \Rightarrow **5.22** (Figure 5.9) by adding increasing quantities of the π -electron-rich guest molecule **3NP** (**5.22**) to a fixed concentration of **5.16** in CD_3CN . (Figure 5.9)

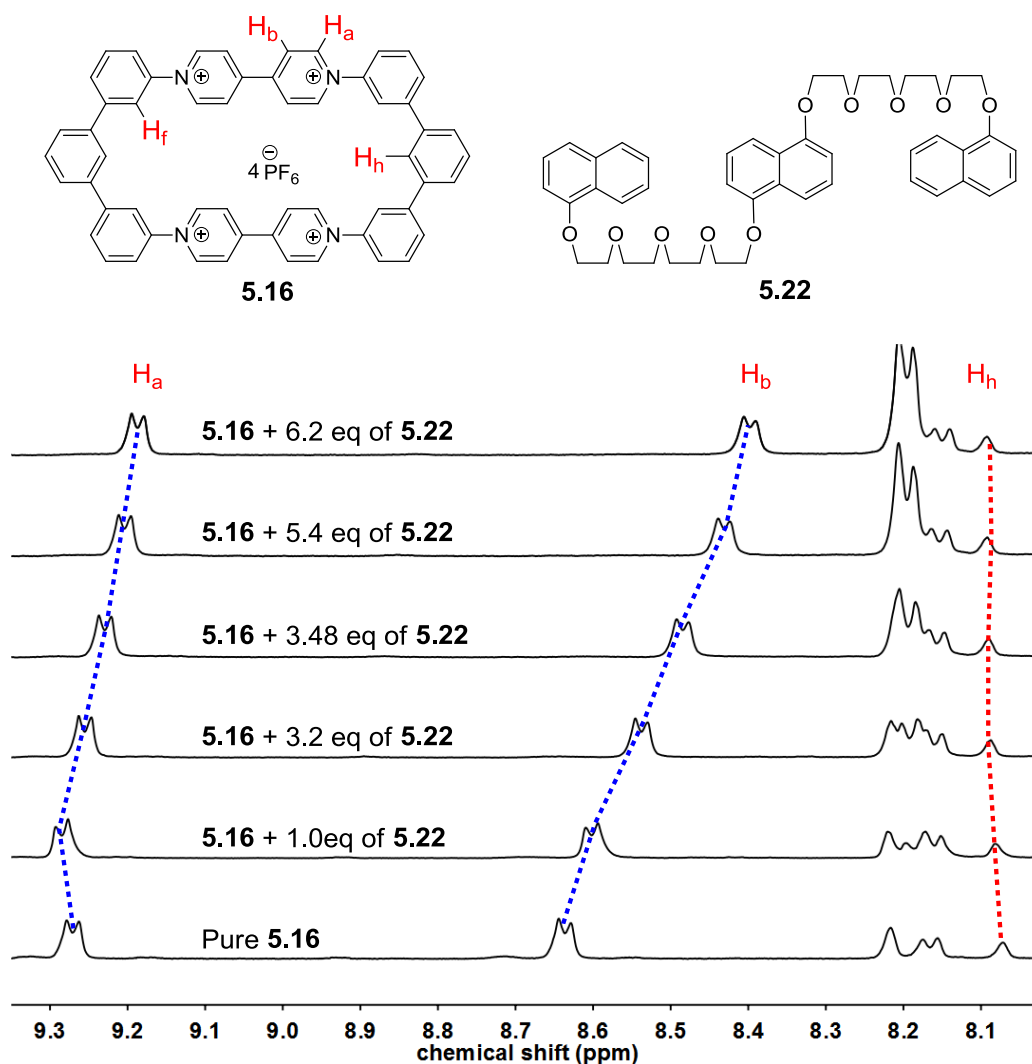


Figure 5.9. ¹H NMR (400 MHz) titration of guest species **5.22** against macrocycle **5.16** in CD₃CN at 298 K. Molar ratios of host and guest are shown.

The proton resonances of **5.16** clearly show significant complexation induced shifts with increasing concentrations of **5.22**. Close examination of the titration shows complex behaviour however. In isolation, the signals for H_a and H_b appear at 9.27 and 8.64 ppm (a separation of 0.63 ppm). At equimolar concentrations of **5.16** and **5.22**, the separation of H_a and H_b in increased (0.08 ppm) resulting in an upfield shift for protons H_a and a downfield shift for protons H_b. However, over the remainder of the titration both signals exhibit ring current shielding from the guest resulting in overall upfield shifts of 0.08 and 0.22 ppm, for H_a and H_b respectively over the course of the titration. In addition, the signal for H_h which is pointing

towards the guest into the interior of the macrocycle exhibits a small but measurable downfield change in chemical shift value over the course of the titration. This suggests that these protons are in the ring current *deshielding* region of the guest molecule, exactly as would be predicted for a "threaded" host-guest complex.

If the binding stoichiometry of complex (**5.16**⇌**5.22**) was assumed to be one to one, the binding constant was calculated to be $153 \pm 26 \text{ M}^{-1}$ using the program Bindfit²⁵⁸ as assessed from the change in chemical shift exhibited by H_h. In addition, comparison of the ¹H NMR titration studies between the **5.19** (Figure 5.8) and **5.22** (Figure 5.9) against the cyclophane **5.16** supports this calculation: at similar relative concentrations the complexation induced shifts for H_a and H_b were 0.01 and 0.05 ppm which are considerably smaller than that observed for **5.16**⇌**5.22** (0.08 and 0.22 ppm). This observation suggests that increasing the number of electron rich naphthalene units does indeed increase the binding constant for the complex. This may be accounted for if **5.16**⇌**5.22** forms an intertwined structure in a similar manner to that seen by the Stoddart group using (CBPQT⁴⁺) **5.4** as the π -electron poor cyclophane.²⁵⁵

5.2.2. Chemically reversible redox studies on macrocycle **5.16**.

After having successfully obtained the pure macrocycle and studied its binding to π -electron rich guests, it was important to study its chemically reversible redox properties. Reversible redox properties are important in determining if this new class of macrocycles may be amenable to being used in switching systems (Figure 5.3).

As described previously for the oligomeric systems reported in this thesis (unimer **3.1**, dimer **3.2** and trimer **3.3**) and the unconjugated macrocycles investigated previously (Figure 5.4),¹²⁵ we first investigated the formation of radical cationic species formed by the addition of triethylamine (TEA). Figure 5.10(A) shows the ¹H NMR spectrum of an orange solution of macrocycle **5.16**, which exhibits clearly resolved signals in the aromatic region (7.5 to 10.0 ppm). Upon addition of TEA, all the signals corresponding

to the protons of the aromatic and heterocyclic rings disappear, as a consequence of the formation of a paramagnetic bis(radical cation) (Figure 5.10B). This change in the ^1H NMR spectrum is accompanied by a change in colour of the solution to deep green, which is characteristic of the formation of radical cationic chromophores of this type (Table 1.1).¹⁰⁹ Addition of excess of TFA to this system, led to recovery of the original color of the solution and the ^1H NMR signals of parent **5.16** (Figure 5.10C). Their slight upfield chemical shift may be a result of the influence of the change in solvent polarity caused by the addition of TEA and TFA species.

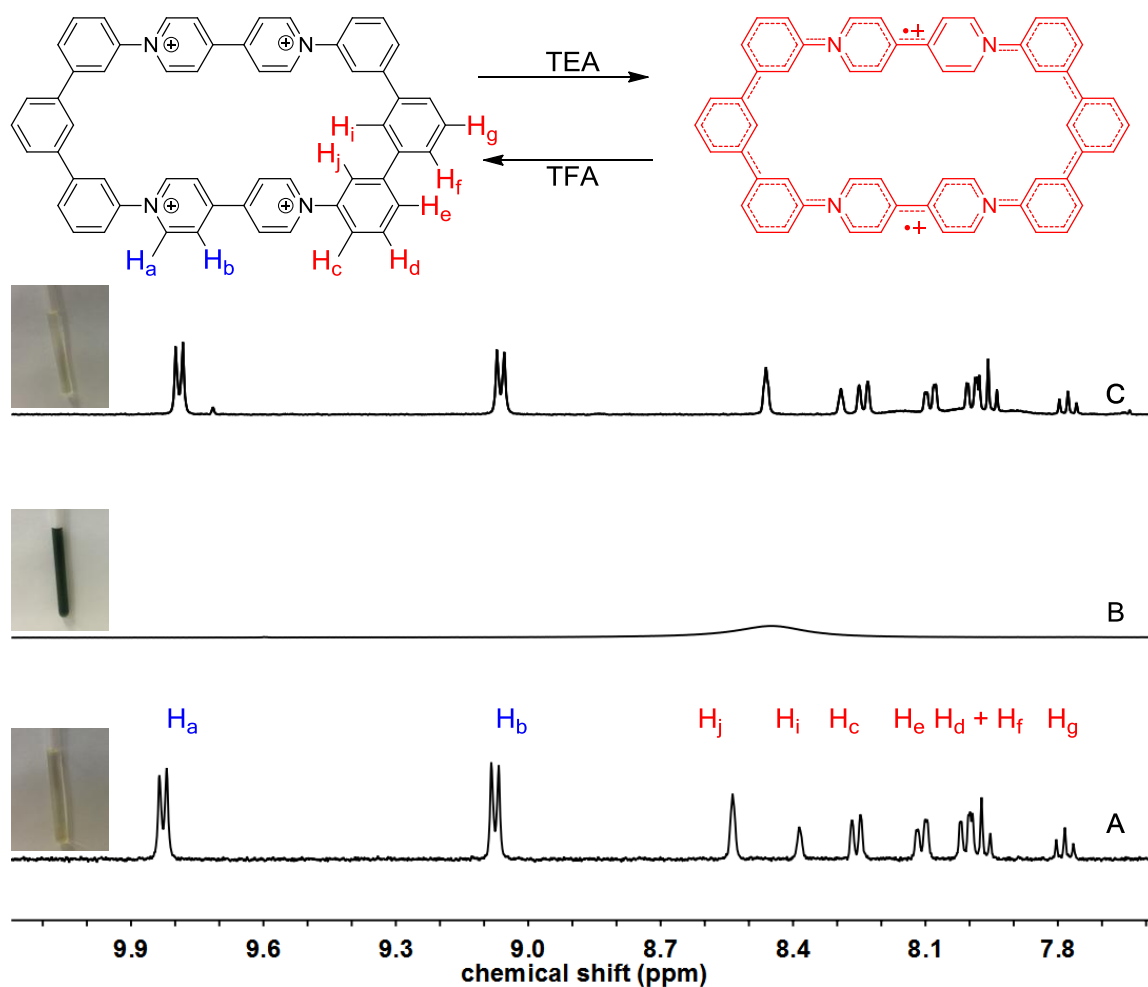


Figure 5.10. Chemical reduction of macrocycle **5.16** to the paramagnetic bis(radical cation) using TEA and reversible reoxidation with TFA monitored by ^1H NMR spectroscopy and corresponding colour changes. The aromatic and heterocyclic rings highlighted in red indicate the region of the spin density in 5.16^{2+} (not bond order) (A) macrocycle **5.16** in acetone- d_6 , (B) after addition of 20 equivs of TEA and (C) subsequent addition of an excess of TFA to B.

5.2.3. Cyclic voltammetry and square wave voltammetry of **5.16**

The electrochemical reduction of **5.16** was studied by cyclic voltammetry (CV) at a polished glassy carbon disc electrode, using anhydrous acetonitrile as solvent containing 0.1 M tetrabutylammonium hexafluorophosphate (TBAPF₆) as supporting electrolyte. Ferrocene was again selected as internal reference (Set to 0.0 V).

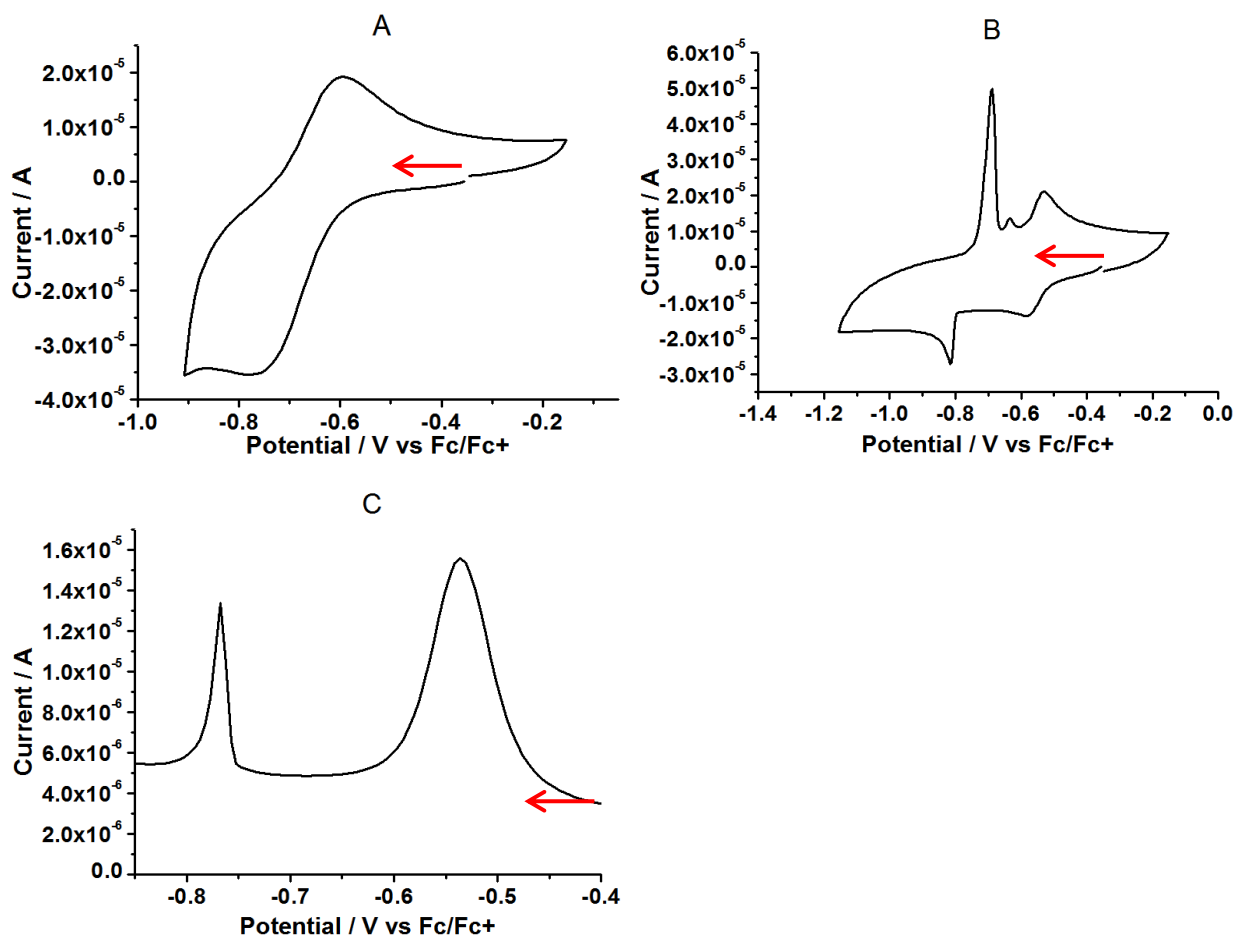


Figure 5.11. Cyclic voltammograms and square wave voltammogram of 0.2 mM compound **5.16** at a glassy carbon disc ($d = 2$ mm) electrode in anhydrous acetonitrile: A) 1st reversible reaction at $\nu = 1.5$ V s⁻¹, B) 2nd not fully reversible reaction at $\nu = 0.5$ V s⁻¹ and C) square wave voltammogram. The arrow indicates the scan direction from the initial potential.

From the CV of macrocycle **5.16** it is apparent that the first reduction/oxidation couple corresponding to the formation of bis(radical cationic) residues is quasireversible in nature ($E_{1/2} = -0.56$ V vs Fc/Fc⁺, Figure 5.11A and Figure 5.11B). In contrast, the large difference in current flow for the second redox couple corresponding to the transformation of the

bis(radical cationic) species to its neutral form ($E_{1/2} = -0.75$ vs Fc/Fc⁺) shows this couple is not fully reversible (Figure 5.11B). The peak-to-peak separations for these two waves are 50 and 130 mV, respectively. Indeed, during this experiment, the second reduction to form the fully reduced viologen species ($2V^0$) leads to some precipitation, which accounts for the sharp appearance of this reduction wave (-0.82 V).

Between the two major re-oxidation waves there is a small but observable anodic peak at -0.636 V) which perhaps could be attributed to precipitation or decomposition phenomena.

SWV was carried out on **5.16** under the same conditions as used for CV measurements. The two reduction waves ($E_p = -0.54$ and -0.77 vs Fc/Fc) are of different intensities, confirming that precipitation is interfering with measuring the complete CV for this new macrocycle.

5.2.4. Electromechanical behaviour of 5.16 \supset 5.22.

In 1994 Smith and co-workers studied the CV of CBPQT⁴⁺ (Scheme 5.1, **5.4**) in the presence of various guest molecules including ethoxy ether substituted benzenes.²⁵⁹ They were able to observe significant shifts (20 mV) in the first oxidation and reduction potentials of the viologens in the macrocycle as a function of the quantity of the guest.

Prior to starting extensive CV studies of our most strongly bound complex (**5.16** \supset **5.22**) it was important to determine the redox properties of the guest 3NP (**5.22**) on its own. As can be seen from Figure 5.12, that **5.22** exhibits two irreversible oxidation waves ($E = 0.79$ and 1.05 V vs Fc/Fc⁺) as found for related structures.²⁶⁰ The two signals can be accounted for by inspection of the structure of **5.22** that has a central naphthalene unit with two electron donating alkoxy substituents whereas the two terminal naphthalene residues have only one electron donating alkoxy substituent each. Therefore, these two distinct naphthalene environments are oxidised to their respective radical cations at distinct oxidation potentials.

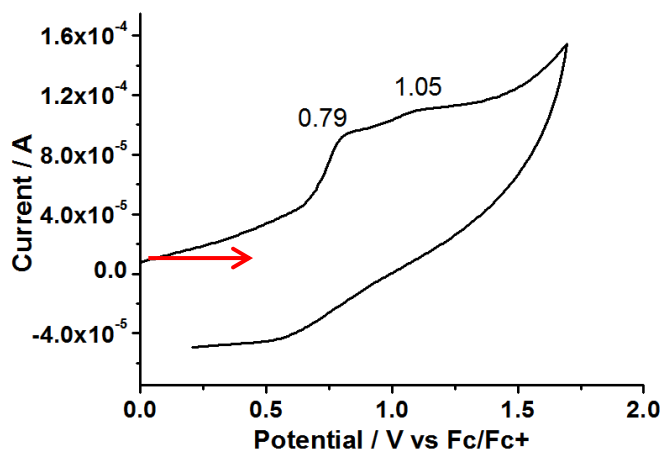


Figure 5.12. Cyclic voltammograms of 0.2 mM compound **5.22** at a glassy carbon disc ($d = 2$ mm) electrode in anhydrous acetonitrile at $v = 500$ mV s^{-1} . The arrow indicates the initial potential sweep.

Comparison of the CVs of the macrocycle **5.16** and guest **5.22** (Figure 5.13) show that their oxidation potentials are distinct, with their redox activities occurring at negative and positive potentials respectively. Therefore, studying the redox behaviour of the macrocycle in the presence of the guest will not result in inconvenient coincidence of signals.

Figures 5.13A and 5.13B show the redox behaviour of the macrocycle **5.16** in the presence of increasing quantities of guest. The addition of the guest does not alter the irreversible nature of the second redox couple. Addition of 10 and 20 equivalents of guest **5.22** to the host **5.16**, results in significant changes in the $E_{1/2}$ and current flow for the redox waves observed for the viologen groups. For example, the peak current of the anodic sweep from neutral form to bis(radical cationic) species decrease significantly (3.07×10^{-5} A), on increasing addition of guest molecule. This demonstrates a reduction in the diffusion rate of the system²⁶¹ which is indicative of the increase in size of the complex compared to the molecular volume of the starting macrocycle.

Furthermore, upon adding 20 equiv. of **5.22** to the system, the first reduction wave moves to an even more negative value, $E_{1/2} = -0.563$ mV ($\Delta E_{1/2} = 8$ mV compared to **5.16**), but also broadens. In addition the peak-to-peak separation is 126 mV for this complex compared to just 50 mV for **5.16**.

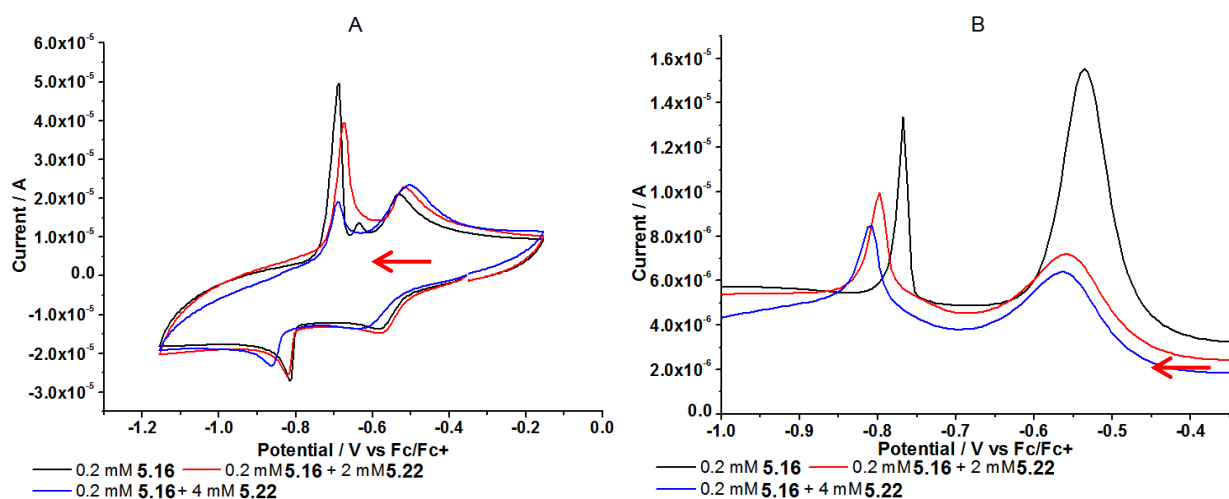


Figure 5.13. Cyclic voltammograms and square wave voltammograms of 0.2 mM compound **5.16** and in the presence of 3NP (**5.22**) at a glassy carbon disc ($d = 2$ mm) electrode in anhydrous acetonitrile at $v = 500$ mV s $^{-1}$.

5.3. Conclusion

This study reports the design and synthesis of a novel fully π -conjugated macrocycle **5.18** which contains two 4,4'-bipyridinium residues.

The binding between **5.16** and π -electron rich guests **5.19** and **5.22** was studied. Titration experiments followed by ^1H NMR spectroscopy clearly demonstrated that binding strength between host **5.16** and **5.22** containing three dialkoxy naphthalene units was greater than with **5.19** which contained just 1 dialkoxy naphthalene units. This may be because the **3NP** was able to form an intercollated complex containing multiple associative π - π stacking interactions.

The redox properties of the new macrocycle, and the novel complexes (**5.16**→**5.19**) were studied in solution. The concentration dependent redox behaviour of the complex **5.16**→**5.22** as measured by CV and SWV clearly demonstrated the formation of the host-guest complex, which exhibited slower diffusion kinetics than the starting materials.

Chapter 6

Characterization of the solid-state electronic properties of viologen-containing compounds

6.1. Introduction

The previous chapters describe the design, synthesis and characterisation of a series of viologen-containing oligomers and macrocycles. This chapter examines the electrical properties of some of these novel compounds in the solid state. Firstly, the thin film conductivity of unimers, dimers and trimers are presented and compared to build up a structure/property relationship for these materials for the first time. Secondly, the results of photocurrent experiments which demonstrate a clear link between the structures of viologen-containing species and their response to absorbed photons.

6.1.1. Overview of conductive viologen-containing compounds

In recent years, the solid-state electrical conductivity of several substituted viologens has been demonstrated, which is the first step towards using them in a new generation of electronic devices. The first studies into the conductivity of these materials were conducted by Allen and co-workers^{262–264} during 1983 and 1984. This group measured the solid-state conductivities of salts of 1,1'-diphenyl-4,4'-bipyridinium (**4.10f**) and its *para*-substituted congeners with 7,7,8,8-tetracyanoquinodimethanide (TCNQ) anion (**6.6**) using a four-probe technique on compacted pellets of microcrystalline samples at 300 K (Figure 6.1). They reported that the degree of conductivity is highly dependent on the level of TCNQ incorporated into the solid with the highest levels of conductivity measured when the TCNQ molecules are present as infinite stacks.

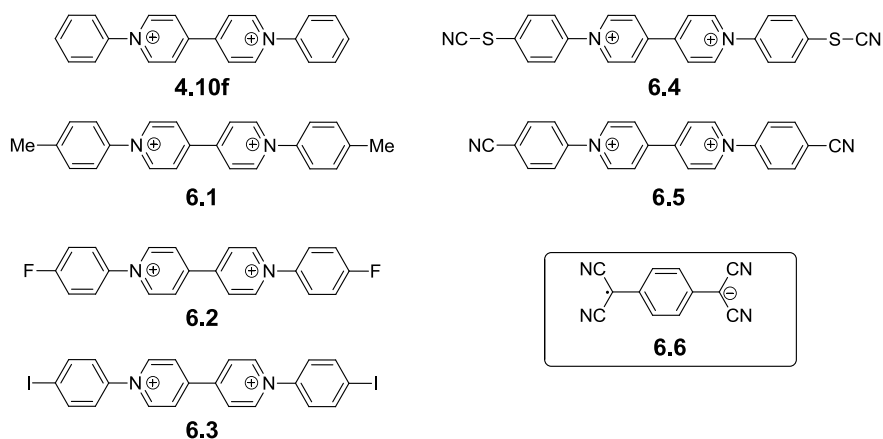


Figure 6.1. Structure of the TCNQ salts of diphenyl-4,4'-bipyridinium and its para-substituted congeners.

In 1994, the electronic properties of the bromide, perchlorate and tetrafluoroborate salts of 1,1'-bis(*p*-cyanophenyl)-4,4'-bipyridinium (CPQ) were measured by Rosseinsky and Monk.²⁶⁵

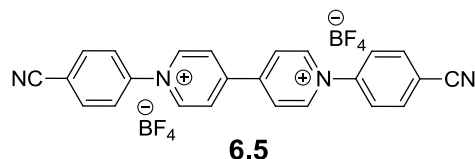


Figure 6.2. Structure of 1,1'-bis(*p*-cyanophenyl)-4,4'-bipyridinium with tetrafluoroborate salts.

In this work the group fabricated a bespoke 'sandwich cell' instrument to measure the conductivity of pressed pellet samples without damaging the surface of the pellets. They found that within the range 0 to 5 tons of applied pressure during pellet formation, the conductivity doubled. They proposed that this increase was as a consequence of improved surface contact between the pressed disc and the Pt electrodes. In addition, the influence of counterions (Br^- , Cl^- , BF_4^- , ClO_4^-) was also investigated. It was found that the nature of the cation had little effect on the conductivity of **6.5** (c. $10^{-8} \text{ S cm}^{-1}$). However, the conductivity of the radical cationic version of **6.5** was approximately 1000 times greater than that of the dication (c. $10^{-5} \text{ S cm}^{-1}$).

More recently Porter and Vaid¹⁷⁹ studied the conductivity of *N,N'*-diphenyl viologen (**4.10f**) in its radical cationic and neutral forms in the solid state. They generated the neutral phenyl viologen by reduction using zinc dust. The radical cationic species was then produced by mixing equimolar quantities of the dication and neutral species in acetonitrile under N₂. The solid-state conductivities were measured from pressed powders in a two-electrode apparatus that consisted of a Delrin block with a 6.35 mm diameter cylinder hole and two 6.35 mm diameter copper cylindrical contacts. They found that both the radical cationic and neutral species exhibit conductivity, but that the neutral viologen is a significantly better conductor than the radical cationic species (Table 6.1). Four years later, the same group investigated the conductivity of an “extended viologen” (**6.8**) which also exhibited the same conductive behavior. In this case, the conductivity of the neutral form ($9.3 \times 10^{-5} (\pm 0.9 \times 10^{-5}) \text{ S m}^{-1}$) was found to be significantly higher than that of the radical cationic species ($4.3 \times 10^{-6} (\pm 0.6 \times 10^{-6}) \text{ S/m}$).¹⁶⁸

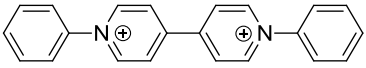
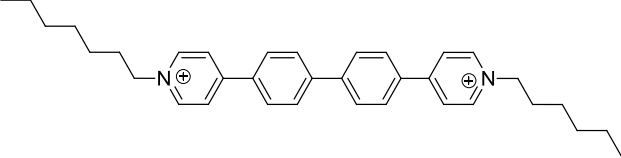
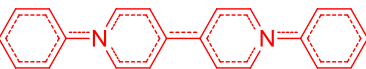
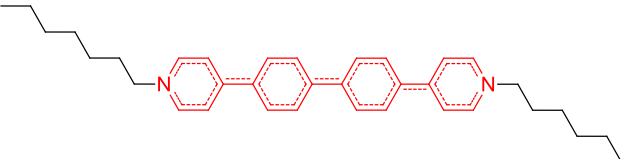
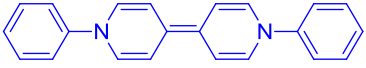
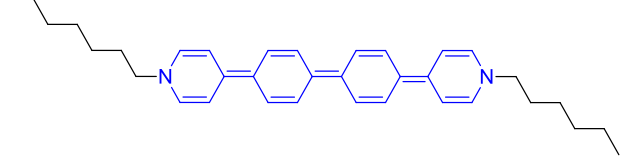
 <p style="text-align: center;">4.10f</p>	 <p style="text-align: center;">6.8</p>
 <p style="text-align: center;">4.10f⁺ : $2.3 \times 10^{-8} (\pm 0.6 \times 10^{-8}) \text{ S/m}$</p>	 <p style="text-align: center;">6.8⁺ : $4.3 \times 10^{-6} (\pm 0.6 \times 10^{-6}) \text{ S/m}$</p>
 <p style="text-align: center;">4.10f⁰ : $3.1 \times 10^{-5} (\pm 0.6 \times 10^{-5}) \text{ S/m}$</p>	 <p style="text-align: center;">6.8⁰ : $9.3 \times 10^{-5} (\pm 0.9 \times 10^{-5}) \text{ S/m}$</p>

Figure 6.3. Solid-state conductivities of the viologen-based species investigated by Port and Vaid.^{168,179}

Each of the conductivity measurements reported above were made using pellets formed from pressed powder. However, these measurements are known to be highly dependent on the sample homogeneity²⁶⁵ which makes it difficult to compare data from a range of sources to build up a true picture of the electronic properties of this class of materials.

In this chapter we produce thin films (<221 nm) of a range of our newly synthesised viologen-based molecules. This is achieved by spin coating concentrated solutions of our samples onto an indium tin oxide (ITO) substrate. This method allows simple measurement of the Current - Voltage (I-V) characteristic of the samples from which the conductivities can be calculated. In addition, we also present data showing that some of these materials exhibit interesting photo-current characteristics.

6.2. Results and Discussion

6.2.1. Preparation of the ITO substrate and thin films

Spin coating is one of the simplest laboratory methods for producing homogeneous thin films. In this work, the viologen containing oligomers were spin coated from acetonitrile solution (12.5 to 80 mg/mL) onto a pre-cleaned 5 channel interdigitated ITO glass slide (resistance of 20 Ω / square, Ossila, Figure 6.4a). A photo of a typical coated cell used in these experiments is shown below. (Figure 6.4b)

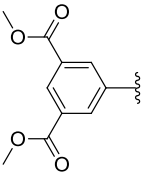
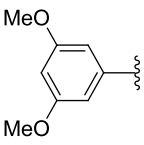
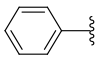
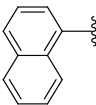


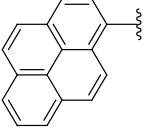
Figure 6.4a. Interdigitated ITO Substrates (Picture from Ossila: <https://www.ossila.com/products/interdigitated-ito-ofet-substrates>). **Figure 6.4b. Photo of a coated ITO cell used in this work**

The ITO channels are the paler areas in this image.

Time constraints did not allow the study of the full series of oligomers produced in chapter 4. Therefore, it was decided to investigate 9 molecules. These viologens were selected to allow for the qualitative comparison between members of each series which vary by oligomer length and electron withdrawing/donating ability of the end group (ether versus ester) or vary by the number of fused aromatic rings in the end group. Films were prepared using saturated solutions, the exact concentration of each solution varied according to solubility. The casting parameters for each film are presented in Table 6.1.

Table 6.1. All of the parameters used in spin coating experiments. (Thickness was measured by Dektak)

Entry	End group (R)	Concentration (mg/mL)	Speed (rpm)	Spin time (s)	Film thickness (nm)
Unimer 3.1		30	1500	100	65
Dimer 3.2		30	1500	100	40
Trimer 3.3		30	1500	100	70
Unimer 4.10d		22	1500	41	221
Dimer 4.13d		38	3500	41	64
Trimer 4.16		21	3500	41	30
Unimer 4.10f		80	5000	41	210
Unimer 4.10g		12.5	1900	41	67

Unimer 4.10h		21	3500	41	16
---------------------	---	----	------	----	----

6.2.2. Conductivity measurement

To measure the conductivity of each sample, the ITO electrode was placed on a Zero Insertion Force (ZIF, from Ossila) board. This allowed an I-V sweep to be made for each sample. The flow of current across the device was measured as a function of applied potential from -100 to 100 V in the dark. Each sample was measured four times to generate a mean I/V graph for each sample from which the slope of the plots were measured. For the cells prepared on ITO substrates, the conductivity (σ) of sample can be obtained with the following equation (Eqn 6.1):

$$\sigma = \frac{dI}{dV} \times \frac{(\text{channel separation})}{(\text{channel length} \times \text{film thickness})}$$

Equation 6.1

In this case, the term $\frac{dI}{dV}$ is the slope of the I/V plot, the channel dimensions are known (separation = 5×10^{-5} m, length = 2.5×10^{-2} m) and the film thickness was measured for each film (table 6.1).

6.2.3. Dependence of the conductivity on the conjugation length.

I/V plots for each sample are presented in appendix 1. From these plots the conductivities for each series of monomeric, dimeric and trimeric viologen containing endgroups with electron withdrawing (**3.1**, **3.2** and **3.3**) and electron donating endgroups (**4.10d**, **4.13d**, **4.16**) were calculated and are presented in Figure 6.5 and Table 6.3.

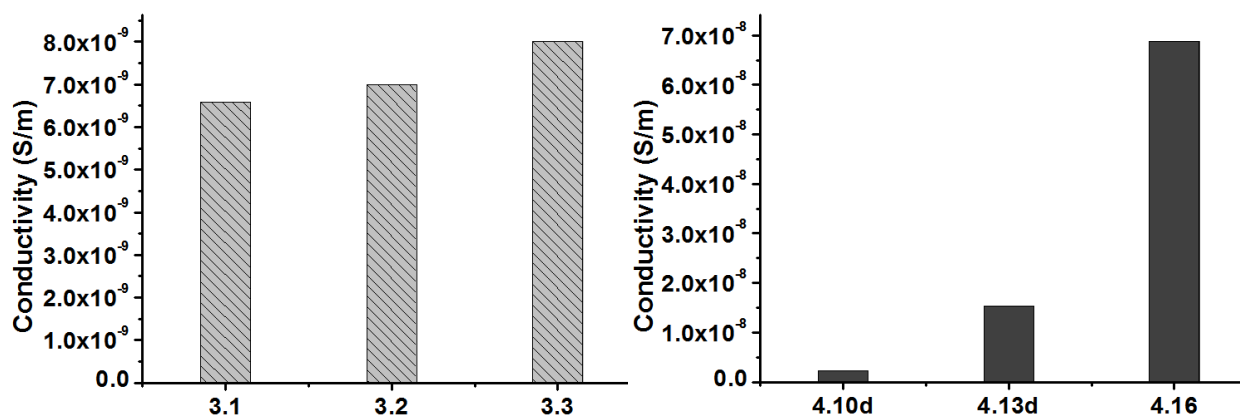


Figure 6.5. The solid state conductivities of unimers (3.1, 4.10d), dimers (3.2, 4.13d) and trimers (3.3 , 4.16) containing ester or ether end groups respectively.

Table 6.2. Average conductivities from thin film electrical conductivity measurements of unimer 3.1 and 4.10d, dimer 3.2 and 4.12d and trimer 3.3 and 4.16.

Entry	Thickness (nm)	Conductivity (S/m)
Unimer 3.1	65	$6.59 \times 10^{-9} (\pm 0.06 \times 10^{-9})$
Dimer 3.2	40	$7.00 \times 10^{-9} (\pm 1.54 \times 10^{-9})$
Trimer 3.3	70	$8.00 \times 10^{-9} (\pm 0.05 \times 10^{-9})$
Unimer 4.10d	221	$2.20 \times 10^{-9} (\pm 0.01 \times 10^{-9})$
Dimer 4.12d	64	$1.54 \times 10^{-8} (\pm 0.001 \times 10^{-8})$
Trimer 4.16	30	$6.87 \times 10^{-8} (\pm 0.006 \times 10^{-8})$

As can be seen from Table 6.2, it was found that with increasing oligomer length from unimeric to trimeric viologen species, their thin film conductivity increased. This trend was more pronounced for the series with electron donating end groups (from $2.20 \times 10^{-9} (\pm 0.01 \times 10^{-9})$ S/m to $6.87 \times 10^{-8} (\pm 0.006 \times 10^{-8})$ S/m) than for the series with electron withdrawing end groups (from $6.59 \times 10^{-9} (\pm 0.06 \times 10^{-9})$ S/m to $8.00 \times 10^{-9} (\pm 0.05 \times 10^{-9})$ S/m).

6.2.4. Dependence of the conductivity on the number of fused aromatic rings in the end group.

After determining how the thin film conductivities depend on the conjugation length, it was decided to investigate the influence that varying the number of fused aromatic rings on the

end group had on on the conductivities of the viologen species. The thin film conductivities for phenyl (**4.10f**), naphthyl (**4.10g**) and pyrenyl (**4.10h**) derivatives are presented in Figure 6.6.

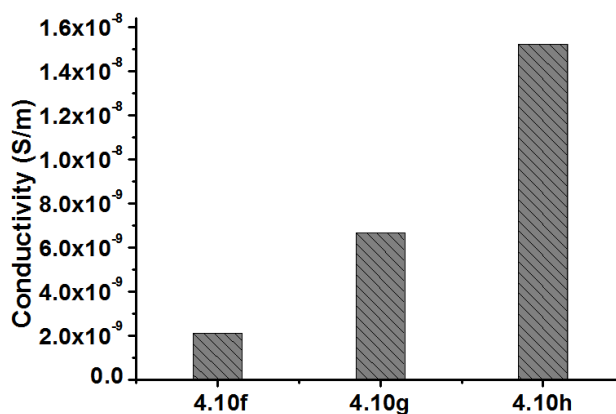


Figure 6.6. The conductivities of unimers **4.10f** (phenyl), **4.10g** (naphthyl) and **4.10h** (pyrenyl) (mean of 4 results).

Table 6.4. Average conductivities from thin film electrical conductivity measurements of unimers **4.10f**, **4.10g** and **4.10h**.

Entry	Thickness (nm)	Conductivity (S/m)
Unimer 4.10f	210	$2.11 \times 10^{-9} (\pm 0.01 \times 10^{-19})$
Unimer 4.10g	67	$6.66 \times 10^{-9} (\pm 0.08 \times 10^{-9})$
Unimer 4.10h	16	$1.52 \times 10^{-8} (\pm 0.01 \times 10^{-8})$

Table 6.4 shows the average conductivity of three unimers with different numbers of fused aromatic rings on their endgroups. It was found that as the number of benzene rings increased, the conductivity improved by an order of magnitude. The measured conductivity of dipyrenyl viologen **4.10h** is 1.52×10^{-8} S/m is as high as the solid state conductivity of the radical cationic species of **4.10f** as measured by Porter and Vaid ($2.3 \times 10^{-8} (\pm 0.6 \times 10^{-8})$ S/m, see figure 6.2). This may be accounted for by more favorable end-group overlap in the solid state or perhaps because of the increased area of delocalization in the viologen species with a higher number of fused aromatic rings on the end group.

6.3. Photocurrent measurements on ether terminated monomeric, dimeric and trimeric viologens (4.10d, 4.13d and 4.16, respectively)

Prior to constructing complex devices including solar cells from new materials, it is important to establish the photoconductive response of the material in isolation. These experiments were carried out on the coated ITO substrates prepared during the conductivity studies (ether terminated viologens **4.10d**, **4.13d** and **4.16**). The films were initially placed in the dark under a continuous applied potential of -15 V. Subsequently the current flow was measured as a function of the wavelength of the incident light as the sample was irradiated over between 300 nm to 800 nm (Figure 6.7).

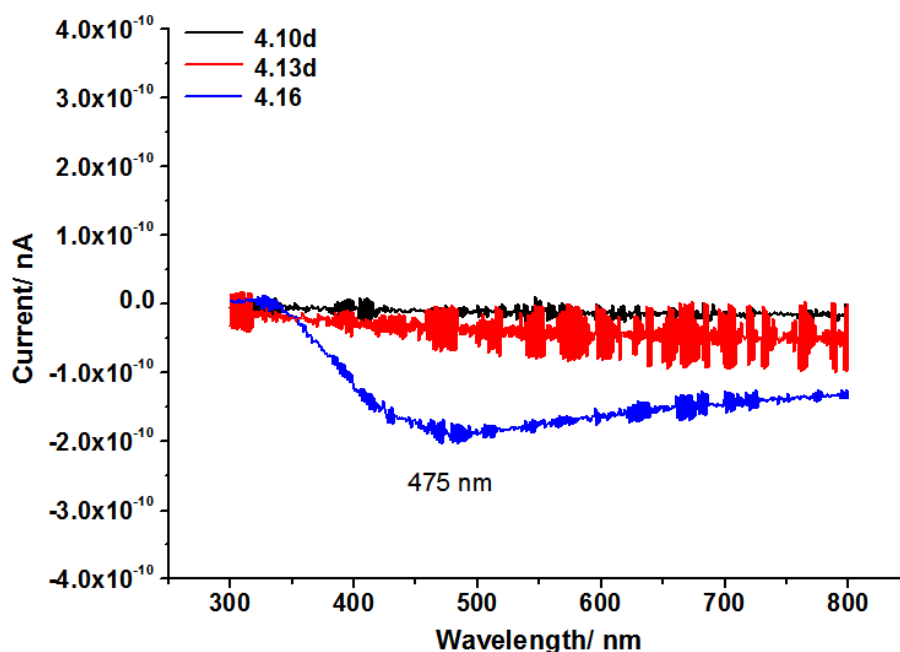


Figure 6.7. Photocurrent response of thin films of samples of 4.10d, 4.13d and 4.16 held at a constant applied potential 15 V as the wavelength of the incident radiation is varied from 300 to 800 nm.

It can be seen from the data (Figure 6.7) that the photocurrent response was dependent on oligomer structure. Neither unimer **4.10d**, nor dimer **4.13d** exhibited any response to incident light over the wavelengths measured. However, trimer **4.16** became conductive under irradiation at the appropriate wavelength: the photocurrent increased significantly when the

wavelength increased from approximately 330 nm to 475 nm. However, when the excitation wavelength was above 475 nm, the generated photocurrent decreased. The position of this maximum enables the band gap between the valence band (VB) to conduction band (CB) to be calculated to be approximately 2.61 eV. This result was reproducible under both positive and negative applied voltage (Figure 6.8).

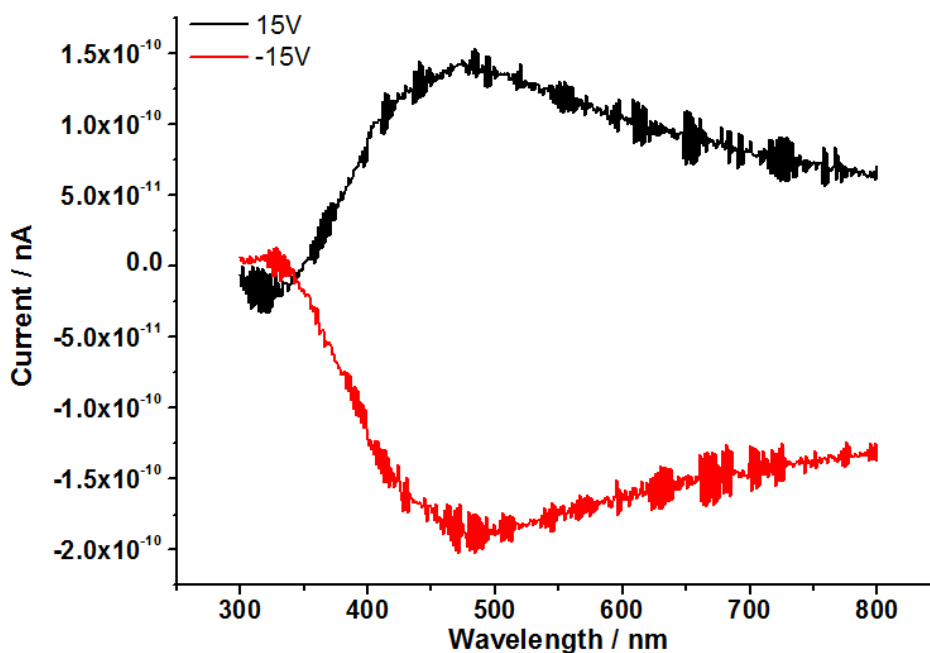


Figure 6.8. Current response of thin films of 4.16 at constant applied potential of either +15 V or -15 V as the wavelength of incident radiation was varied between 300 and 800 nm.

The difference in photocurrent response between unimer **4.10d**, dimer **4.13d** and trimer **4.16** clearly results from their different structures. It may be that as the conjugation length increases, the energy band gap between VB and CB reduces, which may increase the efficiency of photon absorption.²⁶⁶ Alternatively, it may be that the longer oligomer packs more efficiently in the solid state allowing more efficient transport of electrons through the sample.

6.4. Conclusion

In this chapter, the conductivities of a series of 4,4'-bipyridinium-based aromatic oligomers with different end groups have been measured. The results demonstrate that the influence on conductivity of the electron donating or withdrawing endgroups is relatively weak. However, the conductivity increased sharply as the number of fused aromatic rings in the end group increased. In general, conductivity tended to increase from unimer to trimer. These results have demonstrated that as the length or area of conjugation increases, the thin film conductivity tends to increase.

In addition, the photocurrent characteristics of a series viologen species **4.10d**, **4.13d** and **4.16** under a constant voltage were measured for the first time. Only trimer **4.16** exhibited a measureable photocurrent under these irradiation conditions. This initial result shows that structurally optimised conjugated viologen containing systems may have the potential for application in high value products including phototransistors and photovoltaic cells.

Chapter 7

Conclusion and Future Work

7.1. Review of Results

The research described in this thesis has shown that fully π conjugated viologen containing materials can be synthesized in good yield by the Zincke reaction.

It was found that the success of the Zincke reaction was connected to the structure of the nucleophilic amine residue. For example, in the case of the addition of benzene-1,4-diamine to Zincke salt **1.65**, the first addition of one of the amine groups resulted in a reduction of the nucleophilicity of the remaining amine residue. This completely stopped polymerisation/oligomerisation under the conditions tested. To overcome this limitation, the use of the commercially available and electron rich diaromatic diamine 3,3'-dimethoxybenzidine was explored. 4,4'-Bipyridinium-based aromatic oligomers (**3.1-3.3**) were synthesized effectively and their electrochemical properties were investigated by using CV and SEC-UV/vis. Spectroscopically, the UV-vis SEC results for **3.3** demonstrated that the apparently more electron rich, central radical cationic bipyridinium moiety was reduced to a quinoidal, neutral form before the two terminal viologen units which appear comparatively electron poor.

A series of π -conjugated viologen containing oligomers which contained aromatic residues with different end groups or core groups were synthesised and their electrochemical properties were investigated. The discovery of a strong correlation between the half wave potentials and pK_b values is very interesting and will enable the prediction of the reduction potentials as yet unmade substituted viologen species. This could be of great use in designing systems that are to be used in nano-machines, ECD and in catalysis.²⁰²

A novel, fully π -conjugated macrocycle **5.16** which contained two 4,4'-bipyridinium was synthesised. The structure of this macrocycle was found to be suitable to enable supramolecular complexation with π -electron rich guests (**5.19** and **5.22**). Quantitative determination of association constants was carried out using ^1H NMR titration studies. The results clearly demonstrated that the binding strength between host **5.16** and **5.22** containing

three dialkoxy naphthalene units was greater than with guest **5.19** which contained just 1 dialkoxy naphthalene units.

Time constraints did not permit the determination of the thin film conductivity of the full series of oligomers. Therefore, compounds **3.1**, **3.2** and **3.3** containing different numbers of viologens and **4.10f**, **4.10g**, **4.10h** containing endgroups with different numbers of aromatic rings were selected for study. The conductivity results demonstrated that as the conjugation length increased, the thin film conductivity tended to be higher. In addition, oligomeric species **3.3** exhibited interesting photocurrent characteristics under irradiation at visible wavelengths.

7.2. Future work

This work has led to an improved understanding of the electronic behaviour of fully π conjugated viologen containing oligomers. We hope that these results can be used to design new organic semiconductors for electronic device and nano-machines. The first step to achieving this would be to produce simple OPVCs or OTFTs containing our materials and to study their solid state properties.

From Porter's report,^{168,179} it is known that the conductivity of radical-cationic and neutral viologen species is much higher than for the dicationic species tested in this work. Therefore, it would be interesting to produce radical cationic species of our materials and test their conductivities. Moreover, solid-state blends of related compounds and electron rich species including(TCNQ) anion (**6.6**)²⁶²⁻²⁶⁴ have been shown to exhibit extremely high conductivities. It would therefore be interesting to produce similar types of thin films using the viologen species produced in this thesis and study their electronic properties.

Lastly, work on macrocycle **5.18**, is at a very early stage. It would be exciting to see if it can be used to produce more complex supramolecular species including rotaxanes, catenanes and switches in the future.

Experimental Techniques

Chemicals and solvents (from Sigma Aldrich, Fisher Scientific or Alfa Aesar) were generally used without further purification unless otherwise stated. Anhydrous *N,N*-dimethylformamide (DMF) (Alfa Aesar, 99.8%, packaged under argon) was used as received. Tetra-*n*-butylammonium hexafluorophosphate (TBAPF₆) was recrystallized twice from absolute ethanol and dried at 80 °C under vacuum overnight. Acetonitrile was distilled from CaH₂.

¹H and ¹³C NMR spectra were acquired on a Bruker DPX-400 spectrometer operating at 400 MHz and 100 MHz respectively or on a Bruker AV-700 spectrometer operating as 175 MHz for ¹³C nuclei. Residual ¹H signals from the solvent were used as internal calibrants.

Infrared spectra were recorded on a Perkin Elmer 17 20-X spectrometer from thin films cast from acetone, and major absorption bands are reported in wavenumbers (cm⁻¹). For spectroelectrochemical (SEC) measurements, IR spectra were recorded on a Bruker Vertex 70v FTIR spectrometer. UV-Vis spectra were acquired on a Scinco S-3100 diode-array spectrophotometer.

Thin layer chromatography (TLC) was performed using aluminium-backed plates pre-coated with Merck silica gel 60-F₂₅₄. Melting points were determined on a TA Instruments DSC Q2000 instrument. Mass spectra were recorded Thermo Scientific LQT Orbitrap XL under conditions of electrospray ionisation.

Compounds **1.65**, **3.11**, **5.18**, **5.19** and **5.20** were synthesized as described previously.^{182,255,267,268} All reactions were carried out in oven-dried glassware under dry

nitrogen.

Single crystal X-ray

The crystal structure of **5.16** was solved by Dr Ann Chippindale (University of Reading). X-ray diffraction data were collected on an Agilent Technologies Gemini Ultra-S CCD diffractometer, using Cu-K α radiation, equipped with an Oxford Cryosystems low-temperature device operating at 150 K. The structure was solved in "Superflip" and refined in "CRYSTALS". Electron density due to disordered and unidentifiable solvent was treated using the SQUEEZE routine in "PLATON".

Crystal data for 5.16: C₅₆H₄₀F₂₄N₄P₄, *Mr* = 1348.81, monoclinic, *P*2₁/*c*, *a* = 14.1176(3), *b* = 22.1778(4), *c* = 11.2310(2) Å, β = 100.087(2)°, *V* = 3462.05(12) Å³, *T* = 150(2) K, *Z* = 2, *D_c* = 1.294 g cm⁻³, μ (Cu-K α) = 1.919 mm⁻¹, *F*(000) = 1360, independent measured reflections 6635, *R_I* = 0.0728, *wR₂* = 0.830 for 4977 independent observed reflections [$2\theta \leq 71.242^\circ$, $I > 3\sigma(I)$].

EPR measurements

X-band EPR spectra were acquired on a Bruker EMX spectrometer using a TM₁₁₀ cylindrical mode resonator (ER 4103TM). Due to the high dielectric loss of the solvent all samples were contained in 1 mm internal diameter quartz tubes (Wilmad 712-SQ). To allow resolution of hyperfine structure, samples were deoxygenated by a minimum of three freeze-pump-thaw cycles, and spectra were recorded with a 20 μ T modulation amplitude. A DPPH standard [*g* = 2.0036(3)] was used to obtain accurate *g*-values.²⁶⁹

Cyclic voltammetry measurements

Cyclic voltammetry (CV) measurements were performed on 0.2 mM solution of the viologen containing compounds in anhydrous DMF or anhydrous acetonitrile containing 0.1 M TBAPF₆ as supporting electrolyte with a single-compartment

three-electrode cell equipped with glassy carbon disc ($d = 2$ mm) working electrode, coiled platinum wire auxiliary and coiled Ag wire pseudoreference electrodes.

Spectroelectrochemical measurements

Spectroelectrochemical measurements were carried out at 293 K, using an optically transparent thin-layer electrochemical (OTTLE) cell equipped with Pt minigrad working and auxiliary electrodes, a silver microwire pseudoreference electrode, and CaF_2 windows. The course of the spectroelectrochemical experiment was monitored by thin-layer cyclic voltammetry conducted with an EmStat 3 (PalmSens BV) potentiostat. The applied potentials stated in the UV-SEC are approximated from the CV of each compound. The Beer-Lambert Law relates to spectrophotometric analysis, which refers the concentration of a solution to the absorption of light by the solution, as shown in below, where A is the concentration, ϵ is the molar absorption, l is the path-length of the light (1 cm), and c is the concentration of the solution (0.2mM). $A = \epsilon lc$.

Solid-state conductivity and photocurrent measurements

The ITO substrates were cleaned by immersion in ultrasonic bath using the following solvents and times: 1) de-ionized water for 15min to remove the detergent from the substrate. 2) acetone 15min, 3) isopropyl alcohol 15min, followed by blowing dry with N_2 .

The experimental setup for current-voltage measurement is illustrated in below.

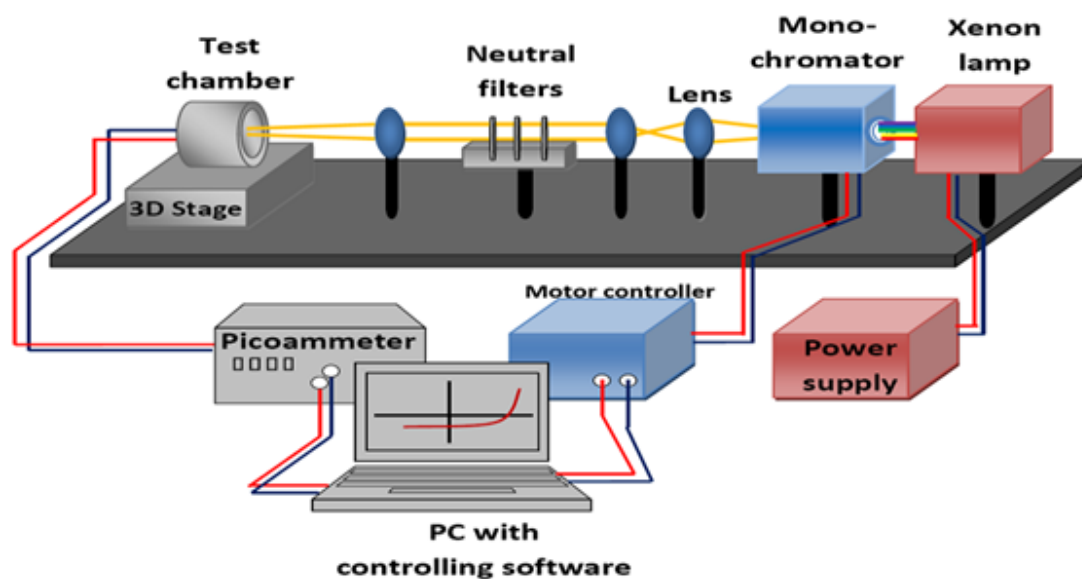
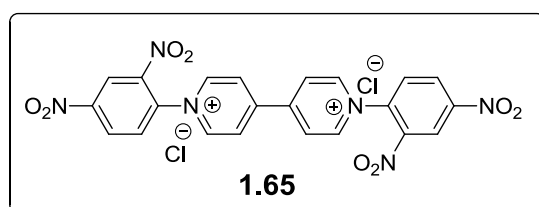


Figure S1. Schematic diagram of the equipment used for current-voltage measurements.

A voltage waveform generator (incorporated in the computer) supplies voltage for the device, and the current was recorded by a picoammeter. A Xenon lamp with its power supply was used as an illumination source. A motorized monochromator was used to vary the wavelength of the light for photospectrum measurement. The monochromator is connected to a computer based controller with software to control wavelength selection.

Detailed synthetic procedures

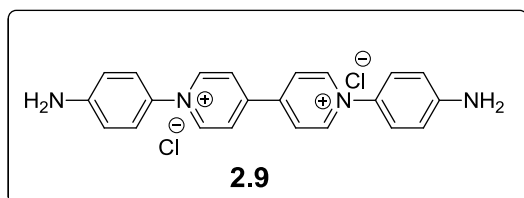
1,1'-bis(2,4-dinitrophenyl)-4,4'-bipyridinium dichloride **1.65**.¹²⁸



4,4'-Bipyridine (1.55 g, 9.94 mmol) and 1-chloro-2,4-dinitrobenzene (7.31 g, 36.1 mmol) were dissolved in anhydrous acetonitrile (15 mL) under argon. The solvent was heated to reflux and

stirred for 9 days until a large amount of pale grey precipitate was formed. A few drops of water were added to the flask and it was warmed until all the precipitate had disappeared, then ethanol was added resulting in the formation of a pale grey precipitate. The precipitate was collected by filtration, then dried *in vacuo* to yield 1,1'-bis(2,4-dinitrophenyl)-4,4'-bipyridinium dichloride (6.50 g, 95%) as a pale grey powder. The crude product was sufficiently pure for immediate use in the next reaction. A portion of this crude precipitate was purified *via* low temperature crystallization from acetonitrile with a drop of water to afford yellow needle crystals. M.p. 243 – 245 °C (Lit 250 °C). ¹H NMR (D₂O, 400 MHz) δ 9.47 (d, 6.8 Hz, 4H), 9.40 (d, 2.4 Hz, 2H_B), 8.91 - 8.95 (m, 6H), 8.30 (d, 8.4 Hz, 2H). ¹³C NMR (D₂O, 100 MHz) δ 153, 150, 147, 138, 131, 131, 128, 123. IR (cm⁻¹) ν 1548 m (NO₂).

1,1'-bis(4-aminophenyl)-[4,4'-bipyridine]-1,1'-dium chloride **2.9**¹²⁹

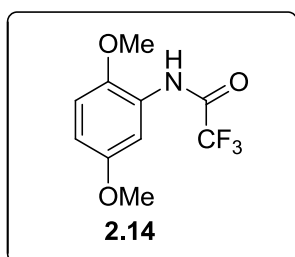


1,1'-Bis(2,4-dinitrophenyl)-4,4'-bipyridinium dichloride (5.90 g, 10.5 mmol) was dissolved in a mixture of EtOH (50 mL) and water (100 mL) with a huge excess of 1,4-diaminobenzene (7.01 g, 65

mmol). The solvent was heated to reflux and stirred strongly for 24 hours. After cooling to room temperature, the solution was concentrated to approximately 2 mL under reduced pressure and added to rapidly stirred THF (300 mL) resulting in the formation of a black precipitate. The precipitate was collected by filtration, then washed with THF (2×100 mL), and

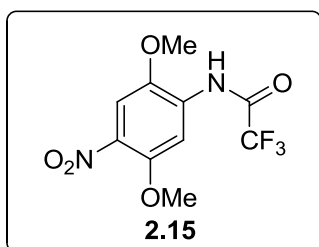
dried *in vacuo*, then recrystallized from water to yield **2.9** as a black powder (3.50g, 81%); M.p. 319 °C (Lit⁵³ 320 °C). ¹H NMR (D₂O, 400 MHz) δ 9.26 (d, 6.8 Hz, 4H), 8.68 (d, 6.8 Hz, 4H), 7.59 (d, 8.8 Hz, 4H), 7.03 (d, 8.8 Hz, 4H). ¹³C NMR (D₂O, 100 MHz) δ 150.5, 149.2, 145.6, 133.4, 126.7, 125.1, 116.4. IR (cm⁻¹) ν 3321 s (NH₂).

N-(2,5-dimethoxyphenyl)-2,2,2-trifluoroacetamide **2.14**¹³⁰



To a stirred solution of 2,5-dimethoxyaniline (8.58 g, 56.0 mmol) in a mixed solvent of chloroform (100 mL) and triethylamine (6.20 g, 61.0 mmol) with ice-bath, was added a solution of trifluoroacetic anhydride (11.7 g, 56.0 mmol) in chloroform (200 mL) slowly. Then the mixture was stirred at room temperature for 20 h. It was then washed with 0.5 N dilute hydrochloric acid (2 × 50 mL), water (2 × 100 mL), brine (2 × 50 mL), then dried over MgSO₄. After evaporating the solvent, the crude product was recrystallized from chloroform and petroleum ether (60~80 °C) to give **2.14** as a light purple powder (9.51 g, 68%). ¹H NMR (CDCl₃, 400 MHz) δ 8.50 (s, 1H), 8.01 (d, 2.8 Hz, 1H), 6.85 (d, 8.8 Hz, 1H), 6.70 (dd, 2.8 & 8.8 Hz, 1H), 3.88 (s, 3H), 3.79 (s, 3H). ¹³C NMR (CDCl₃, 100 MHz) δ 154, 142, 126, 117, 114, 111, 111, 107, 56, 56. [M]¹⁺ calc. C₁₀H₁₀O₃NF₃ for 230.0623, found 230.0621.

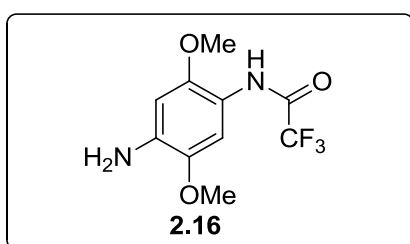
N-(2,5-dimethoxy-4-nitrophenyl)-2,2,2-trifluoroacetamide **2.15**¹³⁰



To a stirred solution of **2.14** (9.05 g, 36.0 mmol) in a mixed solvent of chloroform (100 mL) and acetic acid (50 mL) with ice-bath, was added fuming nitric acid (98%, 25 mL) dropwise. The mixture was stirred for 15 min and then poured to ice water (200 mL). The organic phase was separated and the aqueous layer was extracted with chloroform (2×50 mL). The combined organic phase was washed with 0.5 N aqueous sodium hydrogen carbonate (2×100 mL), water (2×100 mL), and brine (100 mL), then dried

over MgSO_4 . After evaporating the solvent, the crude product was recrystallized with chloroform and petroleum ether to afford **2.15** as a yellow brown powder (3.61 g, 34%). ^1H NMR (CDCl_3 , 400 MHz) δ 8.72 (s, 1H), 8.32 (s, 1H), 7.58 (s, 1H), 3.98 (s, 3H), 3.98 (s, 3H). ^{13}C NMR (CDCl_3 , 100 MHz) δ 155, 155, 149, 135, 131, 108, 106, 57, 57. $[\text{M}]^{1+}$ calc. $\text{C}_{10}\text{H}_{10}\text{O}_5\text{N}_2\text{F}_3$ for 295.0536, found 295.0535.

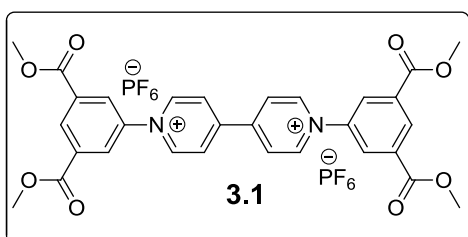
N-(4-amino-2,5-dimethoxyphenyl)-2,2,2-trifluoroacetamide **2.16**¹³⁰



A solution of **2.15** (0.98 g, 3.70 mmol) and stannous chloride (4.62 g, 22 mmol) in ethyl acetate (50 mL) was stirred under reflux for 2 h. After cooling to room temperature, saturated aqueous sodium bicarbonate solution was added until $\text{pH} = 8$. The formed precipitate was

removed by filtration through celite. The organic phases were separated and the aqueous phase was extracted with ethyl acetate (2×50 mL). The organic phase were combined and washed with water (2×50 mL), and brine (2×50 mL), and then dried over MgSO_4 . The solvent was then evaporated to afford N-(4-amino-2,5-dimethoxyphenyl)-2,2,2-trifluoroacetamide **2.16** as a purple solid (0.63 g, 64%). ^1H NMR (CDCl_3 , 400 MHz) δ 8.40 (s, 1H), 7.89 (s, 1H), 6.34 (s, 4H), 3.82 (s, 3H), 3.80 (s, 3H). ^{13}C NMR (D_2O , 100 MHz) δ 154, 153, 143, 141, 115, 105, 99, 56, 56.

Synthesis of dicationic unimer **3.1**

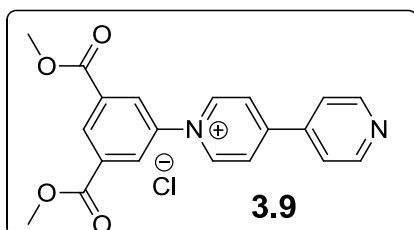


1,1'-bis(2,4-dinitrophenyl)-4,4'-bipyridinium dichloride (2.22 g, 3.96 mmol) was dissolved in a mixture of ethanol (50 mL) and water (50 mL) with excess dimethyl 5-aminoisophthalate (3.52 g, 16.83

mmol). The reaction mixture was heated to reflux and stirred vigorously for 3 days. After

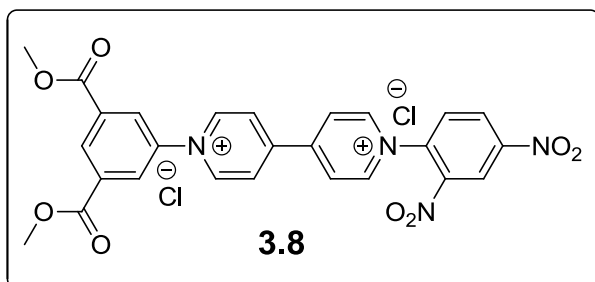
cooling to room temperature, the solvent was evaporated and the yellow solid was washed with THF (200 mL) and EtOAc (200 mL). Anion exchange to PF_6^- was achieved by dissolving the solid (4.60 g) in a mixture of water/methanol (v/v 8:2 50 mL) and adding 10 g of NH_4PF_6 . The resulting precipitate was filtered off, washed with 300 mL of water and 100 mL of ethyl acetate, and then dried under high vacuum overnight to yield **3.1** as a white solid (3.06 g, 93%). ^1H NMR (acetone- d_6 , 400 MHz) δ 9.82 (d, $J = 6.8$ Hz, 4H), 9.14 (d, $J = 6.8$ Hz, 4H), 8.88 (t, $J = 1.3$ Hz, 2H), 8.83 (d, $J = 1.2$ Hz, 4H), 3.99 (s, 12H). ^{13}C NMR (acetone- d_6 , 100 MHz) δ 164.9, 152.0, 147.7, 144.1, 133.9, 133.4, 131.0, 128.4, 53.5. IR (cm^{-1}) $\nu = 1730$ (α,β -unsaturated ester C=O). $[\text{M}-\text{H}]^{1+}$ calc. $\text{C}_{30}\text{H}_{25}\text{N}_2\text{O}_8$ for 541.1605, found 541.1601; $[\text{M}]^{2+}$ calc. $\text{C}_{30}\text{H}_{26}\text{N}_2\text{O}_8$ for 271.0839, found 271.0840.

Synthesis of 1-(3,5-bis(methoxycarbonyl)phenyl)-[4,4'-bipyridin]-1-ium dichloride **3.9**



1-(2,4-dinitrophenyl)-[4,4'-bipyridin]-1-ium chloride **3.10** (3.59 g, 10 mmol) was dissolved in ethanol (50 mL) with a large excess of dimethyl 5-aminoisophthalate (5.04 g, 24.9 mmol). The mixture was heated to reflux and stirred vigorously for 2 days. After cooling to room temperature, the solvent was evaporated and the product reprecipitated twice with ethyl acetate from methanol. The precipitate was collected by filtration, washed with THF (200 mL), and dried *in vacuo* to yield **3.9** as a light green solid (3.61 g, 94%) M.p. 243-246 °C (dec). ^1H NMR (D_2O , 400 MHz) δ 9.29 (d, $J = 6.8$ Hz, 2H), 8.94 (t, $J = 1.2$ Hz, 1H), 8.81 (dd, $J = 4.8$ and 1.6 Hz, 2H), 8.66 (d, $J = 1.2$ Hz, 2H), 8.64 (d, $J = 6.8$ Hz, 2H), 8.01 (dd, $J = 1.6$ and 4.8 Hz, 2H), 4.01 (s, 6H). ^{13}C NMR (D_2O , 100 MHz) δ 166.2, 155.5, 149.9, 144.9, 142.5, 142.3, 132.8, 132.81, 132.78, 129.4, 126.2, 53.3. IR (cm^{-1}) $\nu = 1736$ (ester C=O). $[\text{M}]^{1+}$ calc. $\text{C}_{20}\text{H}_{17}\text{N}_2\text{O}_4$ for 349.1183, found 349.1181.

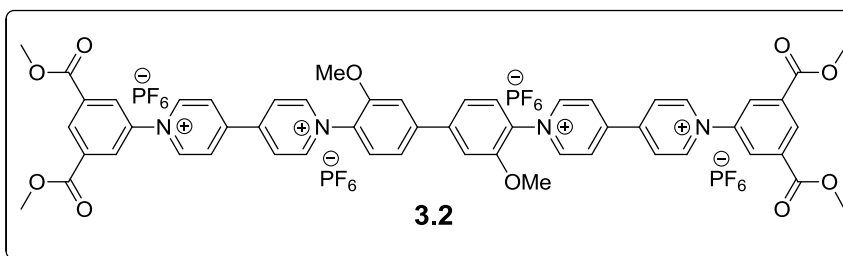
Synthesis of 3.8



1-(3,5-bis(methoxycarbonyl)phenyl)-[4,4'-bipyridin]-1-ium dichloride **3.9** (1.35 g, 3.51 mmol) was dissolved in 8 mL of EtOH with a large excess of 1-chloro-2,4-dinitrobenzene (10.0 g, 49.4 mmol). The solvent was heated to reflux and stirred strongly for 3 days. After

cooling to room temperature, the crystals were filtered off and washed with THF (2 × 100 mL), further washed with EtOAc (2 × 100 mL), and dried *in vacuo* to yield a light brown solid (1.41 g, 59%). M.p. 216-218 °C. ¹H NMR (D₂O, 400 MHz) δ 9.53 (d, *J* = 6.8 Hz, 2H), 9.47 (d, *J* = 7.2 Hz, 2H), 9.42 (d, *J* = 2.4 Hz, 2H), 8.99 (t, *J* = 1.2 Hz, 1H), 8.96 (dd, *J* = 2.4 and 8.8 Hz, 1H), 8.919 (d, *J* = 9.6 Hz, 2H), 8.912 (d, *J* = 9.6 Hz, 2H), 8.72 (d, *J* = 1.2 Hz, 2H), 8.31 (d, *J* = 8.8 Hz, 2H), 4.03 (s, 6H). ¹³C NMR (D₂O, 100 MHz) δ 168.7, 155.7, 153.6, 152.4, 149.3, 148.4, 145.3, 145.0, 140.8, 135.7, 135.5, 133.6, 133.2, 132.0, 130.1, 129.9, 125.3, 55.9. IR (cm⁻¹) ν = 1715 (ester, C=O), 1541 (NO₂). [M]¹⁺ calc. C₂₆H₂₀N₄O₈ for 561.1276, found 561.1266.

Synthesis of tetracationic dimer 3.2

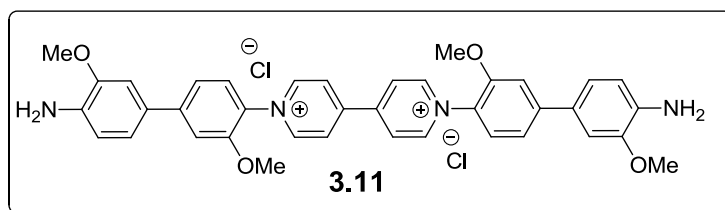


1-(3,5-bis(methoxycarbonyl)phenyl)-1'-(2,4-dinitrophenyl)-[4,4'-bipyridin]-1,1'-dium chloride **3.8** (984 mg,

1.68 mmol) was dissolved in methanol (50 mL) with 3,3'-dimethoxybenzidine (204 mg, 0.84 mmol). The mixture was heated to reflux and stirred for 4 d. After cooling to room temperature, the solvent was evaporated, and the crude product was precipitated twice from MeOH with ethyl acetate to afford a brown solid. Anion exchange to PF₆⁻

was achieved by dissolving the solid in a mixture of water/methanol (10 mL) and adding 3 g of NH_4PF_6 . The resulting precipitate was filtered off, washed with 500 mL of water and 300 mL of ethyl acetate, and then dried under high vacuum overnight to yield **3.2** as a yellow solid (960 mg, 77%). M.p. 312 °C. ^1H NMR (acetone- d_6 with 1% trifluoroacetic acid (TFA); the signal of TFA is not reported; 400 MHz) δ 9.92 (d, $J = 6.8$ Hz, 4H), 9.64 (d, $J = 7.2$ Hz, 4H), 9.21 (d, $J = 6.8$ Hz, 4H), 9.12 (d, $J = 6.8$ Hz, 4H), 8.90 (t, $J = 1.4$ Hz, 2H), 8.87 (d, $J = 1.2$ Hz, 4H), 8.04 (d, $J = 8$ Hz, 2H), 7.91 (d, $J = 1.6$ Hz, 2H), 7.69 (dd, $J = 1.6$ and 8.4 Hz, 2H), 4.13 (s, 6H), 4.02 (s, 12H). ^{13}C NMR (CD_3CN with 1% TFA; the signal of TFA is not included; 175 MHz) δ 165.3, 153.5, 152.2, 151.5, 148.4, 147.1, 145.4, 143.6, 134.3, 130.6, 128.5, 128.1, 121.6, 113.5, 27.9, 53.9. IR (cm^{-1}) $\nu = 1722$ (α,β -unsaturated ester C=O). $[\text{M}]^{4+}$ calc. for $\text{C}_{54}\text{H}_{46}\text{N}_4\text{O}_{10}$ for 227.5798, found 227.5798; $[\text{M}-1\text{H}]^{3+}$ calc. $\text{C}_{54}\text{H}_{45}\text{N}_4\text{O}_{10}$ for 303.1040, found 303.1040; $[\text{M}-2\text{H}]^{2+}$ calc. $\text{C}_{54}\text{H}_{44}\text{N}_4\text{O}_{10}$ for 454.1523, found 454.1519.

Synthesis of 1,1'-bis(4'-amino-3,3'-dimethoxy-[1,1'-biphenyl]-4-yl)-[4,4'-bipyridine]-1,1'-diium chloride **3.11**

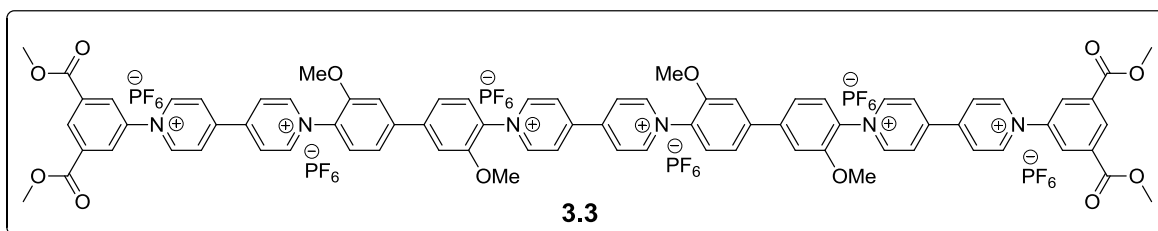


Zincke salt **1.65** (570 mg, 1.00 mmol) was dissolved in 50 mL of methanol/water (5:1, v/v) with 3,3'-dimethoxybenzidine

(732 mg, 3 mmol). The reaction mixture was heated with stirring at reflux for 3 days, and then concentrated to 3 mL and treated with THF (100 mL). The crude product was precipitated twice from MeOH/EtOAc (1:8). The precipitate was filtered off and dried under high vacuum to afford **3.12** as a deep purple solid (653 mg, 95%). M.p. 280 °C (dec.). ^1H NMR (CD_3OD , 400 MHz) δ 9.48 (d, $J = 6.8$ Hz, 2H), 9.19 (d, $J = 6.8$ Hz, 2H), 8.97 (t, $J = 1.2$ Hz, 1H), 8.82 (d, $J = 6.8$ Hz, 2H), 8.70 (d, $J = 1.2$ Hz, 2H), 8.68 (d, $J = 7.5$ Hz, 2H), 7.63 (d, $J = 8.0$ Hz, 1H), 7.44 (s, 1H), 7.42 (d, $J = 8.0$ Hz, 1H), 7.23 (d,

$J = 8.0$ Hz, 1H), 7.20 (s, 1H), 6.92 (d, $J = 8.0$ Hz, 1H), 4.03 (s, 3H), 4.01 (s, 3H), 3.93 (s, 3H). ^{13}C NMR (CD_3OD , 100 MHz) δ 165.7, 153.4, 152.5, 151.4, 149.9, 148.8, 148.5, 147.5, 145.3, 144.4, 137.0, 136.7, 134.6, 133.9, 131.6, 130.8, 130.5, 128.5, 128.1, 127.8, 124.8, 121.5, 120.5, 117.5, 111.9, 110.6, 57.3, 56.4, 53.6. IR (cm^{-1}) $\nu = 3350$ (N-H, primary amine). $[\text{M}]^{2+}$ calc. $\text{C}_{38}\text{H}_{36}\text{N}_4\text{O}_4$ for 612.2731, found 612.2725.

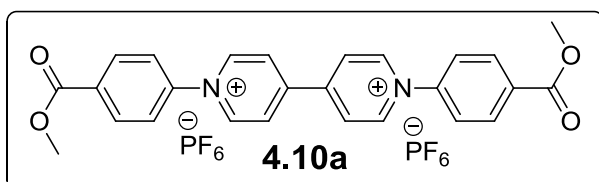
Synthesis of hexacationic trimer **3.3**



Aromatic diamine **3.11** (403 mg, 0.59 mmol) was dissolved in 100 mL of ethanol/water (1:1, v/v) with precursor (**3.8**) (704 mg, 1.20 mmol) and the solution was refluxed for 3 d. The solvent was concentrated to leave approximately 5 mL, and this was added to a rapidly stirred solution of NH_4PF_6 in a mixture of methanol and water (30 mL, 2:8 v/v). After stirring at room temperature for 1 h, the resulting precipitate was filtered off, washed with 300 mL of water and 300 mL of ethyl acetate, and finally purified by column chromatography (elution gradient: acetonitrile to 1% NH_4PF_6 in acetonitrile w/v). Excess salts were removed by precipitating the crude product twice from acetonitrile/water and the product was then dried under high vacuum to give a black solid, **3.3**, (920 mg, 72.5%). M.p. 325 °C (dec.). ^1H NMR (acetone- d_6 with 1% TFA; the signal of TFA is not reported; 400 MHz) δ 9.92 (d, $J = 6.8$ Hz, 4H), 9.64 (d, $J = 7.2$ Hz, 8H), 9.22 (d, $J = 7.2$ Hz, 4H), 9.13 (d, $J = 6.8$ Hz, 4H), 9.10 (d, $J = 6.8$ Hz, 4H), 8.89 (t, $J = 1.2$ Hz, 2H), 8.86 (d, $J = 1.6$ Hz, 4H), 8.05 (t, $J = 7.2$ Hz, 4H), 7.91 (s, 4H), 7.82 (dd, $J = 1.6$ and 8.0 Hz, 4H), 4.13 (s, 12H), 4.02 (s, 12H). ^{13}C NMR (acetone- d_6 with 1% TFA; the signal of TFA is not included; 175 MHz) δ 165.0, 158.7, 158.3, 153.6, 152.2, 151.9, 148.7, 148.7, 147.7, 145.4, 144.2, 133.9, 132.2, 131.0, 128.5, 128.4, 128.2, 128.2, 121.5, 120.2, 117.4, 114.5, 113.3, 57.5, 53.5. IR (cm^{-1}) $\nu =$

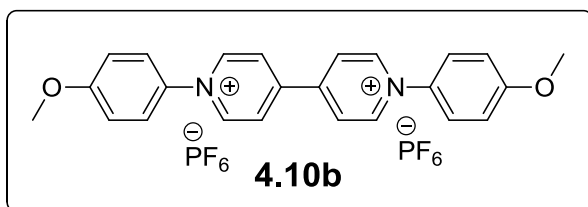
1723 (α,β -unsaturated ester, C=O). $[M-2H]^{4+}$ calc. $C_{78}H_{64}N_6O_{12}$ for 319.1140, found 319.1140; $[M-4H]^{2+}$ calc. $C_{78}H_{62}N_6O_{12}$ for 637.2207, found 637.2210.

Synthesis of 4.10a.



Di-Zincke salt **1.65** (300 mg, 0.53 mmol) was dissolved in a mixture of ethanol (50 mL) and water (15 mL) with excess dimethyl methyl 4-aminobenzoate (324 mg, 2.14 mmol). The reaction mixture was heated to reflux and stirred vigorously for 3 days. After cooling to room temperature, the solvent was evaporated, and the solid was washed with THF (200 mL) and EtOAc (200 mL). The crude product was precipitated from methanol with EtOAc twice. Anion exchange to PF_6^- was achieved by dissolving the solid in 10 mL of water and adding 10 g of NH_4PF_6 . The resulting precipitate was filtered off, washed with 300 mL of water and 100 mL of ethyl acetate, and then dried under high vacuum overnight to yield a brown solid (353 mg, 93%). M.p. 384 °C (dec). 1H NMR (acetonitrile- d_3 , 400 MHz) δ 9.23 (d, $J = 6.9$ Hz, 4H), 8.69 (d, $J = 6.7$ Hz, 4H), 8.36 (d, $J = 8.7$ Hz, 4H_c), 7.91 (d, $J = 8.6$ Hz, 4H), 3.97 (s, 6H). ^{13}C NMR (acetonitrile- d_3 , 100 MHz) δ 166.1, 151.7, 146.7, 146.1, 134.6, 132.4, 128.4, 126.1, 53.4. IR (cm $^{-1}$) $\nu = 1721$ (ester C=O). $[M-H]^{1+}$ calc. $C_{26}H_{21}O_4N_2$ for 425.1496, found 425.1494.

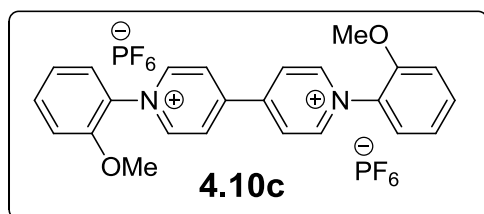
Synthesis of 4.10b.



Di-Zincke salt **1.65** (300 mg, 0.53 mmol) was dissolved in a mixture of ethanol (50 mL) and water (15 mL) with excess 4-methoxyaniline (658 mg, 5.34 mmol). The reaction mixture was heated to reflux and stirred vigorously for 2 days. After cooling to room temperature, the solvent was evaporated, the solid was washed with THF (200 mL) and EtOAc (200 mL). The crude product was precipitated from methanol with EtOAc twice. Anion exchange to PF_6^- was

achieved by dissolving the solid in 10 mL of water and adding 10 g of NH_4PF_6 . The resulting precipitate was filtered off, washed with 300 mL of water and 100 mL of ethyl acetate, and then dried under high vacuum overnight to a yellow solid (332 mg, 95%). M.p. 229 °C. ^1H NMR (acetonitrile- d_3 , 400 MHz) δ 9.14 (d, J = 6.9 Hz, 4H), 8.61 (d, J = 6.8 Hz, 4H), 7.73 (d, J = 9.0 Hz, 4H), 7.91 (d, J = 9.0 Hz, 4H), 3.94 (s, 6H). ^{13}C NMR (acetonitrile- d_3 , 100 MHz) δ 163.3, 150.6, 146.3, 136.2, 128.0, 126.8, 116.5, 56.8. IR (cm $^{-1}$) ν = 1257 (ether C-O). $[\text{M-H}]^{1+}$ calc. $\text{C}_{26}\text{H}_{21}\text{O}_2\text{N}_2$ for 369.1598, found 369.1598.

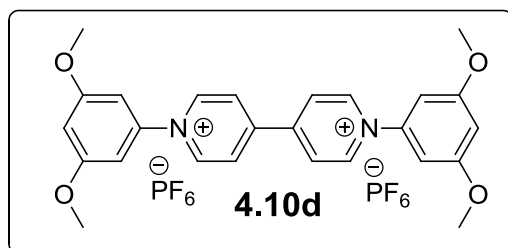
Synthesis of 4.10c.



Di-Zincke salt **1.65** (300 mg, 0.53 mmol) was dissolved in a mixture of methanol (60 mL) and water (15 mL) with excess 2-methoxyaniline (246 mg, 2.00 mmol). The reaction mixture was heated to reflux and

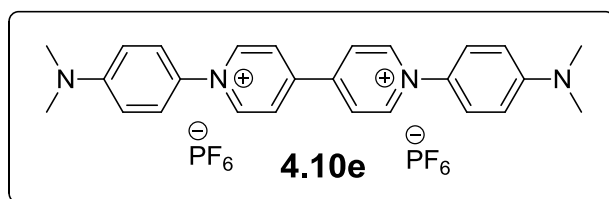
stirred vigorously under argon for 2 days. After cooling to room temperature, the solvent was evaporated, the solid was washed with THF (200 mL) and EtOAc (200 mL). The crude product was precipitated from methanol with EtOAc twice. Anion exchange to PF_6^- was achieved by dissolving the solid in 10 mL of water and adding 10 g of NH_4PF_6 . The resulting precipitate was filtered off, washed with 300 mL of water and 100 mL of ethyl acetate, and then dried under high vacuum overnight to a yellow solid (322 mg, 92%). M.p. 274 °C. ^1H NMR (acetonitrile- d_3 , 400 MHz) δ 9.07 (d, J = 7.0 Hz, 4H), 8.60 (d, J = 7.0 Hz, 4H), 7.77 – 7.73 (m, 2H), 7.63 (dd, J = 8.0 & 1.4 Hz, 2H), 7.40 (dd, J = 8.0 & 1.4 Hz, 2H), 7.32 – 7.28 (m, 2H), 3.92 (s, 6H). ^{13}C NMR (acetonitrile- d_3 , 100 MHz) δ 153.0, 151.6, 148.3, 134.7, 131.6, 127.9, 127.4, 122.5, 114.4, 57.3. IR (cm $^{-1}$) ν = 1277 (ether C-O). $[\text{M-H}]^{1+}$ calc. $\text{C}_{26}\text{H}_{21}\text{O}_2\text{N}_2$ for 369.1598, found 369.1601.

Synthesis of 4.10d.



Zincke salt **1.65** (300 mg, 0.53 mmol) was dissolved in a mixture of methanol (60 mL) and water (15 mL) with excess 3,5-dimethoxyaniline (409 mg, 2.67 mmol). The reaction mixture was heated to reflux and stirred vigorously under argon for 2 days. After cooling to room temperature, the solvent was evaporated, the solid was washed with THF (200 mL) and EtOAc (200 mL). The crude product was precipitated from methanol with EtOAc twice. Anion exchange to PF_6^- was achieved by dissolving the solid in 10 mL of water and adding 10 g of NH_4PF_6 . The resulting precipitate was filtered off, washed with 300 mL of water and 100 mL of ethyl acetate, and then dried under high vacuum overnight to a yellow solid (302 mg, 79%). M.p. 335 °C (dec). ^1H NMR (acetonitrile- d_3 , 400 MHz) δ 9.19 (d, $J = 6.5$ Hz, 4H), 8.60 (d, $J = 6.4$ Hz, 4H), 6.94 (s, 4H), 6.86 (s, 2H), 3.91 (s, 12H). ^{13}C NMR (acetonitrile- d_3 , 100 MHz) δ 162.9, 151.4, 146.6, 144.8, 128.1, 104.0, 103.9, 56.9. IR (cm $^{-1}$) $\nu = 1161, 1213$ (ether C-O). $[\text{M-H}]^{1+}$ calc. $\text{C}_{26}\text{H}_{25}\text{O}_4\text{N}_2$ for 429.1809, found 429.1807.

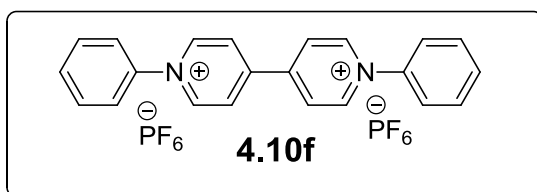
Synthesis of 4.10e



Zincke salt **1.65** (300 mg, 0.53 mmol) was dissolved in a mixture of methanol (60 mL) and water (15 mL) with excess of N,N-Dimethyl-1,4-benzenediamine (545 mg, 4.00 mmol) in a 100 mL round bottom flask which was covered with foil (light sensitive). The reaction mixture was heated to reflux and stirred vigorously under argon for 3 days. After cooling to room temperature, the solvent was evaporated, the solid was washed with THF (200 mL). The crude product was precipitated from methanol with EtOAc twice. Anion exchange to PF_6^- was achieved by dissolving the solid in 10 mL of water and adding 10 g of NH_4PF_6 . The resulting precipitate was filtered off, washed with 300 mL of water and 100 mL of ethyl acetate,

and then dried under high vacuum overnight to a deep purple solid (298 mg, 81%). M.p. 368 °C (dec). ^1H NMR (acetonitrile- d_3 , 400 MHz) δ 9.08 (d, J = 6.2 Hz, 4H), 8.54 (d, J = 6.1 Hz, 4H), 7.62 (d, J = 9.0 Hz, 4H), 6.97 (d, J = 9.0 Hz, 4H), 3.10 (s, 12H). ^{13}C NMR (acetonitrile- d_3 , 100 MHz) δ 15.3.3, 149.0, 145.0, 131.7, 127.6, 125.7, 113.5, 40.6. IR (cm^{-1}) ν = 2820 (*N,N*-dimethyl). $[\text{M-H}]^{1+}$ calc. $\text{C}_{26}\text{H}_{21}\text{O}_2\text{N}_2$ for 395.2230, found 395.2231.

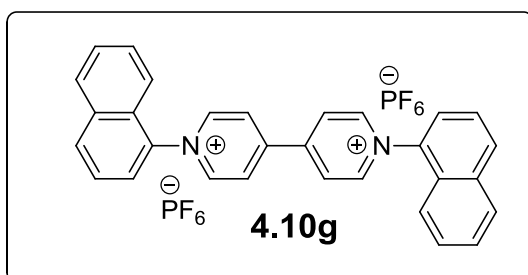
Synthesis of 4.10f



Zincke salt **1.65** (300 mg, 0.53 mmol) was dissolved in a mixture of methanol (60 mL) and water (15 mL) with aniline (465 mg, 5.00 mmol).

The reaction mixture was heated to reflux and stirred vigorously under argon for 3 days. After cooling to room temperature, the solvent was evaporated, the solid was washed with THF (200 mL) and EtOAc (200 mL). The crude product was precipitated from methanol with EtOAc twice. Anion exchange to PF_6^- was achieved by dissolving the solid in 10 mL of water and adding 10 g of NH_4PF_6 . The resulting precipitate was filtered off, washed with 300 mL of water and 100 mL of ethyl acetate, and then dried under high vacuum overnight to a white solid (305 mg, 96%). M.p. 395 °C (dec). ^1H NMR (acetonitrile- d_3 , 400 MHz) δ 9.20 (d, J = 7.0 Hz, 4H), 8.66 (d, J = 6.8 Hz, 4H), 7.80 (s, 10H). ^{13}C NMR (acetonitrile- d_3 , 100 MHz) δ 151.3, 146.6, 143.3, 133.1, 131.6, 128.2, 125.4. $[\text{M-H}]^{1+}$ calc. $\text{C}_{22}\text{H}_{17}\text{N}_2$ for 309.1386, found 309.1391.

Synthesis of 4.10g

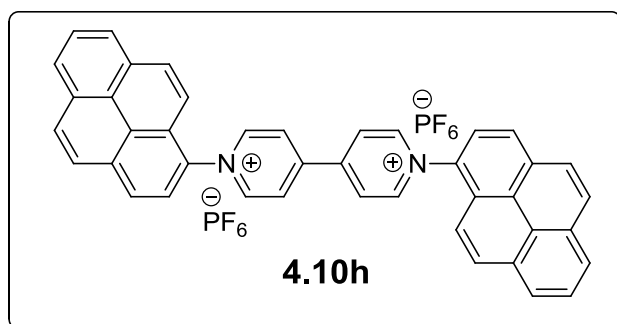


Zincke salt **1.65** (300 mg, 0.53 mmol) was dissolved in a mixture of methanol (60 mL) and water (15 mL) with excess of naphthalen-1-amine (85 mg, 0.6 mmol). The reaction mixture was heated to reflux and stirred vigorously under argon

for 3 days. After cooling to room temperature, the solvent was evaporated, the solid was

washed with THF (200 mL) and EtOAc (200 mL). The crude product was precipitated from methanol with EtOAc twice. Precipitate the crude product from methanol with EtOAc twice. Anion exchange to PF_6^- was achieved by dissolving the solid in 10 mL of water and adding 10 g of NH_4PF_6 . The resulting precipitate was filtered off, washed with 300 mL of water and 100 mL of ethyl acetate, and then dried under high vacuum overnight to a bright yellow solid (323 mg, 87%). M.p. 310 °C. ^1H NMR (acetonitrile- d_3 , 400 MHz) δ 9.23 (d, $J = 6.8$ Hz, 4H), 8.66 (d, $J = 6.7$ Hz, 4H), 8.37 (d, $J = 8.2$ Hz, 2H), 8.23 (d, $J = 8.2$ Hz, 2H), 7.92 (d, $J = 7.3$ Hz, 2H), 7.86 - 7.73 (m, 6H), 7.50 (d, $J = 8.3$ Hz, 2H). ^{13}C NMR (acetonitrile- d_3 , 100 MHz) δ 152.5, 148.4, 139.3, 135.1, 133.6, 130.2, 130.0, 129.1, 128.7, 127.9, 126.3, 125.6, 121.2. $[\text{M-H}]^{1+}$ calc. $\text{C}_{30}\text{H}_{21}\text{N}_2$ for 409.1699, found 409.1701.

Synthesis of 4.10h

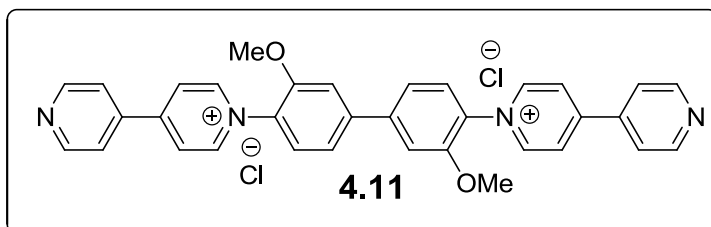


Zincke salt **1.65** (300 mg, 0.53 mmol) was dissolved in a mixture of methanol (60 mL) and water (15 mL) with excess of 1-aminopyrene (270 mg, 1.24 mmol). The reaction mixture was heated to reflux and stirred vigorously under argon for 3 days.

After cooling to room temperature, the solvent was evaporated, the solid was washed with THF (200 mL) and EtOAc (200 mL). The crude product was precipitated from methanol with EtOAc twice. Anion exchange to PF_6^- was achieved by dissolving the solid in 10 mL of water and adding 10 g of NH_4PF_6 . The resulting precipitate was filtered off, washed with 300 mL of water and 100 mL of ethyl acetate, and then dried under high vacuum overnight to a deep fuchsia solid (382 mg, 85%). M.p. 342 °C. ^1H NMR (acetonitrile- d_3 , 400 MHz) δ 9.39 (d, $J = 6.0$ Hz, 4H), 8.85 (d, $J = 5.8$ Hz, 4H), 8.59 (d, $J = 8.3$ Hz, 2H), 8.55 (d, $J = 7.8$ Hz, 2H), 8.51 - 8.44 (m, 6H), 8.38 (t, $J = 9.9$ Hz, 4H), 8.29 (t, $J = 7.6$ Hz, 2H), 7.78 (d, $J = 9.2$ Hz, 2H). ^{13}C NMR (acetonitrile- d_3 , 100 MHz) δ 152.3, 148.9, 136.0, 134.6, 132.3, 132.0, 131.3, 131.2, 128.8, 128.7, 128.1, 127.9, 126.3, 126.2, 125.4, 124.5, 124.3. $[\text{M-H}]^{1+}$ calc. $\text{C}_{42}\text{H}_{25}\text{N}_2$ for 557.2012,

found 557.2009.

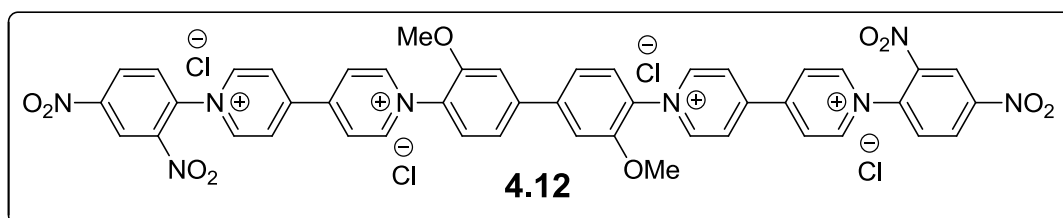
Synthesis of 4.11



Compound **3.10** (1.20 g, 3.34 mmol) was dissolved in a mixture solution of DMAc (30 mL) and water (30 mL) with

aromatic diamine **2.19** (408 mg, 1.67 mmol). The mixture was heated to 95 °C and stirred for 5 d. After cooling to room temperature, the solvent was concentrated to 5 mL roughly, then poured in to 300 mL of THF. The resulting precipitate was filtered off, washed with 300 mL of ethyl acetate, and then dried under high vacuum at 40 °C for 2 hours to yield the brown solid. The crude product was recrystallized from water to afford the brownish yellow solid (1.59 g, 80%). M.p 232 °C. ¹H NMR (methanol-*d*₄, 400 MHz) δ 9.31 (d, *J* = 6.9 Hz, 4H), 8.91 (d, *J* = 6.0 Hz, 4H), 8.73 (d, *J* = 6.9 Hz, 4H_b), 8.16 (d, *J* = 6.2 Hz, 4H), 7.92 (d, *J* = 8.2 Hz, 2H), 7.78 (d, *J* = 1.4 Hz, 2H) 7.71 (dd, *J* = 8.2 & 1.6 Hz, 2H), 4.10 (s, 6H). ¹³C NMR (D₂O; 175 MHz) δ 156.0, 153.9, 151.4, 148.4, 146.0, 144.1, 132.4, 128.3, 126.9, 124.0, 121.8, 113.5, 57.5. [M-H]¹⁺ calc. C₃₄H₂₇O₂N₄ for 523.2129, found 523.2124.

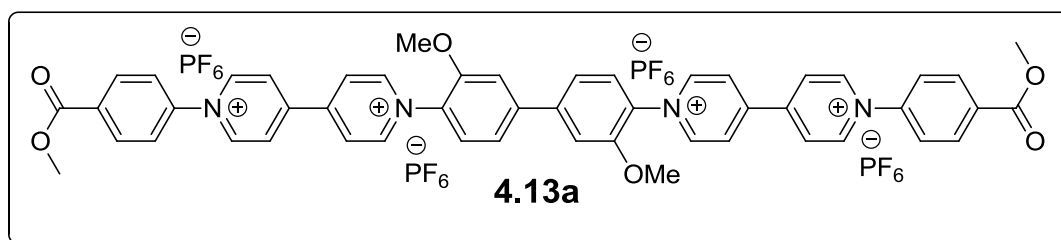
Synthesis of the precursor for general dimer



Compound **4.11** (0.92 g, 1.51 mmol) and 1-chloro-2,4-dinitrobenzene (14.62 g, 72.2 mmol) were dissolved in anhydrous methanol (15 mL). The solvent was heated to 75 °C and stirred 10 days under argon. After cooling to room temperature, the solution was added slowly to a rapidly

stirred mixture solution of THF (100 mL) and EtOAc (200 mL). After stirring at room temperature for 15 min, the resulting yellow precipitate was collected by filtration, washed with EtOAc (2 × 20 mL) and dried *in vacuo* at 40 °C overnight. Purification was achieved by recrystallization from water 3 times, collecting the filtrate, then precipitating with EtOAc to afford the yellow solid (0.72 g, 47.6). M.p. 162 °C. ¹H NMR (D₂O, 400MHz) δ 9.45 (d, J = 6.8 Hz, 4H_a), 9.41 (d, J = 2.4 Hz, 2H_e), 9.36 (d, J = 7.2 Hz, 2H_c), 8.95 (dd, J = 8.8, 2.4 Hz, 2H_g), 8.90 (d, J = 6.8 Hz, 4H_b), 8.81 (d, J = 7.2 Hz, 4H_d), 8.30 (d, J = 8.4 Hz, 2 H_f), 7.82 (d, 8.4 Hz, 2 H_i), 7.69 (s, 2 H_h), 7.66 (d, J = 8.4Hz, 2H_j). ¹³C NMR (methanol-d₄, 100 MHz) δ 154.1, 153.9, 151.9, 151.5, 149.1, 148.6, 146.2, 144.6, 139.8, 132.6, 131.3, 128.5, 128.41, 128.37, 123.3, 121.9, 113.6, 57.6. IR (cm⁻¹) ν = 1539, 1343 (NO₂).

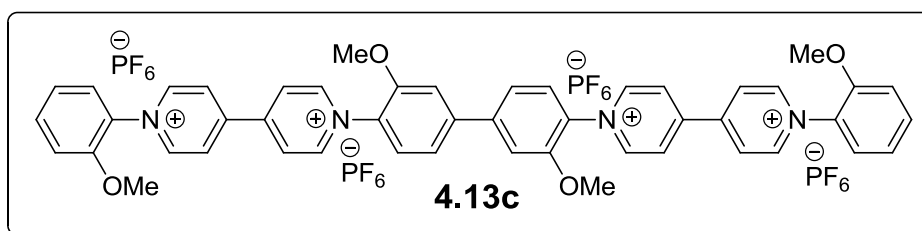
Synthesis of dimer **4.13a**



The precursor **4.12** (150 mg, 0.15 mmol) was dissolved in a mixture of methanol (50 mL) and water (15 mL) with excess methyl 4-aminobenzoate (324 mg, 2.14 mmol). The reaction mixture was heated to reflux and stirred vigorously for 3 days. After cooling to room temperature, the solvent was evaporated, and the crude product was precipitated twice from MeOH with ethyl acetate to afford a brown solid. Anion exchange to PF₆⁻ was achieved by dissolving the solid in a mixture of water/methanol (10 mL) and adding 3 g of NH₄PF₆. After stirring at room temperature for 1 h, the resulting yellow precipitate was collected by filtration, washed with water (2 × 50 mL) and dried *in vacuo* overnight to yield dimer **4.13a** as a yellow solid (195 mg, 95%). M.p 384 °C (dec). ¹H NMR (acetonitrile-*d*₃ with 1% trifluoroacetic acid (TFA); the signal of TFA is not reported; 400 MHz) δ 9.24 (d, J = 6.8 Hz, 4H), 9.16 (d, J = 6.9 Hz, 4H), 8.70 (d, J = 6.8 Hz, 4H), 8.66 (d, J = 6.9 Hz, 4H), 8.57 (d, J = 8.7 Hz, 4H), 7.93 (d, J =

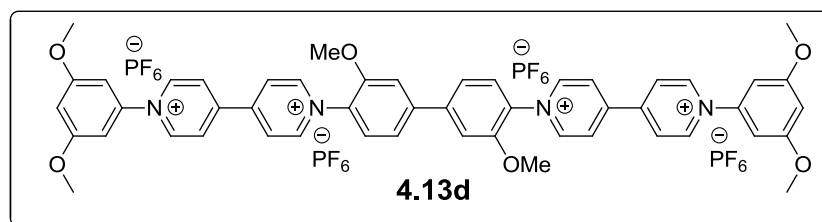
8.7 Hz, 4H), 7.81 (d, $J = 8.4$ Hz, 2H), 7.71-7.69 (m, 4H), 4.08 (s, 6H), 3.98 (s, 6H). ^{13}C NMR (acetonitrile- d_3 with 1% trifluoroacetic acid (TFA); the signal of TFA is not reported; 100 MHz) δ 166.1, 153.4, 152.0, 151.5, 148.3, 146.6, 146.1, 145.3, 132.4, 131.8, 128.4, 128.1, 128.0, 126.1, 121.5, 113.4, 57.8, 53.4. IR (cm^{-1}) $\nu = 1723$ (ester C=O). $[\text{M}-2\text{H}]^{2+}$ calc. $\text{C}_{50}\text{H}_{40}\text{O}_6\text{N}_4$ for 396.1468, found 396.1469.

Synthesis of dimer **4.13c**



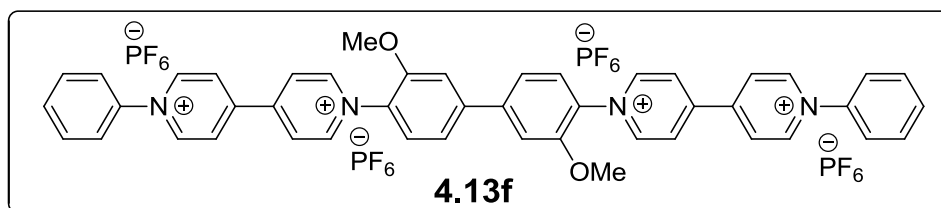
The precursor for general dimer **4.12** (150 mg, 0.15 mmol) was dissolved in a mixture of methanol (60 mL) and water (15 mL) with excess 2-methoxyaniline (246 mg, 2.00 mmol). The reaction mixture was heated to reflux and stirred vigorously under argon for 2 days. After cooling to room temperature, the solvent was evaporated, and the crude product was precipitated twice from MeOH with ethyl acetate to afford a brown solid. Anion exchange to PF_6^- was achieved by dissolving the solid in a mixture of water/methanol (10 mL) and adding 3 g of NH_4PF_6 . After stirring at room temperature for 1 h, the resulting yellow precipitate was collected by filtration, washed with water (2×50 mL) and dried *in vacuo* overnight to yield dimer **4.13c** as a brown solid after filtration and drying (168 mg, 85%). M.p 300 °C(dec). ^1H NMR (acetonitrile- d_3 with 1% trifluoroacetic acid (TFA); the signal of TFA is not reported; 400 MHz) δ 9.16 (d, $J = 7.0$ Hz, 4H), 9.10 (d, $J = 6.1$ Hz, 4H), 8.66 (m, 8H), 7.80-7.64 (m, 10H), 7.41 (d, $J = 8.6$ Hz, 2H), 7.93 (t, $J = 7.5$ Hz, 2H), 4.08 (s, 6H), 3.93 (s, 6H). ^{13}C NMR (acetonitrile- d_3 with 1% trifluoroacetic acid (TFA); the signal of TFA is not reported; 175 MHz) δ 153.4, 152.9, 148.3, 148.3, 134.7, 131.8, 131.6, 128.1, 128.0, 127.97, 127.93, 127.4, 122.5, 121.5, 114.9, 114.4, 113.4, 57.8, 57.3. IR (cm^{-1}) $\nu = 1227$ (ether C-O). $[\text{M}-2\text{H}]^{2+}$ calc. $\text{C}_{48}\text{H}_{40}\text{O}_4\text{N}_4$ for 368.1519, found 368.1511.

Synthesis of dimer 4.13d



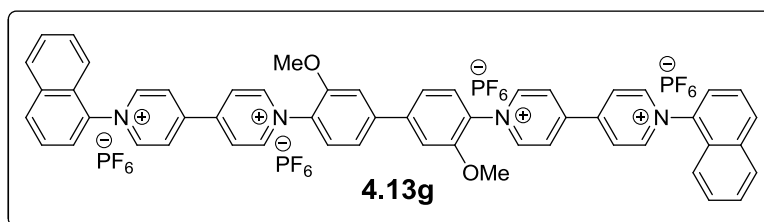
The precursor **4.12** for general dimer (150 mg, 0.15 mmol) was dissolved in a mixture of methanol (60 mL) and water (15 mL) with excess 3,5-dimethoxyaniline (409 mg, 2.67 mmol). The reaction mixture was heated to reflux and stirred vigorously under argon for 2 days. After cooling to room temperature, the solvent was evaporated, and the crude product was precipitated twice from MeOH with ethyl acetate to afford a brown solid. Anion exchange to PF_6^- was achieved by dissolving the solid in a mixture of water/methanol (10 mL) and adding 3 g of NH_4PF_6 . After stirring at room temperature for 1 h, the resulting yellow precipitate was collected by filtration, washed with water (2×50 mL) and dried *in vacuo* overnight to yield dimer **3** as a brown solid (186 mg, 90%). M.p 372 °C (dec). ^1H NMR (acetonitrile- d_3 with 1% trifluoroacetic acid (TFA); the signal of TFA is not reported; 400 MHz) δ 9.21 (d, $J = 6.8$ Hz, 4H), 9.15 (d, $J = 6.8$ Hz, 4H), 8.65 (d, $J = 5.8$ Hz, 8H), 7.80 (d, $J = 8.4$ Hz, 2H), 7.70-7.68 (m, 4H), 6.96 (d, $J = 1.9$ Hz, 4H), 6.88 (s, 2H), 4.07 (s, 6H), 3.93 (s, 12H). ^{13}C NMR (acetonitrile- d_3 with 1% trifluoroacetic acid (TFA); the signal of TFA is not reported; 100 MHz) δ 162.9, 153.4, 151.6, 148.3, 146.6, 145.3, 144.8, 131.8, 128.2, 128.1, 128.0, 121.5, 113.4, 104.1, 103.9, 57.8, 56.9. IR (cm^{-1}) $\nu = 1162$ (ether C-O). $[\text{M}-2\text{H}]^{2+}$ calc. $\text{C}_{48}\text{H}_{44}\text{O}_6\text{N}_4$ for 398.1625, found 398.1629.

Synthesis of dimer **4.13f**



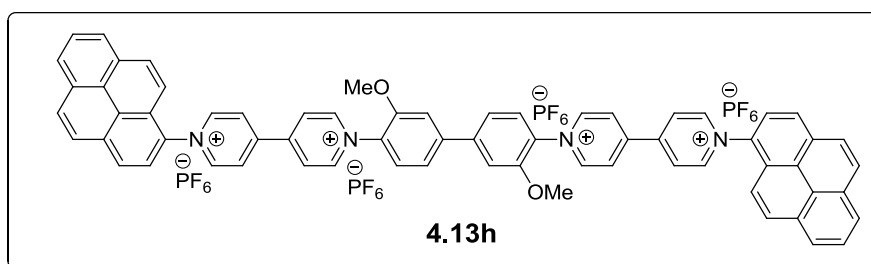
The precursor for general dimer (150 mg, 0.15 mmol) was dissolved in a mixture of methanol (60 mL) and water (15 mL) with aniline (465 mg, 5.00 mmol). The reaction mixture was heated to reflux and stirred vigorously under argon for 3 days. After cooling to room temperature, the solvent was evaporated, and the crude product was precipitated twice from MeOH with ethyl acetate to afford a brown solid. Anion exchange to PF_6^- was achieved by dissolving the solid in a mixture of water/methanol (10 mL) and adding 3 g of NH_4PF_6 . After stirring at room temperature for 1 h, the resulting yellow precipitate was collected by filtration, washed with water (2×50 mL) and dried *in vacuo* overnight to yield dimer **4.13f** as a deep brown solid (164 mg, 87%). M.p 322 °C (dec). ^1H NMR (acetonitrile- d_3 with 1% trifluoroacetic acid (TFA); the signal of TFA is not reported; 400 MHz) δ 9.22 (d, $J = 6.4$ Hz, 4H), 9.13 (d, $J = 6.8$ Hz, 4H), 8.65 (m, 8H), 7.82 (s, 10H), 7.72-7.68 (m, 4H), 6.96 (m, 2H), 6.88 (s, 2H), 4.03 (s, 6H). ^{13}C NMR (acetonitrile- d_3 with 1% trifluoroacetic acid (TFA); the signal of TFA is not reported; 100 MHz) δ 152.5, 152.2, 147.4, 147.3, 145.73, 145.69, 130.7, 127.4, 127.37, 126.9, 126.8, 124.5, 112.5, 111.5, 110.6, 55.6. $[\text{M}-2\text{H}]^{2+}$ calc. $\text{C}_{46}\text{H}_{36}\text{O}_2\text{N}_4$ for 338.1414, found 398.1415.

Synthesis of dimer **4.13g**



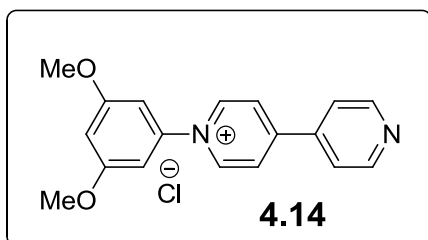
The precursor for general dimer (150 mg, 0.15 mmol) was dissolved in a mixture of methanol (60 mL) and water (15 mL) with excess of naphthalen-1-amine (545 mg, 4.00 mmol). The reaction mixture was heated to reflux and stirred vigorously under argon for 3 days. After cooling to room temperature, the solvent was evaporated, and the crude product was precipitated twice from MeOH with ethyl acetate to afford a brown solid. Anion exchange to PF_6^- was achieved by dissolving the solid in a mixture of water/methanol (10 mL) and adding 3 g of NH_4PF_6 . After stirring at room temperature for 1 h, the resulting yellow precipitate was collected by filtration, washed with water (2×50 mL) and dried *in vacuo* overnight to yield dimer **4.13g** as a brownish yellow solid (191 mg, 92%). M.p 340 °C (dec). ^1H NMR (acetonitrile- d_3 with 1% trifluoroacetic acid (TFA); the signal of TFA is not reported; 400 MHz) δ 9.20 (dd, $J = 6.9, 7.0$ Hz, 8H), 8.74 (d, $J = 6.7$ Hz, 4H), 8.70 (d, $J = 6.7$ Hz, 4H), 8.37 (d, $J = 8.2$ Hz, 2H), 8.22 (d, $J = 7.8$ Hz, 2H), 7.91 (d, $J = 6.7$ Hz, 2H), 7.85-7.71 (m, 12H), 7.49 (d, $J = 8.2$ Hz, 2H), 4.07(s, 6H). ^{13}C NMR (acetonitrile- d_3 with 1% trifluoroacetic acid (TFA); the signal of TFA is not reported; 100 MHz) δ 153.5, 152.4, 151.9, 148.4, 145.3, 139.3, 135.1, 133.6, 131.8, 130.2, 129.8, 129.1, 128.7, 128.1, 128.05, 127.9, 126.4, 125.6, 121.5, 121.2, 113.5, 57.8. $[\text{M}-2\text{H}]^{2+}$ calc. $\text{C}_{48}\text{H}_{40}\text{O}_2\text{N}_4$ for 388.1570, found 388.1573.

Synthesis of dimer **4.13h**



The precursor for general dimer (150 mg, 0.15 mmol) was dissolved in a mixture of methanol (60 mL) and water (15 mL) with excess of 1-aminopyrene (270 mg, 1.24 mmol). The reaction mixture was heated to reflux and stirred vigorously under argon for 3 days. After cooling to room temperature, the solvent was evaporated, and the crude product was precipitated twice from MeOH with ethyl acetate to afford a brown solid. Anion exchange to PF_6^- was achieved by dissolving the solid in a mixture of water/methanol (10 mL) and adding 3 g of NH_4PF_6 . After stirring at room temperature for 1 h, the resulting yellow precipitate was collected by filtration, washed with water (2×50 mL) and dried *in vacuo* overnight to yield dimer **4.13h** as a brownish yellow solid (214 mg, 95%). M.p 343 °C (dec). ^1H NMR (acetonitrile- d_3 with 1% trifluoroacetic acid (TFA); the signal of TFA is not reported; 400 MHz) δ 9.37 (d, $J = 6.0$ Hz, 4H), 9.24 (d, $J = 6.4$ Hz, 4H), 8.88 (d, $J = 6.2$ Hz, 4H), 8.76 (d, $J = 6.4$ Hz, 4H), 8.59 (d, $J = 8.3$ Hz, 3H), 8.54 (d, $J = 7.7$ Hz, 2H), 8.48 (t, $J = 7.6$ Hz, 3H), 8.44 (d, $J = 7.7$ Hz, 4H), 8.38 (t, $J = 9.5$ Hz, 4H), 8.29 (t, $J = 7.6$ Hz, 2H), 7.88 (d, $J = 8.0$ Hz, 2H), 7.76-7.72 (m, 4H), 4.13(s, 6H). ^{13}C NMR (acetonitrile- d_3 with 1% trifluoroacetic acid (TFA); the signal of TFA is not reported; 100 MHz) δ 152.2, 151.0, 150.7, 147.6, 147.2, 146.8, 144.12, 143.8, 134.8, 133.4, 131.0, 130.8, 130.6, 130.1, 129.96, 127.5, 126.9, 126.85, 126.8, 126.7, 126.5, 125.7, 125.05, 124.97, 124.2, 123.2, 123.1, 120.3, 118.5, 112.2, 56.6. $[\text{M}-2\text{H}]^{2+}$ calc. $\text{C}_{66}\text{H}_{44}\text{O}_2\text{N}_4$ for 462.1727, found 462.1727.

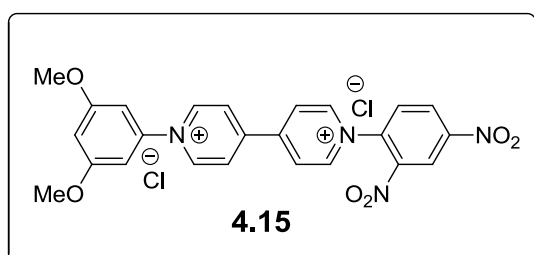
Synthesis of 4.14



1-(2,4-Dinitrophenyl)-[4,4'-bipyridin]-1-ium chloride **3.10** (3.59 g, 10 mmol) was dissolved in ethanol (50 mL) with a large excess of dimethyl 3,5-dimethoxyaniline (5.04 g, 24.9 mmol). The

mixture was heated to reflux and stirred vigorously for 2 days. After cooling to room temperature, the solvent was evaporated and the product reprecipitated twice with ethyl acetate from methanol. The precipitate was collected by filtration, washed with THF (200 mL), and dried *in vacuo* to yield **4.14** as a brown solid (3.08 g, 94%) M.p. 241 °C (dec). ¹H NMR (D₂O, 400 MHz) δ 9.18 (d, *J* = 6.8 Hz, 2H), 8.78 (d, *J* = 6.4 Hz, 2H), 8.55 (d, *J* = 6.8 Hz, 2H), 7.97 (d, *J* = 6.0 Hz, 2H), 6.96 (d, *J* = 2.0 Hz, 2H), 6.84 (t, *J* = 2.0 Hz, 1H), 3.89 (s, 6H). ¹³C NMR (D₂O, 100 MHz) δ 161.4, 154.9, 150.1, 144.6, 143.8, 142.2, 125.9, 122.6, 103.02, 102.95, 56.05. IR (cm⁻¹) ν = 1582, 1329 (NO₂). [M]¹⁺ calc. C₁₈H₁₇O₂N₂ for 293.1285, found 293.1283.

Synthesis of 4.15

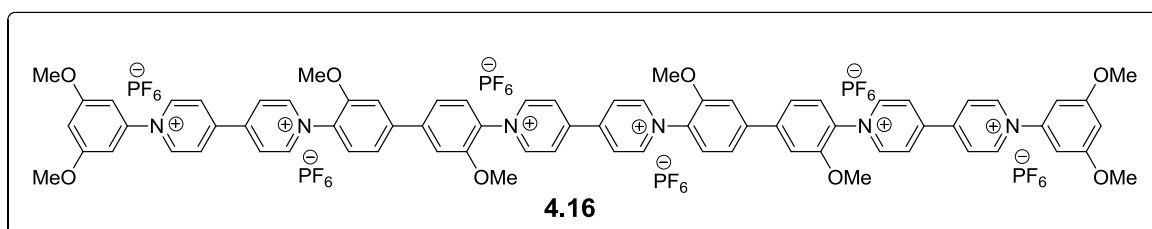


Compound **4.14** (2.10 g, 6.38 mmol) was dissolved in 8 mL of EtOH with a large excess of 1-chloro-2,4-dinitrobenzene (10.0 g, 49.4 mmol). The solvent was heated to reflux and stirred strongly for 3 days. After cooling to room

temperature, the crystals were filtered off and washed with THF (2 × 100 mL), further washed with EtOAc (2 × 100 mL), and dried *in vacuo* to yield a yellow solid (2.04 g, 60%). M.p. 216-218 °C. ¹H NMR (D₂O, 400 MHz) δ 9.47-9.43 (m, 5H), 8.97 (dd, *J* = 2.8, 8.8 Hz, 1H), 8.92 (d, *J* = 6.8 Hz, 2H), 8.83 (d, *J* = 6.8 Hz, 2H), 8.33 (d, *J* = 8.8 Hz, 1H), 7.06 (d, *J* = 2.0 Hz, 2H), 6.95 (t, *J* = 2.0 Hz, 1H), 3.94 (s, 6H). ¹³C NMR (D₂O, 100 MHz) δ 161.4, 152.9, 150.9, 150.4,

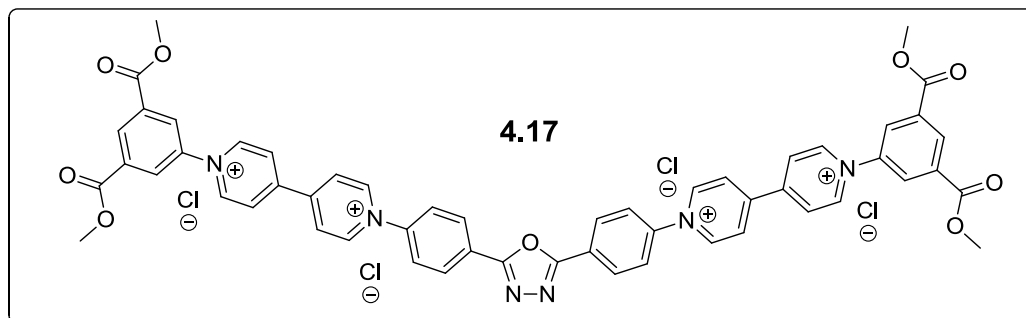
149.7, 146.6, 145.6, 143.7. 142.7, 138.2, 131.0, 130.6, 127.2, 127.1, 122.7, 103.3, 103.1, 56.0.
IR (cm⁻¹) ν = 1542, 1331 (NO₂). [M-1H]¹⁺ calc. C₂₄H₂₁O₅N₄ for 445.1506, found 445.1501.

Synthesis of trimer **4.16**



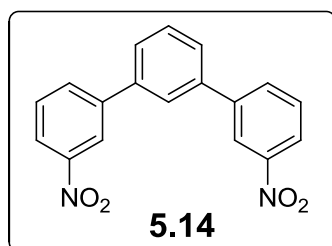
Aromatic diamine **3.11** (403 mg, 0.59 mmol) was dissolved in 100 mL of ethanol/water (1:1, v/v) with precursor (**4.15**) (704 mg, 1.20 mmol) and the solution was refluxed for 3 d. The solvent was concentrated to leave approximately 5 mL, and this was added to a rapidly stirred solution of NH₄PF₆ in a mixture of methanol and water (30 mL, 2:8 v/v). After stirring at room temperature for 1 h, the resulting precipitate was filtered off, washed with 300 mL of water and 300 mL of ethyl acetate, and finally purified by column chromatography (elution gradient: acetonitrile to 1% NH₄PF₆ in acetonitrile w/v). Excess salts were removed by precipitating the crude product twice from acetonitrile/water and the product was then dried under high vacuum to give a brown solid, **4.16**, (1.14 mg, 95%). M.p. 392 °C (dec.). ¹H NMR (acetonitrile-*d*₃ with 1% trifluoroacetic acid (TFA); the signal of TFA is not reported; 400 MHz) δ 9.22 (d, *J* = 6.6 Hz, 8H), 8.69-8.65 (m, 12H), 7.81 (d, *J* = 7.8 Hz, 4H), 7.71 (m, 6H), 6.96 (s, 4H), 6.87 (s, 2H), 4.06 (s, 12H), 3.93(s, 12H). ¹³C NMR (acetonitrile-*d*₃ with 1% trifluoroacetic acid (TFA); the signal of TFA is not reported; 100 MHz) δ 162.9, 153.4, 151.6, 148.2, 146.5, 145.3, 144.8, 131.8, 128.13, 128.07, 127.99, 127.94, 121.5, 113.4, 104.0, 57.8, 56.9. IR (cm⁻¹) = 1162 (ether, C-O), 1541 (NO₂). [M-1H]⁵⁺ calc. C₇₄H₆₅O₈N₆ for 233.0967, found 233.0968.

Synthesis of dimer 4.17



The intermediate compound **3.8** (587 mg, 1 mmol) was dissolved in EtOH (5 mL) with aromatic diamine **4.9** (126 mg, 0.5 mmol). The solvent was heated to reflux and stirred for 4 days. After cooling to room temperature, the solvent was evaporated and the crude product was recrystallized from water (15 mL) and THF (150 mL) to afford crude **4.17** as a brown solid, further purification was achieved by a single recrystallization from water to generate **4.17** as a light brown solid (126 mg, 41% isolate yield). M.p 379 °C (dec). ^1H NMR (D_2O , 400MHz) δ 9.52 (q, 6.8 Hz, 8H_{A/A'}), 8.97 (s, 2H_C), 8.88 (d, 4.8 Hz, 8H_{B/B'}), 8.70 (d, 1.6 Hz, 4H_F), 8.56 (d, 8.4 Hz, 4H_E), 8.13 (d, 8.8 Hz, 4H_D), 4.06 (s, 4H_{OMe}). ^{13}C NMR (D_2O , 700 MHz) δ 166, 165, 151, 151, 146, 146, 145, 142, 133, 133, 129, 129, 127, 127, 126, 125, 53. IR (cm^{-1}) ν 1736 s (ester). $[\text{M}-2\text{H}]^{2+}$ calc. $\text{C}_{54}\text{H}_{40}\text{O}_9\text{N}_6$ for 458.1423, found 458.1417, $[\text{M}-1\text{H}]^{1+}$ calc. $\text{C}_{54}\text{H}_{41}\text{O}_9\text{N}_6$ for 458.6462, found 458.6438.

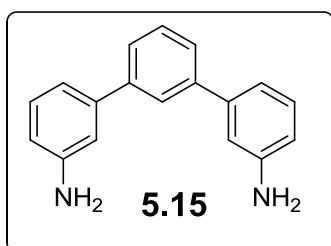
Synthesis of 3,3''-dinitro-*m*-terphenyl (5.14)



1,3-dibromobenzene (1.50 g, 6.36 mmol), 3-nitrophenyl boronic acid (2.23 g, 13.3 mmol), Na_2CO_3 (2.7 g, 25.4 mmol) and $\text{Pd}(\text{OAc})_2$ (~15 mg) were stirred in a mixture of water (30 mL) and DMF (55 mL) at 70 °C overnight. The product was precipitated in water, filtered off and washed with methanol, water, then methanol once again before drying under vacuum for 2 h to afford the intermediate

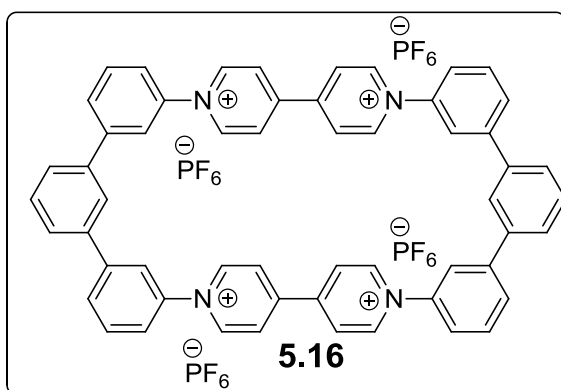
5.14 as a grey powder (1.54 g, 66.5%). M.p. (DSC) 210 °C; ^1H NMR (DMSO- d_6 , 400 MHz) δ 8.59 (s, 2H), 8.30 (d, $J = 7.6$, 2H), 8.28 (d, $J = 8.0$, 2H), 8.16 (s, 1H), 7.86 (d, $J = 8.0$, 2H) 7.79 (t, $J = 8.4$, 2H) 7.67 (t, $J = 7.6$, 1H); ^{13}C NMR (DMSO- d_6 , 400 MHz) δ (ppm) 148.5, 141.4, 138.8, 133.7, 130.4, 130.1, 127.3, 125.9, 122.36, 121.8; IR (cm^{-1}) $\nu = 1528$ (N-O), 1344 (C-N), 888 (C-H Ar). MS (m/z) calc. for $(\text{C}_{18}\text{H}_{12}\text{N}_2\text{O}_4)^+$: 320.0797, found 320.0799.

Synthesis of *m*-terphenylene diamine (5.15)



A solution of palladium(II) acetate (50 mg, 2 mmol) and intermediate **5.14** (1.30 g, 4 mmol) in tetrahydrofuran (20 mL) was stirred until homogenous. A solution of potassium fluoride (1.0 g, 17.2 mmol) in water (8 mL) was added. Liquid polymethylhydrosiloxane (4 mL, 32 mmol) was then added dropwise. The solution was stirred for 3 h. CHCl_3 (100 mL) was added to the reaction mixture and the organic phase was separated and dried over MgSO_4 , then concentrated under vacuum. The resulting oil was easily purified by column chromatography on silica gel (ethanol: hexane 1:4, v/v) to afford the desired diamine as yellow oil (0.83g, 100%). ^1H NMR (DMSO- d_6 , 400 MHz) δ 7.58 (s, 1H), 7.39 (m, 3H), 7.01 (t, $J = 7.02$, 2H), 6.79 (s, 2H), 6.72 (d, $J = 6.7$, 2H), 6.47 (d, $J = 6.5$, 2H) 5.06 (s, 2NH $_2$); ^{13}C NMR (DMSO- d_6 , 100 MHz) δ 149.1, 141.5, 140.9, 129.4, 129.1, 125.2, 124.6, 114.4, 113.2, 112.2; IR (cm^{-1}) $\nu = 3367$ (N-H) 1598 (N-H bend), 1478 (C-N), 907 (N-H wag). MS (m/z) calc. for $(\text{C}_{18}\text{H}_{17}\text{N}_2)^+$: 261.1392, found 261.1384.

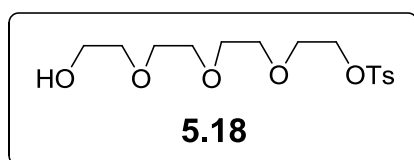
Synthesis of tetracationic macrocycle 5.16



A solution of Zincke salt (**1.65**) (431 mg, 0768 mmol) in a mixture of EtOH (3 mL) and water (2 mL) and a solution of aromatic

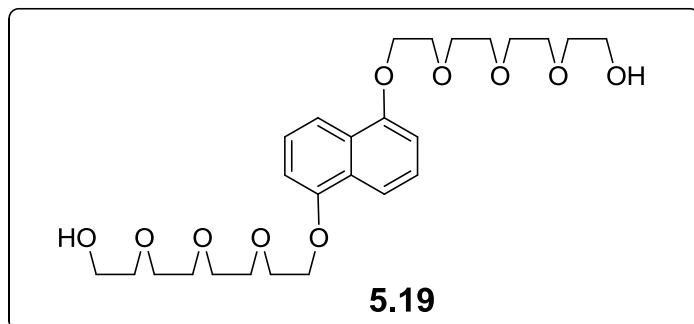
diamine (**5.15**) (200 mg, 0.768 mmol) in DMAc (5 mL) were added drop-wise to a rapidly stirred DMAc (80 mL) at 50 °C *via* two syringes. The reaction mixture was stirred under a positive pressure of argon for 5 d. After cooling to room temperature, the solution was concentrated to approximately 5 mL under reduced pressure and added slowly to a rapidly stirred solution of NH₄PF₆ (20 g) in water (200 ml). After stirring at room temperature for 1 h, the resulting yellow precipitate was collected by filtration, washed with water (2 × 20 mL) and dried in vacuo overnight. Purification was achieved by precipitating into a mixture of acetonitrile: acetone (10:90, v/v) to afford the yellow solid (100 mg, 10%). M.p. 380 °C (dec). ¹H NMR acetone-*d*₆, 400 MHz) δ 9.83 (d, *J* = 6.7 Hz, 4H), 9.08 (d, *J* = 6.7 Hz, 4H), 8.54 (s, 4H), 8.39 (s, 2H), 8.26 (d, *J* = 7.5 Hz, 4H), 8.11 (d, *J* = 6.6 Hz, 4H), 8.05 – 7.91 (m, 6H), 7.78 (t, *J* = 7.7 Hz, 2H). ¹³C NMR (acetonitrile-*d*₃, 100 MHz) δ 150.4, 150.0, 145.5, 144.3, 142.4, 139.5, 139.0, 131.4, 130.9, 130.4, 130.2, 129.8, 127.2, 127.1, 127.0, 124.1, 123.4, 123.2, 123.1. MS (*m/z*) calc. for (C₅₆H₄₀N₄F₁₂P₂)²⁺: 529.1263, found 529.1263.

Synthesis of monotosylated tetraethylene glycol **5.18**²⁶⁸



A solution of tetraethylene glycol (100.0 g, 515 mmol) in THF (230 mL) was added to a solution of sodium hydroxide (6.89g, 172 mmol) in of deionized water (20 mL). The mixture solution was cooled to 0 °C and then the solution of toluene sulfonyl chloride (9.81g, 51.5 mmol) in THF (20 mL) was added dropwise. After 2 hours, the solution was poured into 200 mL deionized water. The organic layers were separated and extracted with DCM. The organic layers were combined and washed with water, dried with MgSO₄, filtered and concentrated under reduced pressure to yield **5.18** as a colourless oil (15.8g, 88%). ¹H NMR (CDCl₃, 400 MHz) δ 7.77 (d, *J* = 8.3 Hz, 2 H), 7.32 (d, *J* = 8.1 Hz, 2 H), 4.14 (m, 2 H), 3.39–3.56 (m, 14 H), 2.42 (s, 3H). (Data in agreement with lit.)²⁶⁸

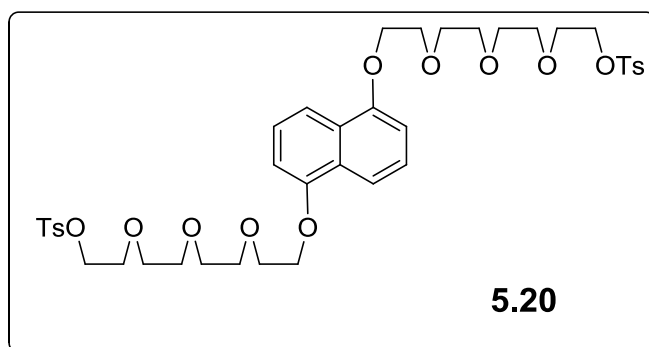
Synthesis of 1,5-dialkoxy naphthalene **5.19**²⁵⁵



1,5-dihydroxynaphthalene (2.0g, 12.49 mmol), K₂CO₃ (4.28g, 31.2 mmol) and 18-crown-6 (25mg, 0.125 mmol) were dissolved in anhydrous acetonitrile (20 mL) under argon. The mixture was

heated to reflux for 1 h, then **5.21** (15.7g, 45.0 mmol) was added to the solution dropwise. After heat to reflux under argon for 1 d, the solvent was evaporated, washed with H₂O, then extracted with EtOAc and DCM. The organic layers were combined, and dried with MgSO₄. The solvent was removed to yield the crude product, which can be easily purified by silica gel column chromatography (ethanol : ethyl acetate 1:4) to afford **5.19** as a reddish oil (8.08 g, 64%). ¹H NMR (CDCl₃, 400 MHz) δ 7.85 (d, *J* = 8.5 Hz, 2H), 7.34 (t, *J* = 8.0 Hz, 2H), 6.84 (d, *J* = 7.6 Hz, 2H), 4.30 (t, *J* = 4.7 Hz, 4H), 3.99 (t, *J* = 5.0 Hz, 4H), 3.81-3.79 (m, 4H), 3.70-3.63 (m, 18H), 3.58-3.56 (m, 4H). (Data in agreement with lit.)²⁵⁵

Synthesis of **5.20**²⁵⁵

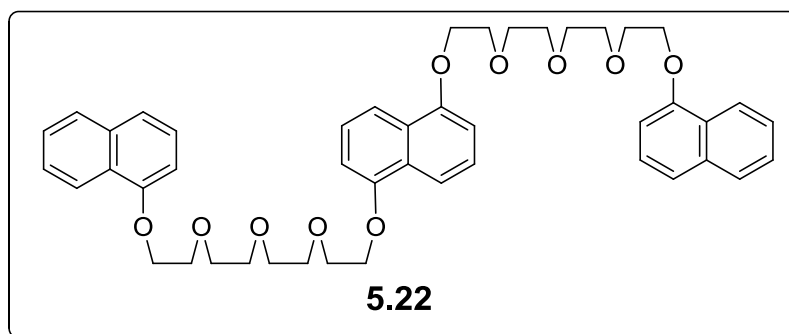


Triethylamine (Et₃N) (2.1g, 20.8 mmol) and N,N'-dimethylaminopyridine (DMAP) (854mg, 6.91 mmol) were added to a solution of **5.21** in dry DCM (175 mL) at 0 °C under a nitrogen atmosphere.

After 5 min, a solution of TsCl (4.0g, 21.24 mmol) was added directly to the reaction. The reaction mixture was allowed to warm up to room temperature and stirred for another 12 h. The solvent was removed, washed with H₂O, extracted with EtOAc and

DCM. The organic layers were combined and dried with MgSO_4 , the solvent was removed to yield the crude product. Purification was achieved by precipitation with acetone and petroleum ether (40-60 °C) to afford **5.20** a yellow oil (3.24 g, 57%). ^1H NMR (CDCl_3 , 400 MHz) δ 7.85 (d, $J = 8.5$ Hz, 2H), 7.35-7.29 (m, 6H), 6.84 (d, $J = 7.6$ Hz, 2H), 4.29 (t, $J = 4.7$ Hz, 4H), 4.13 (t, $J = 4.8$ Hz, 4H), 3.99 (t, $J = 5.0$ Hz, 4H), 3.79-3.77 (m, 4H), 3.67-3.64 (m, 8H), 3.61-3.55 (m, 8H), 2.41 (s, 6H). (Data in agreement with lit.)²⁵⁵

Synthesis of 3NP (5.22)



1-Naphthol (905 mg, 6.28 mmol), K_2CO_3 (427 mg, 3.09 mmol) and 18-crown-6 (100mg, 0.5 mmol) were dissolved in anhydrous acetonitrile (20

mL) under argon atmosphere, the mixture was heated under reflux for 1 h, then 1NP-ditosylate (**5.21**) (984 mg, 1.68 mmol) was added. The reaction mixture was refluxed and stirred under argon for further 2 days. Solvent was evaporated, and the residue washed with H_2O , and then finally extracted into CH_2Cl_2 and dried with MgSO_4 . The solvent was collected and evaporated to yield the crude product, which was purified by silica gel column chromatography (ethyl acetate) to afford **5.22** as an orange oil (2.36 g, 100%). ^1H NMR (CDCl_3 , 400 MHz) δ 8.27 (d, $J = 6.6$ Hz, 2H), 7.85 (d, $J = 8.2$ Hz, 2H), 7.77 (d, $J = 6.8$ Hz, 2H), 7.45 – 7.40 (m, 2H), 7.32 (dd, $J = 16.5, 8.2$ Hz, 4H), 6.77 (d, $J = 7.2$ Hz, 4H), 4.25 – 4.23 (m, 8H), 3.96 (d, $J = 1.9$ Hz, 8H), 3.74 (d, $J = 26.1$ Hz, 16H). ^{13}C NMR (CDCl_3 , 100 MHz) δ 154.5, 154.3, 134.5, 127.4, 126.4, 125.8, 125.1, 122.1, 120.4, 114.6, 105.6, 104.9, 70.9, 70.7, 69.8, 67.8, 67.8. MS (m/z) calc. for $(\text{C}_{46}\text{H}_{53}\text{O}_{10})^{2+}$: 765.3633, found 765.3633.

References

- 1 R. Herrick, *DC/AC circuits and electronics : principles & applications*, Delmar Cengage Learning, New York, 2002.
- 2 Y.-J. Cheng, S.-H. Yang and C.-S. Hsu, *Chem. Rev.*, 2009, **109**, 5868–5923.
- 3 M. L. Mingos and A. S. M. I. H. Committee, *Electronic Materials Handbook: Packaging*, Taylor & Francis, Ohio, 1989.
- 4 D. R. Askeland and P. P. Fulay, *Essentials of Materials Science & Engineering*, Cengage Learning, United States, 2008.
- 5 E. H. Lee, L. A. Eldada, M. Razeghi and C. Jagadish, *VLSI Micro- and Nanophotonics: Science, Technology, and Applications*, Taylor & Francis, Boca Raton, 2010.
- 6 J. A. Carson, *Solar Cell Research Progress*, Nova Science Publishers, New York, 2008.
- 7 N. Committee On Polymer Science And Engineering, *Polymer Science And Engineering: The Shifting Research Frontiers*, National Academies Press, Washington, 1994.
- 8 J. Mark, K. Ngai, W. Graessley, L. Mandelkern, E. Samulski, J. Koenig and G. Wignall, *Physical Properties of Polymers*, Cambridge University Press, Cambridge, 3rd edn., 2004.
- 9 C. D. Papaspyrides and P. Kiliaris, *Polymer Green Flame Retardants*, Elsevier Science Limited, Amsterdam, Netherlands, 2014.
- 10 M. D. Archer and M. A. Green, *Clean Electricity from Photovoltaics*, Imperial College Press, London, 2014.
- 11 H. Shirakawa, E. J. Louis, A. G. Macdiarmid, C. K. Chiang and A. J. Heeger, *J. Chem. Soc. Chem. Commun.*, 1977, 578–580.
- 12 C. K. Chiang, C. R. Fincher, Y. W. Park, A. J. Heeger, H. Shirakawa, E. J. Louis, S. C. Gau and A. G. Macdiarmid, *Phys. Rev. Lett.*, 1977, **39**, 1098–1101.
- 13 Y. Li, P. Sonar, L. Murphy and W. Hong, *Energy Environ. Sci.*, 2013, **6**, 1684–1710.
- 14 D. Rodriguez, S. Savagatrup, E. Valle, C. M. Proctor, C. McDowell, G. C. Bazan, T.-Q. Nguyen and D. J. Lipomi, *ACS Appl. Mater. Interfaces*, 2016, **8**, 11649–11657.
- 15 Y. Huang, W. Wen, S. Mukherjee, H. Ade, E. J. Kramer and G. C. Bazan, *Adv. Mater.*,

- 2014, **26**, 4168–4172.
- 16 R. H. Friend, R. W. Gymer, A. B. Holmes, J. H. Burroughes, R. N. Marks, C. Taliani, D. D. C. Bradley, D. A. Dos Santos, J. L. Brédas, M. Lögdlund and W. R. Salaneck, *Nature*, 1999, **397**, 121–128.
- 17 A. J. Heeger, *J. Phys. Chem. B*, 2001, **105**, 8475–8491.
- 18 K. M. Coakley and M. D. McGehee, *Chem. Mater.*, 2004, **16**, 4533–4542.
- 19 H. Hoppe and N. S. Sariciftci, *J. Mater. Res.*, 2004, **19**, 1924–1945.
- 20 G. A. Sotzing, J. R. Reynolds and P. J. Steel, *Chem. Mater.*, 1996, **8**, 882–889.
- 21 P. R. Somani and S. Radhakrishnan, *Mater. Chem. Phys.*, 2003, **77**, 117–133.
- 22 J. C. Lacroix, G. Trippe-Allard, J. Ghilane and P. Martin, *Adv. Nat. Sci. Nanosci. Nanotechnol.*, 2014, **5**, 15001.
- 23 M. L. Chabinyc and A. Salleo, *Chem. Mater.*, 2004, **16**, 4509–4521.
- 24 C. D. Dimitrakopoulos and P. R. L. Malenfant, *Adv. Mater.*, 2002, **14**, 99–+.
- 25 G. Horowitz, *J. Mater. Res.*, 2004, **19**, 1946–1962.
- 26 H. E. Katz and Z. Bao, *J. Phys. Chem. B*, 2000, **104**, 671–678.
- 27 R. J. Mortimer, *Electrochim. Acta*, 1999, **44**, 2971–2981.
- 28 C. K. Chiang, Y. W. Park, A. J. Heeger, H. Shirakawa, E. J. Louis and A. G. MacDiarmid, *J. Chem. Phys.*, 1978, **69**.
- 29 S. Alavi, S. Thomas, K. P. Sandeep, N. Kalarikkal, J. Varghese and S. Yaragalla, *Polymers for Packaging Applications*, Apple Academic Press, Toronto, 2014.
- 30 N. B. McKeown, *Phthalocyanine Materials: Synthesis, Structure and Function*, Cambridge University Press, Cambridge, 1998.
- 31 W. Hu, *Organic Optoelectronics*, Wiley, Weinheim, 2013.
- 32 U. Mitschke and P. Bauerle, *J. Mater. Chem.*, 2000, **10**, 1471–1507.
- 33 A. Kraft, A. C. Grimsdale and A. B. Holmes, *Angew. Chemie Int. Ed.*, 1998, **37**, 402–428.
- 34 M. Zheng, L. M. Ding, E. E. Gurel and F. E. Karasz, *J. Polym. Sci. Part A Polym. Chem.*, 2002, **40**, 235–241.

- 35 Z. H. Peng, Z. N. Bao and M. E. Galvin, *Adv. Mater.*, 1998, **10**, 680–684.
- 36 M. R. Robinson, S. J. Wang, G. C. Bazan and Y. Cao, *Adv. Mater.*, 2000, **12**, 1701.
- 37 M. Onoda, Y. Manda, T. Iwasa, S. Morita, T. Kawai and K. Yoshino, *Synth. Met.*, 1991, **41**, 1349–1352.
- 38 B. S. Ong, Y. Wu, P. Liu and S. Gardner, *J. Am. Chem. Soc.*, 2004, **126**, 3378–3379.
- 39 J. G. Laquindanum, H. E. Katz and A. J. Lovinger, *J. Am. Chem. Soc.*, 1998, **120**, 664–672.
- 40 W. J. Li, H. E. Katz, A. J. Lovinger and J. G. Laquindanum, *Chem. Mater.*, 1999, **11**, 458–465.
- 41 F. Garnier, R. Hajlaoui, A. El Kassmi, G. Horowitz, L. Laigre, W. Porzio, M. Armanini and F. Provasoli, *Chem. Mater.*, 1998, **10**, 3334–3339.
- 42 Z. Bao, A. Dodabalapur and A. J. Lovinger, *Appl. Phys. Lett.*, 1996, **69**.
- 43 H. Sirringhaus, N. Tessler and R. Friend, *Science*, 1998, **280**, 1741–4.
- 44 Z. L. Li, S. C. Yang, H. F. Meng, Y. S. Chen, Y. Z. Yang, C. H. Liu, S. F. Horng, C. S. Hsu, L. C. Chen, J. P. Hu and R. H. Lee, *Appl. Phys. Lett.*, 2004, **84**.
- 45 H. Sirringhaus, R. H. Friend, X. C. Li, S. C. Moratti, A. B. Holmes and N. Feeder, *Appl. Phys. Lett.*, 1997, **71**.
- 46 T. W. Kelley, D. V. Muires, P. F. Baude, T. P. Smith and T. D. Jones, *MRS Online Proc. Libr. Arch.*, 2003, **771**, L6.5 (11 pages).
- 47 Z. Bao, A. J. Lovinger and A. Dodabalapur, *Appl. Phys. Lett.*, 1996, **69**, 3066–3068.
- 48 H. E. Katz, *J. Mater. Chem.*, 1997, **7**, 369–376.
- 49 C. Wang, H. Dong, W. Hu, Y. Liu and D. Zhu, *Chem. Rev.*, 2012, **112**, 2208–2267.
- 50 R. C. Haddon, A. S. Perel, R. C. Morris, T. T. M. Palstra, A. F. Hebard and R. M. Fleming, *Appl. Phys. Lett.*, 1995, **67**, 121–123.
- 51 S. Kobayashi, T. Takenobu, S. Mori, A. Fujiwara and Y. Iwasa, *Appl. Phys. Lett.*, 2003, **82**, 4581–4583.
- 52 H. E. Katz, J. Johnson, A. J. Lovinger and W. J. Li, *J. Am. Chem. Soc.*, 2000, **122**, 7787–7792.

- 53 A. R. Brown, D. M. de Leeuw, E. J. Lous and E. E. Havinga, *Synth. Met.*, 1994, **66**, 257–261.
- 54 R. J. Chesterfield, J. C. McKeen, C. R. Newman, C. D. Frisbie, P. C. Ewbank, K. R. Mann and L. L. Miller, *J. Appl. Phys.*, 2004, **95**.
- 55 P. R. L. Malenfant, C. D. Dimitrakopoulos, J. D. Gelorme, L. L. Kosbar, T. O. Graham, A. Curioni and W. Andreoni, *Appl. Phys. Lett.*, 2002, **80**.
- 56 R. J. Chesterfield, J. C. McKeen, C. R. Newman, P. C. Ewbank, D. A. da Silva Filho, J.-L. Brédas, L. L. Miller, K. R. Mann and C. D. Frisbie, *J. Phys. Chem. B*, 2004, **108**, 19281–19292.
- 57 J. G. Laquindanum, H. E. Katz, A. Dodabalapur and A. J. Lovinger, *J. Am. Chem. Soc.*, 1996, **118**, 11331–11332.
- 58 T. M. Pappenfus, R. J. Chesterfield, C. D. Frisbie, K. R. Mann, J. Casado, J. D. Raff and L. L. Miller, *J. Am. Chem. Soc.*, 2002, **124**, 4184–4185.
- 59 R. J. Chesterfield, C. R. Newman, T. M. Pappenfus, P. C. Ewbank, M. H. Haukaas, K. R. Mann, L. L. Miller and C. D. Frisbie, *Adv. Mater.*, 2003, **15**, 1278–1282.
- 60 C. J. Tonzola, M. M. Alam, W. Kaminsky and S. A. Jenekhe, *J. Am. Chem. Soc.*, 2003, **125**, 13548–13558.
- 61 A. Babel and S. A. Jenekhe, *Adv. Mater.*, 2002, **14**, 371–374.
- 62 A. Babel and S. A. Jenekhe, *J. Am. Chem. Soc.*, 2003, **125**, 13656–13657.
- 63 K. Nassau, *The physics and chemistry of color: the fifteen causes of color*, Wiley, New York, 2001.
- 64 L. Dai, *Intelligent Macromolecules for Smart Devices: From Materials Synthesis to Device Applications*, Springer, London, 2004.
- 65 J. H. Burroughes, D. D. C. Bradley, A. R. Brown, R. N. Marks, K. Mackay, R. H. Friend, P. L. Burns and A. B. Holmes, *Nature*, 1990, **347**, 539–541.
- 66 T. A. Skotheim, *Handbook of Conducting Polymers, Second Edition*, Taylor & Francis, New York, 1997.
- 67 M. S. AlSalhi, J. Alam, L. A. Dass and M. Raja, *Int. J. Mol. Sci.*, 2011, **12**, 2036–2054.

- 68 L. Brandão, J. Viana, D. G. Bucknall and G. Bernardo, *Synth. Met.*, 2014, **197**, 23–33.
- 69 G. Bergamini and S. Silvi, *Applied Photochemistry: When Light Meets Molecules*, Springer International Publishing, Switzerland, 2016.
- 70 P. Karastatiris, J. A. Mikroyannidis, I. K. Spiliopoulos, M. Fakis and P. Persephonis, *J. Polym. Sci. Part A Polym. Chem.*, 2004, **42**, 2214–2224.
- 71 L. P. Yu and Z. N. Bao, *Adv. Mater.*, 1994, **6**, 156–159.
- 72 M. T. Bernius, M. Inbasekaran, J. O’Brien and W. S. Wu, *Adv. Mater.*, 2000, **12**, 1737–1750.
- 73 M. O’Neill and S. M. Kelly, *Adv. Mater.*, 2011, **23**, 566–584.
- 74 D. D. C. Bradley, *Adv. Mater.*, 1992, **4**, 756–759.
- 75 C. Kallinger, M. Hilmer, A. Haugeneder, M. Perner, W. Spirk, U. Lemmer, J. Feldmann, U. Scherf, K. Mullen, A. Gombert and V. Wittwer, *Adv. Mater.*, 1998, **10**, 920–923.
- 76 R. Mertens, *The OLED handbook: a guide to OLED technology, industry & market*, OLED-Info, Herzlia, Israel, 2012.
- 77 D. M. Chapin, *J. Appl. Phys.*, 1954, **25**, 676–677.
- 78 M. A. Green, K. Emery, Y. Hishikawa and W. Warta, *Prog. Photovoltaics*, 2009, **17**, 85–94.
- 79 P. Peumans and S. R. Forrest, *Appl. Phys. Lett.*, 2001, **79**, 126–128.
- 80 P. Peumans, A. Yakimov and S. R. Forrest, *J. Appl. Phys.*, 2003, **93**, 3693–3723.
- 81 K. Schulze, C. Uhrich, R. Schuppel, K. Leo, M. Pfeiffer, E. Brier, E. Reinold and P. Bauerle, *Adv. Mater.*, 2006, **18**, 2872–2875.
- 82 J. G. Xue, B. P. Rand, S. Uchida and S. R. Forrest, *Adv. Mater.*, 2005, **17**, 66–71.
- 83 P. Wang, S. M. Zakeeruddin, J. E. Moser, M. K. Nazeeruddin, T. Sekiguchi and M. Gratzel, *Nat. Mater.*, 2003, **2**, 402–407.
- 84 Y. Bai, Y. M. Cao, J. Zhang, M. Wang, R. Z. Li, P. Wang, S. M. Zakeeruddin and M. Gratzel, *Nat. Mater.*, 2008, **7**, 626–630.
- 85 M. K. Nazeeruddin, F. De Angelis, S. Fantacci, A. Selloni, G. Viscardi, P. Liska, S. Ito, T. Bessho and M. Gratzel, *J. Am. Chem. Soc.*, 2005, **127**, 16835–16847.

- 86 B. Oregan and M. Gratzel, *Nature*, 1991, **353**, 737–740.
- 87 E. Bundgaard and F. C. Krebs, *Sol. Energy Mater. Sol. Cells*, 2007, **91**, 954–985.
- 88 R. Kroon, M. Lenes, J. C. Hummelen, P. W. M. Blom and B. De Boer, *Polym. Rev.*, 2008, **48**, 531–582.
- 89 B. A. Gregg and M. C. Hanna, *J. Appl. Phys.*, 2003, **93**, 3605–3614.
- 90 V. I. Arkhipov and H. Bassler, *Phys. Status Solidi A-applied Res.*, 2004, **201**, 1152–1187.
- 91 E. E. Havinga, W. Hoeve and H. Wynberg, *Polym. Bull.*, 1992, **29**, 119–126.
- 92 E. E. Havinga, W. Tenhoeve and H. Wynberg, *Synth. Met.*, 1993, **55**, 299–306.
- 93 C. W. Tang, *Appl. Phys. Lett.*, 1986, **48**, 183–185.
- 94 B. C. Thompson and J. M. J. Frechet, *Angew. Chem., Int. Ed.*, 2008, **47**, 58–77.
- 95 D. Izuhara and T. M. Swager, *J. Am. Chem. Soc.*, 2009, **131**, 17724–17725.
- 96 D. Izuhara and T. M. Swager, *Macromolecules*, 2011, **44**, 2678–2684.
- 97 D. C. Giancoli, *Physics: Principles with Applications*, Pearson/Prentice Hall, Upper Saddle River, 2013.
- 98 R. Waser, *Nanoelectronics and information technology : advanced electronic materials and novel devices*, Wiley, Weinheim, 2003.
- 99 W. Shockley, W. Brattain. and J. Bardeen, *APS News – This Mon. Phys. Hist.*, 1947.
- 100 C. Reese, M. Roberts, M. Ling and Z. Bao, *Mater. Today*, 2004, **7**, 20–27.
- 101 C.-W. Chu, S.-H. Li, C.-W. Chen, V. Shrotriya and Y. Yang, *Appl. Phys. Lett.*, 2005, **87**.
- 102 A. Tsumura, H. Koezuka and T. Ando, *Appl. Phys. Lett.*, 1986, **49**, 1210–1212.
- 103 Y.-Y. Lin, D. I. Gundlach, S. F. Nelson and T. N. Jackson, *IEEE Trans. Electron Devices*, 1997, **44**, 1325–1331.
- 104 S. K. Park, Y. H. Kim, J. I. Han, D. G. Moon and W. K. Kim, *IEEE Trans. Electron Devices*, 2002, **49**, 2008–2015.
- 105 Z. A. Bao, A. J. Lovinger and J. Brown, *J. Am. Chem. Soc.*, 1998, **120**, 207–208.
- 106 A. Facchetti, M. Mushrush, H. E. Katz and T. J. Marks, *Adv. Mater.*, 2003, **15**, 33–38.
- 107 L. Michaelis and E. S. Hill, *J. Gen. Physiol.*, 1933, **16**, 859–873.
- 108 P. M. S. Monk, *The viologens : physicochemical properties, synthesis and applications*

- of the salts of 4,4'-bipyridine*, Wiley, New York, 1998.
- 109 D. Barrios, R. Vergaz, J. C. Torres-Zafra, C. Vega, J. M. Sanchez-Pena and A. Vinuales, *Photonics Journal, IEEE*, 2012, **4**, 2105–2115.
- 110 T. L. Hill, *Free Energy Transduction and Biochemical Cycle Kinetics*, Springer-Verlag, New York, 2004.
- 111 C. J. Schoot, J. J. Ponjee, H. T. Vandam, R. A. Vandoorn and P. T. Bolwijn, *Appl. Phys. Lett.*, 1973, **23**, 64–65.
- 112 R. J. Mortimer, D. R. Rosseinsky and P. M. S. Monk, *Electrochromic Materials and Devices*, Wiley, Weinheim, 2015.
- 113 <http://www.gentex.com/corporate/our-history>
- 114 V. Koncar, *Smart Textiles and Their Applications*, Elsevier Science & Technology, Duxford, 2016.
- 115 A. Factor and G. E. Heinsohn, *J. Polym. Sci. Part C Polym. Lett.*, 1971, **9**, 289–295.
- 116 M. Shimomura, K. Utsugi, J. Horikoshi, K. Okuyama, O. Hatozaki and N. Oyama, *Langmuir*, 1991, **7**, 760–765.
- 117 A. T. Balaban, *Pyrylium Salts: Syntheses, Reactions, and Physical Properties*, Academic Press, New York, 1982.
- 118 M. Valášek, J. Pecka, Jindřich, G. Calleja, P. R. Craig and J. Michl, *J. Org. Chem.*, 2005, **70**, 405–412.
- 119 A. K. Nedeltchev, H. Han and P. K. Bhowmik, *Polym. Chem.*, 2010, **1**, 908–915.
- 120 M. Hromádov a V. Kolivoška, M. Gál, L. Pospíšil, R. Sokolov a and M. Valášek, *J. Incl. Phenom. Macrocycl. Chem.*, 2011, **70**, 461–469.
- 121 V. Kolivoška, M. Valášek, M. Gál, R. Sokolov a J. Bulíckov a L. Pospíšil, G. Mészáros and M. Hromádov a *J. Phys. Chem. Lett.*, 2013, **4**, 589–595.
- 122 S. A. X. Huang, K. C. Chuang, S. Z. D. Cheng and F. W. Harris, *Polymer (Guildf.)*, 2000, **41**, 5001–5009.
- 123 T. Zincke, G. Heuser and W. Möller, *Justus Liebigs Ann. Chem.*, 1904, **333**, 296–345.
- 124 N. Zeghibib, P. Thelliere, M. Rivard and T. Martens, *J. Org. Chem.*, 2016, **81**, 3256–

- 3262.
- 125 H. M. Colquhoun, B. W. Greenland, Z. Zhu, J. S. Shaw, C. J. Cardin, S. Burattini, J. M. Elliott, S. Basu, T. B. Gasa and J. F. Stoddart, *Org. Lett.*, 2009, **11**, 5238–5241.
- 126 W. König, *J. für Prakt. Chemie*, 1904, **69**, 105–137.
- 127 J. J. Li, *Name reactions: A collection of detailed mechanisms and synthetic applications: Fourth expanded edition*, Springer-Verlag, Berlin, 2009.
- 128 M. Nanasawa, M. Miwa, M. Hirai and T. Kuwabara, *J. Org. Chem.*, 2000, **65**, 593–595.
- 129 P. M. S. Monk and N. M. Hodgkinson, *J. Electroanal. Chem.*, 1999, **462**, 43–54.
- 130 G.-T. Wang, X. Zhao and Z.-T. Li, *Tetrahedron*, 2011, **67**, 48–57.
- 131 D. Nematollahi and H. Khoshshafar, *Tetrahedron*, 2009, **65**, 4742–4750.
- 132 L. Chen, H. Willcock, C. J. Wedge, F. Hartl, H. M. Colquhoun and B. W. Greenland, *Org. Biomol. Chem.*, 2016, **14**, 980–988.
- 133 D. B. Amabilino and J. F. Stoddart, *Chem. Rev.*, 1995, **95**, 2725–2828.
- 134 F. M. Raymo and J. F. Stoddart, *Chem. Rev.*, 1999, **99**, 1643–1663.
- 135 V. Jain, M. Khiterer, R. Montazami, H. M. Yochum, K. J. Shea and J. R. Heflin, *ACS Appl. Mater. Interfaces*, 2009, **1**, 83–89.
- 136 D. S. Guo, S. Chen, H. Qian, H. Q. Zhang and Y. Liu, *Chem. Commun.*, 2010, **46**, 2620–2622.
- 137 A. Trabolsi, N. Khashab, A. C. Fahrenbach, D. C. Friedman, M. T. Colvin, K. K. Cot í D. Ben fez, E. Tkatchouk, J.-C. Olsen, M. E. Belowich, R. Carmielli, H. A. Khatib, W. A. Goddard, M. R. Wasielewski and J. F. Stoddart, *Nat. Chem.*, 2010, **2**, 42–49.
- 138 W. Zhang, E. DeIonno, W. R. Dichtel, L. Fang, A. Trabolsi, J.-C. Olsen, D. Benitez, J. R. Heath and J. F. Stoddart, *J. Mater. Chem.*, 2011, **21**, 1487–1495.
- 139 C. Kahlfuss, E. Méay, M.-C. Duclos, M. Lemaire, A. Milet, E. Saint-Aman and C. Bucher, *Chem. Eur. J.*, 2014, 2090–2106.
- 140 O. Schiemann, N. J. Turro and J. K. Barton, *J. Phys. Chem. B*, 2000, **104**, 7214–7220.
- 141 T. Ha and P. Tinnefeld, *Annu. Rev. Phys. Chem.*, 2012, **63**, 595–617.
- 142 H.-B. Cheng, Y.-M. Zhang, C. Xu and Y. Liu, *Sci. Rep.*, 2014, **4**.

- 143 T. Nakahira and M. Graetzel, *J. Phys. Chem.*, 1984, **88**, 4006–4010.
- 144 J. C. Barnes, A. C. Fahrenbach, D. Cao, S. M. Dyar, M. Frasconi, M. A. Giesener, D. Ben fez, E. Tkatchouk, O. Chernyashevskyy, W. H. Shin, H. Li, S. Sampath, C. L. Stern, A. A. Sarjeant, K. J. Hartlieb, Z. Liu, R. Carmieli, Y. Y. Botros, J. W. Choi, A. M. Z. Slawin, J. B. Ketterson, M. R. Wasielewski, W. A. Goddard and J. F. Stoddart, *Science*, 2013, **339**, 429–433.
- 145 B. L. Feringa, W. F. Jager and B. de Lange, *Tetrahedron*, 1993, **49**, 8267–8310.
- 146 J. E. Green, J. Wook Choi, A. Boukai, Y. Bunimovich, E. Johnston-Halperin, E. DeIonno, Y. Luo, B. A. Sheriff, K. Xu, Y. Shik Shin, H.-R. Tseng, J. F. Stoddart and J. R. Heath, *Nature*, 2007, **445**, 414–417.
- 147 J. Iehl, M. Frasconi, H. P. Jacquot de Rouville, N. Renaud, S. M. Dyar, N. L. Strutt, R. Carmieli, M. R. Wasielewski, M. A. Ratner, J. F. Nierengarten and J. F. Stoddart, *Chem. Sci.*, 2013, **4**, 1462–1469.
- 148 C. L. Bird and A. T. Kuhn, *Chem. Soc. Rev.*, 1981, **10**, 49–82.
- 149 R. J. Mortimer and T. S. Varley, *Chem. Mater.*, 2011, **23**, 4077–4082.
- 150 J. Palenzuela, A. Viñuales, I. Odriozola, G. Cabañero, H. J. Grande and V. Ruiz, *ACS Appl. Mater. Interfaces*, 2014, **6**, 14562–14567.
- 151 E. M. Kosower and J. L. Cotter, *J. Am. Chem. Soc.*, 1964, **86**, 5524–5527.
- 152 A. G. Evans, N. K. Dodson and N. H. Rees, *J. Chem. Soc. Trans. 2*, 1976, 859–863.
- 153 I. P. Krainov, O. M. Tsyguleva and S. F. Kramarenko, *Theor. Exp. Chem.*, 1988, **23**, 699–704.
- 154 K. Wadhwa, S. Nuryyeva, A. C. Fahrenbach, M. Elhabiri, C. Platas-Iglesias and A. Trabolsi, *J. Mater. Chem. C*, 2013, **1**, 2302–2307.
- 155 Y.-C. Zhang, D.-W. Zhang, H. Wang, Y. Zhou and Z.-T. Li, *Polym. Chem.*, 2015, **6**, 4404–4408.
- 156 K. Murugavel, *Polym. Chem.*, 2014, **5**, 5873–5884.
- 157 M. Kathiresan, L. Walder, F. Ye and H. Reuter, *Tetrahedron Lett.*, 2010, **51**, 2188–2192.
- 158 I. Yamaguchi, H. Higashi, S. Kimura and M. Sato, *Helv. Chim. Acta*, 2010, **93**, 819–828.

- 159 M. Hromádov a M. Valášek, N. Fanelli, H. N. Randriamahazaka and L. Pospíšil, *J. Phys. Chem. C*, 2014, **118**, 9066–9072.
- 160 J. Romanova, V. Liegeois and B. Champagne, *Phys. Chem. Chem. Phys.*, 2014, **16**, 21721–21731.
- 161 J. Romanova, V. Liégeois and B. Champagne, *J. Phys. Chem. C*, 2014, **118**, 12469–12484.
- 162 A. Beneduci, S. Cospito, A. Crispini, B. Gabriele, F. P. Nicoletta, L. Veltri and G. Chidichimo, *J. Mater. Chem.*, 2013, **1**, 2233–2240.
- 163 J. Fortage, C. Peltier, C. Perruchot, Y. Takemoto, Y. Teki, F. Bedioui, V. Marvaud, G. Dupeyre, L. Pospíšil, C. Adamo, M. Hromádov a I. Ciofini and P. P. Lainé *J. Am. Chem. Soc.*, 2012, **134**, 2691–2705.
- 164 M. E. Alberto, B. C. De Simone, S. Cospito, D. Imbardelli, L. Veltri, G. Chidichimo and N. Russo, *Chem. Phys. Lett.*, 2012, **552**, 141–145.
- 165 P. P. Lainé F. Bedioui, F. Loiseau, C. Chiorboli and S. Campagna, *J. Am. Chem. Soc.*, 2006, **128**, 7510–7521.
- 166 A. Funston, J. P. Kirby, J. R. Miller, L. Pospíšil, J. Fiedler, M. Hromádov a M. Gál, J. Pecka, M. Valášek, Z. Zawada, P. Rempala and J. Michl, *J. Phys. Chem. A*, 2005, **109**, 10862–10869.
- 167 M. Pumera, J. Jindřich, M. Valášek and J. Pecka, *Electrophoresis*, 2005, **26**, 4465–4467.
- 168 W. W. Porter, T. P. Vaid and A. L. Rheingold, *J. Am. Chem. Soc.*, 2005, **127**, 16559–16566.
- 169 S.-H. Chiu, A. M. Elizarov, P. T. Glink and J. F. Stoddart, *Org. Lett.*, 2002, **4**, 3561–3564.
- 170 P. R. Ashton, V. Baldoni, V. Balzani, A. Credi, H. D. A. Hoffmann, M. V. Martínez Díez, F. M. Raymo, J. F. Stoddart and M. Venturi, *Chem. Eur. J.*, 2001, **7**, 3482–3493.
- 171 A. H. Flood, S. Nygaard, B. W. Laursen, J. O. Jeppesen and J. F. Stoddart, *Org. Lett.*, 2006, **8**, 2205–2208.
- 172 J. M. Belitsky, A. Nelson, J. D. Hernandez, L. G. Baum and J. F. Stoddart, *Chem. Biol.*, 2007, **14**, 1140–1151.

- 173 C. M. Gothard, C. J. Bruns, N. A. Gothard, B. A. Grzybowski and J. F. Stoddart, *Org. Lett.*, 2012, **14**, 5066–5069.
- 174 T. Ikeda, I. Aprahamian and J. F. Stoddart, *Org. Lett.*, 2007, **9**, 1481–1484.
- 175 K. Da Zhang, J. Tian, D. Hanifi, Y. Zhang, A. C. H. Sue, T.-Y. Zhou, L. Zhang, X. Zhao, Y. Liu and Z. T. Li, *J. Am. Chem. Soc.*, 2013, **135**, 17913–17918.
- 176 V. A. Constantin, D. Bongard and L. Walder, *Eur. J. Org. Chem.*, 2012, **2012**, 913–921.
- 177 V. Kolivoška, M. Gál, Š. Lachmanová and M. Valášek, M. Hromádová and L. Pospíšil, *Anal. Chim. Acta*, 2011, **697**, 23–26.
- 178 V. Kolivoska, M. Gal, L. Pospisil, M. Valasek and M. Hromadova, *Phys. Chem. Chem. Phys.*, 2011, **13**, 11422–11429.
- 179 W. W. Porter and T. P. Vaid, *J. Org. Chem.*, 2005, **70**, 5028–5035.
- 180 S. Goswami, S. Jana and H.-K. Fun, *CrystEngComm*, 2008, **10**, 507–517.
- 181 R. L. LaDuca, M. P. Desciak, R. S. Rarig and J. A. Zubieta, *Z. Anorg. Allg. Chem.*, 2006, **632**, 449–453.
- 182 E. N. Marvell, G. Caple and I. Shahidi, *J. Am. Chem. Soc.*, 1970, **92**, 5641–5645.
- 183 B. J. Coe, J. L. Harries, M. Helliwell, L. A. Jones, I. Asselberghs, K. Clays, B. S. Brunshwig, J. A. Harris, J. Garín and J. Orduna, *J. Am. Chem. Soc.*, 2006, **128**, 12192–12204.
- 184 C. S. Johnson and H. S. Gutowsky, *J. Chem. Phys.*, 1963, **39**, 58–62.
- 185 W. R. Dunham, J. A. Fee, L. J. Harding and H. J. Grande, *J. Magn. Reson.*, 1980, **40**, 351–359.
- 186 G. Grampp, B. Y. Mladenova, D. R. Kattnig and S. Landgraf, *Appl. Magn. Reson.*, 2006, **30**, 145–164.
- 187 M. Krejčík, M. Daněk and F. Hartl, *J. Electroanal. Chem. Interfacial Electrochem.*, 1991, **317**, 179–187.
- 188 Manuel P. Soriaga, J. Stickney, L. A. Bottomley and Y.-G. Kim, *Thin Films: Preparation, Characterization, Applications*, Soriaga, 2002.
- 189 S. Tretiak, A. Saxena, R. L. Martin and A. R. Bishop, *Phys. Rev. Lett.*, 2002, **89**, 97402.

- 190 I. Franco and S. Tretiak, *J. Am. Chem. Soc.*, 2004, **126**, 12130–12140.
- 191 K. Arihara, T. Ohsaka and F. Kitamura, *Phys. Chem. Chem. Phys.*, 2002, **4**, 1002–1005.
- 192 D. A. Smith, *Metabolism, pharmacokinetics and toxicity of functional groups : impact of the building blocks of medicinal chemistry in ADMET*, Royal Society of Chemistry, Cambridge, 2010.
- 193 G. P. Klimisha, I. P. Krainov, Y. G. Protsenko and B. G. Distanov, *Khimiya geterotsiklicheskikh Soedin.*, 1979, 264.
- 194 H. Kamogawa and S. Sato, *Bull. Chem. Soc. Jpn.*, 1991, **64**, 321–323.
- 195 P. Wardman, *J. Phys. Chem. Ref. Data*, 1989, **18**.
- 196 Y. Lei and J. K. Hurst, *J. Phys. Chem.*, 1991, **95**, 7918–7925.
- 197 D. E. Helbling, J. Hollender, H.-P. E. Kohler and K. Fenner, *Environ. Sci. Technol.*, 2010, **44**, 6628–6635.
- 198 B. Singh, H. R. Bhat, M. K. Kumawat and U. P. Singh, *Bioorg. Med. Chem. Lett.*, 2014, **24**, 3321–3325.
- 199 K. A. Thoreson and K. McNeill, *Dalt. Trans.*, 2011, **40**, 1646–1648.
- 200 Y. Klichko, M. Liong, E. Choi, S. Angelos, A. E. Nel, J. F. Stoddart, F. Tamanoi and J. I. Zink, *J. Am. Ceram. Soc.*, 2009, **92**, s2–s10.
- 201 C. Cheng, P. R. McGonigal, S. T. Schneebeli, H. Li, N. A. Vermeulen, C. Ke and J. F. Stoddart, *Nat. Nanotechnol.*, 2015, **10**, 547–553.
- 202 O. Buyukcakir, S. H. Je, D. S. Choi, S. N. Talapaneni, Y. Seo, Y. Jung, K. Polychronopoulou and A. Coskun, *Chem. Commun.*, 2016, **52**, 934–937.
- 203 A. Read, D. Hansen, S. Aloji, W. G. Pitt, D. R. Wheeler and G. D. Watt, *Renew. Energy*, 2012, **46**, 218–223.
- 204 D. Hansen, J. Hadley, A. Read, E. Manwill, W. Pitt and D. Wheeler, *ECS Trans.*, 2011, **41**, 1737–1745.
- 205 D. C. Hansen, G. Watt, J. Nichols, M. B. Andrus, D. R. Wheeler and S. H. Choi, *ECS Trans.*, 2008, **16**, 2057–2063.
- 206 L. Kress, A. Neudeck, A. Petr and L. Dunsch, *J. Electroanal. Chem.*, 1996, **414**, 31–40.

- 207 J.-M. Lehn, in *Supramolecular Chemistry*, Wiley-VCH Verlag GmbH & Co. KGaA, 2006, pp. 1–9.
- 208 G. M. Whitesides, J. P. Mathias and C. T. Seto, *Science (80-.)*, 1991, **254**, 1312–1319.
- 209 J.-M. Lehn, *Science (80-.)*, 2002, **295**, 2400–2403.
- 210 J.-M. Lehn, *Proc. Natl. Acad. Sci.* , 2002, **99**, 4763–4768.
- 211 P. J. Cragg, *Supramolecular Chemistry: From Biological Inspiration to Biomedical Applications*, Springer Netherlands, Amsterdam, 2010.
- 212 A. F. Pozharskii, A. Soldatenkov and A. R. Katritzky, *Heterocycles in Life and Society: An Introduction to Heterocyclic Chemistry, Biochemistry and Applications*, Wiley, New York, 2011.
- 213 V. Percec, *Hierarchical Macromolecular Structures: 60 Years after the Staudinger Nobel Prize I*, Springer International Publishing, Basel, 2014.
- 214 R. Yerushalmi, A. Scherz, M. E. van der Boom and H.-B. Kraatz, *J. Mater. Chem.*, 2005, **15**, 4480–4487.
- 215 R. J. Wojtecki and A. Nelson, *J. Polym. Sci. Part A Polym. Chem.*, 2016, **54**, 457–472.
- 216 T. F. A. de Greef and E. W. Meijer, *Nature*, 2008, **453**, 171–173.
- 217 W. M. Latimer and W. H. Rodebush, *J. Am. Chem. Soc.*, 1920, **42**, 1419–1433.
- 218 C. Fouquey, J.-M. Lehn and A.-M. Levelut, *Adv. Mater.*, 1990, **2**, 254–257.
- 219 J. M. Lehn, *Chem., Macromol. Synp.*, 1993, **69**, 1–17.
- 220 L. J. Prins, D. N. Reinhoudt and P. Timmerman, *Angew. Chem., Int. Ed.*, 2001, **40**, 2382–2426.
- 221 F. H. Beijer, H. Kooijman, A. L. Spek, R. P. Sijbesma and E. W. Meijer, *Angew. Chem., Int. Ed.*, 1998, **37**, 75–78.
- 222 W. L. Jorgensen and J. Pranata, *J. Am. Chem. Soc.*, 1990, **112**, 2008–2010.
- 223 J. Pranata, S. G. Wierschke and W. L. Jorgensen, *J. Am. Chem. Soc.*, 1991, **113**, 2810–2819.
- 224 T. J. Murray and S. C. Zimmerman, *J. Am. Chem. Soc.*, 1992, **114**, 4010–4011.
- 225 A. Gooch, A. M. McGhee, L. C. Renton, J. P. Plante, C. I. Lindsay and A. J. Wilson,

- Supramol. Chem.*, 2009, **21**, 12–17.
- 226 D. A. Bell and E. V. Anslyn, *J. Org. Chem.*, 1994, **59**, 512–514.
- 227 D. A. Bell and E. V. Anslyn, *Tetrahedron*, 1995, **51**, 7161–7172.
- 228 S. Djurdjevic, D. A. Leigh, H. McNab, S. Parsons, G. Teobaldi and F. Zerbetto, *J. Am. Chem. Soc.*, 2007, **129**, 476–477.
- 229 B. A. Blight, A. Camara-Campos, S. Djurdjevic, M. Kaller, D. A. Leigh, F. M. McMillan, H. McNab and A. M. Z. Slawin, *J. Am. Chem. Soc.*, 2009, **131**, 14116–14122.
- 230 S. G. Newman, A. Taylor and R. J. Boyd, *Chem. Phys. Lett.*, 2008, **450**, 210–213.
- 231 R. P. Sijbesma and E. W. Meijer, *Chem. Commun.*, 2003, 5–16.
- 232 P. S. Corbin and S. C. Zimmerman, *J. Am. Chem. Soc.*, 1998, **120**, 9710–9711.
- 233 P. S. Corbin, S. C. Zimmerman, P. A. Thiessen, N. A. Hawryluk and T. J. Murray, *J. Am. Chem. Soc.*, 2001, **123**, 10475–10488.
- 234 Y. Hisamatsu, N. Shirai, S. Ikeda and K. Odashima, *Org. Lett.*, 2009, **11**, 4342–4345.
- 235 X. Li, Y. Fang, P. Deng, J. Hu, T. Li, W. Feng and L. Yuan, *Org. Lett.*, 2011, **13**, 4628–4631.
- 236 R. P. Sijbesma, F. H. Beijer, L. Brunsveld, B. J. B. Folmer, J. H. K. K. Hirschberg, R. F. M. Lange, J. K. L. Lowe and E. W. Meijer, *Science (80-.)*, 1997, **278**, 1601–1604.
- 237 S. H. M. Sontjens, R. P. Sijbesma, M. H. P. van Genderen and E. W. Meijer, *J. Am. Chem. Soc.*, 2000, **122**, 7487–7493.
- 238 J. C. Ma and D. A. Dougherty, *Chem. Rev.*, 1997, **97**, 1303–1324.
- 239 O. B. Berryman, V. S. Bryantsev, D. P. Stay, D. W. Johnson and B. P. Hay, *J. Am. Chem. Soc.*, 2007, **129**, 48–58.
- 240 C. A. Hunter, K. R. Lawson, J. Perkins and C. J. Urch, *J. Chem. Soc. Trans. 2*, 2001, 651–669.
- 241 B. Odell, M. V Reddington, A. M. Z. Slawin, N. Spencer, J. F. Stoddart and D. J. Williams, *Angew. Chem., Int. Ed. Engl.*, 1988, **27**, 1547–1550.
- 242 M. Asakawa, W. Dehaen, G. L'abb é S. Menzer, J. Nouwen, F. M. Raymo, J. F. Stoddart and D. J. Williams, *J. Org. Chem.*, 1996, **61**, 9591–9595.

- 243 W. R. Dichtel, O. S. Miljanic, J. M. Spruell, J. R. Heath and J. F. Stoddart, *J. Am. Chem. Soc.*, 2006, **128**, 10388–10390.
- 244 I. Aprahamian, W. R. Dichtel, T. Ikeda, J. R. Heath and J. F. Stoddart, *Org. Lett.*, 2007, **9**, 1287–1290.
- 245 A. B. Braunschweig, W. R. Dichtel, O. S. Miljanic, M. A. Olson, J. M. Spruell, S. I. Khan, J. R. Heath and J. Fraser Stoddart, *Chem. ASIAN J.*, 2007, **2**, 634–647.
- 246 I. Aprahamian, O. S. Miljanic, W. R. Dichtel, K. Isoda, T. Yasuda, T. Kato and J. F. Stoddart, *Bull. Chem. Soc. Jpn.*, 2007, **80**, 1856–1869.
- 247 P. R. Ashton, T. T. Goodnow, A. E. Kaifer, M. V Reddington, A. M. Z. Slawin, N. Spencer, J. F. Stoddart, C. Vicent and D. J. Williams, *Angew. Chem., Int. Ed. Engl.*, 1989, **28**, 1396–1399.
- 248 P. R. Ashton, R. Ballardini, V. Balzani, A. Credi, M. T. Gandolfi, S. Menzer, L. Perezgarcia, L. Prodi, J. F. Stoddart, M. Venturi, A. J. P. White and D. J. Williams, *J. Am. Chem. Soc.*, 1995, **117**, 11171–11197.
- 249 D. B. Amabilino, P. R. Ashton, L. Perezgarcia and J. F. Stoddart, *Angew. Chem., Int. Ed. Engl.*, 1995, **34**, 2378–2380.
- 250 W. R. Dichtel, J. R. Heath and J. Fraser Stoddart, *Philos. Trans. R. Soc. London A Math. Phys. Eng. Sci.*, 2007, **365**, 1607–1625.
- 251 O. Š. Miljanić, W. R. Dichtel, S. I. Khan, S. Mortezaei, J. R. Heath and J. F. Stoddart, *J. Am. Chem. Soc.*, 2007, **129**, 8236–8246.
- 252 O. Š. Miljanić and J. F. Stoddart, *Proc. Natl. Acad. Sci.*, 2007, **104**, 12966–12970.
- 253 L. Liu, Y. Zhang and B. Xin, *J. Org. Chem.*, 2006, **71**, 3994–3997.
- 254 R. J. Rahaim and R. E. Maleczka, *Org. Lett.*, 2005, **7**, 5087–5090.
- 255 S. Basu, A. Coskun, D. C. Friedman, M. A. Olson, D. Ben fez, E. Tkatchouk, G. Barin, J. Yang, A. C. Fahrenbach, W. A. Goddard and J. F. Stoddart, *Chem. Eur. J.*, 2011, **17**, 2107–2119.
- 256 D. B. Amabilino, J. F. Stoddart and D. J. Williams, *Chem. Mater.*, 1994, **6**, 1159–1167.
- 257 P. R. Ashton, D. Philp, M. V Reddington, A. M. Z. Slawin, N. Spencer, J. F. Stoddart and

- D. J. Williams, *J. Chem. Soc. Chem. Commun.*, 1991, 1680–1683.
- 258
- 259 E. Smith, R. Lilienthal, R. Fonseca and D. Smith, *Anal. Chem.*, 1994, **66**, 3013–3020.
- 260 M. N. Cortona, N. R. Vettorazzi, J. J. Silber and L. E. Sereno, *J. Braz. Chem. Soc.*, 1997, **8**, 377–382.
- 261 O. Hammerich and B. Speiser, *Organic Electrochemistry, Fifth Edition: Revised and Expanded*, Taylor & Francis, Abingdon, 2015.
- 262 G. J. Ashwell, G. H. Cross, D. A. Kennedy, I. W. Nowell and J. G. Allen, *J. Chem. Soc. Perkin Trans. 2*, 1983, 1787–1791.
- 263 G. J. Ashwell and J. G. Allen, *J. Phys.*, 1983, **44**, 1261–1264.
- 264 G. J. Ashwell, J. G. Allen, E. P. Goodings and I. W. Nowell, *Phys. Status Solidi Appl. Res.*, 1984, **82**, 301–306.
- 265 D. R. Rosseinsky and P. M. S. Monk, *J. Chem. Soc. Faraday Trans.*, 1994, **90**, 1127–1131.
- 266 M. Pollak and B. I. Shklovskii, *Hopping transport in solids*, North Holland, Amsterdam, 1991.
- 267 S. K. Nimkar, A. H. Anderson, J. M. Rimoldi, M. Stanton, K. P. Castagnoli, S. Mabic, Y. X. Wang and N. Castagnoli, *Chem. Res. Toxicol.*, 1996, **9**, 1013–1022.
- 268 P. S. Shirude, V. A. Kumar and K. N. Ganesh, *Eur. J. Org. Chem.*, 2005, **2005**, 5207–5215.
- 269 J. Krzystek, A. Sienkiewicz, L. Pardi and L. . Brunel, *J. Magn. Reson.*, 1997, **125**, 207–211.

Appendix 1

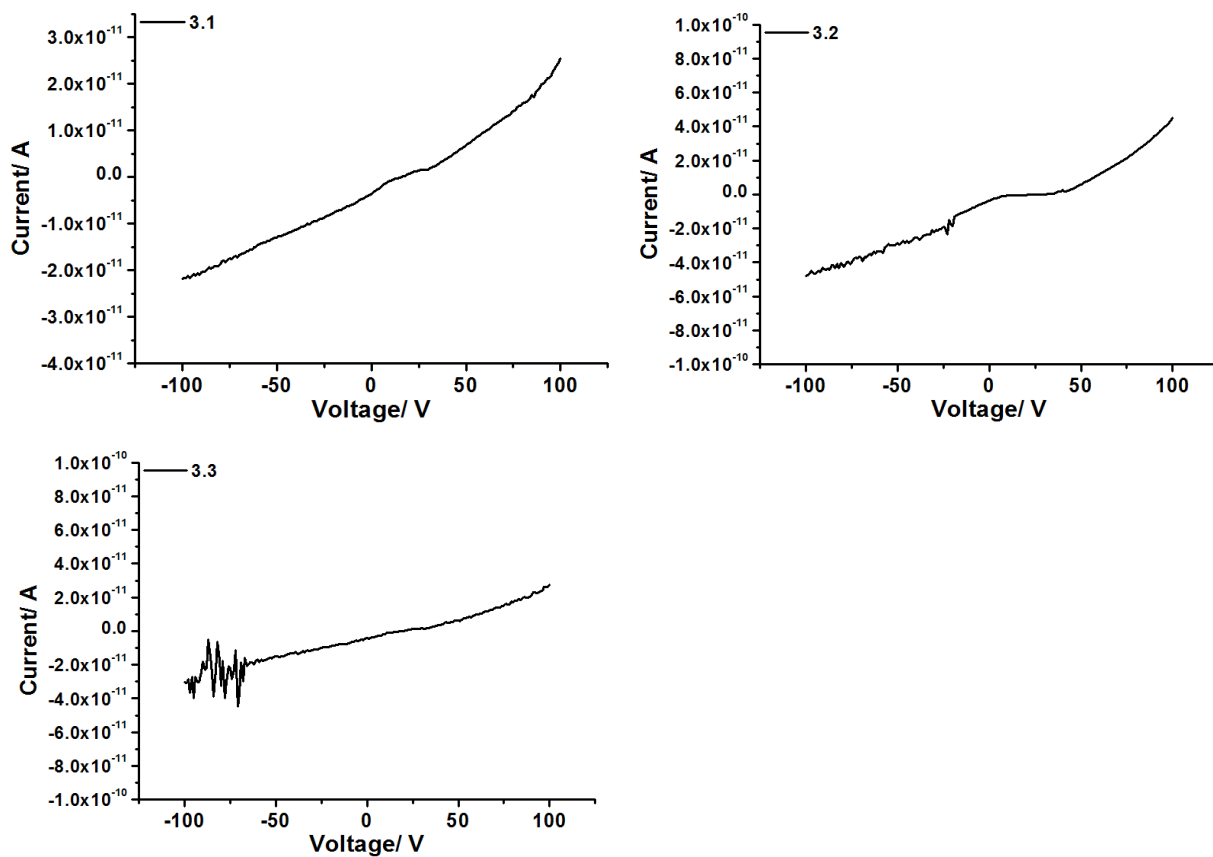


Figure S2. The I/V plot of unimer 3.1, dimer 3.2 and trimer 3.3 containing ester end groups, respectively.

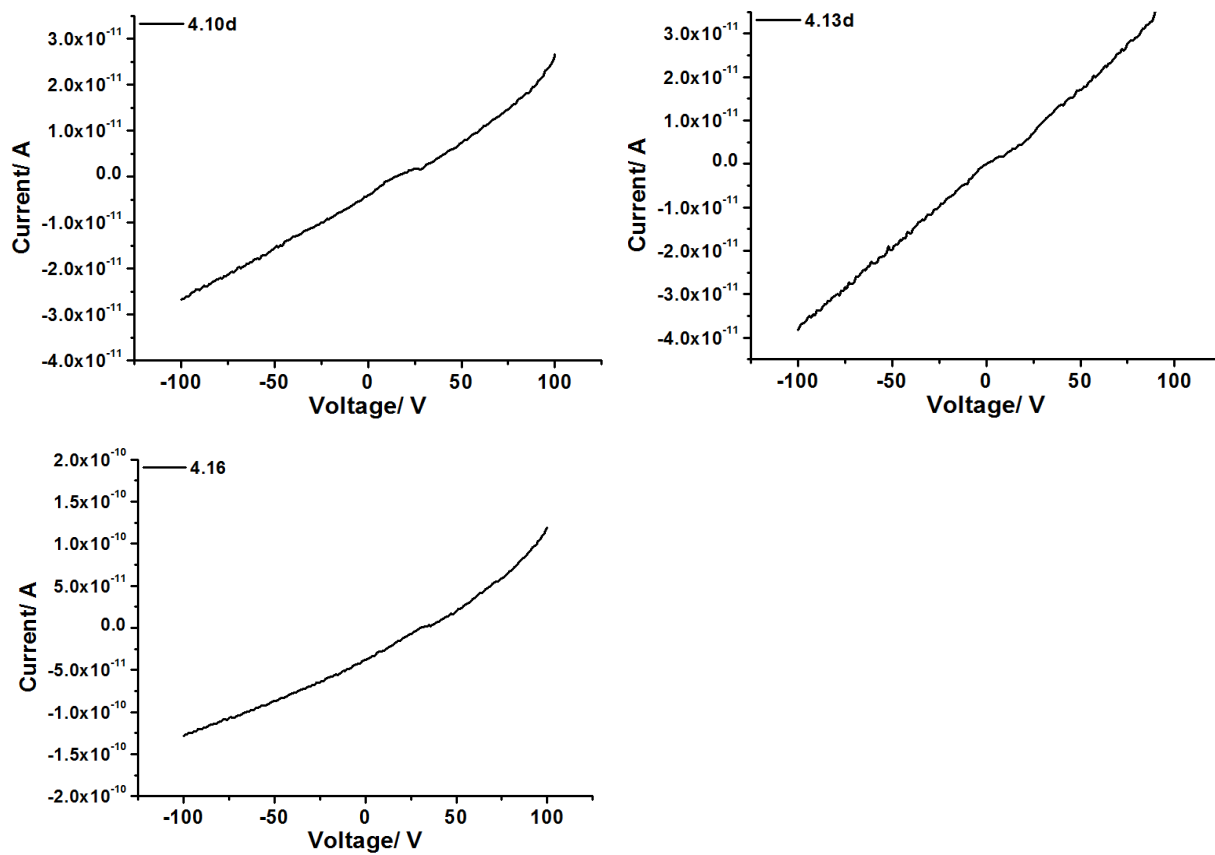


Figure S3. The I/V plot of unimer 4.10d, dimer 4.13d and trimers 4.16 containing ester end groups, respectively

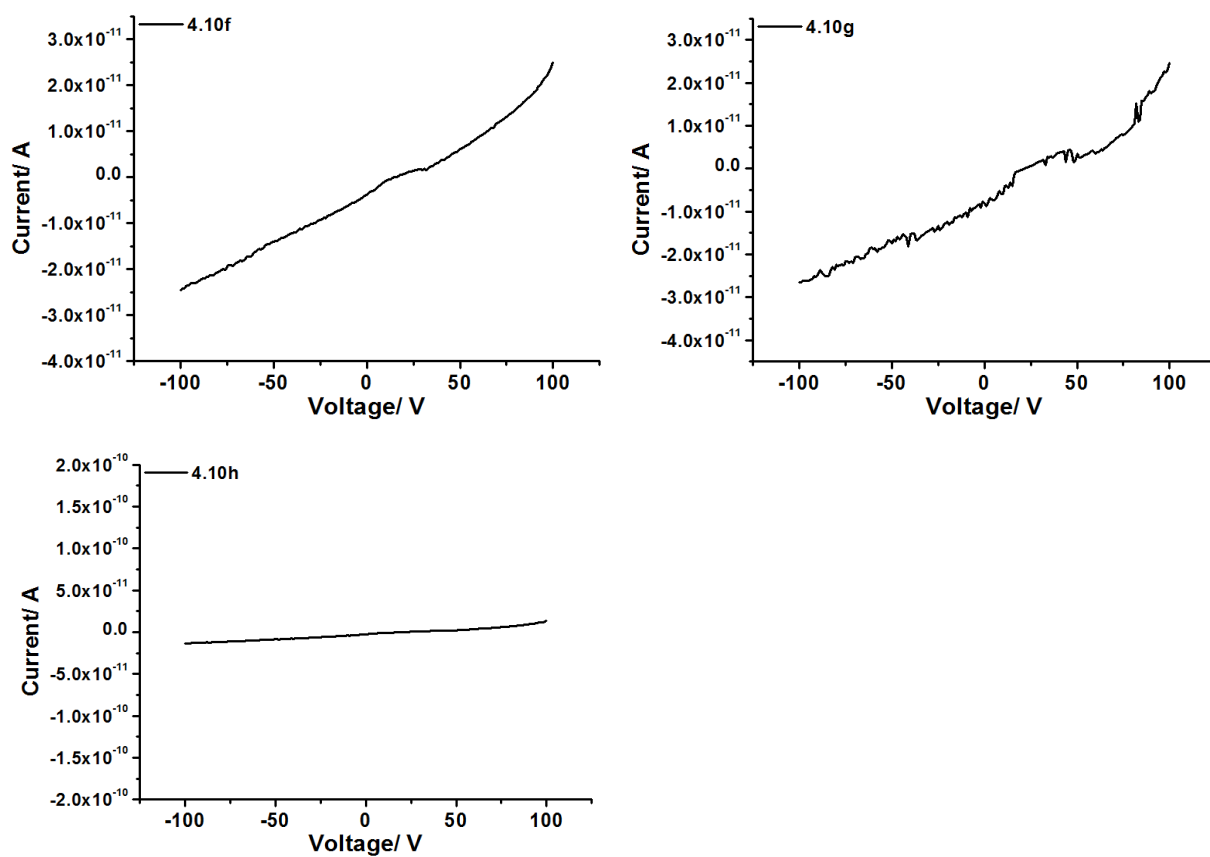


Figure S4. The I/V plot of unimer 4.10f, 4.10g, 4.10h containing varying numbers of fused aromatic rings residues on the end group.

Appendix 2

In order to fully understand the redox-induced changes in **5.16**, thin-layer ultraviolet-visible spectroelectrochemical (UV-vis SEC) measurements were carried out at 293 K with 0.2 mM **5.16** in DMF/0.1 M TBAPF₆.

The observed spectral changes for compound **5.16** exhibit isosbestic points, excluding the possibility of side reactions on the timescale of the experiment. The cathodic steps were reversible and parent electronic absorption spectra were recovered upon reoxidation.

Figure S5 shows the UV-Vis spectral monitoring of the electrochemical reduction of tetracationic macrocycle **5.16** at the two well-defined cathodic waves shown in Figure S5. Conversion of the tetracationic species to the bis(radical cation) results in new absorption bands at 435 nm, 600 nm and 715 nm (Figure S5A), which indicates the formation of radical cationic viologen. Continued decrease in the applied cathodic potential results in the formation of a second transformation associated with intense absorption band at 445, and decrease absorption bands at 600 nm and 715 nm.

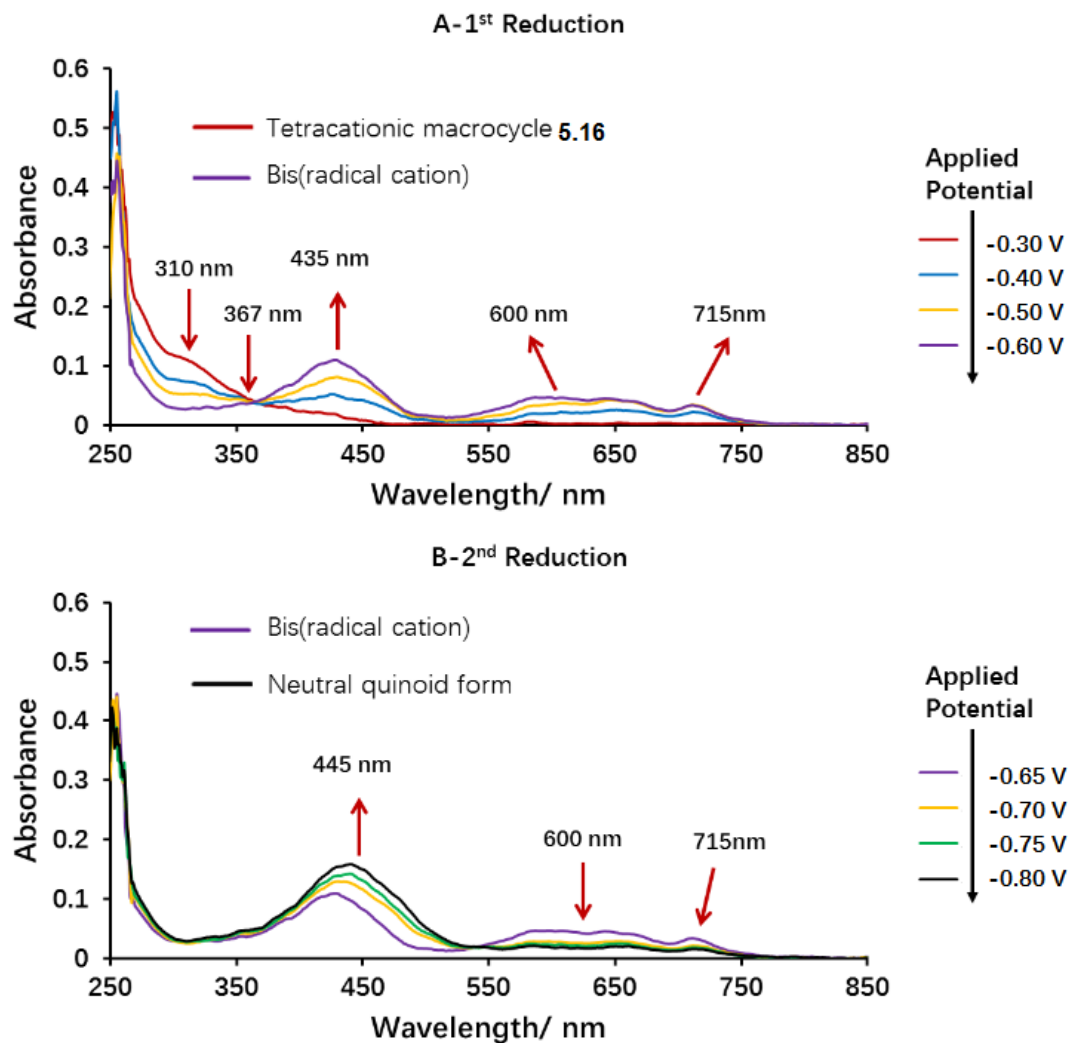


Figure S5. Reversible UV-vis spectral changes accompanying the stepwise electrochemical reduction of macrocycle 5.16 to bis(radical cation) (spectrum A) and the neutral quinoid form (spectrum B). Spectra recorded in anhydrous DMF/0.1 M TABPF₆, using an OTTLE cell.

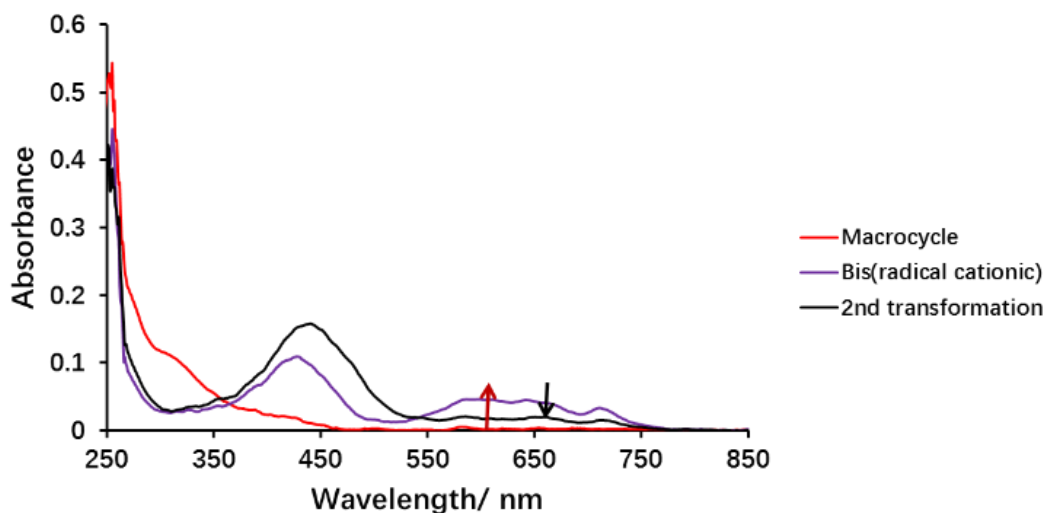


Figure S6. UV-vis spectral changes accompanying the stepwise reduction of tetracationic **5.16** to its second transformation species.

Figure S6 shows an overlaid plot of the UV/vis spectra of the three stable, spectroscopically distinct species in the redox cycle of **5.16**. The increase in intensity of the absorption band of radical cationic viologen at 615 and 700 nm as the molecule becomes reduced to the bis(radical cationic) species (Red arrow). This compares to a change in intensity of black arrow when moving from the bis(radical cationic) species to the fully reduced, 1st transformation. These data suggest that the 2nd transformation species of **5.16**, which is formed at approximately -0.80 V, did not fully reduce. This was caused by the precipitation of the box after reduction.

Appendix 3

“Efficient access to conjugated 4,4'-bipyridinium oligomers using the Zincke reaction:
Synthesis, spectroscopic and electrochemical properties”